The effects of paint-based protective films on the actual temporal water-side performance characteristics of steam surface condenser tubes

by
John Goodenough

Dissertation presented for the degree of Doctor of Philosophy in the Faculty of Engineering at Stellenbosch University

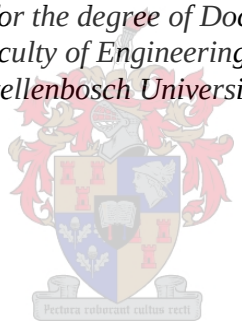

Supervisor: Prof Hanno Carl Rudolf Reuter
Co-supervisor: Dr Mike Owen

March 2017

Declaration

By submitting this dissertation electronically, I declare that the entirety of the work contained therein is my own, original work, that I am the sole author thereof (save to the extent explicitly otherwise stated), that reproduction and publication thereof by Stellenbosch University will not infringe any third party rights and that I have not previously in its entirety or in part submitted it for obtaining any qualification.

Date: ..... March 2017 .....

Abstract

Paint-based protective films (PPFs) are applied to the internal surface of steam surface condenser tubes to mitigate corrosion and erosion. The performance impact resulting from fresh-water fouling on these PPFs is experimentally investigated using actual cooling water from a thermal coal-fired power station. Four different paint types are tested alongside unmodified stainless steel, titanium, and brass tubes for direct comparison, using a purpose-built test apparatus featuring six co-current flow double-pipe heat exchangers arranged in parallel. Exposure times vary between 85 days and 280 days providing novel information pertaining to these PPFs in terms of their performance over time.

Cooling water exiting the condenser is drawn from a take-off valve fitted before the cooling duct enters the wet-cooled cooling tower, and passes through the test apparatus at 4 L/s. The cooling water passes once through each test tube at the condenser design velocity before being returned to the cooling tower pond. Each tube is heated using water instead of steam, to provide consistent and repeatable outer convection conditions. By measuring a total of 24 bulk fluid temperatures and 12 volumetric flow rates, the heat transfer, and hence fouling factor, for each tube is determined during tests.

In order of decreasing predominance: biological fouling, precipitation fouling (scaling), and particulate fouling (deposition) are identified on all the test tubes. The unmodified admiralty brass tube provides the best overall performance because its copper ions retard the biological fouling rate. The non-biocidal PPFs experience similar fouling to all the non-copper alloy tubes tested, where their asymptotic fouling factors are almost five times greater than the copper-bearing alloy tested. The data gained using the testing techniques described herein allows the dominant fouling mechanism to be identified and can be used to better design water treatment management, as well as direct further PPF development towards reducing biological fouling tendencies. One of the biocidal PPFs that is tested reaches a lower fouling factor than an unmodified stainless steel tube after 85 days of exposure under the same conditions. These results are compared to the plant's condenser fouling factor, calculated using a one dimensional condenser model. The agreement between the fouling factor measured on single tubes compared to the fouling factor of the condenser validates the testing and further means that the fouling data can be used to enhance condenser design and management using PPFs.

Keywords: Paint, coating, condenser, fouling, biofouling, performance, corrosion, thermal conductivity

Uittreksel

Verf-gebaseerde beskermende film (VBF) word toegepas aan interne oppervlaktes van stoom oppervlakte kondenser buise om roes te versag. Die prestasie impak gevolg van vars-water aangroei op die VBF is eksperimenteel ondersoek deur gebruik van werklike verkoelings water van termiese steenkool krag stasie. Vier verkillende verf tiepes word getoets langs onveranderde vlekvrye staal, titanium en koper buise vir direkte vergelyking, deur gebruik van doel-geboude toets aparatus wat ses mede-huidige vloei dubbel pyp hitte uitruilers uitgele in parallel. Blootstelling tye kan verskil tussen 85 dae en 280 dae verskaf unieke informasie met betrekking tot die VBF in terme van die prestasie oor tyd terwyl die onderwerp van die indentiese water wat in diens ervaar word.

Verkoelings water wat die kondenser verlaat, word vertrek van ’n uitlaat klep wat toegerus is voor die verkoelings uitlaat pyp die nat-verkoelde verkoelings toring in loop, en loop deur die toets aparatus teen 4 L/s. Die verkoelings water loop een keer deur elke toets buis van die kondenser ontwerpde snelheid voor dit teruggekeer word na die verkoelings toring dam. Elke buis is verhit deur water inplaas van stoom, om ’n konstante en vertroubare buite konveksie toestand te voorsien. Deur ’n totaal van 24 grootmaat vloeistof temperature en 12 volumetriese floei koers, die hitte oordrag, en van daar die aangroei faktor van elke buis word bepaal geduirende die toets.

Biologiese aangroei, skalering, en deeljies (ingesteldheid) word geidentifiseer as die oorheersende meganisme op al die toets buise, hoewel die onveranderde Admiralty braas buise voer die beste algehele prestasie want die koper ione bewoon bakterele sellulere asemhaling. Die nie-biociden VBF ervaring het soortgelyk aangroei vir al die nie-koper allooi buise wat getoets was, waar hulle asimptotiese aangroei faktore in orde was vyf keer groter as die koper-draende allooi wat getoets was. Die data laat toe dat die dominante aangroei meganisme geidentifiseer word en dan beter gebruik kan word vir beter ontwerpde water behandeling beheer, so wel as direk verdere VBF ontwikkeling vir die vermindering van biologiese aangroei neigings. Een van die biociden VBF wat getoets was, het ’n laer biologiesie aangroei bereik as ’n nie geverfde stainless steel buise na 85 dae onder dieselfde blootstelling. Hierdie resultate is vergelyk met die kragstasie se kondenser aangroei faktor, wat bepaal is deur ’n een dimensionelle kondenser model. Die ooreenkoms tussen die aangroei faktor wat gemeet is op enkle buise in vergelyking van die aangroei faktor van die kondenser bevestig die toets, en die data kan dus gebruik word vir die verbetering van kondenser ontwerp en bestuur, deur die gebruik van VBF.

Sleutelwoorde: verf, laag, kondenser, aangroei, biologiese aangroei, pre, roes, gradering, termiese geleiding

Acknowledgements

My deepest gratitude is given to my supervisor and mentor Professor Hanno Carl Rudolf Reuter. Thank you for your continued dedication, exceptional support, and leadership throughout the years of our friendship. Your teaching is extraordinary and I shall always endeavor to apply the knowledge you have passed onto me.

My parents have made this project possible and I could not have achieved any of this without them. My father has guided me along an amazing journey, lighting the way ahead. Thank you for believing in us and never giving up. My mother, with her ironclad faith in all our efforts, has been a stronghold in any adversity. To my sister and brother-in-law, thank you and I appreciate your never-ending help, encouragement and support.

Members of the power utility who were instrumental in this research are deeply appreciated. In particular Dhiraj Maharaj, the plant station manager who supported this project from its inception. Louw Nagal, Keith Northcott, Kelley-Reynolds Clausene, Francois de Preez, Alain Micheals, and Gontse Mathibedi are expressly thanked for their contributions.

To my co-supervisor Dr Micheal Owen, thank you for your exceptional guidance, as well as your determined support in seeing this project to completion.

Contents

List of figures

List of tables

Nomenclature

Symbols

A	Area (m)
A_{Nu}	Experimentally determined regression coefficient in equation (3.23)
B_{Nu}	Experimentally determined regression exponent in equation (3.23)
CF	Cleanliness factor
C	Rate constant in equation (3.33) (W/(m^2 K d))
c_p	Specific heat at constant pressure (J/(kg K))
C^*	Rate constant in equation (3.32)
d	Diameter (m)
d_1	PPF modified inner diameter / fouled inner diameter of tube (m)
d_2	Tube inner unmodified diameter of tube (m)
d_3	Annulus inner diameter = tube outer diameter (m)
d_4	Annulus outer diameter (m)
EB	Energy balance term in equation (3.37)
$\frac{e}{d_1}$	Relative surface roughness (m/m)
F	Volumetric flow rate (m^3/s)
f_d	Darcy friction factor
g	Gravitational constant, 9.79 (m/s^2)
h	Convection coefficient (W/(m^2 K))
i_{fg}	Latent heat of vaporization (J/kg)
k	Thermal conductivity (W/(m K))
k_1	Factor in equation (3.22)
k_{eff}	Equivalent thermal conductivity of PPF and tube combined (W K/m)
L	Length (m)
MB	Mass balance term in equation (3.39)
Δp	Pressure drop (Pa)

P_p	Pumping power (W)
$\bar{Q}$	Average heat transfer rate (W)
Q	Heat transfer rate (W)
Q_{duty}	Heat rejected by the condenser to the cooling system (W)
Q_{fuel}	Heat input into the boiler (W)
R	Thermal resistance to heat transfer (K/W)
$R_f{}^*$	Fouling factor based on the difference in overall heat transfer coefficients (equation (3.30)) (m^2 K/W)
R_f	Fouling factor ($m^2 \cdot$ K/W)
R_f^∞	Asymptotic fouling factor (m^2 K/W)
R''_{PPF}	Equivalent fouling factor of PPF (m^2 K/W)
R_f^0	Asymptotic fouling factor at time 0 (m^2 K/W)
T	Temperature (K)
t	Time (d)
T_1	Condenser inlet water temperature (K)
T_2	Condenser outlet water temperature (K)
ΔT_{LM}	Log mean temperature difference (K)
U_0	Overall heat transfer coefficient at time zero (clean tube condition) (W/(m^2 K))
v	Velocity (time averaged) (m/s)

Greek letters

β	Constant in equation (3.31) (d)
ϵ	Surface roughness (m)
ϵ^*	Machine epsilon (related to the processor smallest digit)
μ	Dynamic viscosity (kg/s.m)
ρ	Density (kg/m^3)
ζ	Step size used in numerical differencing

Subscripts

ann	Annulus
con	Condensate
cond	Condenser
e	Electromagnetic flow meter / energy
f	Fouling / foulant / fluid

gen	Generator
h	Hydraulic
in	Inlet
m	Mean
max	Maximum
mf	Mean film
out	outlet
PPF	Paint-based protective film
Δp	Between pressure tappings
s	Steam
t	Time / total
u	Ultrasonic flow meter
w	Wall or waterside

Dimensionless groups

Nu	Nusselt number, hd/k
Pr	Prandtl number, $\mu c_p/k$
Re	Reynolds number, $\rho v d/\mu$

Acronyms

CFD	Computational fluid dynamics
CFU	Colony forming units
EPDM	Ethylene propylene diene monomer (a synthetic rubber)
h_g	Convection coefficient for condensation of a pure vapor on a single horizontal tube (W/(m^2 K))
LP	Low pressure
LSI	Langelier Saturation Index
LMTD	Log mean temperature difference
PID	Piping and instrumentation diagram
PPF	Paint-based protective film applied to a heat exchanger surface to offer protection between the working fluid and the surface
PVC	Polyvinyl chloride (a synthetic plastic)
RSI	Ryznar Stability Index
RTD	Resistance temperature detector

TEMA Tubular Exchangers Manufacturers Association

TT Test tube

USD United States Dollar

The cross-section schematic shown below illustrates the relevant diameters and symbols:

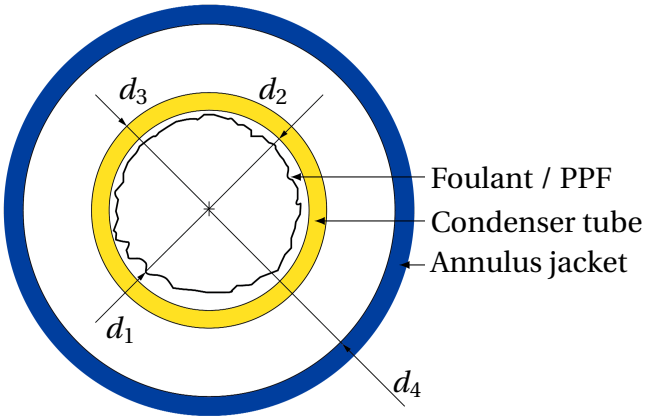

Chapter 1

Introduction

1.1 Background

1.1.1 Steam surface condensers

Steam surface condensers are shell-and-tube type heat exchangers, typically having tens of thousands of thin-walled tubes arranged in bundles. They condense steam on the outer surface of their tubes by removing latent heat of vaporization, ultimately condensing the steam back to its liquid state. Surface condensers are distinguished from direct contact condensers where the coolant is sprayed directly into a chamber containing the steam vapor and there is no physical barrier. Hereafter condenser shall refer solely to surface condensers. In vapor power cycles, reducing the specific volume of the steam allows it to be pumped back to the boiler completing the cycle. The tubes are cooled by passing cooling water through the inside of each of the tubes. Cooling water is either taken from a body of water (such as a lake, river or sea) or it is circulated through a cooling tower.

The impact of the condenser on the cycle efficiency is significant – it is the second largest heat exchanger in the power plant (second only to the boiler). It provides the lowest possible temperature to reject low-grade energy to the heat sink in the power cycle (Silver, 1963). That is to say it provides the lowest possible back pressure at the turbine exhaust exit because most of the condensation takes place under the vapor dome at saturated conditions so temperature and pressure are constant. Consider the Rankine cycle plotted in terms of temperature and entropy in figure 1.1.

The process 1-2 represents the expansion of superheated steam through the turbine. At point 2 the wet steam enters the condenser and is condensed to point 3, a slightly sub-cooled liquid. From 3 to 4 the liquid condensate is pumped back to the boiler, before being heated along line 4-1, and entering the turbine as superheated steam. Since the area enclosed by the points 1-2-3-4 represents the net heat input which from the first law of thermodynamics for a closed system is equal to the power output from the cycle, it becomes clear that as the condenser lowers the condensing pressure (line 2-3), it greatly improves the power output

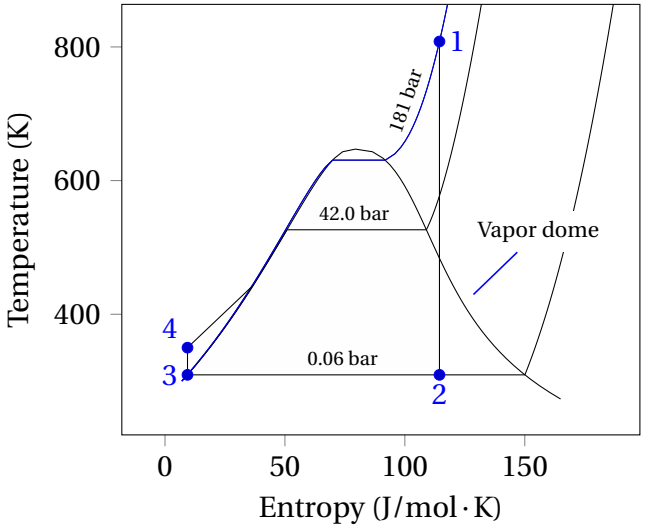

Figure 1.1: Temperature-entropy diagram of the Rankine power cycle

from the cycle. The condenser performance directly affects the cycle efficiency, and the cycle cannot operate if the condenser is compromised.

Steam surface condensers perform a number of principle functions that include:

1. condensing steam with the lowest possible steam-side pressure drop (and associated temperature drop) across the condenser;
2. acting as a physical barrier between cooling water and ultra-pure demineralized boiler feedwater;
3. removing non-condensible gases that accumulate within the steam by means of an evacuation system;
4. deaerating and reheating the condensate;
5. storing condensate before it is pumped back to the condenser;
6. serving as a collection point where drains from auxiliary equipment (ranging from sub-cooled liquid to liquid-gas mixtures to superheated steam) can be safely reclaimed into the steam system;

The first function to minimize the pressure drop experienced by the steam across the condenser is achieved by designing the shell and tube bundles to include steam passages or lanes through which the steam passes. These passages evenly distribute the steam over the tubes (figure 1.2). The change in specific volume of the steam as it condenses, caused by coalescing gas molecules to form liquid drops, within the fixed volume of the condenser shell, creates the low pressure which drives the steam flow.

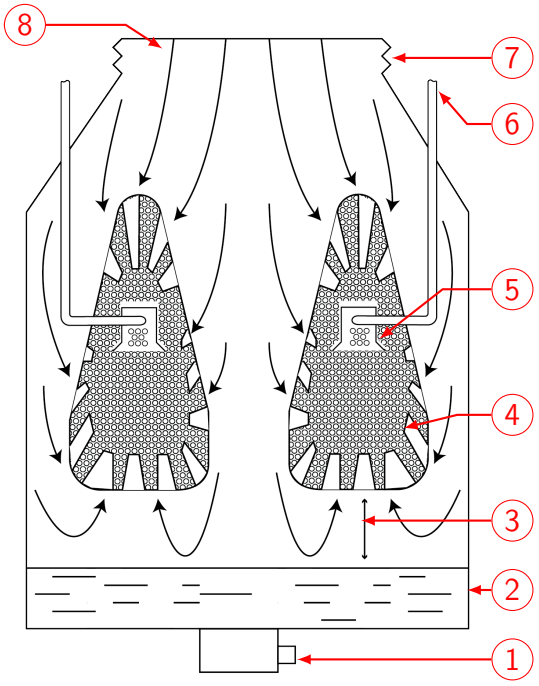

Figure 1.2: Simplified end view of condenser – (1) condensate return, (2) hotwell, (3) condensate reheat section, (4) laned tube bundle, (5) air-extraction zone, (6) Air vapor take-off, (7) expansion joint, (8) steam from turbine,

The steam itself is raised from boiler feedwater which is meticulously purified as this becomes critical in high pressure boilers and turbines used in the power industry. Contaminants in the boiler feedwater can lead to many detrimental effects ranging from corrosion and scaling of the boiler tubes to impingement damage on the turbine blades. The purification of the boiler feedwater is a costly operation, and such a level of purity cannot be economically achieved for the cooling water used in the condenser (owing to the large water consumption of open-type cooling systems discussed later). The cooling water in the condenser therefore has a much higher level of contaminants and the second function of the condenser is to act as a physical barrier between the cooling water and the ultra-pure steam. These contaminants can quickly pollute the demineralized water in the steam cycle if leaks develop within the condenser. The situation is exacerbated by virtue of the fact that the condenser operates below atmospheric pressure and hence it is imperative that the integrity of condenser tubes are protected as far as possible. A relatively thin tube wall (between 0.5 and 1.2 mm) is all that separates the cooing water and the steam. Condenser tubes are therefore made from alloys which resist corrosion and erosion as well as maintain a high thermal conductivity.

The third function arises from the fact that the condenser is the lowest pressure point in the steam cycle, and hence any non-condensible gases within the steam will accumulate within the condenser. Notwithstanding all efforts to en-

sure an airtight steam space, practical limitations mean that some non-condensible gases (predominantly air) inevitably leak into the steam system. Liquid-ring vacuum pumps or steam-jet-air-ejectors are used to extract these non-condensible gases from the so-called air extraction zone within the condenser. This region is the coldest region in the condenser, usually designed to be near the geometric center of the tube bundles. Perforated ducting piped to this point in the steam space is used to vent the non-condensibles as they collect in the air extraction zone as depicted in figure 1.2.

Ideally steam should be condensed to the saturation temperature and then returned to the boiler. However, in practice it is possible that condensate is cooled below the saturation temperature - a condition referred to as subcooling or condensate depression. The subcooled condensate is able to dissolve more oxygen which adversely affects corrosion within the boiler. Another detrimental consequence of subcooling is that it increases the amount of fuel required by the boiler since the condensate has to be heated until the saturation temperature is reached before phase change can occur. The level of subcooling should therefore always be minimized as far as possible, which is the fourth function of the condenser, and most condensers are designed such that steam is directed counter-current to falling condensate to heat subcooled condensate to the saturation temperature. Suitable space below the tube bundles is provided for this.

The hotwell is a chamber at the bottom of the condenser below the reheat section that serves the fifth function of the condenser: to collect the falling condensate and temporarily store it before it is sent back to the boiler. The size of the hotwell is designed to meet the operational needs of the boiler, and the level is closely monitored as well as the temperature of the condensate within the hotwell.

Since the condenser has the lowest pressure in the steam cycle, many of the auxiliary steam processes also dump steam (and condensate from the flash vessel) into the condenser. Therefore the last function means that the condenser is fitted with spargers and impingement plates at drain points to slow down the high energy steam flows which need to be condensed, and distribute them safely into the flowing steam. Additionally during operation of the steam turbine, occasions arise when the main turbine steam flow bypasses the turbine and this high kinetic energy flow must also be suitably condensed by the condenser.

1.1.2 Condenser tubes

Condenser tubes are made from thin-walled metal alloys which include: copper alloys, stainless steels, and titanium. The tubes range in length but generally vary between 6 m and 12 m, and are supported along their length using support plates. Each tube end is rolled into a tube sheet plate. After meeting structural requirements of dynamic loading (vibration is often a catastrophic failure cause in condensers), the tubes themselves must offer good thermal performance as they are the heat transfer surface of the condenser. The cross section of a con-

denser tube in figure 1.3 shows the condensate film and resulting heat transfer path (neglecting any fouling on the outer surface which is typically much smaller compared to the waterside fouling). Note that condensers typically experience film-wise condensation as opposed to drop-wise condensation, because of surface weathering of the tube outer surface. As for the internal surface, fouling, corrosion, and erosion of the waterside surface occur because of the cooling water flowing through the tube. Fouling is the unwanted deposition of material on the heat transfer surface which adversely affects the hydraulic and thermal performance and is dealt with in detail later.

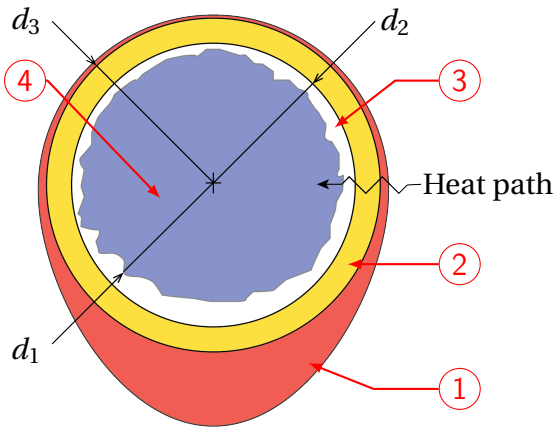

Figure 1.3: Cross section of condenser tube – (1) condensate film, (2) tube wall, (3) waterside foulant (rough surface profile) (4) cooling water

Corrosion mechanisms affecting condenser tubes include:

- General corrosion
- Erosion-corrosion
- Under-crevice corrosion
- Stress corrosion cracking
- Pitting corrosion
- Hydrogen embrittlement
- Microbial induced corrosion

Erosion not only influences corrosion but also leads to parent wall material loss. Both corrosion and erosion are detrimental to the structural integrity of the condenser tubes and depend on the cooling water used. A detailed treatise of

characteristics of condenser tube materials is provided in the subsequent chapter, although it is important to note that a major difference between fresh water and sea water (including brackish water) is the concentration level of chloride ions which greatly impacts the protective oxide films of certain alloys (especially those of stainless steels). Once the condenser tube is permeated, cooling water quickly enters the steam space (operating below atmospheric pressure). Consequently the once-pure condensate becomes contaminated, and depending on the severity of the tube leak the unit may have to be shut down in order to effect repair.

After the boiler has been shut down, the cooling water is drained from the condenser so that access to the tube sheet can be gained through the water box openings. Thereafter the tube is isolated from service by plugging it at both ends, before bringing the unit back into operation. This is a costly exercise and eventually life-extension strategies are sought to extend the service of the condenser until it can be retubed. One such strategy is the application of paint-based protective films (PPFs) to the internal surface of the tube to protect the remaining tube material from further damage.

1.1.3 Paint-based protective films as a life-extension and failure mitigation strategy

Paint-based protective films (PPFs) are inert polymeric coatings that are applied to heat transfer surfaces to protect them from corrosion and to a lesser extent erosion. PPFs successfully form a protective barrier between the parent tube material and the cooling water, preventing corrosion (Sato *et al.*, 1985), and have thus been shown to be a viable option for extending condenser life (Fraze & Woodruff, 1997). They have further been observed to reduce the rate of fouling in other heat exchanger applications (Gawlik *et al.*, 1998) but this has not been fully investigated in steam surface condensers. PPFs can improve the average cleanliness of the condenser over time if they are carefully designed and operated, such that they decrease the rate of fouling, and they therefore ultimately improve the average overall performance.

1.2 Fouling of heat transfer surfaces

1.2.1 Definition of fouling

Fouling may be defined as the formation of unwanted deposits on heat transfer surfaces, which tend to increase the resistance to heat transfer and fluid flow (Somerscales, 1981). Moreover, Somerscales (1981) identifies the Kern-Seaton relation (Kern & Seaton, 1959) to be the generally accepted starting point of many fouling models.

Kern & Seaton (1959) describe the net rate of fouling to be the difference between formation processes and removal processes, i.e.

$$\text{Net fouling rate} = \begin{pmatrix}\text{Rate of formation of}\\ \text{the fouling deposit}\end{pmatrix} - \begin{pmatrix}\text{Rate of removal of the}\\ \text{fouling deposit}\end{pmatrix} \tag{1.1}$$

The formation processes involve bulk processes occurring in the fluid (which depend on concentrations of different species), transportation of these species to the heat transfer surface, and the attachment of the deposit to the surface.

Similarly the removal processes include dissolution of the deposit as it ionizes, erosion (re-entrainment) as particulate material leaves the surface, and spalling as large masses of material are transported away from the surface. Fouling can therefore be categorized according to the dominant mechanism by which it occurs.

Epstein (1981) organizes fouling into six types based on the principle mechanism which causes that type of fouling:

1. **Precipitation fouling (scaling)** - refers to the precipitation of dissolved minerals on heat transfer surfaces. Scaling occurs when substances in solution have inverse solubility with temperature, and the precipitation occurs on heated surfaces. Typical scaling examples in cooling water are calcium carbonate (Bhatt, 2006) and magnesium carbonate (Wu & Cremaschi, 2013).

2. **Particulate fouling** - refers to the accumulation of solids suspended in the process fluid onto the heat transfer surface

3. **Chemical reaction fouling** - refers to chemical reactions which result in the deposition of products at the heat transfer surface, although the surface material has no part in the reaction.

4. **Corrosion fouling** - refers to the formation of corrosion products at the heat transfer surface that occur when the surface material reacts with the fluid.

5. **Biological fouling** - refers to the attachment of living organisms to the surface. In this context biological fouling refers to micro fouling, compared to macro fouling which involves the obstruction of the flow area due to foreign matter (which may be organic or inorganic).

6. **Freezing fouling** - refers to the solidification of a liquid or its constituent when sub-cooled by the heat transfer surface. This type of fouling does not occur in steam surface condensers.

Composite fouling involves two or more fouling mechanisms present in the same fouling media, which may interact with one another (Yu, 2007), cited by Izadi *et al.* (2011). A review of composite fouling of heat transfer equipment

is presented by Sheikholeslami (2000). The author highlights the lack of attention given to composite fouling, such as occurs when biological fouling and inorganic (precipitation and particulate) fouling are both taking place. Therefore controlled testing on model systems is required to isolate these interactive effects and subsequent testing can be used to determine their combined effects (Sheikholeslami, 2000).

1.2.2 Fouling mechanisms affecting steam surface condensers

Open recirculating cooling water systems using fresh water, such as the one depicted in figure 1.4, likely suffer from precipitation, particulate, and biological fouling. To a lesser extent corrosion fouling may also be of concern.

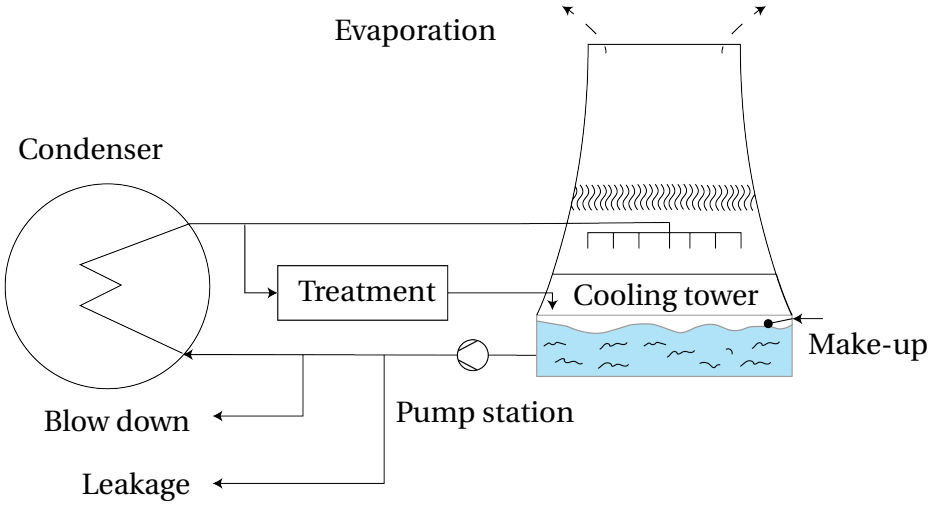

Figure 1.4: Schematic of an open recirculating cooling system with a wet-cooled natural draft cooling tower

The process of evaporation in such systems leads to increasing concentrations of salts in the cooling water (IHS ESDU 2008). Therefore at regular intervals a fraction of the water is purposefully discharged and replaced with make-up water: a practice referred to as blowdown. Leakage is another issue necessitating the input of make-up water. Often the make-up water is sourced from a lake or river, which means that contaminants enter the system via the make-up water. Thus a percentage of the water returning to the cooling tower pond in figure 1.4 is passed through a chemical and physical treatment process, normally using flocculants, clarifier, and biocides etc.

1.2.3 Biological fouling

Micro biological fouling, referred to as biological fouling hereafter, is the fouling caused by the uncontrolled reproduction of bacteria, algae, and fungi on heat

exchanger surfaces (IHS ESDU, 2008; Rice *et al.*, 1993). Nimmons (1979), cited by Characklis (1981), found the thermal conductivity of a biofilm to vary between 0.57 and 0.71 W/(m K) (at 27 °C), which clearly explains the severe impact biofilms cause on heat transfer.

The biofilm growth rate depends heavily on the bulk water temperature, and all micro-organisms have an optimum temperature for maximum growth (Bott, 1995). Clearly depicted in figure 1.5 is the non-linear dependence of biofilms on the bulk water temperature and in particular the biofilm that was tested reaches a maximum between 35 °C and 40 °C.

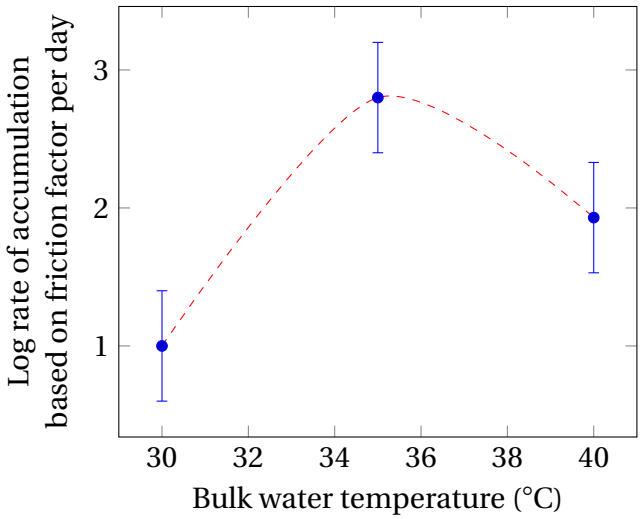

Figure 1.5: Influence of bulk water temperature: measured log rate of biofilm thickness in an experimental flow system (source: Characklis & Marshall (1990))

Bott (1995) found another particular bacteria species (Escherichia coli) to also have its maximum growth in this temperature range. This is an important consequence as will be seen later, where the cooling water used in the experimentation is near this range.

1.3 Field testing of the waterside fouling of condenser tubes at a thermal power plant

1.3.1 Characteristics of the power plant used in this study

The actual cooling water that passes through condenser tubes is a mixture of water, inorganic and organic species. Therefore any meaningful holistic experimental testing of PPFs needs to account for all of these species within the cooling water. However, to prepare water with exactly the same composition is exceedingly difficult. Accordingly water from an actual power plant with an open-type

recirculating cooling water system is used. The power plant is a large coal-fired power plant with six boiler turbine sets and four natural draft wet-cooling towers. The power plant draws raw water from a combined gravity and earth-fill type dam located on a river.

1.3.2 Source water

Over the years the make-up water conditions have deteriorated considerably. The Department of Water Affairs and Forestry (DWAF) (2006), cited by the Department of Water Affairs (DWA) (2009), found that the following causes of this:

- non-compliant sewage treatment plants that discharge into the river network;
- mining pollution;
- irrigation systems which feed back into the rivers, introducing fertilizers and other contaminants;
- urban run-off especially from increased formal and informal settlements (many of which are also not compliant);
- industrial pollution.

1.3.3 History of PPFs used at the power plant

Consider the history of PPFs used at the thermal power plant chosen for this study shown in figure 1.6. The selected power plant has been in operation for many years, having all six units equipped with admiralty brass tubed condensers (26 000 tubes each). In 2004 non-destructive eddy current testing indicated a general wall thinning of these tubes of almost 50 %. Tube leaks increased as a result of pitting corrosion and other failure mechanisms associated with corrosion and erosion. To extend the lifespan of these tubes until the next retubing opportunity, the first PPF was thus applied in 2007 to the unit 4 main condenser. Only 30 % of the condenser tubes were selected for the PPF application, based on the tubes that had the largest deterioration (determined from eddy current analysis). A phenolic epoxy film was applied at an average thickness of 200 µm. By passing a spray lance down the length of each tube and using a cone nozzle, this solvent-borne product was sprayed directly onto the tube surface. This technique is unsuitable for thinner films and the volatility of the solvents create hazardous conditions within the confined space of the condenser water box.

To overcome the application hazards, solvent-free epoxies were selected. Concerns of the increased thermal resistance offered by the relatively thick PPFs necessitated advances in the PPF application technologies to provide thinner films. Thence a pigging technique was developed, which involves injecting a fixed quantity of paint into one end of the tube and then propelling a tight-fitting plug down

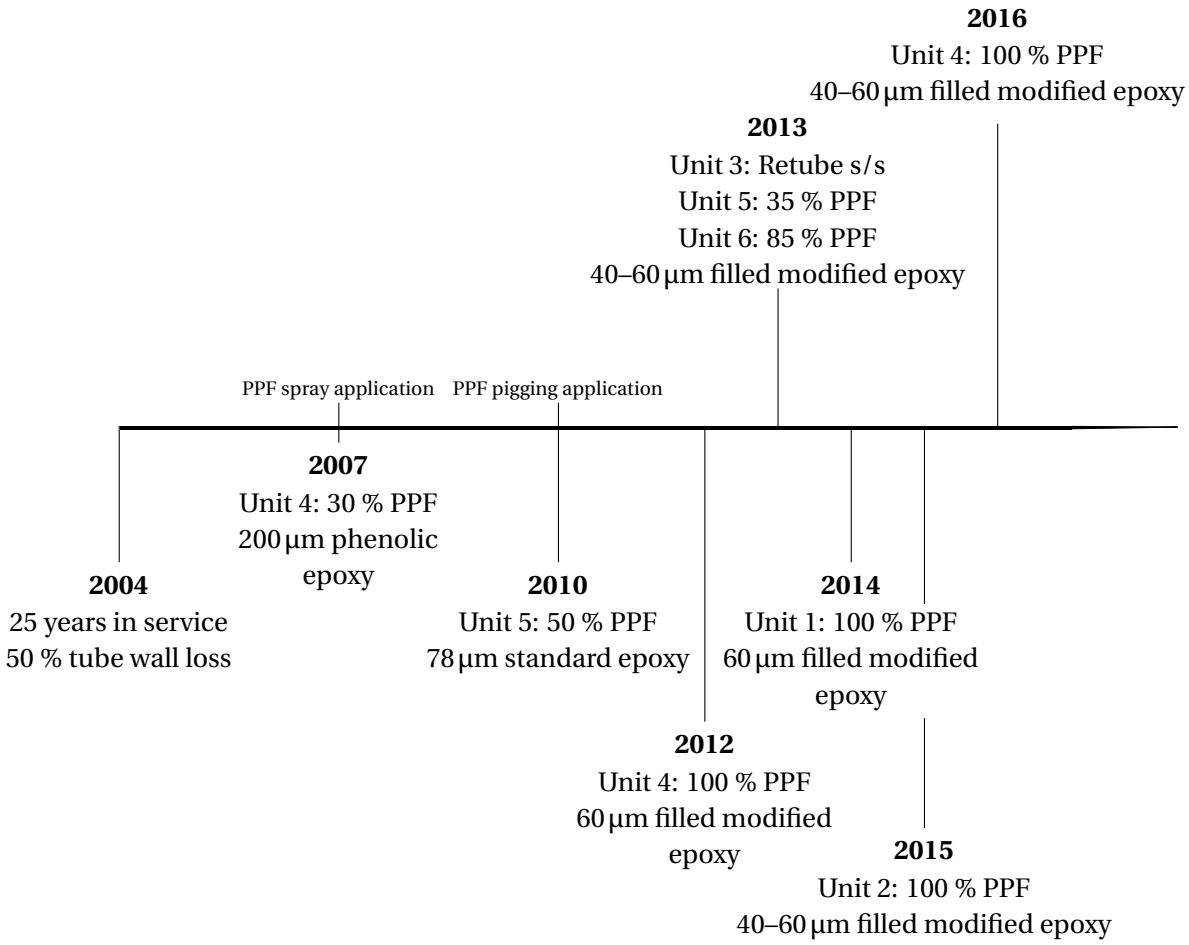

Figure 1.6: Timeline of the history of PPFs used at the selected thermal power plant

the tube's length forcing the paint onto the tube surface. By 2010 the average film thickness was reduced to 78 µm. 50 % of the tubes of the unit 5 condenser were thus painted with a modified epoxy that is solvent-free. The success of this application technique warranted further development of the solvent-free epoxies in terms of their conductivity (which varies between 0.5 and 0.6 W/(m K), measured by Goodenough (2013)).

Various fillers were tested and by 2012 the entire condenser of unit 4 was coated with a filled modified epoxy. At this time the average film thickness was 60 µm. In 2013 films with a thickness in the range of 40–60 µm were realized. Over the development period of these PPFs there has been a significant development in the physical properties of the paint to ensure a uniform film is achieved that is free from sagging, discontinuities and other defects. The application of PPFs on these condensers did result in fewer tube leaks, but knowledge of their propensity for fouling is scant.

1.4 Definitions and presuppositions

1.4.1 Definitions

The following terms are defined for use throughout this thesis:

Biofouling: Biological micro-fouling including the fouling caused by bacteria, algae, and fungi. Compared to biological macro-fouling that includes mussels, dead fish, and other organic debris that cause an obstruction to flow of the fouling fluid.

Condenser: Steam surface condenser of the shell-and-tube type.

Convection coefficient: Refers to the convection heat transfer coefficient.

Foulant: Refers to the deposited material on the tube surface which causes fouling, i.e. includes inorganic and organic matter.

Cooling water: The fresh water used in open-recirculating cooling systems, such as the one used by the abovementioned power station.

Paint-based protective films (PPFs): Paint refers to synthetic polymeric resins used with various fillers to form a thin protective film. Other sources in literature often refer to these PPFs as coatings, although strictly speaking the term coating refers to films applied to an external surface. Only films applied to the internal surface of the tubes are considered herein.

Power station: The thermal coal-fired power station where the aforementioned apparatus is installed. Since this utiltiy is a national keypoint its identity is not disclosed.

QEMSCAN®: Quantitative Evaluation of Minerals by SCANning electron microscopy is an automated scanning electron microscope used in this study for determining inorganic foulant species. The QEMSCAN® analysis is conducted by an independent laboratory.

Sea-cure®: A proprietary stainless steel made by *Plymouth Tube Co* (Plymouth Tube Co, 2013) specifically made for seawater applications with an enhanced pitting corrosion resistance.

Test apparatus: An experimental heat transfer testing apparatus designed, built, and operated by the author to fulfill this study.

1.4.2 Presuppositions pertaining to the PPFs in this study

The following presuppositions are made:

- The principal PPF tested in this study has already met the minimum coating requirements by passing the following tests:
  - pull-off dolly adhesion;
  - salt water immersion (ASTM D870-02, 2002);
  - 3 000 hour salt spray;
  - cathodic disbondment;
  - taber-wheel abrasion (D4060);
  - as well as six years in-service monitoring and evaluation.
- Two further PPFs are presented in this study that have not undergone all of the above mentioned tests, so these PPFs are clearly defined to be prototype PPFs (they are currently in second level development).
- Unless otherwise stated no coating failures are encountered, such as sagging, pin-holes, and / or peeling.
- Coating films that are tested herein are complete and continuous along the length of the test tubes.

1.5 Context of this research

Within Stellenbosch University, Kröger (1998) and Reuter (2010) have made significant advances in cooling towers. This study aims to complement their work by addressing the other major component of this cooling cycle, namely the condenser. The performance of PPFs applied to individual condenser tubes was first tested at Stellenbosch University in 2006 (Honing & Kröger, 2006). Continuing with this research in 2013, Goodenough (2013) measured the thermal performance of three different PPF coatings. The results from these tests showed great potential for PPFs but raised unanswered questions of quantifying their performance over time.

The research herein holistically considers the first steps in optimizing steam surface condenser life-cycle performance by utilizing PPFs, which not only prevent corrosion and erosion but also resist fouling. This has relevant industrial application, as this technology is currently being used to maintain existing condensers in South Africa; over one million tubes have been coated between 2008 and 2016.

1.6 Research objectives and motivation

1.6.1 Research hypothesis

It is hypothesized that the overall condenser performance (which is a combination of thermal effectiveness as well as availability) can be improved by applying

specially designed PPFs to new condenser tubes. Provided the PPF limits fouling, corrosion, and erosion such that the average performance over time is better than the average performance without the PPF, this hypothesis will be true. It is the subject of this research project to evaluate this hypothesis.

1.6.2 Objectives

With reference to steam surface condensers[1] the objectives of this project are to:

1. design, build, and operate an experimental testing facility at a power station, which is used to investigate fouling deposition and conditions inside condenser tubes with and without PPFs and evaluate their performance;

2. use this apparatus to gain a better understanding of the actual conditions condenser tubes experience in terms of combined fouling, erosion, and corrosion;

3. determine the time when PPFs should be applied within the condenser life cycle, by:

    a) investigating whether they can effectively reduce fouling, whilst mitigating corrosion, on several representative condenser tube materials, such as: admiralty brass, stainless steel, and titanium;

    b) comparing the relative performance over time of these tubes with and without PPFs ;

    c) validate these tests on single tubes with actual condenser data.

1.6.3 Motivation

Since more than 40 % of the thermal energy input in a steam power cycle has to be rejected to the environment via the cooling system (Kröger, 1998), proper condenser management is vital (Putman, 2001). Maximizing its performance effectively lowers environmentally harmful emissions and keeps costs to a minimum. Walker *et al.* (2012) estimated the combined economic impact of condenser fouling of a representative coal-fired power plant (550 MW) in the United States to range from $0.4 million/yr to $2.2 million/year (normalized to 2009 USD). This represents a loss of revenue between 0.34 % and 0.88 %. Coupled with the loss of production resulting from tube failures (caused by corrosion and erosion), it is clear that significant improvements need to be made in the steam surface condenser design and operation.

One solution is using a *materials system approach*, whereby a protective coating is incorporated into the design of the equipment, rather than implemented as a "band-aid" (Stringer, 1998). Although, Stringer (1998) considered coatings

[1] These objectives are equally applicable to tubular heat exchangers

predominately used in the boiler and turbine, equal importance must be allocated to the condenser as it forms an integral inter-dependent component in the power cycle.

PPFs have been found to be an effective countermeasure against corrosion and erosion (Fraze & Woodruff, 1997). They have therefore been used to extend the life of condenser tubes (Fraze & Woodruff, 1997) by preventing excessive tube failures (leaks) caused by accelerated corrosion (such as pitting) and/or erosion mechanisms. Now questions arise whether PPFs can be incorporated into the condenser system before failures occur, ultimately improving performance by: reducing fouling tendency, whilst eliminating corrosion and erosion, thereby extending availability, and ultimately yielding better average performance over time.

If this is the case, it needs to be established which PPF types should be used and most importantly when they should be applied. This research aims to address these questions in order to present industry with the necessary knowledge and decision making tools to optimize condenser performance.

1.7 Thesis outline

Chapter 1 introduces the role of the steam surface condenser in power plants. Requirements and operating conditions experienced by condenser tubes are then discussed to explain the need for PPFs. Next the power plant that is selected for this study is described together with its history using PPFs. Finally the objectives are stated with the motivation for this research project.

Chapter 2 surveys relevant literature pertaining to condenser tube material characteristics, previous testing of PPFs, as well as antifouling PPFs. Ways of measuring fouling resistance using various experimental apparatuses are then summarized. Lastly fouling and condenser modelling is discussed.

Chapter 3 describes the experimental investigation undertaken for the study of PPFs tested using water from the power plant described in chapter 1. The design features, operating principles, and equipment validation is covered in detail. Results from three fouling tests are presented: test A uses bare condenser tubes, test B uses non-biocidal PPF modified tubes, and test C uses biocidal PPF-modified tubes. The resulting fouling data is used in the succeeding chapter.

Chapter 4 compares the single tube test data (from the previous chapter) to the actual condenser measured data. Using the design data of the condenser, a performance factor is found in order to calculate the actual fouling factor of the condenser as a function of time. Once the results are positively compared, criteria for using PPFs in condensers are put forward.

Chapter 5 concludes the thesis by addressing the objectives with the corresponding conclusions found in the study. Recommendations are given to assist condenser operators, designers, and researchers.

Appendix A states formula for determining the thermophysical properties of water as a function of temperature.

Appendix B provides supplementary specifications and photographs of the test apparatus.

Appendix C gives the calibration and commissioning data as well as the annular convection coefficient regression coefficients.

Appendix D summarizes all the relevant raw and processed data measured during experimentation.

Appendix E contains sample calculations.

Appendix F shows the complete water analysis comparisons.

Chapter 2

Literature survey

2.1 Characteristics of condenser tube materials

The effects of corrosion and fouling on the performance of different condenser tube materials is assessed by Michels *et al.* (1979). They concluded that the water quality is the "single most important factor in governing condenser tube performance." Cooling water is treated to reduce the levels of pernicious ions, bacteria and solids suspended in the water. However, as the quality of cooling water sources decreases, and environmental legislation becomes more stringent, water treatment often cannot keep up – the cooling water still contains many impurities as it enters the condenser. These impurities foul, corrode, and erode the condenser tubes.

Fouling and corrosion products adhere to the tube wall thereby increasing the conductive thermal resistance between the wall and the cooling water. Moreover fouling decreases the cross-sectional flow area and increases the hydraulic pressure drop. As the fouling develops, the thermal and hydraulic performance of the tube deteriorates over time. To combat the temporal performance deterioration over time, condensers are generally over-designed with a cleanliness factor typically between 85 % and 95 % (Heat Exchange Institute, 2012). However, according to Pullen & Lherminier (2005) condensers operated without continuous condenser tube cleaning systems (CCTS) typically experience a performance degradation over one year such that the average cleanliness is only 70 % or less. This means that there can be a vast difference between the design condition and the actual average performance of condensers.

Putman (2001) groups condenser tube materials into three broad categories: copper-based alloys (admiralty brass, aluminium-brass, cupronickel etc.), stainless steels, and titanium. Copper-based alloys were some of the first condenser tube materials used, although stainless steels and titanium have been subsequently sought after for their improved corrosion and erosion resistance. These attributes come at a price, namely a lower thermal conductivity, decreased biological fouling resistance and in some instances (like titanium) vibration-related

issues.

Copper-based alloys are susceptible to crevice (under-deposit) corrosion, dealloying (either dezincification or denickelification), erosion-corrosion (Putman, 2001), and ammonia induced stress corrosion cracking (Putman, 2001; Michels *et al.*, 1979). According to Putman (2001) the corrosion resistance of copper-based alloys results from the formation of an inert cuprous oxide film. It is very important that this film is uniformly formed during initial start-up of a condenser (Michels *et al.*, 1979). However, as indicated by Michels *et al.* (1979) cooling water may be left stagnant for several months inside the condenser during plant commissioning. Contaminants may then prevent a uniform cuprous oxide layer from forming, which can lead to premature tube failure due to pitting corrosion (Michels *et al.*, 1979).

Conversely, Putman (2001) declares that cupric oxides form a thick porous layer which can impact the conductivity of copper-based alloys, and therefore should be cleaned once or twice per year. Although little published information exists, Maurer & Franson (1988) suggest that brass alloys form a corrosion product which can result in a minimum performance loss of 10 % when the tubes are stored after manufacture for an undisclosed period of time. Maurer & Franson (1988) make reference to university tests conducted by McAllister *et al.* (1961) at the Gulf States Utilities Company's Neches Power Station. Their apparatus used river water that passed through the plant condenser and test tubes were testing in several double-pipe heat exchangers. The annuli were arranged in series, although some heat exchangers were operated in a co-current fashion whilst others in a counter-current fashion without any stated consideration for the differences in heat fluxes. Heat was supplied by steam passing through copper spiraled tubes within the annuli and no mention is made of the entrance effects or three-dimensional heat effects of the copper spiral tubing. Chlorine was dosed twice daily to reduce biological growth. Although river water was used, during their test period of 120 days the water was contaminated by sea water where chloride levels peaked at 6 000 ppm. When comparing the results between copper alloys and stainless steel the authors suggest initially the fouling rates are the same, but as the chloride levels drastically changed the stainless steel proceeded to have a lower fouling rate than the copper alloys. This does not distinguish between the temporal effects of fouling and the change in composition (namely the dramatic chloride ion change). The authors admit that no account of pitting was made.

Maurer & Franson (1988) then use McAllister's data (McAllister *et al.*, 1961) to plot the relative fouling between copper alloys and stainless steel in figure 2.1. Maurer & Franson (1988) state that the stainless steel suffered from fouling only and suggest that an "exposure aging" results on the copper alloys where fouling and corrosion take place. However, McAllister *et al.* (1961) actually applied a PPF to one of two admiralty brass tubes and said there was no corrosion taking place beneath the film. In fact the brass and PPF-modified brass tubes behaved in exactly the same manner which contradicts the statement by Maurer & Franson (1988).

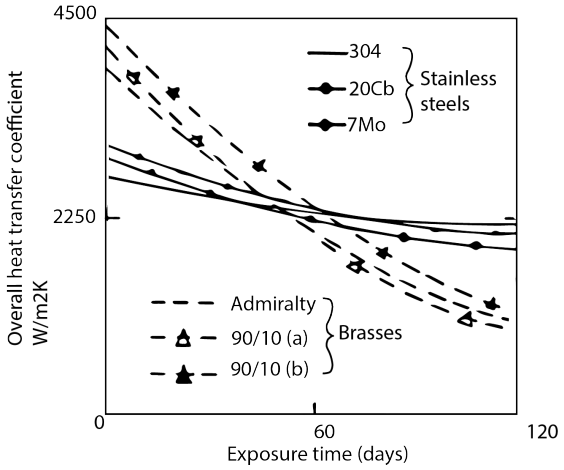

Figure 2.1: Overall heat transfer coefficient change with time for several condenser tube alloys (Maurer & Franson, 1988)

Shor (1988) indicated that the decrease in the thermal conductivity of their copper-nickel tubes after eight years of service caused a difference in overall heat transfer coefficient of only 6 %, but this was determined by comparing heat transfer of new tubes to existing tubes and it is not clear whether this decrease was a result of a cupric oxide layer.

According to Maurer & Franson (1988) stainless steels are susceptible to galvanic corrosion, hydrogen embrittlement, and crevice corrosion (between dissimilar metals). They are also vulnerable to pitting corrosion particularly as a result of high chloride levels. To improve their performance in sea water applications, various stainless steel alloys have been derived, such as Sea-cure®: a super ferritic stainless steel designed to have improved resistance to chlorides (Stiebler, 1988).

Titanium tubes have the highest corrosion resistance, which Putman (2001) accounts to the protective oxide layer that forms when titanium is in contact with moisture. Despite this, titanium still suffers from issues such as galvanic corrosion (especially when tube sheets are made from a dissimilar material), vibration damage and hydriding (Fulford *et al.*, 1987). Titanium is also not immune to biological fouling (attachment of living organisms to the surface) unlike copper-based alloys which tend to resist biological fouling (Michels *et al.*, 1979). In fact the biofouling rates for the materials discussed are ranked as follows (Characklis & Marshall, 1990):

copper-nickel (lowest)
brass
titanium ↓ Increasing biofouling
stainless steel (highest)

From this literature assay it is clear that when considering tube materials for steam surface condensers it is necessary to consider not only the corrosion of the

parent material, but also the interaction of fouling mechanisms which affect the combined thermal and mechanical performance of the tube over time.

2.2 Performance testing of PPFs in heat exchanger applications

Table 2.1 shows that some of the earliest testing of PPFs applied to steam surface condenser tubes is reported by McAllister *et al.* (1961) who tested a silicone dispersion in phenolic (77 µm thick) and a standard phenolic (127 −178 µm thick) baked on admiralty brass tubes. Although these PPFs were applied to individual test tubes, the application of baked paints is not practical for in-situ applications in condensers. Comparing the results between the bare tube and PPF-modified tubes, they concluded a very small increase in heat transfer for the thinner film and a slightly larger increase for the thicker one. The authors did not believe any corrosion took place under the coating, but no evidence was provided to indicate how this was checked.

Sato *et al.* (1985) found that the PPFs they tested had excellent corrosion resistance but did not prevent biological fouling. Powdered copper was later added as a filler to overcome this. With reference to the unfilled polyester and epoxy resins applied to copper alloy condenser tubes, the authors purport that generally the PPF thickness was designed such that the heat transfer resistance (overall coated heat transfer coefficient minus the uncoated overall heat transfer coefficient) offered by the PPF should not exceed 3×10^{-5} m$^2 \cdot$h°C/kcal (2.6×10^{-5} m^{2}K/W). To achieve this standard, the authors specify the PPF thicknesses of polyester and epoxy cannot exceed 22 µm and 7 µm respectively. The continuity of these films was not explicitly examined. However, according to Sato *et al.* (1985), laboratory tests proved that accelerated galvanic corrosion does not occur at points where the PPF is discontinuous. The authors do not specify how the PPF thickness should be measured nor do they attempt to quantify the uncertainty in measuring such thin films.

Sato *et al.* (1985) compared the relative performance between two compartments of the same condenser at the Sakai-Port Power Station, one of which was coated with an in-situ PPF. It is stated that application of the PPF resulted in an improved condenser vacuum of about 4 mm Hg between the two compartments. Mussalli (1989) attributes this to the reduction in corrosion and fouling, although Sato *et al.* (1985) does not characterize the cleanliness of the uncoated compartment at the start of the test. The heat transfer resistance of the PPF was found to be 3.2×10^{-5} m^{2}K/W (compared to the design fouling resistance of 2.6×10^{-5} m^{2}K/W) as shown in table 2.1. However, the PPF had blistered at both ends of the test tubes after 6 months, which may have been caused by cathodic protection. Despite this the authors suggest there was no indication of corrosion.

Table 2.1: Summary of the performance testing of PPFs in literature

Author	APL type	Filler	Nominal thickness μm	Tube	k_{PPF} W/(m K)	k_{eff} W/(m K)	R''_{PPF} m^2 K/W
McAllister *et al.* (1961)	Silicone dispersion in phenolic (naked)††	None	76.2	Admiralty brass		Not available	
	Phenolic (baked)††	None	127-178			Not available	
Sato *et al.* (1985)	Unknown	None	16-28	Aluminium brass	–	–	3.2×10^{-5}
Sato & Nagata (1985)	Epoxy	None	7 (max)	Admiralty brass	–	–	Design: 2.6×10^{-5}
	Polyester	None	22 (max)		–	–	
ESEERCO (1987), cited by Mussalli (1989)	Epoxy phenolic	–	Not available	Admiralty brass		Not available	
	Polyester	None	Not available			Not available	
Mussalli (1989) (originally Hager *et al.* (1988))	Epoxy phenolic	None	38-76	Cupronickel (o.d. 28.2 mm)	–	–	1.8×10^{-5}
	Epoxy phenolic	Metal	38-76		–	–	1.8×10^{-5}
	Polyester	None	50		–	–	3.5×10^{-5}
	Polyester	Copper (antifoulant)	50		–	–	3.5×10^{-5}
	Phenolic I (baked)††	None	152-203		–	–	42×10^{-5}
	Phenolic II (baked)††	None	102-152		–	–	42×10^{-5}
	Cu-Ni	None	1		–	–	1.8×10^{-5}
	Fluorinated urethane	None	Not available		–	–	28×10^{-5}
	Epoxy	None	Not available		–	–	77×10^{-5}
Horn & Woodruff (1996)	Epoxy	Aluminium oxide	50-100	Admiralty brass		Not available	
Fraze & Woodruff (1997)	Epoxy, siloxirane	None	Not available	90/10 Cu/Ni	–	–	17.6×10^{-5}
	Epoxy, modified siloxirane	None	Not available		–	–	8.5×10^{-5}
	Epoxy, modified phenolic	None	Not available		–	–	17.3×10^{-5}
	Epoxy, urethane primer	None	Not available		–	–	32.1×10^{-5}
	Epoxy	None	Not available		–	–	57.2×10^{-5}
	Silicone, urethane primer	None	Not available		–	–	40.5×10^{-5}
Gawlik *et al.* (1998)	ST-TMP‡, ZnP primer††	Silicon carbide	760	Carbon steel		Not available	
	PPS‡‡, ZnP primer††	Silicon carbide				Not available	
Sugama (2006)	PPS ‡‡	–	Not available	Carbon steel	0.40	–	–
	PPS‡‡	Carbon microfiber	Not available		1.03	–	–
Curran (2009)	Epoxy (100 % solids)	None	75	Brass† (o.d. 21 mm, i.d. 16.4 mm	–	2.737	–
	Epoxy phenolic	None	75		–	8.82	–
	Epoxy phenolic	Type unavailable	Not available		–	14.764	–
Kukulka & Leising (2010)	PTFE based	–	25.4	Compact plate heat exchanger	0.25		
	PPG E-coating	None	25.4		0.7	–	–
	Epoxy based	None	76.2-127		0.53	–	–
Goodenough (2013)	Epoxy (100 % solids)	None	50	Cartridge brass (o.d. 25.4 mm, i.d. 23 mm)	0.51 ± 0.03	11.3	9.82×10^{-5}
	Epoxy, modified (100 % solids)	Type unavailable	46		1.29 ± 0.11	27.2	3.57×10^{-5}
	Epoxy, modified (100 % solids)	Type unavailable	44, 130		2.27 ± 0.25	43.9, 19.3	1.98, 5.6 ($\times 10^{-5}$)

†type unavailable
††not suitable for in-situ application
‡styrene/methyl methacrylate
‡‡polyphenylenesulfide

Mussalli (1989) investigated nine PPFs as a strategy to extend the condenser life span by repairing existing tubes. The PPFs included epoxies, polyesters, phenolics as well as a fluorinated urethane. Heat transfer tests were performed on a test heat exchanger of a shell-and-tube type. Velocity measurements were recorded using a pitot tube in order to determine the flow rate through each tube. Tests were performed over a six month period and used actual cooling water so that the biological fouling tendencies of the coatings could be determined. However, the authors admit that variations in operating conditions meant that their results had to be corrected in terms of a mean overall heat transfer coefficient. The estimated coating resistances are given in table 2.1. Several of the coatings experienced failures, particularly delamination. The economic analysis considered by Mussalli (1989) (accuracy of ±20 %) proved to be very sensitive to site specific conditions (cooling water temperatures, type and level of fouling) and plant economic parameters (such as fuel costs).

Horn & Woodruff (1996) suggested PPFs as an alternative method to extend condenser life by protecting the tube from degradation, but also suggested PPFs could be used to enhance performance. The authors claim that tubes with PPFs are easier to clean than uncoated tubes. Experience of the Florida Power Corporation (Tsou & Woodruff, 1994) with PPFs indicate that uncoated tubes needed to be cleaned twice as often compared to coated tubes, because of barnacle growth fouling the tubes (Horn & Woodruff, 1996). At the time, Horn & Woodruff (1996) estimated the service life of the PPFs to be at least 5 years. However after 17 months of service at Florida Power Corporation's Bartow Unit 2 condenser, the 90-10 Cu-Ni tubes coated with an epoxy phenolic PPF had blisters on almost all of the ends of the tubes. Cathodic protection using impressed current, was assumed to have caused these blisters (Horn & Woodruff, 1996). Similar blistering of a PPF subjected to cathodic protection is reported by Horn & Mitchell (2002).

Fraze & Woodruff (1997) also reported the feasibility of using PPFs as an alternative to retubing. Phull (1991), commissioned by Fraze & Woodruff (1997), performed tests using a heated block on the outside of the condenser tubes (approximately 1 m in length). They compared the heat transfer resistance offered by the PPFs, but did not explicitly determine the conductivity of the PPFs. However, in this apparatus the upstream fluid temperature was measured using an external probe, which means that in fact a surface temperature, and not the bulk temperature, was recorded.

Fraze & Woodruff (1997) considered the following polymers to be viable options for PPF applications: metal modified siloxirane, modified epoxy, polyamine epoxy, and Teflon modified epoxy phenolic. They concluded that tubes that had a PPF applied remained cleaner longer than those that did not. Furthermore, since the PPF heat transfer resistance was comparable or smaller than typically fouled tubes, the authors decided that PPFs could "perform with no negative effect on unit heat rate" (Fraze & Woodruff, 1997). This supports the finding of ESEERCO (1987), cited by Mussalli (1989), who found that properly applied condenser PPFs did "not reduce heat transfer appreciably".

Polymeric resins (antioxidant (PDA)-modified ST-TMP and polyphenylene-sulfide) with and without silicone carbide fillers were evaluated in laboratory and field tests by Gawlik *et al.* (1998) in geothermal heat exchanger applications. These fillers were used to enhance the thermal conductivity of the PPFs by up to 92 % (Gawlik *et al.*, 1998), even though the actual values were not reported.

PPFs used in geothermal applications operate in the temperature range from 90 °C to 110 °C (Gawlik *et al.*, 1998) compared to PPFs used in steam surface condensers which operate at temperatures ranging from 40 °C to 60 °C. Furthermore, the PPFs were applied to carbon steel tubes using a fill and drain technique in the vertical position, before the tubes were installed in the heat exchanger. This differs from the PPFs studied by Fraze & Woodruff (1997) which were applied in-situ, where the tubes were horizontally orientated. Lastly the PPFs investigated by Gawlik *et al.* (1998) featured a zinc-phosphate primer which is unlike the PPFs used in steam surface condensers.

The laboratory tests conducted by Gawlik *et al.* (1998) were conducted on steel panels. Whereas their field evaluation of the PPFs were conducted on 6 m long tubes (25.4 mm outside diameter) with PPF thicknesses of the order of 760 µm (measured using x-ray photographs). These tubes were tested in double-pipe counter-flow heat exchangers.

Horn & Mitchell (2005) presented a method of applying a PPF (less than 25.4 µm by passing a volume of paint through the tube either using plug that is forced along the tube by compressed air, or by pulling it through the tube with a rod (or line). Their focus was to fill existing pits and thereby extend the condenser life span by eliminating accelerated degradation at these pits. The authors indicate the performance of the PPF (100 % solids epoxy) in terms of an overall cleanliness factor of 0.927 for 0.6 mil (15 µm) of coating and 0.692 for 1.6 mil (41 µm) of coating.

Sugama (2006) tested carbon steel heat exchanger tubes used in geothermal binary-cycle power plants with polyaryl thermoplastic PPFs such as polyphenlenesulfide (PPS), polyphenletheretherketone (PEEK), and polyphenyletherketone (PEK). These polymers are melt-crystallized, i.e. baked at high temperature (generally above 250 °C) which make them unsuitable for in-situ applications in steam surface condensers. Although, the inclusion of 5 % by weight of carbon microfibers increased the thermal conductivity of PPS from 0.4 W/(m K) to 1.03 W/(m K).

In contrast to the plugging technique used by Horn & Mitchell (2005), the spray technique used by Curran (2009) resulted in a film having a circumferential variation of up to 37.5 µm. Curran (2009) states that the PPF film needs to be less than 100 µm to "avoid impacting heat transfer". No mention of the required coating conductivity is given with this specified thickness. However, Curran (2009) cited tests performed by Honing & Kröger (2006) which show the effective coated-tube conductivity of these PPFs at an average thickness of 75 µm (table 2.1).

Kukulka & Leising (2010) studied surface coatings applied to plate heat exchangers exposed to untreated lake water. Three coatings were tested: a Teflon

based coating (0.25 W/(m K)), an electro-plated coating manufactured by PPG Industries (0.7 W/(m K)), and an epoxy based coating (0.53 W/(m K)). The coatings eliminated all corrosion, and delayed the effects of fouling (Kukulka & Leising, 2010).

Goodenough & Reuter (2014) measured the thermal conductivity of three different PPFs applied to cartridge brass tubing: an epoxy (unfilled), a modified epoxy (unfilled), and a modified epoxy with conductive filler. Their conductivities were found to be 0.51 W/(m K), 1.29 W/(m K), and 2.27 W/(m K) respectively. The heat transfer testing was performed on new tubing 3 m long, using a double-pipe counter-flow heat exchanger with heated water used to simulate condensing steam.

Considering the summarized data in table 2.1, it is clear that PPFs have not been considered for application on alloys such as titanium and stainless steel in steam surface condensers. Generally PPFs have only been considered as a life extension strategy in steam surface condensers applied to copper-based alloys. The fact that PPF failures are not reported in the most recent literature but have been reported in earlier sources (Sato *et al.*, 1985; Mussalli, 1989), suggests that PPF technology has improved in terms of application and corrosion resistance.

Thermal performance has been reported in terms of one or more of the following measures: the coating conductivity, the effective coated-tube conductivity and/or the coating factor. Extreme caution must be exercised when comparing results in terms of the effective coated-tube conductivity and coating factor because both these measures are dependent on the tube material, size, and coating thickness (Goodenough & Reuter, 2014).

The reported PPF performance measures are also given as fixed values, although no consideration is given to any variation with time. Fouling of PPFs used in steam surface condenser applications is not quantified adequately to enable parametric predictions to be made about their average performance with time.

2.3 Fouling mitigation

The manual for fouling in fresh water systems, IHS ESDU 2008, summarized by Pugh *et al.* (2009), organized the principle mitigation methods of fouling of fresh water systems into three groups: chemical treatment and cleaning, mechanical cleaning, and anti-fouling coatings. Cho *et al.* (2006) studied the effect of physical water treatment on fouling mitigation in cooling tower applications, particularly that of calcium carbonate precipitation fouling. Müller-Steinhagen *et al.* (2011) divide mechanical cleaning into projectiles, wire brushes, and scrapers. Müller-Steinhagen *et al.* (2011) attributes the lack of widespread use of anti-fouling coatings to their relatively poor thermal conductivity and adhesion.

In particular, Müller-Steinhagen *et al.* (2011) identified the lack of correlation between industrial anti-fouling strategies and academic results. The reason offered is that academic institutions and industry have traditionally tackled the

problem of fouling from different perspectives. As a result bi-annual fouling conferences have been organized over the last 17 years to allow for closer collaboration between industry and academia.

2.3.1 Anti-fouling PPFs

Yokouchi *et al.* (1996) performed comparative tests of different silicone-based anti-fouling coatings and an electro-conductive coating applied to panels in a model canal filled with seawater. The authors discovered significant performance differences between the different manufacturers of the silicone-based coatings. For example after six months of immersion, the onset of marine organisms attaching themselves to one of the coated panels, led Yokouchi *et al.* (1996) to conclude that the coating became ineffective at that time. After nine months the electro-conductive coatings de-laminated.

Electroless plating is a coating technique which deposits metallic ions from an aqueous solution onto the substrate through a chemical reduction reaction, which does not use electrical energy (Balaraju *et al.*, 2003). Due to its nonstick properties, polytetra fluorethylene (PTFE) composite coatings have been developed for heat exchangers to prevent fouling (Trueba *et al.*, 2006). However, these coatings are not readily applied in-situ and have therefore not been used as PPFs for steam surface condensers.

Al-Otaibi (2008) compared the scale deposition of calcium sulfate on coated carbon steel and titanium. The coating (Sakaphen coating Si 57E, applied by Sakaphen GmbH Company) had a thickness of 200 µm and a quoted thermal conductivity equal to 3 W/(m K). The coating caused a 60 % reduction in calcium scale deposition compared to the titanium (Al-Otaibi, 2008).

The deposition of nano films of copper-nickel on titanium to mitigate micro biofouling was investigated by Vishwakarma *et al.* (2009). These nano films were applied using the pulsed laser deposition technique on titanium coupons. Their study centered around using titanium as part of the steam generator in a 500 MW fast breeder reactor (nuclear) plant, where the tubes are filled with sodium and have water on their external surface. Therefore the nano-films are applied to the external surface and thence the pulsed laser deposition technique is feasible. For steam surface condensers the PPF is applied to the internal surface of the relatively small inner diameter tubes, and such techniques are not readily available. Despite this Vishwakarma *et al.* (2009) measured lower bacterial adhesion on the copper-nickel nanofilms compared to the unmodified titanium.

Wells & Sytsma (2009) reviewed coatings used to mitigate macro biological fouling, particularly that caused by freshwater mussels, of hydropower facilities in the Columbia River Basin. Silicone- and fluoro-polymer-based foul-release coatings were identified as good candidates for application at these facilities, including circulating water piping and condenser water boxes (Wells & Sytsma, 2009). However, Wells & Sytsma (2009) concluded that there were problems with all the commercially available coatings at that time.

In terms of biological fouling there has been much development in foul-release coatings, such as siloxane-polyurethane (Sommer *et al.*, 2010), particularly used in the marine industry. Instead of biocide coatings which release harmful biocides, these foul-release coatings provide a surface which makes it easy to remove settled organisms (Sommer *et al.*, 2010). No reports of the thermal performance of these coatings used in steam surface condenser applications are available.

It is concluded that anti-fouling coatings have shown potential to improve heat exchanger performance, by lessening the effects of fouling. Despite much research that has been performed, little to no work has been conducted specifically quantifying the fouling tendency of PPFs used in steam surface condensers. Since these PPFs also generally differ from the anti-fouling coatings cited in the aforementioned literature, there is insufficient knowledge of this topic.

2.4 Measuring the fouling resistance

2.4.1 Online testing methods of measuring condenser fouling

Online condenser fouling may either be measured indirectly or directly. Indirect methods calculate the cleanliness factor by using actual plant data and compare this value to the design cleanliness factor. However, caution must be exercised when using this method as the calculated cleanliness factor represents fouling as well as any other steam-side changes in the convection coefficient. Additionally, fluctuations in plant variables must be handled by suitable selection of data points as shown by Prieto *et al.* (2001).

The direct measurement of fouling on steam surface condensers is complicated by the presence of excess non-condensible gases which accumulate from air ingress (Putman & Harpster, 2002). Air ingress occurs from equipment leaks in the steam circuit and these non-condensible gases accumulate in the condenser, causing an increase in the thermal resistance to heat transfer. To separate these two effects Putman & Harpster (2002) proposed measuring the total increase in thermal resistance of the condenser from its design condition, and then subtracting either the resistance offered by the cooling water fouling or that caused by the presence of the non-condensible gases.

According to Putman & Harpster (2002) the cooling water fouling may be measured using two methods: either the method given by the ASME standard, *Steam surface condensers* (ASME, 2010) or Bridger Scientific Inc. (Garey, 1997). The first method measures the outlet temperatures of two adjacent tubes in the condenser, one of which is to be cleaned prior to the test and the other is left in the fouled condition. Due to the spacial proximity of the tubes the outer convection coefficients, as well as the mass flow rates and inlet temperatures, are assumed to be identical. The second method also uses two adjacent tubes in the condenser, although one tube is blocked on either end allowing a temperature probe to be inserted into the tube such that the steam saturation temperature

may be measured. A flow meter is installed upstream of the fouled tube, and the inlet and outlet water temperatures are measured.

2.4.2 Offline testing methods of measuring condenser fouling

Offline condenser fouling testing is either performed on test tubes removed from the condenser, or individual new tubes that are of the same material. Knudsen (1981) reviewed several apparatus types and techniques for measuring the fouling of heat transfer surfaces. Of these methods, the most apt to measuring the fouling of steam surface condenser tubes are: indirect electric heating, sensible heating from a fluid, and latent heating by a condensing vapor.

Indirect electrical heating can be achieved by winding resistance wire around the tube, or placing a thick-walled jacket over the tube with a resistance heater embedded in the jacket. The latter technique introduces an additional uncertainty of the contact resistance (Knudsen, 1981). Awad *et al.* (2007) used electric heaters in this way to study the effect of surface temperature on fouling rates. Specifically, the authors considered water flowing at 0.8 m/s having a suspended colloidal solution of solid particles (alluvium) with a concentration of 1 gm/L and a surface temperature in the range from 55 °C to 95 °C.

Izadi *et al.* (2011) also used the indirect electrical heating technique to measure the composite fouling of sea water on 90/10 Cu/Ni tubing. The sea water samples were filtered through 10 µm filter paper to remove suspended solids. Most of the biological spores were removed in this way according to the author. Moreover, the tests were performed at 76 °C which suggests that the composite fouling was a result of precipitation and corrosion fouling rather than biological fouling.

Sensible heating from a fluid uses an annular test section to test fouling on the inner or outer surface of test tubes (Knudsen, 1981). The test fluid can pass either through the annular region (fouling the outer surface of the tube) or inside the test tube (fouling the inside surface). The heating fluid then flows in a counter-current or co-current fashion, although Knudsen (1981) suggests that co-current flow can be advantageous to reduce variability in the surface temperature.

Using a tube-in-tube heat exchanger (double-pipe heat exchangers connected in a serpentine) as well as brazed-plate heat exchangers, Wu & Cremaschi (2013) investigated the effect of fouling in condensers for cooling tower applications. The potential for fouling of the water sample was measured in terms of the Langelier Saturation Index (LSI) (Langelier, 1936). According to Wu & Cremaschi (2013) this number is calculated as the difference between the actual pH of the water sample and the pH at which concentration of the calcium carbonate in that water sample would be in equilibrium with total alkalinity. Wu & Cremaschi (2013) found that during these fouling tests the entire water loop experienced fouling. Only about 4-5% of the total amount of fouling occurred within the test heat exchanger. This raises an important consideration in the design of fouling apparatuses.

The ASTM standard D4778-10 (2015) describes a test method to measure the fouling deposited (in terms of a mass measurement) on a test tube under heat transfer conditions. Cooling water passes over a heated section of the test tube (10 cm-20 cm) whilst keeping the flow rate and heat flux constant. A cartridge heater is inserted into the test tube (of 9.5 mm or 12.5 mm outside diameter) ensuring a snug fit. The cooling water passes through the annulus formed by fitting an acrylic tube (of 25 mm outside diameter) over the test tube. Thus, fouling occurs on the outside of the test tube. Since PPFs are applied to the internal surface of the tube, this apparatus is not directly applicable. Also the mass measurement of deposit is not directly relatable to calculating the fouling thermal resistance since the deposit porosity often varies.

Casanueva *et al.* (2003) designed and constructed a portable pilot plant to study the effects of different tube materials, diameters, and various chemical treatments on biological fouling caused by seawater. The schematic of their pilot plant is shown in figure 2.2. The shell and tube heat exchanger (3.1 m long) was constructed from PVC to prevent galvanic corrosion. The equipment was housed inside a standard 20 ft container to allow for in-situ testing using actual plant cooling water. The authors obtained a mean conductivity of the fouling film equal to 0.273 W/(m K) after 98 days of experimentation, but they conceded that since this was obtained under very specific conditions it was not possible to extrapolate to other fouling situations.

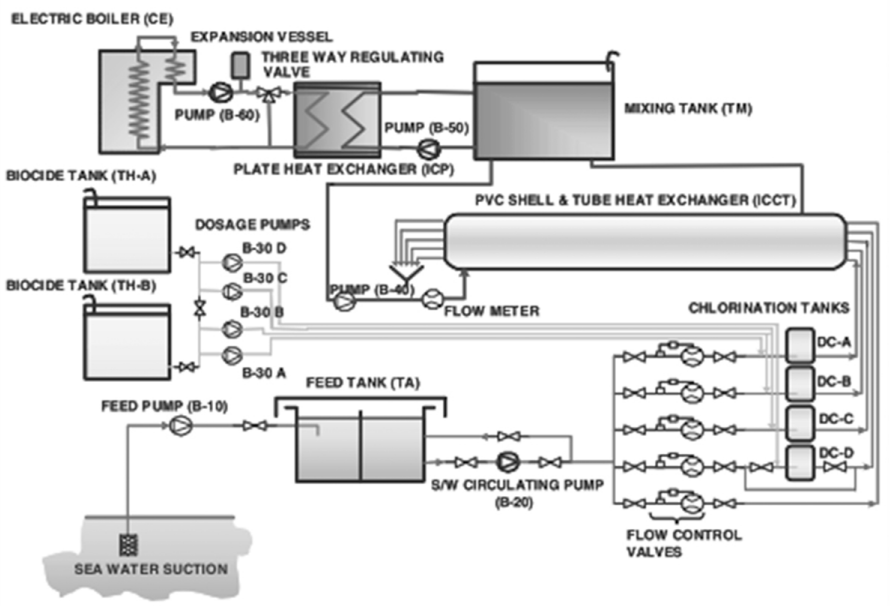

Figure 2.2: Schematic of pilot plant (source: Casanueva *et al.* (2003))

The apparatus described by Knudsen (1981) using a condensing vapor to heat a fouling fluid is formed by orientating a vertical test tube concentrically inside

a larger tube. However, according to Knudsen (1981) a major problem with condensing vapor is the variation in the condensing fluid convection heat transfer. Both surface weathering and the presence of non-condensible gases can change the condensation coefficient of heat transfer.

Another method, which is not included by Knudsen (1981), is radiant heating as proposed by Shinzato *et al.* (1990). The authors purport an accuracy of 1×10^{-5} m^2 K/W of the measured fouling factor using this method of heating.

2.4.3 Fouling modeling

Fouling modeling is an important facet of designing and operating heat exchangers. Müller-Steinhagen (2011) reviews fouling modeling from 1960 to 2011. The Kern-and-Seaton model (equation 1.1) was integrated with respect to time and resulted in the following:

$$R_f = R_f^{\infty}(1 - e^{-\text{constant} \times \text{time}}) \tag{2.1}$$

where R_f^{∞} is the asymptotic fouling resistance. This approach had several limitations, the most notable of which is that it included empirical parameters that could only be obtained from operational data and also did not include chemical reactions (Müller-Steinhagen, 2011). Despite these shortcomings, from 1960 to about 1980 the Kern-and-Seaton model (equation 1.1) and the Tubular Exchangers Manufacturers Association (TEMA) fouling resistances were fundamental in most of the fouling models and heat exchanger designs.

Thereafter the work of Epstein (1983) altered the modeling approach such that fouling is considered to be made up of five processes: initiation, transport to the surface, attachment, removal (transport from the surface), and ageing. Numerous models to correlate available data followed, except many correlations can only be applied to idealized fouling cases. Müller-Steinhagen (2011) suggests that this may be a result of the non-linear nature and unsteady properties of fouling in addition to the numerous variables and different processes.

Recent developments to model fouling include: neural networks, computational fluid dynamics (CFD) and molecular modeling. Fan & Zhong (2013) developed a novel model based on Fuzzy stage identification and Chebyshev neural network, which showed better prediction of experimental work performed on a steam surface condenser than an asymptotic fouling model. Nebot *et al.* (2007) modified the kinetic fouling model defined by Konak (1973), in order to investigate the effect of water velocity and tube material on fouling of steam surface condensers cooled by seawater. This evidence shows fouling models have been applied to steam surface condensers, but there are no reports of fouling models incorporating the effects of PPFs.

2.4.4 Condenser modeling

The inherent complexity associated with the condensation process within condensers makes the steam-side convection coefficient difficult to predict. Vapor shearing, condensate inundation and the presence of non-condensible gases are the most notorious processes affecting the condensing coefficient. Pioneering analysis in this field, performed by Silver (1963), put original ideas forward pertaining to the analysis of such effects, although the authors admit that (at that time) the ideas were yet unproven.

Individually these effects have been studied. For example, tube inundation effects were studied by Kern & Seaton (1959) in simple tube arrays. Rose (1980) developed approximate equations describing the convection coefficient in the presence of non-condensible gases. Recently Lakshmi *et al.* (2011) analyzed film condensation of pure vapors flowing normal to a horizontal condenser tube, whilst the tube experiences constant heat flux. All of these effects combined with spatial variations in the conditions within the condenser, such as non-uniform steam loading, means that the problem of condenser modeling often resorts to discretization of the condenser and ultimately computational fluid dynamic (CFD) techniques are used.

CFD models can either be two- or three-dimensional (Ramón & González, 2001; Prieto *et al.*, 2003; Tarrad & Majeed, 2010). Using a CFD model, Rhodes & Hardy (2005) were able to study the impact on performance of the Pilgrim Nuclear power station condenser, caused by changes in the following variables: a partially-filled waterbox, tube plugging, air-inleakage, and steam leakage from the moisture separator dump valve. Their CFD mesh consisted of 338 142 cells, although air extraction equipment was not explicitly modeled. Model verification indicated a maximum temperature difference of 4 °C between the measured and calculated temperature rise across the west shell of the condenser. The authors suggested that this temperature difference can be a result of a difference between the actual heat rejected by the condenser and that assumed as a boundary condition in the model.

CFD modeling is gaining popularity and has been shown to be a successful tool in condenser performance modeling. There does however appear to be no such models which account directly for PPFs. Additionally there is a lack of evidence suggesting that fouling models that change with time have been incorporated in previous CFD models.

2.5 Summary

Relevant characteristics of condenser tube materials are reviewed. To combat corrosion and erosion, PPFs have been used. The reported PPF performance measures are quoted as fixed values and no consideration is given to their variation with time. In terms of mitigating fouling, anti-fouling coatings in literature

have been shown to improve heat exchanger performance, by lessening the effects of fouling. However, the literature does not provide sufficient information regarding the water-side fouling of PPFs, thus warranting further research. The fouling resistance can be measured either online with the condenser, or offline where separate tubes are tested outside the condenser. Various methods in literature are considered for their suitability to test the fouling characteristics of PPFs. The chapter concludes by discussing fouling models as well as condenser modeling.

Chapter 3

Experimentation

3.1 Introduction

The waterside fouling of archetypal steam surface condenser tubes is experimentally investigated so that the temporal performance effects of incorporating paint-based protective films (PPFs) can be quantified. Several different alloy tubes, with and without PPFs, are thus subjected to the identical water that also passes through an actual steam surface condenser. A conventional coal-fired thermal power plant is selected for this investigation. The plant has an open-type recirculating cooling water system with four natural draft wet-cooled cooling towers which supply cooling water to six surface condensers. This means the condensers suffer from fresh-water fouling[2]. Owing to the size, variability in condensation processes, inaccessibility, and poorly instrumented properties of the actual plant condenser, an off-line apparatus is used instead. Actual plant cooling water is tapped from the plant's cooling water system at a point downstream of the condenser and just before the cooling water enters the wet-cooling tower (figure 3.1).

The significance of using actual cooling water in real time will become apparent later. The distance between the tap-off point and the condenser is approximately 50 m, but the temperature measured at the condenser outlet water box compares within 1 °C of that measured at the tap-off point. Water exiting the condenser is specifically chosen because it is the hottest point in the cooling system and therefore has the highest propensity for scaling. Even though scaling takes place within the condenser before this point, causing inversely soluble ions to precipitate out of solution, the cooling water exiting the condenser is still supersaturated with scalants. Furthermore this water is above 30 °C and is therefore in the range of highest biofilm development (chapter 1). The cooling tower pond was not considered as a good candidate location because of the striation that occurs vertically in the pond. Also the water entering the condenser is around 20 °C

[2]Coversely some power plant condensers use sea water in open-type cooling systems and in these instances chloride ion concentrations are about an order of magnitude greater.

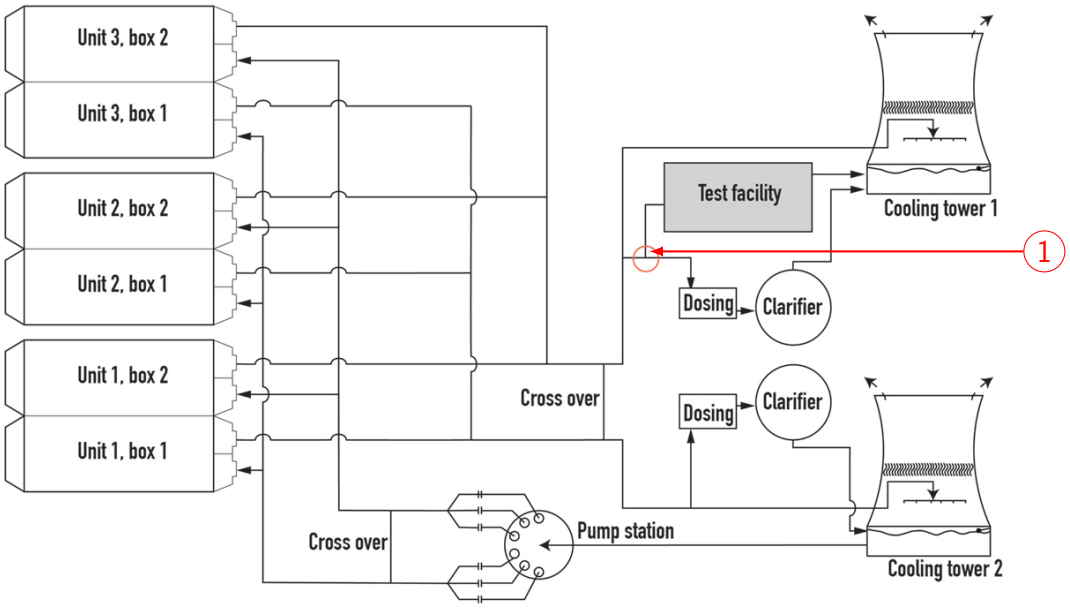

Figure 3.1: Apparatus installation in relation to the plant cooling water network – (1) tap-off point

and therefore not in the region of maximum biofouling potential as it is at the condenser outlet. Therefore this tap-off point was not considered suitable. The plant cooling water is referred to as the fouling fluid hereafter.

Knudsen (1981) explains how steam is the least desirable medium to heat the fouling surface in experimental apparatuses due to its inherent variability caused by surface weathering and non-condensible gases. Therefore sensible heating is used in this apparatus to simulate the condensing steam in the actual condenser – maintaining repeatable and known conditions such as heat flux and flow rate. Six identical double-pipe heat exchangers are formed by locating PVC tubes concentrically over each of the test tubes creating a water jacket around each tube. The double-pipe heat exchangers are then arranged in a parallel configuration. Heated potable water passes through the annular region of each heat exchanger which heats the outer surface of the test tube, whilst the actual cooling water passes through the inside of the test tube at the design flow rate for the condenser. The heat exchangers are operated in a co-current fashion such that the fouling fluid and heated potable water flow in the same direction. This configuration achieves a more uniform tube wall temperature compared to a counter-flow configuration.

Figure 3.2 depicts how the equivalent heat transfer conditions experienced by a tube inside a condenser are simulated by the heated water inside the test heat exchangers. Both the tube inside (a) the condenser and (b) the double-pipe heat exchanger have the fouling fluid passing through the inside of the tube, as

the foulant deposits at the fluid-solid interface. The velocity of the heated water is then controlled such that the sensible convective heat transfer coefficients are comparable to those for condensing steam.

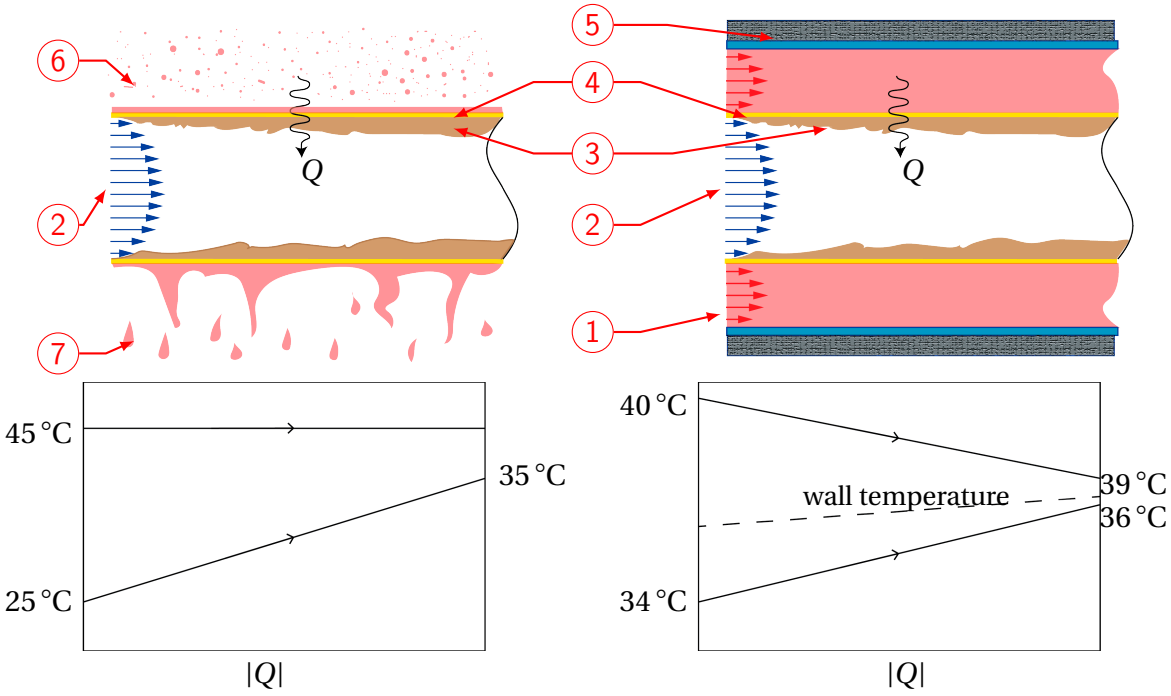

(a) condenser (b) double-pipe heat exchanger

Figure 3.2: Illustration comparing heat transfer conditions within the condenser and the double-pipe heat exchanger – (1) heated water flowing through annulus, (2) fouling fluid, (3) foulant, (4) tube wall, (5) insulation, (6) steam, (7) falling condensate

3.2 Apparatus description

3.2.1 Apparatus housing

An aluminum-clad mild steel space frame houses the apparatus as shown in figure 3.3. The structure is insulated using 40 mm polystyrene foam which is sandwiched between the aluminum cladding. Using a 5 kW air-conditioner, the air temperature within the housing is controlled around 28 °C. There is only one access door on the housing which is 1.2 m wide and allows installation and removal of the full-length test tubes (see appendix B). Figure 3.3 demonstrates the transportability of the entire apparatus, which is maneuvered and loaded onto the trailer using two purpose-built castor wheeled trolleys.

Figure 3.3: Photograph of the apparatus housing – (1) trailer, (2) piping connection point, (3) housing, (4) air-conditioner, (5) domed roof

3.2.2 Support structure

A stainless steel frame supports four polypropylene plates, that fix the heat exchangers jackets in the hexagonal arrangement shown in figure 3.4. These 20 mm thick support plates are stack drilled to aid manufacturing accuracy and are fitted with slotted brackets that allow three dimensional positioning during alignment so that the heat exchangers can be evenly supported along their length. The polypropylene is chosen for its good thermal insulation property thereby minimizing heat transfer with the heat exchangers.

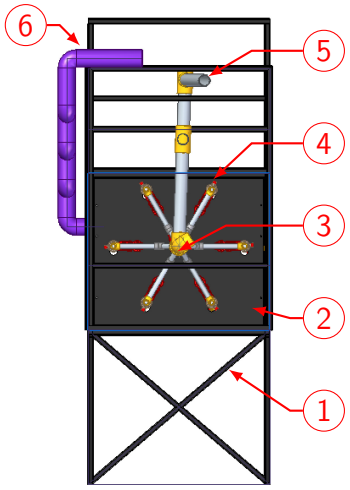

Figure 3.4: Simplified front view of the apparatus showing hexagonal arrangement of the heat exchangers – (1) stand, (2) support baffle, (3) distribution manifold, (4) heat exchanger, (5) return line, (6) inline heater

3.2.3 Double-pipe co-current flow heat exchanger

New condenser tubes are placed inside these heat exchangers that are made from class 12 PVC with a nominal diameter of 40 mm. The tubes are supported at their mid-length using the centralizing plates depicted in figure 3.5. These PVC plates are 1 mm thick and have four points that contact the tube, to minimize disruption of the flow. Once again PVC is chosen due to its good thermal insulation property (0.1 W/(m K) (Cengel & Ghajar, 2011)).

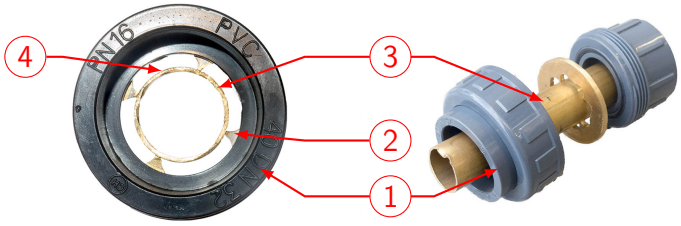

Figure 3.5: Photographs showing a centralizing disc inside the heat exchanger union at its midpoint – (1) PVC union, (2) stabilizing pin (1 of 4), (3) test tube, (4) annulus

Rubber (EPDM) o-rings seal the outer jacket onto the test tube and allow fixing and removal of the tubes without damaging them. Specially designed and manufactured glands are used as shown in the exploded view of figure 3.6.

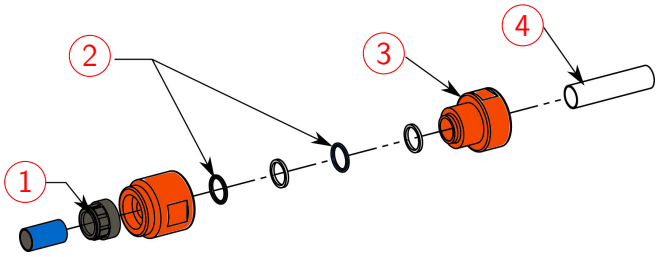

Figure 3.6: Exploded view of a tube gland – (1) PVC union, (2) o-rings, (3) gland compression nut, (4) test tube

3.2.4 Pump and piping material selection

The pump used to circulate the heated water (photographs provided in appendix B) is a chemical pump which means that all its wetted surfaces are made of polypropylene. This reduces the chance of corrosion products contaminating the heated water and hence the outside of the test tubes. Furthermore, PVC piping is selected because it is chemically inert and has a low thermal conductivity.

3.3 Measurement techniques

3.3.1 Measured variables

The apparatus simulates waterside fouling whilst controlling variables including flow rate, heat flux and differential pressure across the test tubes. The comparative testing between parallel test tubes quantifies their fouling tendency with and without linings. Using this technique, direct feedback is also obtained from the apparatus principally indicated by the outlet temperatures of the test tubes. The results are used to separate the waterside effects from the steam-side dynamics inside the condenser to better model the condenser performance and hence optimize its surface treatment strategy.

The heat transfer of each heat exchanger is calculated to quantify the performance effects of fouling occurring on each test tube. The inlet and outlet temperatures of both the fouling fluid and heated water as well as their flow rates need to be measured. Furthermore the surface roughness of the inner surface of the tube, which has a significant influence on the heat transfer, needs to be determined as it changes with fouling. Since the surface roughness cannot be measured directly whilst the tube is being tested, the static pressure drop is measured using static pressure tappings. In comparison the outer surfaces of the tubes are assumed to be smooth and do not change with time because no fouling takes place as the heated water has negligible foulants present. This assumption is verified after testing has concluded by visually inspecting the outer surface of each tube.

The piping and instrumentation diagram in figure 3.7 shows the six heat exchangers arranged in parallel, and the legend is given in table 3.1.

Table 3.1: PID legend

	Isolating valve		Diaphragm control valve
	Solenoid valve		Regulating valve
	Three way valve		Pump
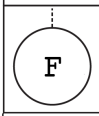	Local flow rate	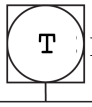	Remote temperature
	Pressure drop		Air vent

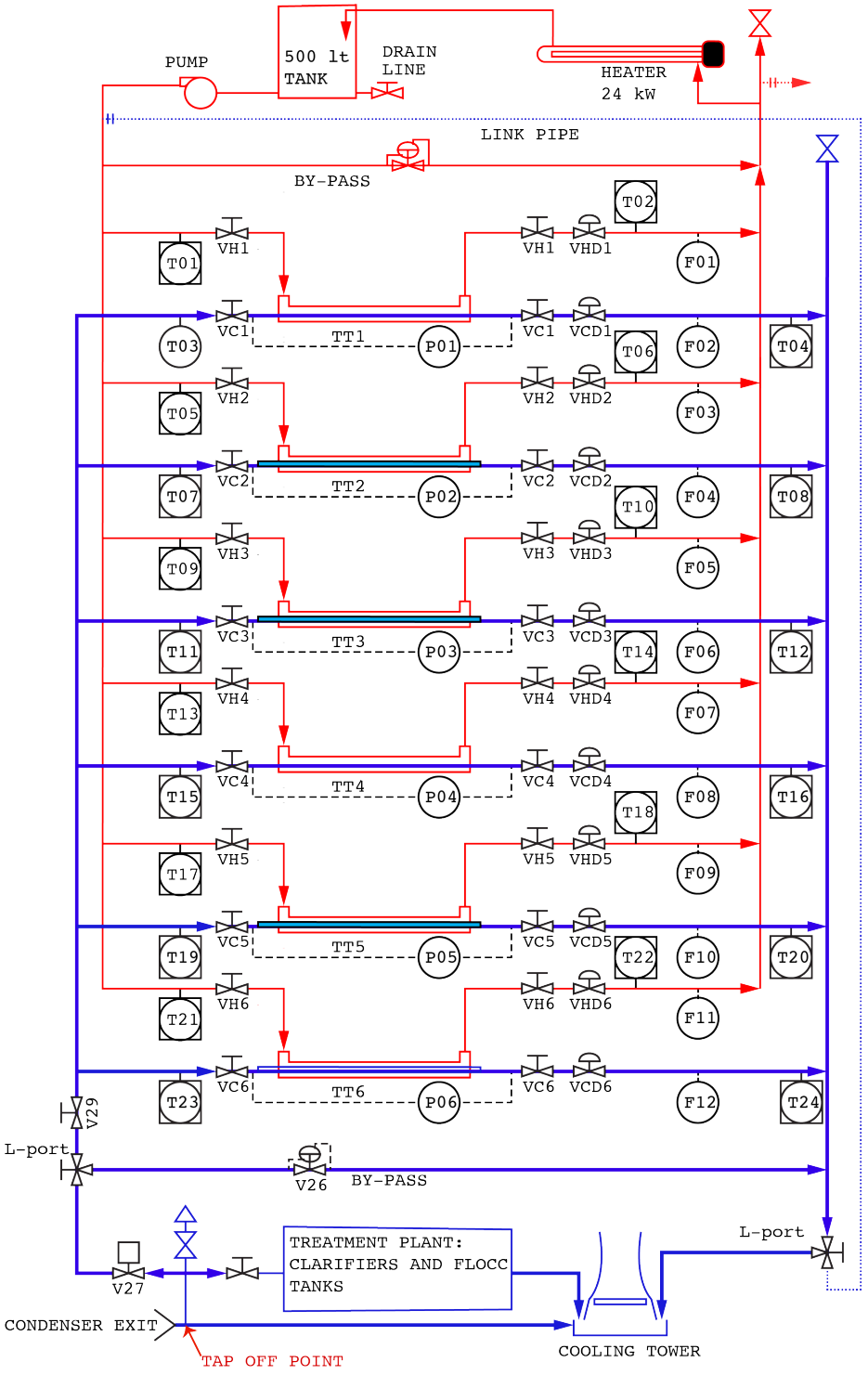

Figure 3.7: Piping and instrumentation diagram showing variable measurement locations and set-point flow rates

In figure 3.7 temperature measurement points are denoted T. The flow rate measurement points are denoted F. The static pressure measurements are denoted p and dashed lines indicate the piping from the manometers to the tapping saddles. Note that the fouling water is distinguished with a thicker line style on the diagram and valves are distinguished where C refers to the fouling fluid and H refers to the annular fluid.

3.3.2 Flow distribution

Purpose-built manifolds distribute the flow equally to the heat exchangers. The pipe lengths between the manifolds and test tubes are identical because of the symmetric arrangement as shown in figure 3.8. Further this distribution point creates significant mixing of the water streams. After splitting the flow into six branches, an entrance length of 25 diameters is provided upstream before the foulant enters each heat exchanger. The flow is thus conditioned to become fully developed before entering the heat exchangers.

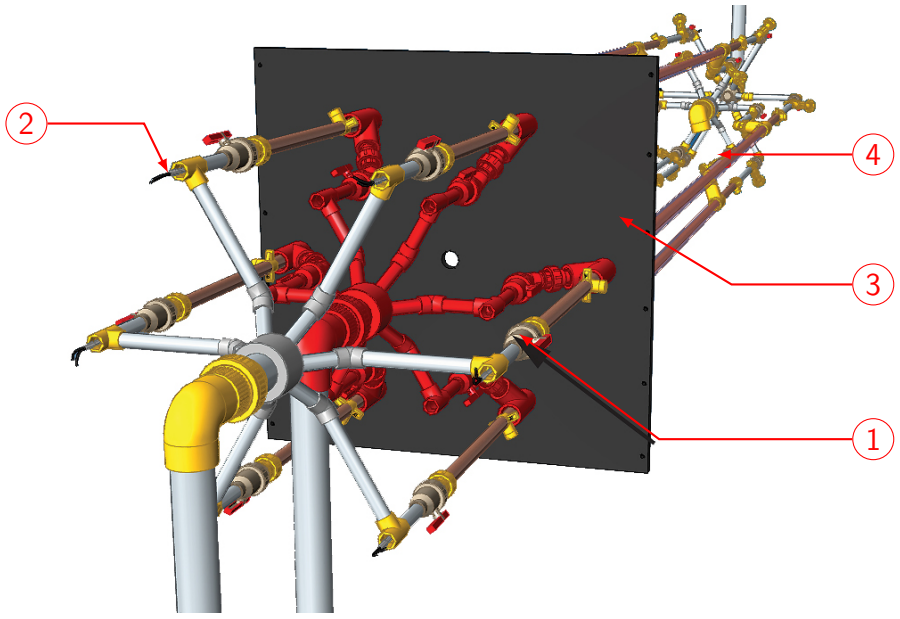

Figure 3.8: Perspective view of distribution manifolds – (1) isolating valve, (2) temperature probe, (3) support baffle (1 of 4), (4) co-current flow heat exchanger

Flow rates are measured through individual tubes using a common ultrasonic flow meter at regular time intervals. The flow meter is fitted at the outlets of the heat exchangers such that it has 25 upstream diameters and 5 downstream diameters without flow disturbances. The foulant water flow rates are checked using an electromagnetic flow meter. This flow meter also continuously logs the total flow rate through all six test tubes and allows the total flow to be trended.

3.3.3 Temperature measurement

Bulk temperatures are measured at the inlet and outlet to each heat exchanger. Class AA PT1000 stainless steel sheathed resistance temperature detector (RTD) probes are inserted at ninety degree junctions in the direction of the flow. The high resistance of these probes provide the necessary resolution for measuring temperature differences across the heat exchangers within 0.1 °C. The 6.14 mm diameter probe is inserted to a depth of 100 mm and the sensor size is 20 mm ensuring effective mixing as well as representative bulk temperature measurements.

A total of 24 insertion probes measure the inlet and outlet temperatures of each of the heat exchangers. Since the probes are inserted about 300 mm upstream and downstream of the heat exchanger, closed-cell polyurethane insulation is fitted over the piping installed between the probes and the heat exchanger. This ensures the point at which the temperatures are measured are representative of the actual bulk temperatures at the heat exchanger interfaces. Further at the exit of the test tubes, a control valve creates the necessary mixing to allow the downstream probe to measure a representative bulk temperature of the water exiting the tubes. The RTDs are connected to the datalogger using a four-wire connection (the most accurate method for these sensors) and their excitation is limited to approximately 200 µA to limit self-heating effects of the sensors.

Three point calibration is conducted on four probes at: 10 °C, 30 °C, and 50 °C. Each one of these probes is located at the inlet and outlets of heat exchanger number 1. The remaining probes are calibrated at 30 °C only, but are compared to the probes from heat exchanger one during the isothermal test. Independent calibration tests traceable to the South African National Accreditation System (SANAS) show that the probes are accurate to within 0.1 °C (see appendix C). Moreover installation accuracy is verified from results during the isothermal test as indicated in table 3.2. The high electrical resistance of these sensors is purposefully chosen so that they achieve a resolution of three decimal places, which is very important because the temperature differences between inlet and outlet readings are used in subsequent calculations. And likewise for the annuli the isothermal test results are given in table 3.3.

Table 3.2: Measured temperatures during isothermal testing of the test tubes

		Heat exchanger					
Temperature		1	2	3	4	5	6
Tube inlet	°C	20.933	20.967	21.013	20.991	20.947	20.929
Tube outlet	°C	20.940	21.012	20.934	20.904	20.983	20.962
Difference	°C	-0.01	-0.04	0.08	0.09	-0.04	-0.03

Table 3.3: Measured temperatures during isothermal testing of the annuli

		Heat exchanger					
Temperature		1	2	3	4	5	6
Annulus inlet	°C	26.014	25.936	26.049	26.000	26.031	26.048
Annulus outlet	°C	26.021	26.004	26.065	26.054	26.052	26.119
Difference	°C	-0.01	-0.07	-0.02	-0.05	-0.02	-0.07

3.3.4 Static pressure drop measurement

The static pressure drop is measured along the internal (fouled) surface of the test tubes using inverted u-tube type manometers that are connected to a common manifold. The pressure tappings are drilled through the test tube just before and after the outer jacket of the heat exchanger. Pipe saddles are fitted over the test tubes to form a static annular chamber as photographed in figure 3.9.

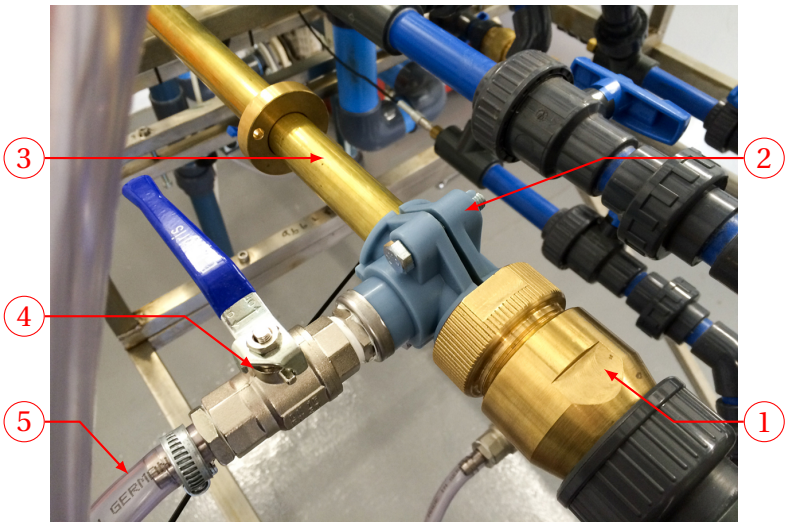

Figure 3.9: Photograph showing a static pressure tapping – (1) tube gland (2) pressure saddle, (3) test tube, (4) valve, (5) tubing

Clear PVC tubing is used between the tapping saddles and the inverted manometers, allowing visual verification that no air bubbles are present. 10 mm diameter manometer tubing is found to be large enough to ensure sufficient damping when measuring the height differences. Each tapping hole must be free of swarf and have no burrs protruding inside tube in order to truly measure the static pressure. To achieve this, each tapping hole is drilled sequentially using 0.8 mm, 1.0 mm and then 1.2 mm drill bits. Thereafter needle reamers are used to ream the holes to a final diameter of 1.6 mm. Backwashing is performed before each

test to unclog the static tapping holes in the event that they become obstructed with fouling matter.

3.3.5 Flow metering

Before beginning the experiment, the flow rate measurements taken using the ultrasonic meter are verified by comparing them to the electromagnetic flow meter (accuracy 0.5 %). The piping is configured in a so-called calibration loop whereby clean water circulates through the inside of each test tube and then through the annulus forming a common stream. The results indicate that the differences are within the experimental uncertainty (see appendix C for further details).

3.4 Operation and control

3.4.1 Tube preparation and installation

After receiving the test tubes, the protective plastic is removed before the outer surface is polished. Polishing removes any oxide layer on the outer surface of the tubes, whereas the inside of the tubes are relatively clean as a result of their transport plugs. Each test tube is then rigorously cleaned using acetone, and they are carefully installed into each heat exchanger whilst preventing any contamination from handling. The centralizing discs installed in the center of the heat exchangers (figure 3.5) are centered and held in place by a threaded union. Thereafter the o-rings are installed in the tube glands and they are tightened by hand to prevent over-tightening.

3.4.2 Heat transfer tests

Heat transfer tests are performed regularly while the fouling test is underway. This entails recording flow rates and temperatures over an approximate 90 min period. Usually this is performed early in the morning (08:00 AM) during which the fouling water temperature has negligible fluctuation and is deemed to be at steady state (expanded upon later). Owing to the design of the apparatus and non-intrusive ultrasonic flow meter, these tests do not interfere in any way with the fouling conditions within the test tubes and hence they undergo similar conditions compared to the actual tubes in the condenser.

3.4.3 Water quality sampling and analysis

Water samples are collected at a 20 mm tap-off valve, installed immediately after the y-strainers, before the fouling fluid enters the apparatus. This valve is fully opened and allowed to run for two minutes before filling a 500 mL polyethylene

sample bottle. The sample bottles are completely filled to minimize any interaction with air inside the container, and they are delivered to the analysis laboratory within two hours of sampling.

Table 3.4 shows the pertinent results from analyzing water at two different points: the first sample point is at the top of the clarifier and the second is at the tap-off valve upstream of the apparatus (refer to figure 3.1). Water from the top of the clarifier is collected using a collection bottle fixed to a pole and this method is used by the station personnel to sample and monitor the cooling water quality. As indicated in table 3.4 the results from the two different sample points are comparable, despite being on different days and this suggests that the tap-off point of the apparatus has been suitably designed to use water representative of the actual cooling water within the condenser. The full results from the analysis are included in appendix F.

Table 3.4: Water analysis comparison

		Sample point			
Descriptor	Limits	Clarifier	Apparatus		
Sample date		2015/12/24	2016/1/27	2016/4/2	2016/8/5
pH 25 °C	8.1-8.6	8.85	8.64	8.59	8.88
Total dissolved solids mg/l			2040	1511	1638
Chloride (Cl) mg/l	400	174	268	172	173
Sulphate (SO_4) mg/l	1000	688	946	727	695
Turbidity (NTU)	100	81.3	32.2	32.9	274
Total hardness mg $CaCO|_3$/l			752	538	636
Suspended solids mg/l			60	43	374
LSI	0		0.92	0.65	1.17
RSI	6.5-7		6.79	7.29	6.55

Further scrutiny of table 3.4 reveals chloride and sulphate ion concentration levels less than the station limits. Therefore it is expected that corrosion levels are within acceptable levels. However the total hardness is very high, and there is a high potential for scaling. This is supported by the Langelier Saturation Index (LSI) and the Ryznar Stability Index (RSI) that describe the following ranges of scaling potential:

- LSI > 0: water is super saturated and tends to precipitate calcium carbonate.
- LSI = 0: water is in equilibrium and saturated with calcium carbonate. No scaling is likely to occur.

- LSI < 0: water is below the saturation level and therefore tends to dissolve solid calcium carbonate.
- RSI < 6 supersaturated and water tends to form calcium carbonate scale.
- 6 < RSI < 7 water is considered to be approximately at saturation equilibrium with calcium carbonate.
- RSI > 7 water is below the saturation level and therefore tends to dissolve solid calcium carbonate, although corrosion of mild steel becomes a problem.

The turbidity (a measure of the cloudiness of the water) in table 3.4 varies between 23 and 274 (which is greater than the station limit of 100). This variance is caused by an increase in the concentration of suspended solids and is indicative of a fluctuation in the makeup water or operational change of the clarifiers. In any event such variations are common to all the tubes because of the design of the apparatus and in this way fluctuations in water chemistry are common for all the tubes and can be identified as such when comparing tubes relative to their control tube. Moreover the water quality is so poor that the influence of minor fluctuations in the water quality do not detract from the fouling data, since the dominant fouling mechanism is clearly identified when comparing relative data. In fact the fluctuations are sufficiently small that the change in fouling factor is contained within the experimental uncertainty estimates.

3.4.4 Periodic maintenance

Fortnightly maintenance activities include cleaning the strainers, checking the heated water tank level, and backwashing the static pressure tappings. Macro debris is removed from the y-strainers, by isolating the strainers sequentially so as to not interrupt flow to the apparatus. Potable water is used to top up the level of the hot tank, and is used to backwash the static pressure tappings to remove any blocked debris.

3.4.5 Tube removal, drying and sectioning

Tubes are removed by simply loosening the locking nut of the tube glands that secures the o-rings in place. In this way the foulant layer is not altered during tube removal. Under sterile conditions the tubes are sectioned immediately and the foulant layer is scraped and swabbed for bacterial analysis. The sectioned tubes are then stored at room temperature for 48 hours on a slight incline to completely dry them. Finally they are transported to a laboratory for QEMSCAN® analysis; this scanning electron microscope analyzes the mineralogical composition of the deposits.

3.5 Analysis

3.5.1 Heat exchanger analysis of the double-pipe co-current flow heat exchanger

The following assumptions are made concerning the analysis of the heat exchanger:

- Steady state conditions are assumed to exist only during the 90 minute period when flow rates are sampled on discrete days during the fouling tests. Over this period temperatures are sampled every 20 seconds and averaged every three minutes. The bulk inlet water temperature trends during each 90 minute sample period is observed to be less than about 0.1 °C/h. This is less than the measurement uncertainty of the temperature probes and thus the steady state assumption is reasonable.
- The fluids are assumed to be incompressible which means constant specific heat approximations are used.
- Thermophysical fluid properties are evaluated using pure water data for both the foulant and heated water, despite the presence of other species in the foulant. The error from this is considered small as the foulant is fresh water and also any small error introduced from this assumption is contained in the regression uncertainty of the annular fluid (the annular Nusselt number is experimentally determined using the same water as discussed later).

Asserting these assumptions, the log mean temperature difference (LMTD) method (Incropera *et al.*, 2007; Cengel & Ghajar, 2011) is applicable to each of the six heat exchangers (figure 3.10). For co-current (parallel) flow it can be shown that the total rate of heat transfer between the two fluids is

$$Q = UA\Delta T_{\mathrm{LM}} \tag{3.1}$$

where U is overall heat transfer coefficient, and A is the surface area contacted by the heated water in the annulus[3] and ΔT_{LM} is the LTMD equal to

$$\Delta T_{\mathrm{LM}} = \frac{T_{\mathrm{in,ann}} - T_{\mathrm{in}} - T_{\mathrm{out,ann}} + T_{\mathrm{out}}}{\ln \frac{T_{\mathrm{in,ann}} - T_{\mathrm{in}}}{T_{\mathrm{out,ann}} - T_{\mathrm{out}}}} \tag{3.2}$$

The overall heat transfer coefficient is equal to the reciprocal of the total thermal resistance between the foulant and the heated water in the annulus (Incropera *et al.*, 2007)

$$(UA)^{-1} = R_t \tag{3.3}$$

[3] U is thus defined in terms of the outer surface of the tube since the outer diameter of the test tube does not change during the test because no fouling takes place in the annulus.

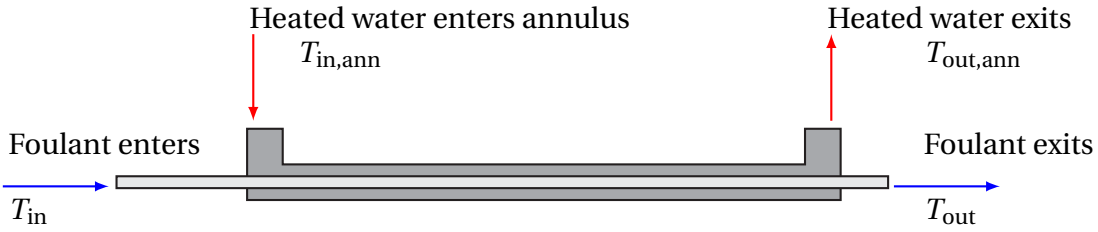

Figure 3.10: Schematic of a heat exchanger (not to scale)

The total thermal resistance is equal to the sum of the individual resistances

$$R_t = \frac{1}{h_{ann} A_{ann}} + \frac{\ln(d_3/d_2)}{2\pi k_t L} + \frac{\ln(d_2/d_1)}{2\pi k_{PPF} L} + \frac{R_f}{A} + \frac{1}{hA} \tag{3.4}$$

where k_{PPF} is the PPF conductivity and R_f is the fouling factor based on the unfouled diameter. The convection coefficients h and h_{ann} describe the convection on the inside and outside of the tube surfaces respectively. In fact they depend on the friction factor which has to determined first.

3.5.2 The analogy between friction factor and convection Nusselt number

The Darcy friction factor f_d, referred hereafter as friction factor, is a dimensionless parameter relating the pressure drop along internal flows to the average velocity according to (Cengel & Ghajar, 2011)

$$\Delta p = f_d \frac{L_{\Delta p}}{d} \frac{\rho v^2}{2} \tag{3.5}$$

Fundamentally the friction factor relates to the skin friction coefficient of the tube, and it is important to describe the pressure drop and hence the pumping power required for the heat exchanger. Further, the friction factor characterizes the surface which determines the turbulent boundary layer. From experiments with smooth tubes, Konakov, cited by Gnielinski (2009), found the fully-turbulent friction factor to be

$$f_d = \left[1.8 \log_{10}(\mathrm{Re}) - 1.5\right]^{-2} \tag{3.6}$$

Importantly the surface roughness tends to increase as the tube surface accumulates foulant (in addition to the obvious reduction in cross-sectional area). To account for this, the pressure drop is physically measured (see section 3.3.4) in order to determine the friction factor (using equation (3.5)).

The change in friction factor also plays a role in the convective heat transfer. Since the friction factor influences the turbulent boundary layer, and this dictates the convective heat transfer, there exists an analogy between the friction factor and the convective heat transfer known as the *Chilton-Colburn* analogy (Cengel & Ghajar, 2011)

$$\mathrm{Nu} = 0.125 f_d \mathrm{RePr}^{\frac{1}{3}} \tag{3.7}$$

where Nu is the dimensionless Nusselt number, i.e the ratio of convective to conductive heat transfer across the tube surface, viz.

$$\mathrm{Nu} = \frac{hd}{k_f} \tag{3.8}$$

The accuracy of equation (3.7) is generally improved through experimental data incorporated in various convection correlations.

3.5.3 Literature correlation to calculate the inner convection coefficient

For fully-developed convective heat transfer across the smooth tube surface, Dittus and Boelter, cited by Kröger (1998), found the Nusselt number to be a function of Reynolds number and Prandtl number according to

$$\mathrm{Nu} = 0.0265\mathrm{Re}^{\frac{4}{5}}\mathrm{Pr}^{0.3} \tag{3.9}$$

when the fluid is being cooled by the tube surface. When the fluid is heated by the surface they propose

$$\mathrm{Nu} = 0.0243\mathrm{Re}^{\frac{4}{5}}\mathrm{Pr}^{0.4} \tag{3.10}$$

Compare this to the correlation found by Rabas & Cane (1983) (used by the ASME performance test code PTC12.2-2010):

$$\mathrm{Nu} = 0.0158\mathrm{Re}^{0.835}\mathrm{Pr}^{0.462} \tag{3.11}$$

More recently, Gnielinski (2009) expanded on the work of Petukhov & Krillov (1958) to find

$$\mathrm{Nu} = \frac{\left(\frac{f_d}{8}\right)\mathrm{RePr}}{1 + 12.7\left(\frac{f_d}{8}\right)^{\frac{1}{2}}\left(\mathrm{Pr}^{\frac{2}{3}} - 1\right)} \tag{3.12}$$

valid for $2300 < \mathrm{Re} < 10^6$, $0.5 < \mathrm{Pr} < 10^4$, and $0 < d_1/L < 1$. Taking into account the entrance length of test tube provided in the design of the heat exchanger, the

internal flow is fully developed by the time it enters the heat exchanger. Therefore equation (3.12) is applicable and the inner convection coefficient is

$$h = \frac{\mathrm{Nu}k}{d_1} \tag{3.13}$$

with the fouling fluid thermal conductivity (k) evaluated at the mean bulk temperature, i.e.

$$T_m = \frac{1}{2}\left(T_{\mathrm{in}} + T_{\mathrm{out}}\right) \tag{3.14}$$

The effect of surface roughening is considered as the foulant alters the surface profile of the internal surface of the tube. The roughness Reynolds number (Lienhard & Lienhard, 2008) is

$$\mathrm{Re}_\epsilon = \mathrm{Re}\frac{\epsilon}{d_1}\left(\frac{f_d}{8}\right)^{\frac{1}{2}} \tag{3.15}$$

where $\frac{\epsilon}{d_1}$ is the relative surface roughness. Although this cannot be measured directly during the test, the relative surface roughness is estimated from the measured friction factor, i.e. rewriting the correlation for the friction factor given by Kröger (1998), yields

$$\frac{\epsilon}{d_1} = e^{((1.14-f_d{}^{-0.5})/0.86)} \tag{3.16}$$

Provided the roughness Reynolds number is less than 5, equation (3.12) is used with the measured friction factor (Lienhard & Lienhard, 2008). If the roughness Reynolds number is between 5 and 70 the flow is transitionally rough and equation (3.12) is still used with the measured friction factor to estimate the Nusselt number, albeit with less accuracy. When the roughness Reynolds number is above 70 the flow is termed fully rough and Bhatti & Shah (1987), cited by Lienhard & Lienhard (2008), recommends the following correlation

$$\mathrm{Nu} = \frac{\left(\frac{f_d}{8}\right)\mathrm{RePr}}{1+\left(\frac{f_d}{8}\right)^{\frac{1}{2}}\left(4.5\mathrm{Re}_\epsilon{}^{0.2}\mathrm{Pr}^{0.5}-8.48\right)} \tag{3.17}$$

3.5.4 The annular convection coefficient

The annular convection analysis follows analogously to the inner tube, although slight differences arise from the velocity profile inside the annulus. The annular Reynolds number is based on the hydraulic diameter

$$\mathrm{Re}_{\mathrm{ann}} = \frac{\rho_{\mathrm{ann}}\, v_{\mathrm{ann}}\,(d_4 - d_3)}{\mu_{\mathrm{ann}}} \tag{3.18}$$

Recently Dirker & Meyer (2005) showed the annular friction factor depends on the diameter ratio of the annulus. Gnielinski (2009) uses this in an effective Reynolds number for the annulus so that

$$f_{d,\text{ann}} = \left(1.8\log_{10}\text{Re}^*\right)^{-2} \tag{3.19}$$

where

$$\text{Re}^* = \text{Re}_{\text{ann}} \frac{\left(1+\left(\frac{d_4}{d_3}\right)^2\right)\ln\left(\frac{d_4}{d_3}\right)+\left(1-\left(\frac{d_4}{d_3}\right)^2\right)}{\left(1-\left(\frac{d_4}{d_3}\right)^2\right)\ln\left(\frac{d_4}{d_3}\right)} \tag{3.20}$$

Using this annular friction factor, Gnielinski (2009) found the following correlation with the annulus jacket insulated:

$$\text{Nu}_{\text{ann}} = \frac{\left(\frac{f_{d,\text{ann}}}{8}\right)\text{Re}_{\text{ann}}\text{Pr}_{\text{ann}}}{k_1 + 12.7\left(\frac{f_{d,\text{ann}}}{8}\right)^{0.5}\left(\text{Pr}_{\text{ann}}{}^{\frac{2}{3}}-1\right)}\left[1+\left(\frac{d_h}{L}\right)^{2/3}\right]0.75\left(\frac{d_4}{d_3}\right)^{-0.17} \tag{3.21}$$

with

$$k_1 = 1.07 + \frac{900}{\text{Re}_{\text{ann}}} - \frac{0.63}{(1+10\text{Pr}_{\text{ann}})} \tag{3.22}$$

Equation (3.21) is the most comprehensive literature correlation describing the Nusselt number for fully developed annular convective flow. However, the heat exchangers in the apparatus have edge effects induced by the transition from circular to annular areas. Thence it is necessary to physically measure the actual annular Nusselt number for various Reynolds numbers before commencing the fouling testing. Using the results from bare tube tests allows the outer convection coefficient to be determined, and the Nusselt number is regressed in terms of the Reynolds number in the form:

$$\text{Nu}_{\text{ann}} = A_{\text{Nu}}\text{Re}_{\text{ann}}{}^{B_{\text{Nu}}}\text{Pr}_{\text{ann}}{}^{0.3} \tag{3.23}$$

where A_{Nu} and B_{Nu} are the experimentally determined coefficients.

3.6 Performance measures: the fouling factor and cleanliness factor

3.6.1 Total thermal resistance method

The fouling factor, R_f, is found by solving equation (3.4), once the other thermal resistance terms are evaluated. The convection coefficients for the inner and

annular surfaces of the tube are calculated using equations (3.12) and (3.23) respectively.

$$R_f = A\left[\frac{\Delta T_{\text{LM}}}{Q} - \frac{1}{h_{\text{ann}} A_{\text{ann}}} - \frac{\ln(d_3/d_2)}{2\pi k_t L} - \frac{\ln(d_2/d_1)}{2\pi k_{\text{PPF}} L} - \frac{1}{hA}\right] \tag{3.24}$$

The cleanliness factor is defined to be the quotient between the actual overall heat transfer coefficient and the equivalent clean overall heat transfer coefficient, viz.

$$\text{CF} = \frac{U}{U_{\text{clean}}} \tag{3.25}$$

Technically changes in the overall heat transfer coefficient arise during the test not only from the increased conduction resistance offered by the fouling layer, but also from changes in the flow rates. In particular the change in friction factor affects the flow rate and hence the internal convection coefficient. In fact the apparatus is designed with a pressure regulating valve in parallel with the manifolds, to maintain the differential pressure across the test tubes. However, the slight changes referred to here are within the deadband of the regulating valve. Furthermore, there are minuscule variations in the annular flow rate during the test arising from current fluctuations to the pump motor. To separate these effects the measured overall heat transfer coefficient is normalized by dividing it by the 'theoretical' clean overall heat transfer coefficient. This is calculated by solving for the equivalent flow rate based on a smooth tube whilst keeping the pumping power constant. The procedure is as follows:

1. Calculate the fouled overall heat transfer coefficient at time t.

$$U = \frac{\bar{Q}}{\pi d_3 L \cdot \Delta T_{\text{LM}}} \tag{3.26}$$

2. Determine the pumping power.

$$P_P = \Delta p \times \frac{\pi d_1^2}{4} \times v \tag{3.27}$$

3. Guess the hypothetical smooth tube velocity.

4. Calculate the smooth tube friction factor using this guessed velocity and equation (3.6).

5. Check the guessed velocity and iterate until the following is true:

$$f_{\text{d,smooth}} \frac{L_{\Delta p}}{d_1} \frac{\rho v_{\text{smooth}}^2}{2} \times \frac{\pi d_1^2}{4} \times v_{\text{smooth}} = P_P \tag{3.28}$$

6. Using the iterated smooth tube velocity, solve for the corresponding internal convection coefficient and hence solve for the equivalent 'clean' overall heat transfer coefficient.

$$U_{\text{clean}} = \left\{ \pi d_3 L \cdot \left[\frac{1}{h_{\text{ann}} A_{\text{ann}}} + \frac{\ln(d_3/d_2)}{2\pi k_t L} + \frac{\ln(d_2/d_1)}{2\pi k_{\text{PPF}} L} + \frac{1}{h_{\text{clean}} A} \right] \right\}^{-1} \tag{3.29}$$

3.6.2 Difference in overall heat transfer coefficient method

Another measure of the fouling factor, denoted $R_f{}^*$, is found by comparing the inverse overall heat transfer coefficient at time t to the inverse of the initial overall heat transfer coefficient, denoted U_0. Assuming no other changes in heat transfer, annular flow rate etc. the fouling factor calculated in this manner is

$$R_f{}^* = \frac{1}{U} - \frac{1}{U_0} \tag{3.30}$$

3.7 Fouling modeling

The model for fouling first provided by Kern & Seaton (1959), cited by Bott (1995), is

$$R_f(t) = R_f^{\infty}(1 - e^{\beta t}) \tag{3.31}$$

where R_f^{∞} is the asymptotic fouling value, and β is a constant dependent on the system properties.

In fact Konak (1973) generalized this model as the n^{th} power so that

$$\frac{\mathrm{d}R_f}{\mathrm{d}t} = C^*(R_f^{\infty} - R_f)^n \tag{3.32}$$

C^* is a rate constant, and setting $n = 1$ reduces back to equation (3.31). It has been shown from experimental evidence that biological fouling follows a sigmoidal curve (Characklis *et al.*, 1981). Therefore Nebot *et al.* (2007) proposed the following modified form of the Konak (1973) model

$$\frac{\mathrm{d}R_f}{\mathrm{d}t} = C(R_f^{\infty} - R_f) \cdot Rf \tag{3.33}$$

where C is the rate constant that represents how quickly the asymptotic fouling resistance value is reached. Integrating equation (3.33) with $R_f = R_f^0$ at time $t = 0$ to $R_f = R_f$ at time $t = t$ yields

$$R_f = \frac{R_f^{\infty}}{1 + \left(\frac{R_f^{\infty}}{R_f^0} - 1 \right) \cdot \mathrm{e}^{-CR_f^{\infty} t}} \tag{3.34}$$

The rate constant C, initial fouling resistance R_f^0, and asymptotic fouling resistance R_f^{∞} are calculated using non-linear regression techniques.

3.8 Calibration and validation

3.8.1 Commissioning the apparatus using a calibration loop

Once the entire temperature measurement system is calibrated (appendix C), commissioning begins with an isothermal test with no load using a link pipe between the tube exit and annulus inlet forming the calibration loop illustrated in figure 3.11.

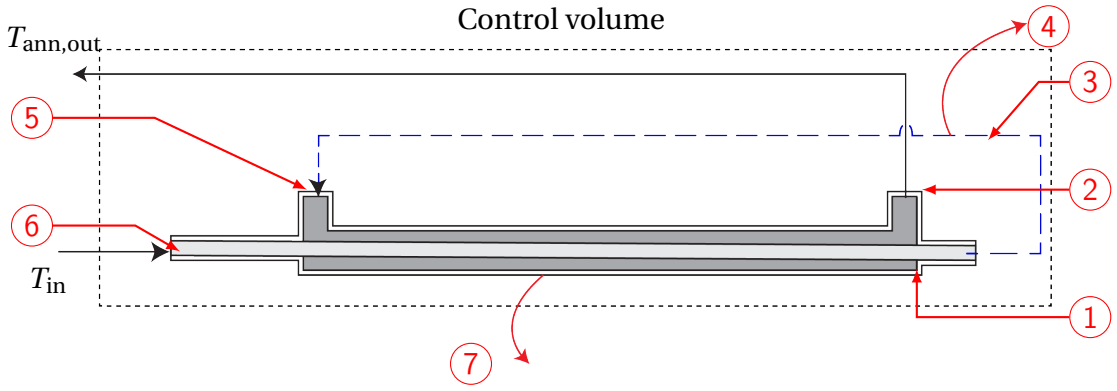

Figure 3.11: Diagram showing the link pipe installed during no load testing – (1) insulation, (2) annulus exit, (3) link pipe (only used during calibration), (4) heat transfer from piping between tube outlet and annulus inlet, (5) annulus inlet, (6) tube inlet, (7) heat transfer from heat exchanger jacket

Potable water is pumped through each test tube and then redirected through each annulus of the heat exchangers before returning to a 2 000 L reservoir. The water in the reservoir is left overnight to reach equilibrium with the ambient air (approximately 20 °C). Inside the container the air temperature is controlled around 28 °C using the air-conditioner as this provides enough of a temperature differential between the air inside the container and the water temperature to at least estimate the heat losses when the heat exchangers see an 8 °C temperature difference between the bulk fluid temperature and the air temperature. Although the water temperature during testing is actually around 35 °C, a similar magnitude temperature differential exists. The choice of using a separate reservoir at 20 °C is simply because this is found to provide a very stable temperature. If the test were performed at an elevated temperature a chiller would need to be used in conjunction with the heaters. Ultimately this is not required as this test is used to verify sufficient insulation and check the probe installation accuracy.

The link pipe further allows individual flow rates to be taken with the ultrasonic flow meter and compared to the reference electromagnetic flow meter (figure 3.12). In the legend JFC and JFH refer to the fouling fluid and annular flow measurements respectively. The appended numbers are the heat exchanger

numbers. The resulting calibration factors are tabulated for each tube in appendix C.

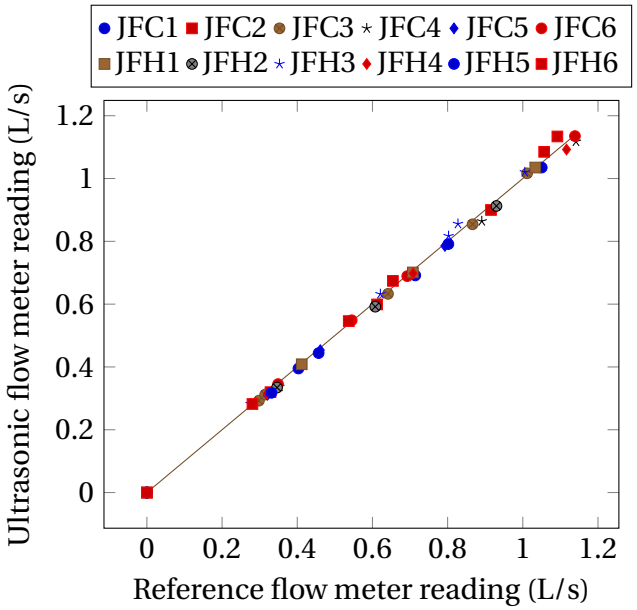

Figure 3.12: Measured flow rates using the ultrasonic flow meter compared to the reference electromagnetic flow meter

3.8.2 Balance checks: mass and energy

The first law of thermodynamics is satisfied at steady state when

$$Q_{\text{ann}} = Q + Q_{\text{surrounding}} \tag{3.35}$$

where Q_{ann} is the total heat transfer rate from the heated water in the annulus, Q is the total heat transfer rate to the foulant inside the test tube, and $Q_{\text{surrounding}}$ is the heat transfer rate to the surroundings.

Using the aforementioned calibration piping layout (section 3.8.1) the heat transfer rate to the surroundings (based on the control volume shown in figure 3.11) is

$$Q_{\text{surrounding}} = mc_p(T_{\text{in}} - T_{\text{out,ann}}) \tag{3.36}$$

The temperature differences $T_{\text{in}} - T_{\text{out,ann}}$ measured during an isothermal test shown in table 3.5 are less than the measurement uncertainty of the probes. From the fact that the temperature differences are less than the uncertainty of the probes, it follows that sufficient insulation is used to isolate the test heat exchangers such that the heat transfer rate to the surroundings is negligibly small.

Table 3.5: Measured temperature differences during isothermal test to verify sufficient insulation of the heat exchangers

Heat exchanger	T_{in} (°C)	$T_{\text{ann},out}$ (°C)	Difference
1	19.634	19.655	0.02
2	19.645	19.637	-0.01
3	19.630	19.672	0.04
4	19.702	19.587	-0.12
5	19.658	19.666	0.01
6	19.637	19.739	0.10

In general Q_{ann} and Q in equation (3.35) will vary according to the uncertainty in the measurements of the temperatures and flow rates. This error is referred to as the energy balance term, quantified as

$$\text{EB} = \frac{Q - Q_{\text{ann}}}{Q_{\text{max}}} \tag{3.37}$$

Provided the energy balance is less than the accuracy of the instrumentation, the results are deemed acceptable although, to improve the accuracy of subsequent calculations the average heat transfer is used calculated as

$$\bar{Q} = \frac{1}{2} \times \left[mc_{\text{p}}(T_{\text{out}} - T_{\text{in}}) + m_{\text{ann}} c_{p,\text{ann}}(T_{\text{ann,in}} - T_{\text{ann,out}}) \right] \tag{3.38}$$

The accuracy of the flow rates is specifically checked by the mass balance between the electromagnetic flow meter (which measures the bulk flow through the test tubes) and the ultrasonic flow meter (which measures the individual flow rates through each test tube). Conservation of mass dictates that the sum of the individual flow rates must equal the total flow, in which case the difference in the measured values is quantified as the mass balance term

$$\text{MB} = \frac{m_{\text{e}} - \Sigma m_{\text{u}}}{m_{\text{max}}} \tag{3.39}$$

The mass balance term is compared to the uncertainty in the flow rate measurements between the ultrasonic and electromagnetic flow meters.

3.8.3 Convection tests to regress the annular Nusselt number in terms of Reynolds number

The annular convection regression coefficients A_{Nu} and B_{Nu} are experimentally determined at the beginning of each test (listed in appendix C). Effectively this calibrates the apparatus by determining the annular convection coefficient taking into account the actual tube thermal conductivity, minor tube eccentricity and other experimental variables. The measured Nusselt numbers are then compared to the predicted values using equation (3.21). The results are practically

within 20 % of the theoretical values – the differences are attributed to transitional flow caused by the edge effects due to the heat exchanger inlet and outlet geometry. See figure C.1 in appendix C for further details.

3.8.4 Experimental procedure

The flow chart in figure 3.13 illustrates the procedure followed from commissioning the apparatus to obtaining fouling test results.

After completing the no load commissioning tests using the calibration loop (section 3.8.1), convection tests are performed. These tests begin by heating the potable water in the hot reservoir to approximately 45 °C which takes up to 1 hour from room temperature. A temperature controller and solid state thyristor are used to vary the heat input from the heaters, and maintain the set temperature of the hot reservoir. The annular flow rates are adjusted using manual angle control valves (VHD1 to VHD6, figure 3.7). The solenoid valve V27 is then energized so that fouling water from the tap-off point is passed through the test tubes and discharged to the cooling tower pond. Flow rates through the test tubes are adjusted using the manual diaphragm control valves VCD1 to VCD6 (figure 3.7).

Once steady state has been reached the flow rates, temperatures, and pressure drops are recorded. Thereafter the annular flow rates are adjusted and the system is allowed to stabilize before recording the new data. At least three different tests are repeated at varying annular flow rates over the range 0.3 L/s to 1.1 L/s so that the annular convection coefficient can be regressed suitably as a function of Reynolds number (section 3.5.4). All of these tests are completed within 6 hours in order to ensure that no significant fouling can take place during the initial convection testing.

Next the flow rates are returned to their respective set points without altering anything else on the apparatus. The fouling test begins and the tubes remain undisturbed for the duration of the test. Figure 3.13 shows that three fouling tests are thus performed for this study:

- **Test A:** Before studying PPF-modified tubes, three pairs of similar tubes are tested to verify the equality between conditions experienced by the two tubes of the same pair. Comparing the tubes before coating means that the subsequent results on PPF-modified tubes cannot be refuted on the basis of dissimilar conditions between each heat exchanger. Thus no PPFs are applied in test A, instead all the bare tube pairs are tested in parallel to investigate the efficacy of the apparatus.

- **Test B:** One particular type of PPF is tested on three different tube alloys: admiralty brass, duplex stainless steel, and titanium. The PPF is a modified epoxy with a conductive filler which has already been used extensively on previous condensers in South Africa. The two brass tubes remain in the apparatus so that they can continue to be tested during the next test.

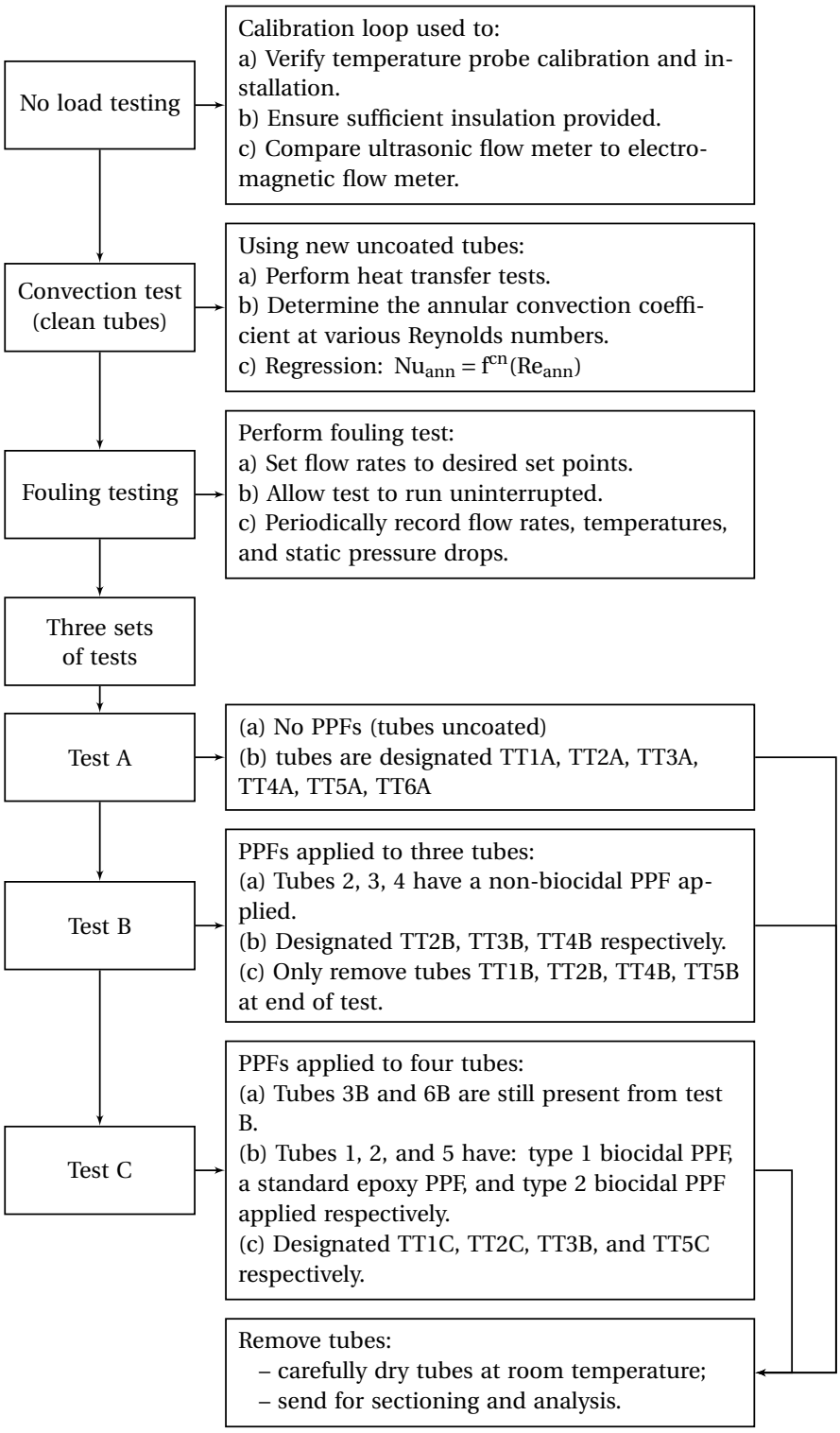

Figure 3.13: Flow chart showing the experimental procedure

- **Test C:** In this test two prototype biocidal PPFs are compared to a standard epoxy, i.e. an epoxy that is not modified in terms of thermal or antifouling properties. An unmodified Sea-cure® tube serves as a control tube for the test.

3.9 Uncertainty analysis

The fouling factor determined from measurements[4] depends on the following 16 measured variables:

$$R_f = \mathrm{f}^{\mathrm{cn}}\left(d_4, d_3, d_2, d_1, L, k_t, L_{\Delta p}, T_{\mathrm{in}}, T_{\mathrm{out}}, T_{\mathrm{ann.in}}, T_{\mathrm{ann,out}}, F, F_{\mathrm{ann}}, \Delta H, A_{\mathrm{Nu}}, B_{\mathrm{Nu}}\right) \tag{3.40}$$

However, because of the fact that the annular convection coefficient is experimentally determined before the fouling tests (see section 3.5.4), errors arising from the following variables are common: d_4, d_3, d_2, L, and k_t. Consequently these errors are contained in the annular convection coefficient regression. Thus equation (3.40) simply reduces to

$$R_f = \mathrm{f}^{\mathrm{cn}}\left(d_1, L_{\Delta p}, T_{\mathrm{in}}, T_{\mathrm{out}}, T_{\mathrm{ann.in}}, T_{\mathrm{ann,out}}, F, F_{\mathrm{ann}}, \Delta H, A_{\mathrm{Nu}}, B_{\mathrm{Nu}}\right) \tag{3.41}$$

Following the Taylor Series Method (TSM) described by Coleman & Steele (2009), an estimate of the overall uncertainty in the measured fouling factor is

$$\Delta R_f = \sqrt{\sum_{j=1}^{11}\left(\frac{\partial R_f}{\partial X_j}^2 \Delta X_j{}^2\right)} \tag{3.42}$$

where X_j is the j^{th} variable of equation (3.41). The uncertainty sources ΔX_j are listed in table 3.6 together with their error estimates. In particular ΔA_{Nu} and ΔB_{Nu} are estimated from previous studies using a similar apparatus (Goodenough, 2013).

The partial derivatives in equation (3.42) are numerically evaluated using the central differencing formula.

$$\frac{\partial R_f}{\partial X_j} = \frac{R_f\left(X_j(1+\zeta)\right) - R_f\left(X_j(1-\zeta)\right)}{2\zeta X_j} \tag{3.43}$$

where the step size ζ is determined according to machine epsilon (ϵ^*):

$$\zeta = \sqrt{\epsilon^*} X_{j_i} \tag{3.44}$$

[4] This analysis is readily extended for the uncertainty in the friction factor

Table 3.6: Uncertainty sources and estimates

Uncertainty source	Uncertainty estimate ΔX_j
Annulus internal diameter	5 µm
Tube diameter	0.5 µm
Heat transfer length	0.5 mm
Temperature	0.05 °C
Flow rate	0.0025 L/s
Manometer height difference	5 mm
A_{Nu}	6 %
B_{Nu}	1.6 %

3.10 Data processing

Table 3.7 summarizes the data processing, using the relevant theory from the previous section.

Table 3.7: Tabulated data processing

Measured variables	Calculated terms
Geometry: → diamaters (d_4, d_3, d_2, d_1) → effective length (L_{eff})	Hydraulic diameters: tube ($d_h = d_1$); annulus ($(d_h)_{\text{ann}} = d_4 - d_3$) surface areas: tube ($\pi d_1 L_{\text{eff}}$); annulus ($\pi d_3 L_{\text{eff}}$) cross-sectional areas: tube ($\pi \frac{{d_1}^2}{4}$); annulus ($\pi \frac{({d_4}^2 - {d_3}^2)}{4}$)
Temperatures: → inlets; outlets	Bulk foulant temperature ($\frac{1}{2}(T_{\text{in}} + T_{\text{out}})$); bulk annular temperature ($\frac{1}{2}((T_{\text{ann}})_{\text{in}} + (T_{\text{ann}})_{\text{out}})$) thermophysical properties: ρ, μ, c_p, k_w cross-sectional areas: tube ($\pi \frac{{d_1}^2}{4}$); annulus ($\pi \frac{({d_4}^2 - {d_3}^2)}{4}$)
Flow rates: → tube (F); annulus (F_{ann})	Mass flow rates: tube ($m = \rho F$); annulus ($m_{\text{ann}} = \rho_{\text{ann}} F_{\text{ann}}$) mean velocity: tube ($v$); annulus ($v_{\text{ann}}$) mean heat transfer: $\bar{Q} = \frac{1}{2} \times \left[m c_{\text{p}} (T_{\text{out}} - T_{\text{in}}) + m_{\text{ann}} c_{p,\text{ann}} (T_{\text{ann,in}} - T_{\text{ann,out}}) \right]$

Twelve volumetric flow rates are measured sequentially within a 60 min period. Each flow rate measurement is the arithmetic mean of the values recorded during a 2 min sampling period during which values are sampled every 15 s. Setup and stabilization of the ultrasonic flow meter requires approximately 3 minutes. Simultaneously the data logger samples all 24 temperature probes every 20 seconds and records the arithmetic mean over 3 min intervals. Pressure drop measurements are recorded once during this procedure, since they remain stable over the 60 min period.

3.11 Experimental results

3.11.1 Test A: performance of the purpose-built facility measured using unmodified tubes

Before testing the fouling tendency of PPFs, the performance of the test facility is experimentally investigated by installing three tube pairs of different but unmodified alloys, i.e. without any PPFs. The purpose is to show that the apparatus creates similar conditions between tube pairs before modification of the tubes using PPFs; principally measured in terms of the pressure drop and fouling factor for each tube. This test is referred to as test A.

Tube selection and designation is tabulated in table 3.8. The following alloys are used: cartridge brass, Sea-cure® (a stainless steel) and titanium. Cartridge brass has not been used as a condenser tube alloy since about 1900 (Putman, 2001), being superseded by the advent of admiralty brass – a copper alloy with 1 % tin and 0.04 % arsenic with greatly enhanced resistance to galvanic corrosion. However, cartridge brass is used only in test A for the purposes of testing equality between tube pairs. Furthermore, scrutiny of table 3.8 also reveals that the brass tubes have a slightly larger outer diameter. This is due to the fact that the condensers operating at the selected plant are designed using metric standards, and so their tubes have a 24 mm outer diameter. In contrast, imperial-sized condensers commonly have 25.4 mm outer diameter tubes. Because cartridge brass tubes with a 25.4 mm outer diameter were the only brass tubes available for testing, the facility is designed to accommodate one pair of tubes with a 25.4 mm outer diameter. The effective heat transfer length of all the tubes throughout this study is 3.199 m.

Table 3.8: Tube designation and specifications for test A

Tube	Material	PPF	Outer diameter d_3 (mm)	Inner diameter d_2 (mm)
TT1A	Sea-cure®	none	23.93	22.59
TT2A	Sea-cure®	none	23.89	22.57
TT3A	Cartridge brass	none	25.35	22.05
TT4A	Titanium	none	23.91	22.74
TT5A	Titanium	none	23.97	23.14
TT6A	Cartridge brass	none	25.33	22.19

Next the twelve volumetric flow rates, denoted F, recorded for test A are given in terms of the test tubes (table 3.9) and annuli (table 3.10). The difference in the set points of tubes 3 and 6 compared to all the others, is to account for the difference in diameters as previously discussed. They are adjusted such that all tubes have the same bulk velocity set point. The differences in the actual flow

rates is deemed small enough to successfully compare the measured pressure drop, and hence friction factor, on each of the tubes.

Table 3.9: Flow rates through test tubes for test A (velocity in brackets)

Tube	Set point (L/s)	Actual mean (L/s)	Standard deviation (L/s)	Max (L/s)	Min (L/s)
TT1A	0.700	0.741 (1.81m/s)	0.0209	0.7787	0.7012
TT2A	0.700	0.669 (1.68m/s)	0.0437	0.7083	0.5822
TT3A	0.710	0.677 (1.70m/s)	0.0210	0.7063	0.6444
TT4A	0.700	0.732 (1.77m/s)	0.0286	0.7738	0.6655
TT5A	0.700	0.729 (1.75m/s)	0.0249	0.7688	0.6578
TT6A	0.710	0.645 (1.66m/s)	0.0674	0.7324	0.5383

Table 3.10: Flow rates through annuli for test A (velocity in brackets)

Annulus	Set point (L/s)	Actual mean (L/s)	Standard deviation (L/s)	Max (L/s)	Min (L/s)
1	1.000	0.934 (1.83m/s)	0.083	0.996	0.792
2	1.000	0.893 (1.64m/s)	0.096	1.009	0.719
3	0.800	0.880 (1.92m/s)	0.022	0.909	0.843
4	1.000	0.966 (1.80m/s)	0.037	1.052	0.922
5	1.000	0.960 (1.82m/s)	0.048	1.073	0.839
6	0.800	0.866 (1.85m/s)	0.110	0.982	0.759

At the start of test A, before fouling has occurred, the friction factors are measured and compared to the theoretical smooth tube values (equation 3.6) so that the accuracy of the pressure drop measurement system can be verified. A sample calculation is provided in appendix E. The results shown in table 3.11 show good agreement and confidence is thus gained in the pressure drop measurement.

Table 3.11: Measured versus theoretical smooth tube friction factors (f_d) measured at the start of test A

Tube	Measured friction factor	Smooth tube friction factor	Difference (%)
TT1A	0.01834	0.01961	-6.43
TT2A	0.01984	0.01989	-0.24
TT3A	0.02335	0.0221	5.70
TT4A	0.02092	0.02044	2.29
TT5A	0.01730	0.01970	-12.18
TT6A	0.02071	0.01960	5.68

Now the measured friction factor is plotted as a function of time in figure 3.14 in terms of each tube pair. Subfigures (a), (b), and (c) compare Sea-cure®, cartridge brass, and titanium tube pairs respectively. Clearly figures 3.14 (a) and (c) show identical trends, with a very small increase in friction factor as test A progresses. On the contrary, the friction factor of the cartridge brass shown in figure 3.14 (b) shows a marked increase in friction factor (point 1). This is caused by corrosion fouling as expounded on upon later. However, it is noted that for each tube pair the friction factors are nearly identical. This is a very positive result indicating homogeneity in the test conditions for each tube pair.

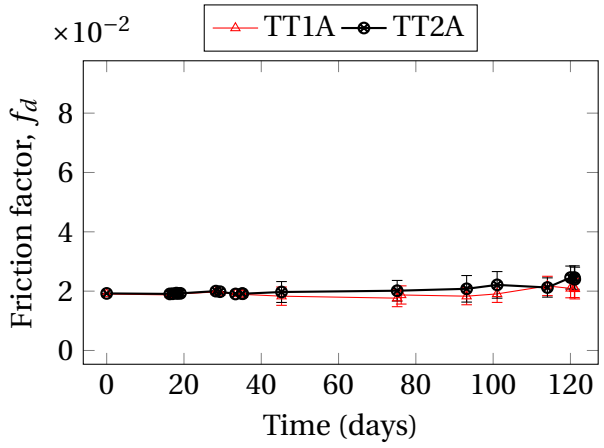

(a) Comparison between unmodified Sea-cure® tubes

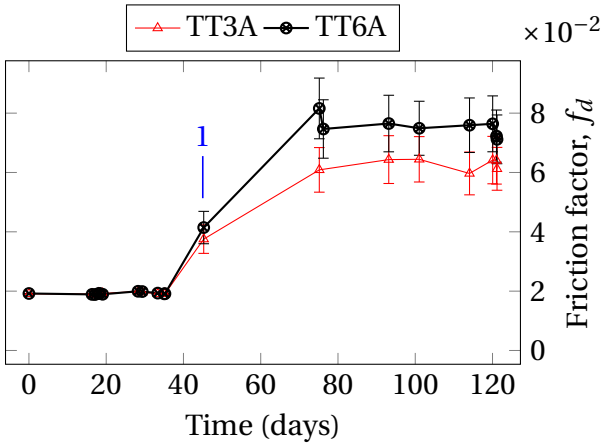

(b) Comparison between unmodified cartridge brass tubes

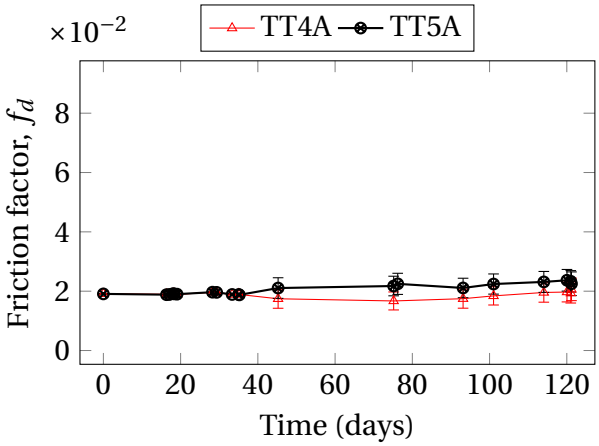

(c) Comparison between unmodified titanium tubes

Figure 3.14: Measured friction factors from test A

The next performance measure is the fouling factor (determined using equation (3.24)) shown in figure 3.15. For all the tube pairs there is a slight decrease in fouling factor up to day 20 which may be explained by a slight increase in heat

transfer resulting from surface roughening due to the onset of fouling. After this initiation period there is a definite increase in the fouling factor as fouling develops. Figures 3.15 (a) and (c) are practically the same within their uncertainty bands. However, point 1 in figure 3.15 highlights the sharp increase in fouling of the cartridge brass tubes. In comparison the fouling factors of the stainless steel and titanium in figures 3.15 (a) and (c) respectively, show a slower rate of fouling. After 120 days the cartridge brass tubes had the highest fouling factors, followed by the Sea-cure® and titanium tubes (both of which have nearly the same fouling factors).

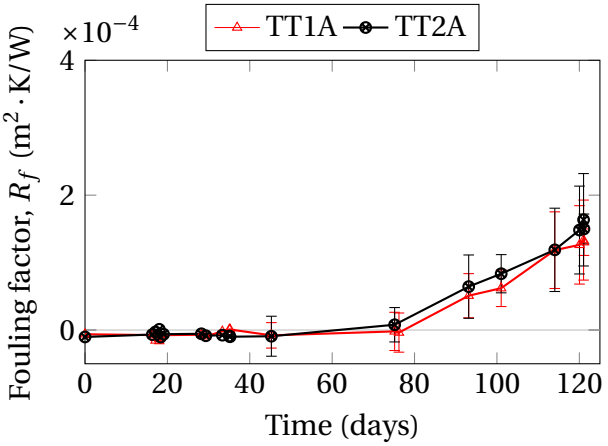

(a) Comparison between unmodified Sea-cure® tubes

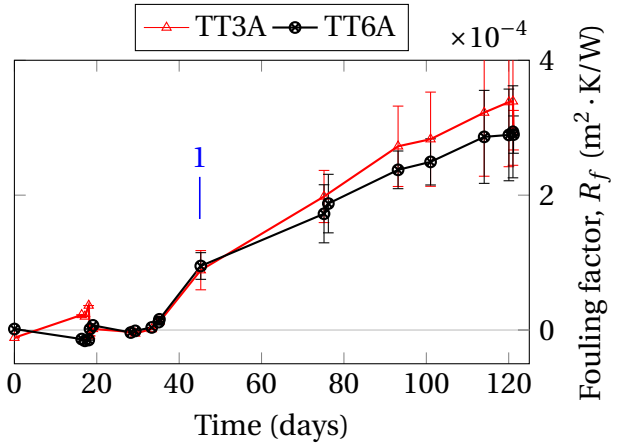

(b) Comparison between unmodified cartridge brass tubes

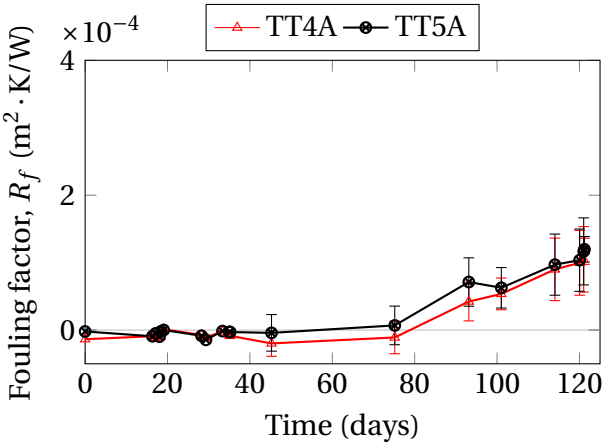

(c) Comparison between unmodified titanium tubes

Figure 3.15: Measured fouling factors from test A – (1) sharp incresae in fouling of cartridge brass

The unusual increase in the measured friction and fouling factors on the cartridge brass compared to the other tubes, warrants a detailed investigation of

tubes TT3A and TT6A after completing test A. The tubes are longitudinally sectioned and photographed in figure 3.16. Extensive fouling is apparent and moreover point 3 in figure 3.16 shows that the parent material has undergone discoloration beneath the foulant.

Figure 3.16: Photograph of TT3A after longitudinal sectioning – (1) heavily fouled area (note the surface roughness), (2) top half of tube, (3) foulant removed to show the discolored parent brass

QEMSCAN® analysis performed at an independent laboratory shows strong evidence that dezincification has occurred on the cartridge brass tubes. Dezincification, a form of corrosion fouling, occurs when zinc is selectively dissolved out of the brass alloy because of the zinc's higher reactivity. This is clearly shown in figure 3.17. Ranjbar (2010) experienced the same result on yellow brass (which differs from cartridge brass by 3 % zinc). Similar pink areas of copper rich 'plugs' caused by the dezincification are noted in their results. Obviously cartridge brass is not used in condenser applications because of its susceptibility to dezincification and is only used during test A to verify equality between test tubes. The remaining tests are all performed on admiralty brass.

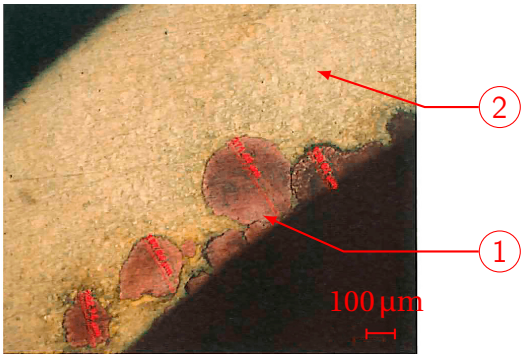

Figure 3.17: Micrograph of TT3A after cross sectioning showing dezincification – (1) copper-rich pit, (2) parent tube

Lastly figure 3.18 compares R_f to $R_f{}^*$ calculated using equations (3.24) and (3.30) respectively (sample calculation in appendix E). The similarity between R_f and $R_f{}^*$ provides confidence in the measurement and analysis, since $R_f{}^*$ does not depend on the regression of the annular convection coefficient. Figure 3.18 in appendix D compares similarly for the subsequent tests B and C.

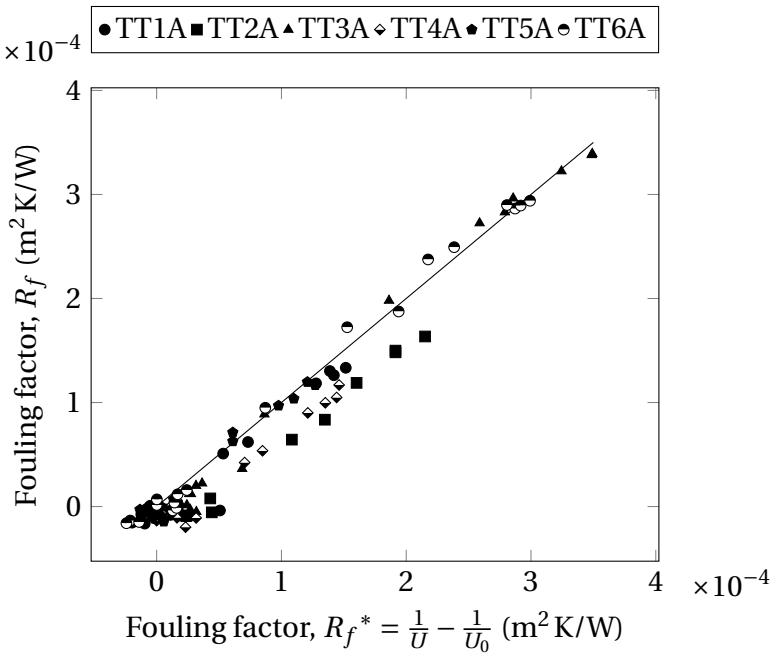

Figure 3.18: Measured fouling factors compared using equations (3.24) and (3.30)

In conclusion the apparatus is efficacious in its design since it can successfully replicate similar fouling conditions on different tube alloy pairs before the application of PPFs. Measured in terms of the friction and fouling factors, the results indicate that each tube pair perform similarly and within the uncertainty bounds. A discussion of the experimental results gained using PPFs is considered next.

3.11.2 Test B: non-biocidal PPF

Tube designation for test B is tabulated in table 3.12. The table reveals that a PPF is applied to tubes TT2B, TT3B, and TT4B, while the remaining tubes are unmodified and serve as control tubes. The PPF used in this test is currently being used extensively as a life-extension measure (see section 1.3.3), and the thermal conductivity of this PPF has already been tested (Goodenough, 2013). With careful addition of a thermally-conductive filler, its conductivity is increased to 1.2 W/(m K) from 0.5 W/(m K). Furthermore the same PPF is applied on three different tube alloys to ensure that the fouling results are irrefutable. Lastly the

application is overseen by the author and visual inspection reveals a continuous film free from defects.

Table 3.12: Tube designation and specifications for test B

Tube	Material	PPF	PPF thickness
TT1B	Duplex stainless steel[1]	none	–
TT2B	Duplex stainless steel[1]	Thermally-enhanced PPF	44 µm
TT3B	Admiralty brass	Thermally-enhanced PPF	55 µm
TT4B	Titanium	Thermally-enhanced PPF	56 µm
TT5B	Titanium	none	–
TT6B	Admiralty brass	none	–

1: UNS S3108

The PPF thicknesses given in table 3.12 are measured during the application process because this is found to be the most accurate method of determining the PPF thickness. Firstly a known volume of paint is injected into the test tube. Secondly a proprietary pig is propelled down the length of the tube forcing the paint against the tube. A thin film of paint remains while the excess paint is collected at the tube exit and measured. Lastly by subtracting the exiting volume of paint from the initial volume allows the average PPF thickness to be calculated based on the uncoated internal diameter of the tube.

Similarly to test A, at the start of test B before fouling has occurred, the friction factors are measured and compared to the theoretical smooth tube values (equation 3.6) in table 3.13. Once again there is good agreement and thus the tapping hole drilling procedures (section 3.3.4) are repeatable.

Table 3.13: Measured versus theoretical smooth tube friction factors (f_d) measured at the start of test B

Tube	Measured friction factor	Smooth tube friction factor	Difference (%)
TT1B	0.01895	0.01957	-3.1 %
TT2B	0.01773	0.01950	-9.09 %
TT3B	0.01900	0.01937	-1.88 %
TT4B	0.01871	0.01945	-3.84 %
TT5B	0.01949	0.01939	0.048 %
TT6B	0.01991	0.01943	2.47 %

The friction factors measured during test B are plotted in figures 3.19 (a), (b), and (c) for the stainless steel, admiralty brass, and titanium tube pairs respectively. Initially there is a slight increase in the friction factor that is common for all the tubes, but between days 40 and 60 point 1 indicates a relatively large increase in all the friction factors. This increase in friction factor is caused by an

increase in surface roughness of the tube caused by fouling deposits, as seen visually and also confirmed later when considering the measured fouling factors.

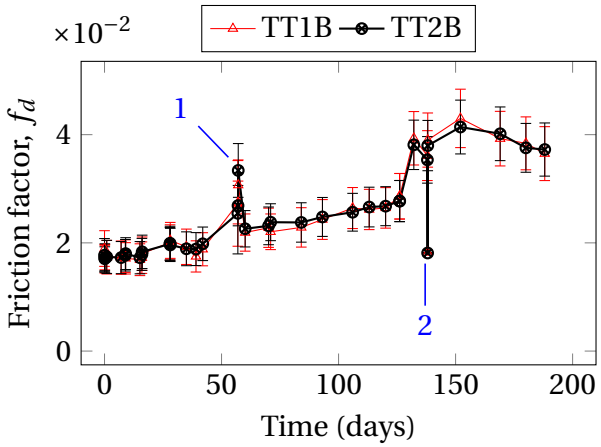

(a) Comparison between duplex stainless steel and PPF-modified duplex stainless steel

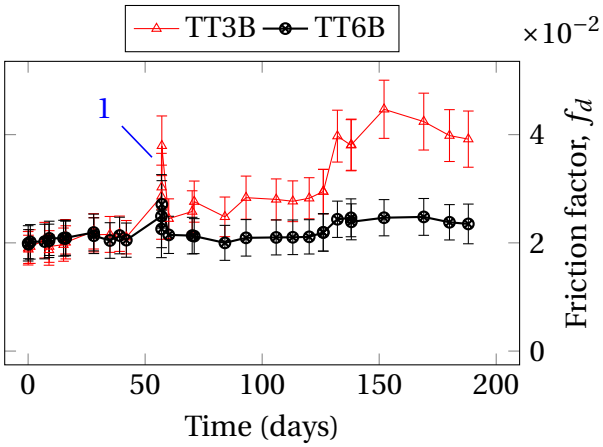

(b) Comparison between admiralty brass and PPF-modified admiralty brass

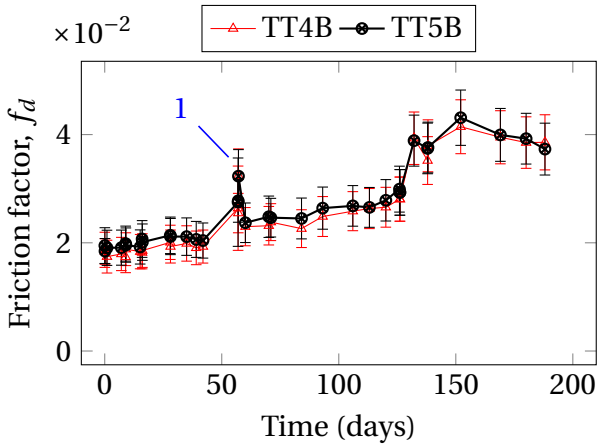

(c) Comparison between titanium and PPF-modified titanium

Figure 3.19: Measured friction factors from test B – (1) flow rates reduced by 40 % between day 40 and 60, (2) flow through stainless steel tubes increased to 150 % for 90 min

During this period there is a notable decrease in the mean velocities as shown in figure 3.20. Due to an operational error, raw water was actually injected into the cooling water system leading to partial blockage of the y-strainers fitted upstream of the apparatus. Examination of the strainers at day 60 revealed extraordinarily excessive macrofouling (photograph given in figure B.6 in appendix B). This anomaly explains the reduction in flow rate and the corresponding increase in friction factor. After rectifying the operational error the flow rates returned to

normal and all the friction factors returned to a value close to that preceding the incident. Thereafter all the tubes except the unmodified admiralty brass (TT6B) show the same increasing trend in friction factor up to day 124. The admiralty brass has a much slower trend of increasing friction factor indicating less fouling.

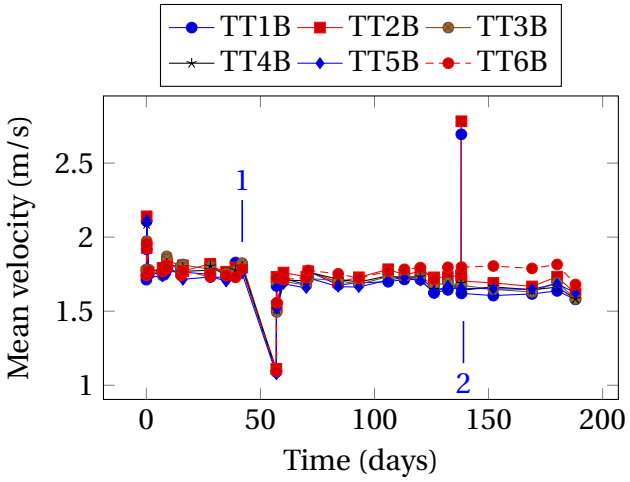

Figure 3.20: Bulk fouling fluid velocity from test B – (1) velocity reduced by 40 % between day 40 and day 60, (2) flow rate through stainless steel tubes (only) increased to 150 % for 90 min

It is important to state that although the flow rate varied during this 20 day period, all six tubes experienced the same inevitable fluctuation in plant parameter equally. The design of the apparatus, in particular the purpose-built manifolds, afforded this similarly between tubes and ensures that the relative results between test tubes are still valid. Moreover this type of online testing at the plant provides very realistic conditions, such as the aforementioned anomaly, which can be nearly impossible to simulate in isolated bench-top type experiments.

Lastly, on day 124 the flow rates through the stainless steel tubes were simultaneously and purposefully increased to 150 % of their set point (point 2 in figure 3.19 (a)) to study the relative tenacity of the foulant layer. The sharp decrease in friction factor measured immediately after this increase in mean velocity through the tubes indicates the foulant layer is not particularly stable, although once the flow rate was restored the friction factor quickly returned to its original value within a number of days.

Next consider the measured fouling factors during test B (figure 3.21). Point 1 shows the slight decrease in fouling factor on all the tubes, similar to the observation made during test A. Thereafter the fouling factor really begins to increase after about day 18 continuing up to day 40. Point 2 shows the sharp increase in fouling factor between days 40 and 60 because of the reduction in flow rate as

previously discussed. Once the flow rates were reset the fouling factors drop to a value slightly higher than that before day 40.

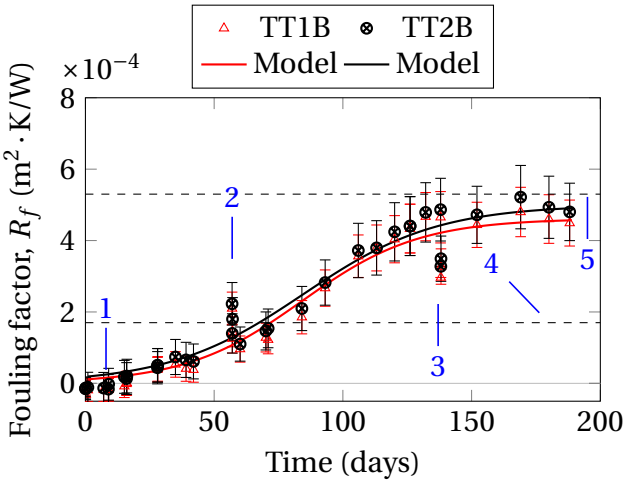

(a) Comparison between duplex stainless steel and PPF-modified duplex stainless steel

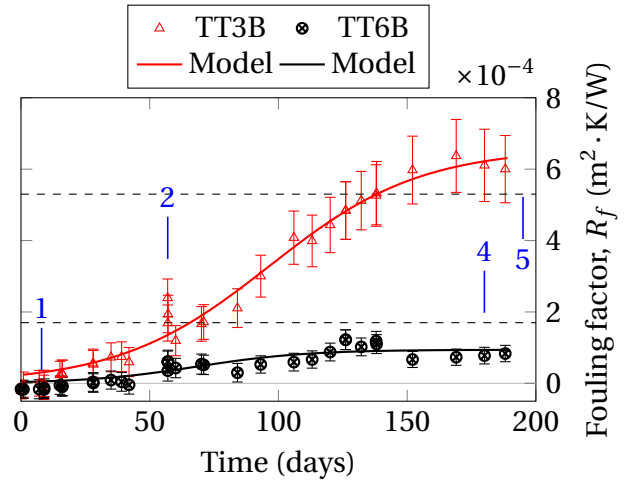

(b) Comparison between admiralty brass and PPF-modified admiralty brass

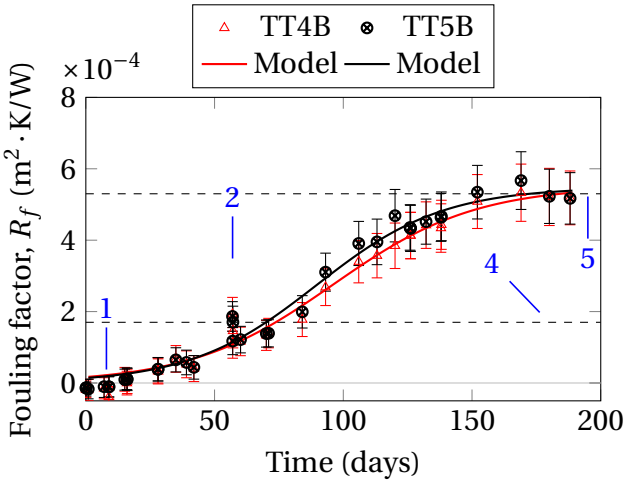

(c) Comparison between titanium and PPF-modified titanium

Figure 3.21: Measured fouling factors from test B – (1) initial slight increase in heat transfer from surface roughening, (2) flow rates reduced by 40 % between day 40 and 60, (3) flow through stainless steel tubes increased to 150 % for 90 min, (4) TEMA fouling factor for cooling tower waters (TEMA, 1999), (5) TEMA fouling factor for hard river waters (TEMA, 1999)

An increase in fouling factor is observed from this point and the stainless steel and titanium tube pairs (figures 3.21 (a) and (c) respectively) show nearly identical behavior. That is to say the PPF-modified duplex stainless steel and PPF-modified titanium tubes unmodified tubes foul exactly the same as their unmod-

ified control tubes. The unmodified admiralty brass tube (figure 3.21 (b)) has a significantly lower fouling factor than any of the other tubes.

The fouling model proposed by Nebot *et al.* (2007) is applied to this data by using non-linear regression methods to solve for the coefficients in equation (3.34). The resulting regression coefficients, tabulated in table 3.14, are employed in plotting the sigmoid curves shown in figure 3.21.

Table 3.14: Asymptotic fouling factors, rate constants, and times to reach inflexion points on the sigmoid fouling curves

Tube	R_f^∞ $m^2\,K/W$	C	$t_{\frac{1}{2}}$ day	R_f^0 $m^2\,K/W$
TT1B	$4.53\cdot10^{-4}$	105.97	83	$8.1\cdot10^{-6}$
TT2B	$4.9\cdot10^{-4}$	85.31	82	$1.45\cdot10^{-5}$
TT3B	$6.48\cdot10^{-4}$	55.38	94	$2\cdot10^{-5}$
TT4B	$5.39\cdot10^{-4}$	72.67	94	$1.28\cdot10^{-5}$
TT5B	$5.42\cdot10^{-4}$	79.05	88	$1.17\cdot10^{-5}$
TT6B	$9.16\cdot10^{-5}$	659.23	68	$1.4\cdot10^{-6}$

The model fits the data well for all the tubes, and it is particularly effective in dealing with the fluctuation in fouling between days 40 and 60. Moreover the test is deemed to have reached asymptotic value judging by the uniformity in the data after 160 days. In fact its asymptotic value is just below the Tubular Exchangers Manufacturers Association (TEMA) recommended fouling factor for cooling tower waters with untreated make up water (velocity greater than 0.91 m/s) equal to $1.7\times10^{-4}\,m^2\,K/W$ (TEMA, 1999). In contrast all the non-copper bearing tubes (and the PPF-modified brass tube) have asymptotic values closer to the fouling factor TEMA suggests for very hard river water equal to $5.3\times10^{-4}\,m^2\,K/W$.

Another way of presenting these results is shown in figure 3.22 where the cleanliness factor (equation 3.25) is plotted against time. The initial cleanliness factors (point 1) are within 5 % of 1.0 – the slight differences arise from the regression uncertainty in the annular convection coefficient. The fouling results previously discussed are reflected in figures 3.22 (a), (b), and (c) although an increase in fouling factor causes a decrease in cleanliness factor. The best performance is still achieved by the unmodified admiralty brass (figure 3.22 (b)) and the asymptotic cleanliness factor is almost 0.8. All the other tubes reach a cleanliness factor of about 0.4 after 180 days of exposure, i.e. clearly significant fouling has occurred. The addition of the PPF to the admiralty brass (TT3B) has therefore changed the cleanliness factor in a detrimental manner. In an actual condenser once the cleanliness factor drops to such an extent, operational limits would force the unit to be derated and / or shutdown until the condenser could be cleaned. Notwithstanding the regular cleaning, typical design values

used for brass alloys are 0.75-0.8 and 0.85-0.95 for stainless steels and titanium alloys. Thus the cleanliness factors measured here are significantly lower than the expected design values after only 185 days exposure which indicates a severe amount of fouling.

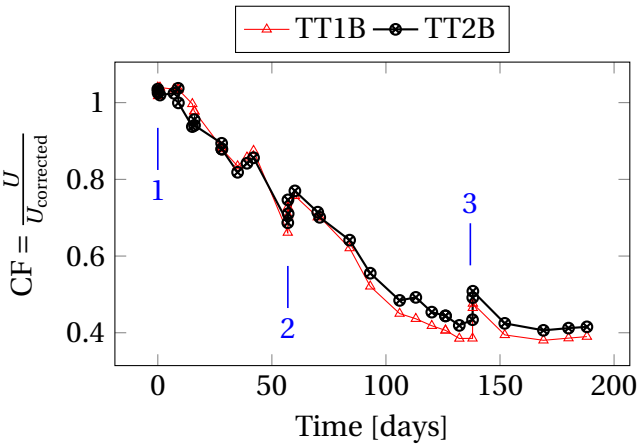

(a) Comparison between duplex stainless steel and PPF-modified duplex stainless steel

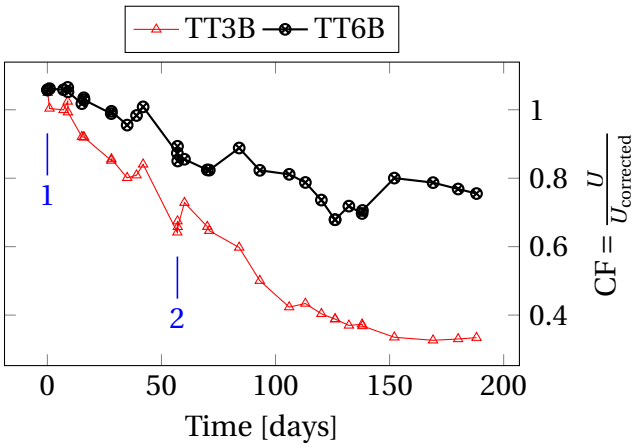

(b) Comparison between admiralty brass and PPF-modified admiralty

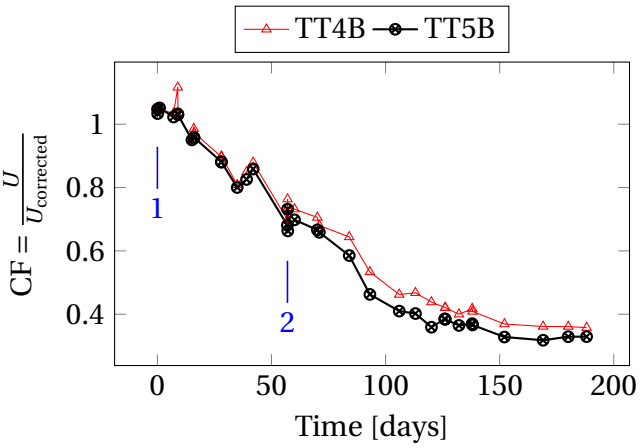

(c) Comparison between titanium and PPF-modified titanium

Figure 3.22: Cleanliness factor versus time measured during test B – (1) corrected heat transfer <5 % deviation from 1.0 because of regression uncertainty, (2) flow rates reduced by 40 % between day 40 and 60, (3) flow rates through tubes stainless steel tubes (only) increased to 150 % for 90 min

Based on the following observations, biofouling is suspected to be the biggest contributor to the difference in fouling between the copper-bearing alloy tube and all the other tubes:

- There is a substantial difference between the fouling behavior of the admiralty brass tube (copper-bearing) and all the other tubes. In particular the admiralty brass has the lowest fouling factor, and this coincides with the ranking of tube alloys in terms of their biofouling resistance given by Characklis & Marshall (1990) (chapter 2).
- The shape of the fouling data (figure 3.21) fits a sigmoidal curve very closely, which is the same pattern observed for biofilm formation (Nebot *et al.*, 2007; Bott, 1995).
- The application of the PPF on TT6B has effectively isolated the brass beneath the PPF from contacting the fouling fluid. The resulting fouling of TT6B is identical to the stainless steel and titanium tubes. This means that the same fouling phenomena is affecting: stainless steel, titanium, and a polymeric surface (all of which are fairly inert), but different behavior only occurs on the brass.

To confirm this suspicion, an analysis of the sessile bacteria residing in the biofilm is required. Therefore bacterial counts were performed after 126 days of exposure during test B (Appendix D, table D.67). Using sterile swabs, samples are taken from the outlet of each test tube. They are then submitted to an independent laboratory for analysis, and the results are given in figure 3.23 in terms of the number of aerobic and anaerobic bacterial forming colonies per milliliter (CFU/mL).

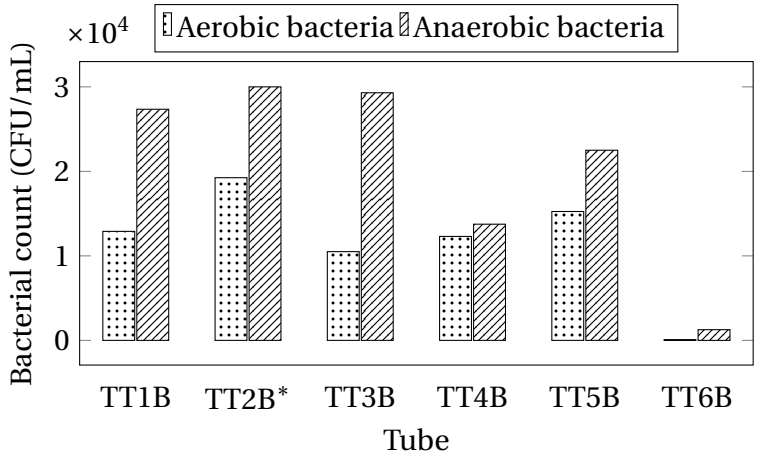

Figure 3.23: Bacterial counts after 126 days of exposure – * indicates colony greater than 30 000 CFU/mL

Clearly TT6B, the bare admiralty brass tube, has aerobic and anaerobic bacterial counts that are at least one order of magnitude less than any other tube (by over 20 times). This is very likely a consequence of the toxicity of the copper ions in the brass alloy. These results agree with the biofouling tendency ranking of

tube alloys given by Characklis & Marshall (1990) (see page 19). From this data it is concluded that biofouling is occurring at the plant and importantly the development of the biofouling is identical for the PPF tested and all the non-copper bearing alloys. In other words the formation of the biofilm is as likely to occur on duplex stainless steel, titanium, or the PPF tested here, because all of these surfaces are inert and therefore do not retard the microbiological activity. In contrast the admiralty brass is copper-bearing and significantly retards the biofouling.

Micrographs from QEMSCAN® analyses shown in figures 3.24 (a) and (b) are of duplex stainless steel and PPF-modified duplex stainless steel respectively. Likewise figures 3.25 (a) and (b) are micrographs of PPF-modified titanium and titanium respectively. In both cases the PPF is indicated in green and attention is drawn to the relative thickness of the film compared to the scale layer (mainly calcium carbonate scale shown in blue). The admiralty brass tube pair is not sectioned since they are tested further in the next test.

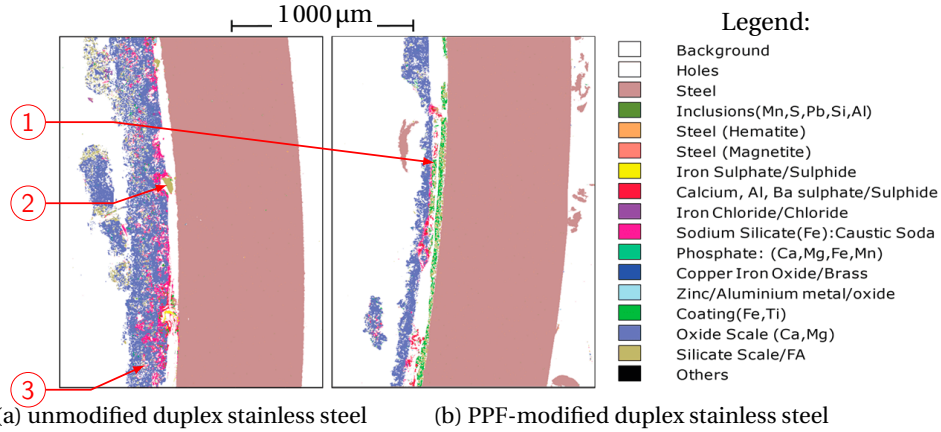

(a) unmodified duplex stainless steel (b) PPF-modified duplex stainless steel

Figure 3.24: QEMSCAN® cross-sectional micrographs of stainless steel tubes: TT1B and TT2B – (1) PPF (shown in green), (2) foulant (silicate, shown in brown), (3) foulant (mainly calcium carbonate, shown in blue)

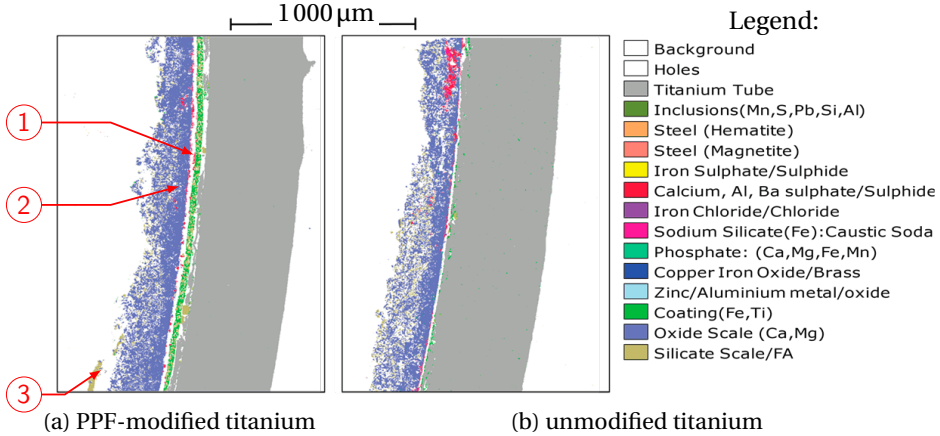

(a) PPF-modified titanium (b) unmodified titanium

Figure 3.25: QEMSCAN® cross-sectional micrographs of titanium tubes: TT4B and TT5B – (1) PPF (shown in green), (2) foulant (mainly calcium carbonate, shown in blue), (3) silicate scale (shown in brown)

The inorganic mineralogical composition of the foulant deposited is found to be made of 70 % calcium carbonate. Silicate scale is also present in the deposit; silicate scale is inherently tenacious and difficult to remove. There is no evidence of corrosion or erosion indicated in the analysis.

In summary the results from test B indicate composite fouling. That is to say predominantly biofouling, precipitation (scaling of calcium and magnesium carbonates), and then to a lesser extent particulate fouling (silt) are occurring co-currently. The copper ions present in the unmodified admiralty brass tube inhibit the biofouling, which results in a fouling factor that is about 5 times less than all the other fouling factors of the other tubes (including the PPF-modified tubes). Bacterial counts confirm this and the pattern of fouling matches closely with a sigmoid curve which is characteristic for biofouling (Nebot *et al.*, 2007). Furthermore, the same PPF that is tested on three different tube alloys experiences the same fouling behavior (within the measurement uncertainty) regardless of which tube alloy it is applied on. Clearly the PPF completely isolates the parent material from contacting the fouling fluid. These results spurred the further development of a PPF featuring biocidal properties as discussed next.

3.11.3 Comparisons between unmodified and PPF-modified tubes' foulant adhesiveness

A method of comparing foulant adhesiveness is required since all condenser tubes will eventually foul. Proper management of the condenser will then necessitate removal of this foulant usually by using one or more of the following means: chemical cleaning, abrasive grit blasting, and high pressure water-jet lancing. The latter is chosen for determining the foulant adherence in the tubes tested during test B.

High pressure water-jet lancing uses a positive displacement pump to force water through a spinning nozzle that creates a whirling jet of high velocity water. This nozzle is guided down the length of the tube using a flexible lance, as the impinging water jet breaks up the foulant before washing it out. Typically cleaning pressures of 200 bar are used, although in cases having very tenacious deposits ultra-high pressures are used between 1 000 bar and 2 500 bar.

Considering the deposit encountered during test B, a relatively low cleaning pressure of 20 bar is used so that multiple passes of the lance are required to clean each test tube. The relative adherence is then easily indicated by comparing the number of passes or dwell time (total time the lance is operating within the entire tube) required to clean the tube as shown in figure 3.26. Cleanliness is readily verified on these tubes by visual inspection as well as mass measurement. The transverse speed of the lance is approximately 60 s per pass. After 8 passes, tubes still not fully clean are then cleaned at 80 bar. Both PPF modified tubes require less than half the time to fully clean the foulant, indicating much better cleanability of the PPFs.

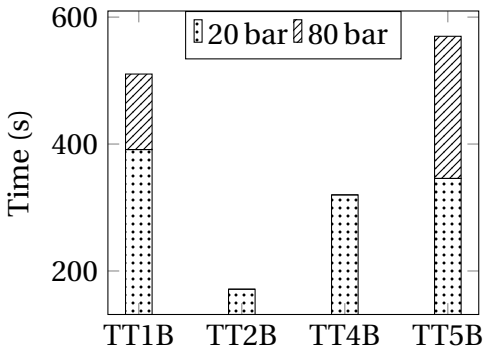

Figure 3.26: Dwell times necessary for removal of foulants on each tube using high pressure water lancing

3.11.4 Test C: biocidal PPFs

Two prototype PPFs are developed with varying amounts of proprietary biocidal fillers added to them: termed type 1 biocidal PPF and type 2 biocidal PPF respectively. Whereas type 1 contains 20 % biocidal filler by weight, type 2 features 50 % biocidal filler. The tube designation is tabulated in table 3.15.

Table 3.15: Tube designation and specifications for test C

Tube	Material	PPF	PPF thickness
TT1C	Duplex stainless steel	Type 1 biocidal PPF*	44 µm
TT2C	Duplex stainless steel	Standard epoxy type PPF	64 µm
TT3B	Admiralty brass	Thermally-enhanced PPF	55 µm
TT4C	Sea-cure®	none	–
TT5C	Sea-cure®	Type 2 biocidal PPF*	65 µm
TT6B	Admiralty brass	none	–

* These two PPFs are prototype coatings (refer back to section 1.4 for coating testing details)

At the start of test C, before fouling has occurred, the friction factors are measured and compared to the theoretical smooth tube values (equation 3.6) for all the new tubes, i.e. TT3B and TT6B are excluded since they are already fouled from test B. Table 3.16 shows good agreement and the pressure drop measurement is repeatable.

Table 3.16: Measured versus theoretical smooth tube friction factors (f_d) measured at the start of test C

Tube	Measured friction factor	Smooth tube friction factor	Difference (%)
TT1C	0.01846	0.01987	-7.13 %
TT2C	0.01816	0.01977	-8.13 %
TT4C	0.01964	0.01972	-0.41 %
TT5C	0.01752	0.01950	-10.18 %

Comparison between the friction factors of the type 1 biocidal PPF-modified and the standard epoxy type PPF-modified duplex stainless steel (figure 3.27 (a)) reveals identical behavior between the two tubes. There is a progressive increase in friction factor. Similar observations are made concerning the two tubes carried over from test B, i.e. unmodified admiralty brass (TT6B) and the (non-biocidal) PPF-modified admiralty brass (TT3B). The explanation for why the tubes from test B, once at asymptotic fouling values, show an increase in fouling during test C is explained by the change in test parameters. The flow rates are set lower in test C, so that the fouling test can be conducted at a mean fluid velocity close to 1.2 m/s compared to the set point in test B of 1.8 m/s.

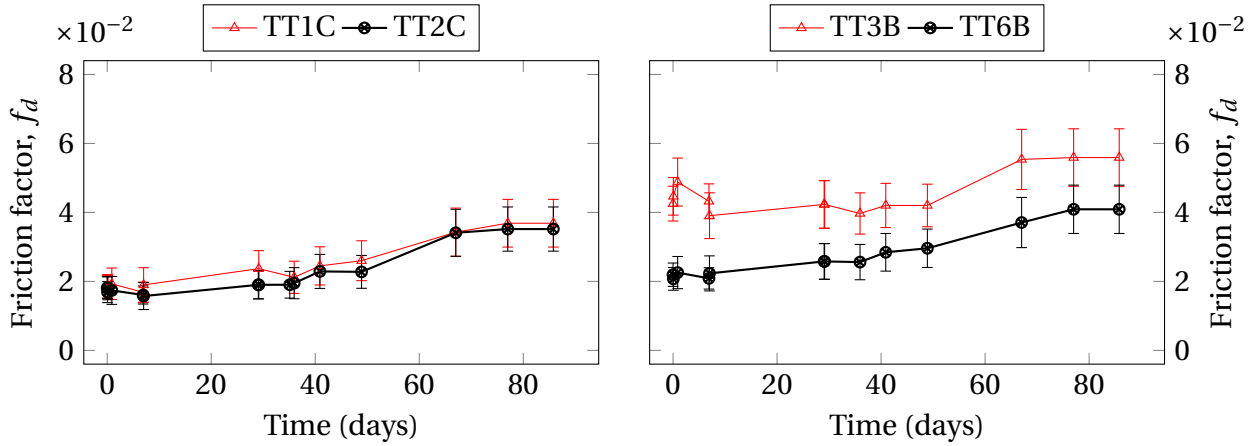

(a) Comparison between type 1 biocidal PPF-modified and standard epoxy type PPF-modified duplex stainless steel

(b) Comparison between admiralty brass and PPF-modified admiralty brass (different y-axis scale)

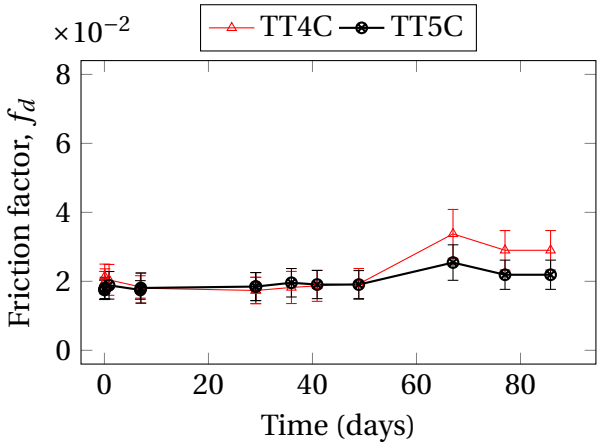

(c) Comparison between un-modified Sea-cure® and type 2 biocidal PPF-modified Sea-cure®

Figure 3.27: Measured friction factors from test C

The lower fouling fluid velocity is chosen to accelerate the test, since a lower bulk fluid velocity has a lower shear stress at the surface which translates into a decrease in the rate of removal of foulant (equation 1.1). Consequently the fouling factors of tubes TT3B and TT6B should be expected to change in accordance with the new fouling fluid velocity and ultimately will reach new asymptotic values. Additionally there is also a change in the mean bulk water temperature of the fouling fluid, which is expounded upon later. Lastly from figure 3.27 (c) the friction factor of the bare Sea-cure® increases more rapidly than the type 2 biocidal PPF-modified tube after day 50.

Analogous to the friction factors, the fouling factors show the same patterns in figure 3.28.

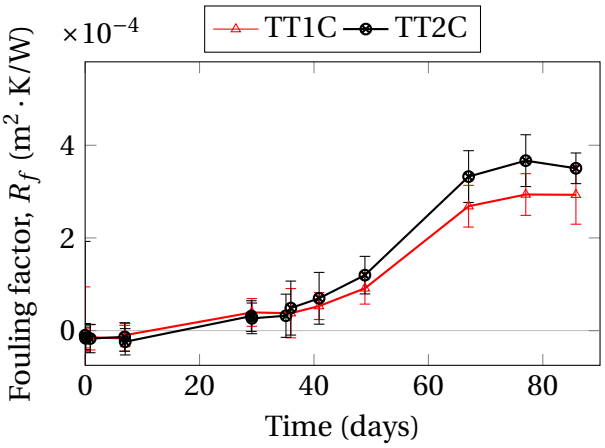

(a) Comparison between type 1 biocidal PPF-modified and standard epoxy type PPF-modified duplex stainless steel

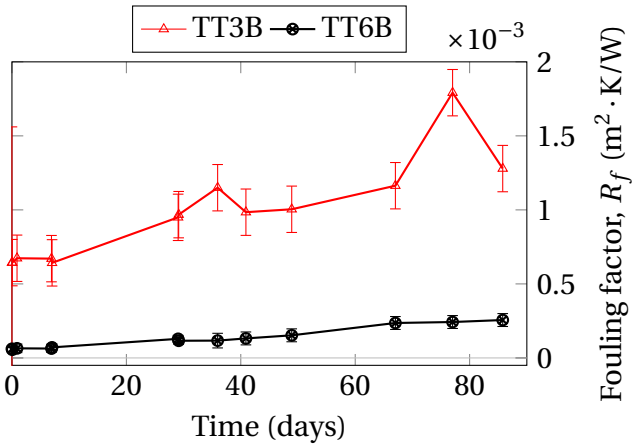

(b) Comparison between admiralty brass and PPF-modified admiralty brass (different y-axis limits)

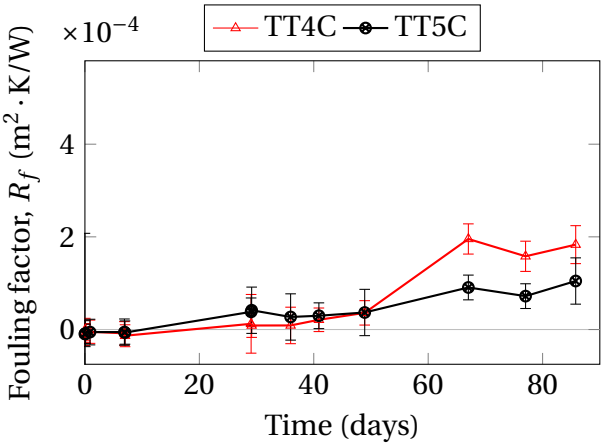

(c) Comparison between un-modified and type 2 biocidal PPF-modified Sea-cure®

Figure 3.28: Measured fouling factors from test C

After 85 days of exposure TT1C and TT2C have fouling factors of 2.930×10^{-4} $m^2 \cdot K/W$ and $3.5023 \times 10^{-4} m^2 \cdot K/W$ respectively. This rate of fouling is similar to that observed in test B after the same exposure time, even though the flow rates in test C were purposefully reduced to accelerate the test. This apparent contradiction may be explained by considering the fact that the average bulk fouling water temperature for test B is 39 °C, whereas the average bulk fouling water temperature for test C is 47 °C. Recalling figure 1.5, it is possible then that this increased bulk water temperature of the fouling fluid slowed the biofilm formation during test C despite the reduced flow rates. Likewise cleanliness factors are shown in figure 3.29.

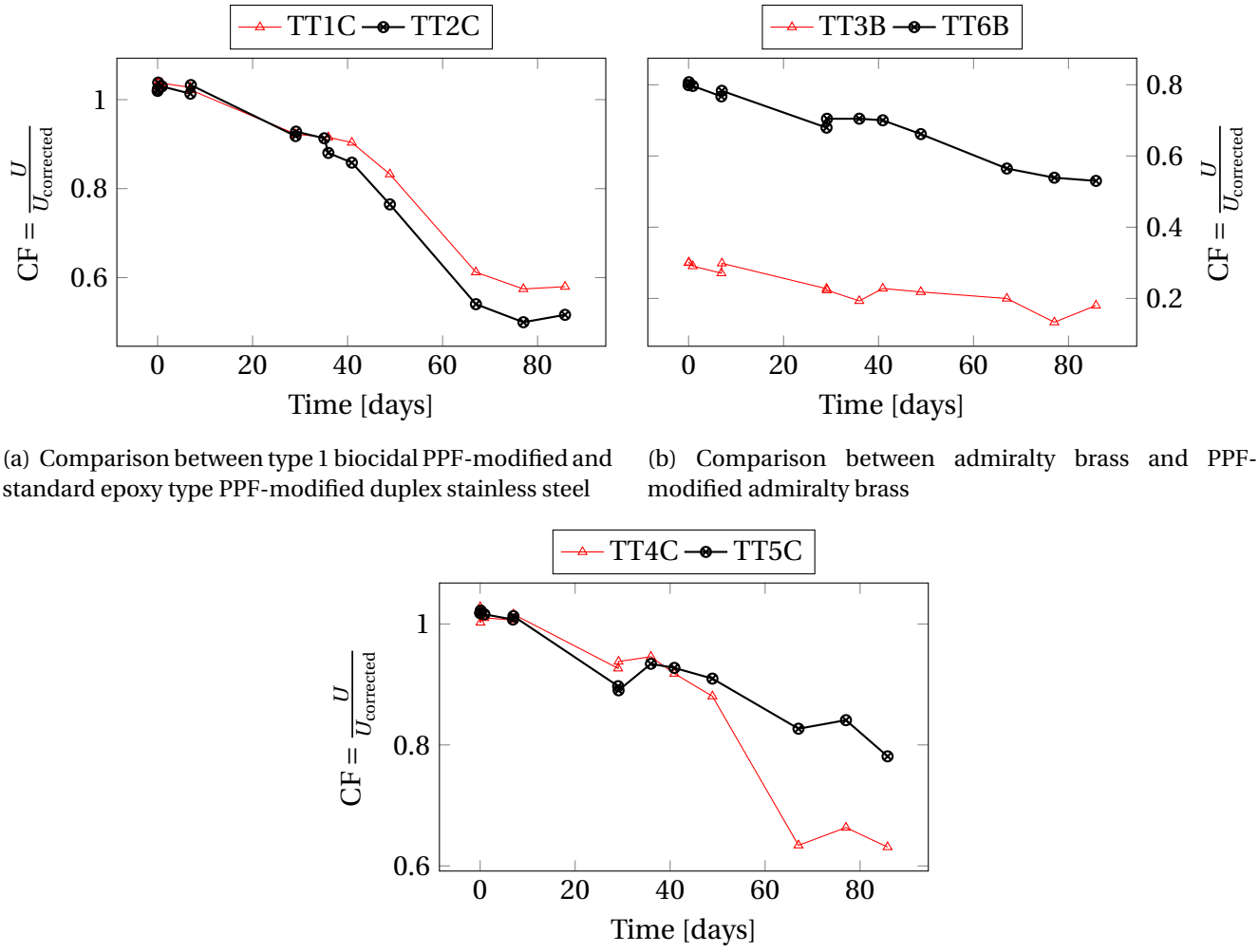

(a) Comparison between type 1 biocidal PPF-modified and standard epoxy type PPF-modified duplex stainless steel

(b) Comparison between admiralty brass and PPF-modified admiralty brass

(c) Comparison between un-modified and type 2 biocidal PPF-modified Sea-cure® and Sea-cure®

Figure 3.29: Cleanliness factor versus time measured during test C

Similar to test B the cleanliness factors are within 5 % of 1.0 at the start of

the test, except for tubes TT3B and TT6B. These tubes have cleanliness factors corresponding to those measured at the end of test B since they are not removed or altered in any way between test B and C. Figure 3.29 (c) shows that the type 2 biocidal PPF-modified Sea-cure® achieves a better performance (cleanliness factor equal to 0.79) than the unmodified Sea-cure® tube (cleanliness factor equal to 0.62) after the same exposure time. This evidence suggests the potential for this coating to retard the biofouling significantly so that it may be used as an antifouling coating rather than purely a means to mitigate corrosion and erosion. However, further development of this coating is required.

3.12 Summary

The water-side composite fouling of several condenser tubes is measured using the apparatus that is designed and built for this project. The following tubes are tested: admiralty brass, duplex stainless steel, Sea-cure® stainless steel, and titanium. Four types of PPFs are applied to these alloys and tested in parallel to identical unmodified control tubes. The first of the PPFs is a thermally enhanced coating that is already being used on existing condensers and the second type of PPF is a standard epoxy coating. The other two PPFs are prototype coatings that are modified with biocidal fillers of varying quantities.

The asymptotic fouling factor of admiralty brass is 9.4×10^{-5} m$^2 \cdot$K/W whereas duplex stainless steel and titanium have fouling factors equal to 4.6×10^{-4} m$^2 \cdot$K/W and 5.4×10^{-4} m$^2 \cdot$K/W respectively. The mean fouling factor measured on the non-biocidal PPF is 5.7×10^{-4} m$^2 \cdot$K/W. Therefore the brass is found to have the best thermal performance as its fouling factor is approximately five times less than these other tubes. The non-biocidal PPF performs the same as the stainless steel and titanium within the measurement uncertainty.

This PPF does however show merit in terms of its clean-ability, i.e. the ease with which the foulant may be removed. This is tested using high-pressure water jet lancing, and the results indicate the PPFs require approximately half the time to clean compared to the stainless steel and titanium tubes in the test.

The large difference in these fouling factors is explained by the influence of biofouling which is found to be the biggest contributor to the fouling factor measured on all the non-copper bearing alloys. This conclusion is drawn from the results of sessile bacterial counts that show the admiralty brass has two orders of magnitude less bacteria after 126 days of exposure. Moreover the fouling data closely fits the sigmoidal curve proposed by Nebot *et al.* (2007) which is archetypal of biofouling. Pressure drop measurements concur with these trends as tubes with the largest fouling have the highest pressure drop and hence friction factors.

One of the biocidal PPF-modified tubes has a lower fouling factor than the stainless steel tube tested alongside it after 85 days of exposure, which indicates the biocide is effective thus far in the development of this prototype coating.

Chapter 4

Relating the experimental results obtained on single test tubes to the actual condenser performance

4.1 Introduction

The apparatus used for the experimental study featured in chapter 3 is installed at a coal-fired thermal power plant. The plant has six generator units that have been in operation for over 35 years. The simplified steam-water power cycle illustrated in figure 4.1 shows the energy transferred from the fuel combusted in the boiler (Q_{fuel}), the power extracted by the turbine (P_{gen}), the heat rejected by the condenser to the cooling water (Q_{cond}), and the power used by the boiler feed pump and auxiliaries ($P_{\text{auxiliary}}$). Design values are indicated with a '+' superscript. Applying the first law of thermodynamics to the cycle means that

$$P_{\text{gen}} - Q_{\text{boiler}} + Q_{\text{cond}} - P_{\text{auxilliary}} = 0 \tag{4.1}$$

When operating in turbine-follow mode the power output from the generator is maintained at its fixed set point by varying the fuel firing rate of the boiler (Putman, 2001). This implies that P_{gen} is constant. For the purposes of this analysis the power requirement of the condensate pumping system is considered constant in relation to the changes in the other energy terms.

The aim of the subsequent analysis is to relate the experimental results obtained on single test tubes (chapter 3) to the actual condenser performance. This is achieved by determining the fouling factor of the condenser and comparing it to the measured values on the single-tube tests. The friction factor is not considered because the pressure drop across the condenser tubes is not readily available and depends heavily on the condenser water box design. Thus the fouling factor is used as a comparative performance measure. In so doing, not only is the experimental data validated, but importantly the effect on plant performance is

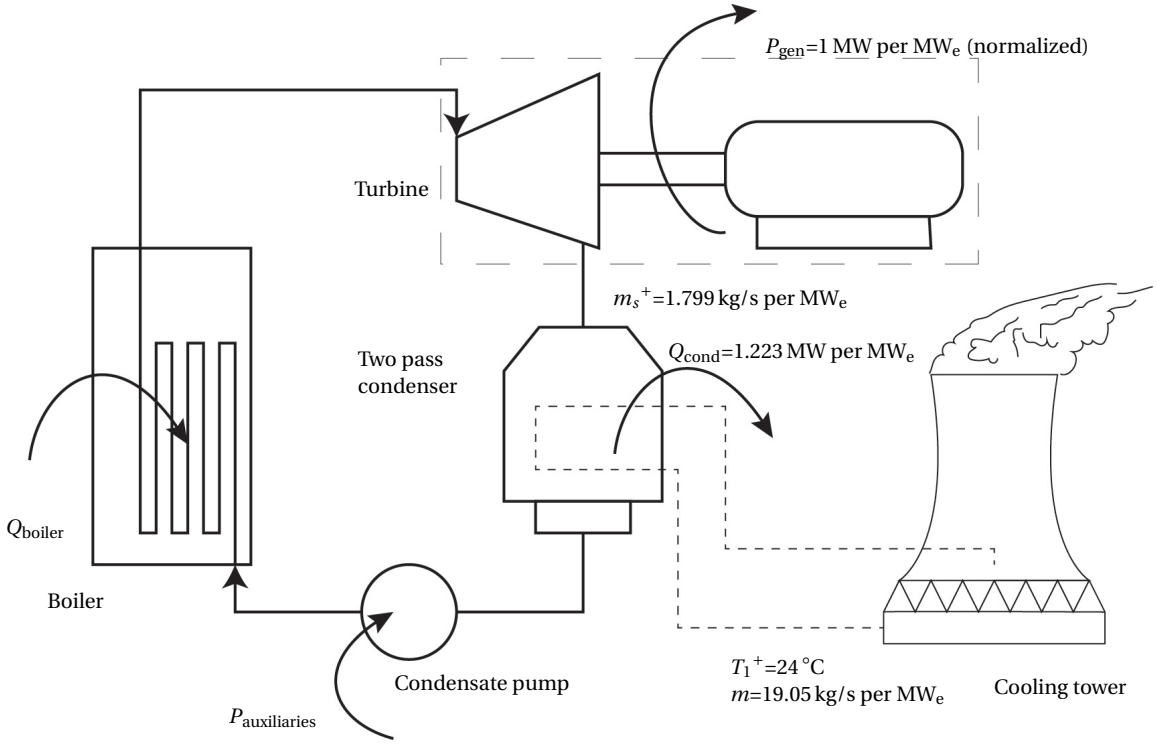

Figure 4.1: Simplified illustration of the steam-water power cycle used by the power plant (design values normalized per 1 MW$_e$)

quantified. Useful tools arise from the fouling model developed herein, which allow plant operators to predict fouling dynamicy on tubes with and without PPFs ultimately aiding their decision making resources.

4.2 Theory for condensation on a single horizontal condenser tube

Much of the analysis presented in the preceding chapter is applicable to condensation on a single horizontal tube, the salient difference arises in determining the outer convection coefficient as discussed next. Consider steam condensing over a single tube at saturation temperature T_s and cooling water entering at T_1 and exiting at T_2. The log mean temperature difference (LMTD) across the tube is

$$\Delta T_{LM} = \frac{T_2 - T_1}{\ln\left(\frac{T_s - T_1}{T_s - T_2}\right)} \tag{4.2}$$

The convection coefficient given by Kröger (1998) for condensation on a sin-

gle isothermal horizontal tube is

$$h_g = 0.728 \left[\frac{g \rho_{\text{con}}^2 i_{fg} {k_l}^3}{\mu_{\text{con}} d_3 (T_s - T_w)} \right]^{1/4} \tag{4.3}$$

where T_s is the steam temperature and T_w is the wall temperature. Condensate properties, subscripted con, are evaluated at the mean film temperature, i.e.

$$T_{mf} = \frac{1}{2}(T_s + T_w) \tag{4.4}$$

With cooling water flowing through the tube, the temperature difference between the condensing steam and the bulk cooling water temperature varies along the length of the tube. However, using an average wall temperature allows the average condensing coefficient to be determined. The overall heat transfer coefficient is thus

$$U = \left(\frac{1}{h_g} + \frac{\ln \frac{d_3}{d_1}}{\frac{2}{d_3} k} + \frac{1}{h \frac{d_2}{d_3}} \right)^{-1} \tag{4.5}$$

where the average wall temperature is estimated according to

$$\frac{T_s - T_w}{T_s - \frac{1}{2}(T_1 + T_2)} = \frac{U}{h_g} \tag{4.6}$$

4.3 Condensation phenomena inside a steam surface condenser

The preceding analysis considers condensation of a pure vapor on a single tube, however a condenser has several thousand tubes bundled together. The implication of the surrounding tubes is that liquid condensate impacts lower tubes as it falls. Often referred to as condensate inundation, this phenomenon greatly reduces the heat transfer across the lower tubes. The falling condensate agglomerates together with the existing film on lower tubes thereby increasing the film thickness and hence thermal resistance.

The steam within the condenser is not a pure vapor – it is a mixture of water vapor and non-condensible gases (predominantly air). These non-condensible gases permeate into the steam system through imperfect joints, cracks and other inevitable perforations (as well as boiler makeup water). The presence of non-condensible gases adversely affects condensation convection as the gases accumulate and increase the partial pressure at the tube-vapor interface. Steam must

then diffuse across the layer of non-condensible gases surrounding the tube before condensing at the surface which effectively adds a thermal resistance to the heat transfer path. Condensers are equipped to vent these non-condensible gases using vacuum pumps or air ejectors. The air removal section is thus located at the coolest area in the bundle (generally the geometric center) and consists of perforated ducting in the steam space that draws off the non-condensible gases using vacuum pumps or air ejectors. Steam flows from the turbine neck down the condenser through the bundles toward the air removal section. As it passes over the tubes, the steam condenses such that by the time the mixture reaches the air removal section it consists of mostly non-condensible gases and only a small fraction of water vapor remains.

The steam flow also tends to shear the condensate film on tubes in areas of higher steam velocity. This enhances the heat transfer by lowering the conduction resistance offered by the condensate film and increasing the convection. All of these effects in the condenser alter the heat transfer coefficient from tube to tube and depend on specific condenser parameters; namely geometry, non-condensible gas concentration, steam flow, and condensing temperature.

4.4 Design performance factor

Condenser designers perform detailed analyses of the aforementioned steam-side effects occurring within the condenser; much of this data is implicitly contained in the design specifications supplied with the condenser. For example, consider the design data stated in table 4.1 describing the condenser. The design condenser duty is calculated using

$$Q_{\text{duty}} = m_s(i_s - i_{\text{con}}) \tag{4.7}$$

where m_s is the steam flow rate, i_s is the incoming steam enthalpy, and i_{con} is the condensate enthalpy. Additional heat duty from the feed water heater and flash box is small in comparison (approximately 0.2 %).

Table 4.1: Design data supplied with the plant condenser

Load MW	Back pressure kPa	Steam flow kg/s	Condenser duty MW
40 %	4.59	118.718	272.4
60 %	5.47	171.964	387.5
80 %	6.49	225.530	501.9
100 %	7.82	285.971	629.8

To reconcile the actual design condenser performance with the single tube correlations, define a performance factor (Putman, 2001) such that:

$$\text{PF} = \frac{h_s}{h_g} \tag{4.8}$$

where h_s is the design steam-side convection coefficient of the condenser and h_g is the effective single-tube condensation coefficient at the same steam temperature. The specific geometry and tube materials are given in table 4.2 and the following assumptions are made:

1. The approach steam quality is assumed to be 0.96.
2. The concentration of non-condensible gases does not vary from the design conditions.
3. The performance factor is only a function of steam flow.
4. Cooling water enters the condenser at 24 °C flowing at 9 800 kg/s.

Table 4.2: Modelling parameters for the plant condenser

Total number of tubes	26 000
Number of tube passes	2
Tube length	12 m
Tube outer diameter	24.00 mm
Original tube material	Admiralty brass, 111 W/(m K), wall thickness: 1.2 mm
Retubed tube material	Duplex stainless steel, 14 W/(m K), wall thickness: 0.7 mm

Consider the design case in table 4.1 of maximum load. The outlet cooling water temperature is then

$$T_2 = \frac{Q_{\text{duty}}}{mc_p} + T_1 = 39.4\,^{\circ}\text{C} \tag{4.9}$$

The saturation steam temperature corresponding to the back pressure of 7.82 kPa is 41.8 °C. The expected overall heat transfer coefficient is

$$U^+ = \frac{Q_{\text{duty}}}{A\Delta T_{\text{LM}}} = \frac{629.8 \times 10^6}{(\pi \times 0.024 \times 12 \times 26000)(7.8929)} = 3\,392\,\text{W/(m}^2\,\text{K)} \tag{4.10}$$

The performance factor is found by iterative solution such that the following is satisfied:

$$\frac{1}{U^+} = \frac{1}{\text{PF}h_g} + \frac{\ln\frac{d_3}{d_1}}{\frac{2}{d_3}k} + \frac{1}{h\frac{d_2}{d_3}} \tag{4.11}$$

where the inner convection coefficient h is calculated using the following modified form of equation (3.12) to account for developing flow (Kröger, 1998):

$$\mathrm{Nu} = \frac{\left(\frac{f_d}{8}\right)(\mathrm{Re}-1000)\,\mathrm{Pr}\left[1+\left(\frac{d}{L}\right)^{0.67}\right]}{1+12.7\left(\frac{f_d}{8}\right)^{0.5}\left(\mathrm{Pr}^{2/3}-1\right)} \tag{4.12}$$

The solution is found to be PF = 0.414. The results for the 40 %, 60 %, and 80 % design loads are plotted together with this result in figure 4.2 as function of steam flow.

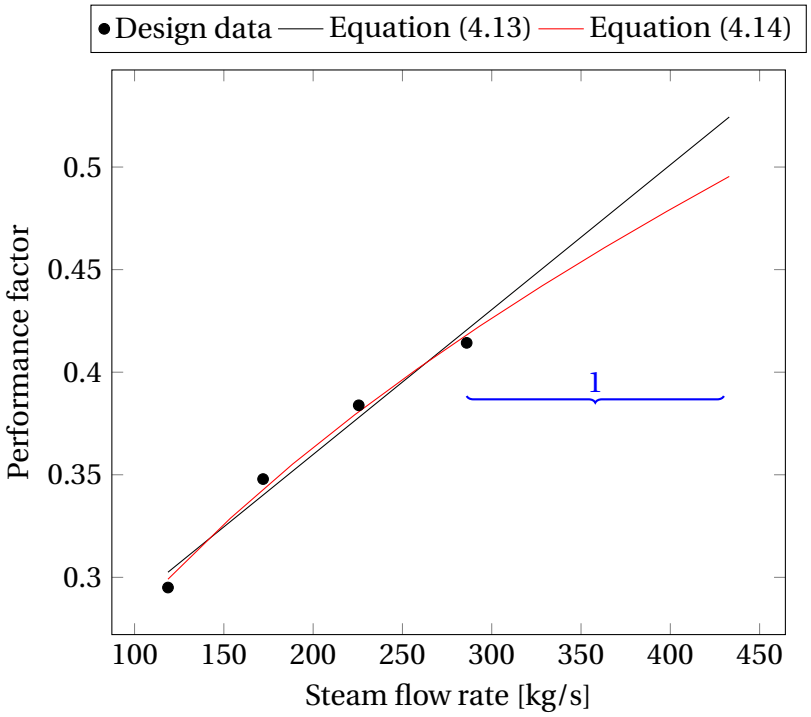

Figure 4.2: Performance factor as a function of steam flow – (1) extrapolated region

Linear regression yields

$$\mathrm{PF} = 0.0007060\,m_s + 0.2186902 \tag{4.13}$$

However the effect of vapor shearing depends on the square root of the vapor velocity. Therefore it is reasonable to assume the performance factor would also vary non-linearly with steam flow rate, i.e. vapor shear velocity. Thus a power fit yields

$$\mathrm{PF} = 0.0198080\,m_s^{0.5} + 0.0832726 \tag{4.14}$$

The region labelled 1 in figure 4.2 is extrapolated since the operational steam flow exceeds the expected maximum design duty condition, as a result of severe fouling of the condenser as will be shown later.

4.5 Actual condenser performance

During the period in which the single tube tests are performed, the following plant measured data is obtained: inlet and outlet water temperatures, the steam flow rate, and the hotwell condensate temperature. Other parameters such as the backpressure are not available. Also the condenser was retubed with a stainless steel alloy (table 4.2) which is taken into consideration. Thence the fouling factor for the condenser is calculated and plotted in figure 4.3 over the last year. Data points where the unit load was less than 60 % load are excluded, which explains for some of the discontinuities in the data. Data above 60 % load ensures the unit load is between the range over which the performance factor is regressed (figure 4.2).

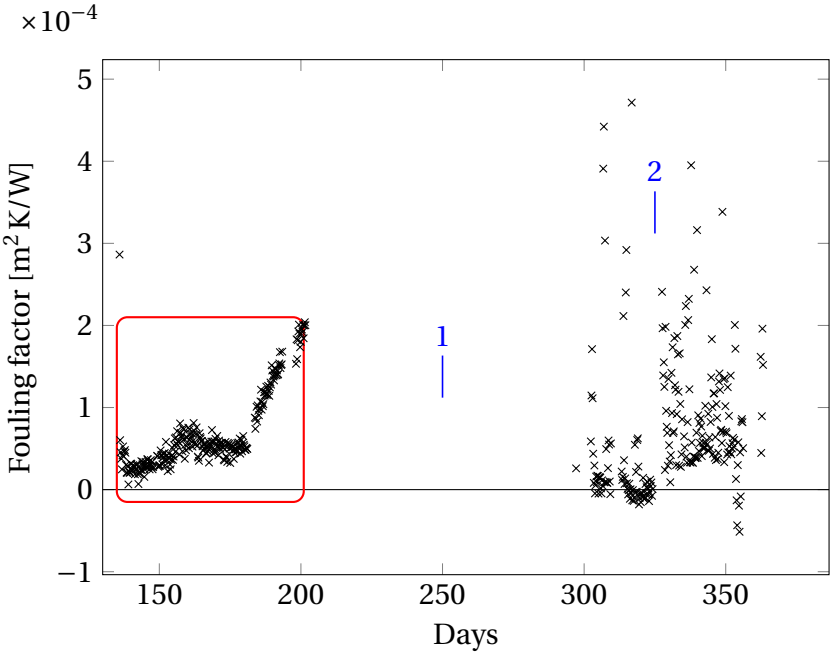

Figure 4.3: Estimated fouling factor of the plant condenser – (1) unit offline for turbine maintenance (2) noise caused by air-ingress (red box shows selected data for model comparison in figure 4.4)

Data between days 136 and 201 is selected for further scrutiny (figure 4.4) because several days before day 136 the unit was shutdown and the condenser was cleaned using high-pressure water-jet lancing. It is presumed that this cleaning removed most, if not all, of the foulant. Therefore this data provides the unique opportunity to compare the following fouling model obtained from single-tube

data from tube TT1B (equation 3.34), with values from table 3.14 in chapter 3):

$$R_f = \frac{0.0004534}{1 + \left(\frac{0.0004534}{0.0000081} - 1\right) \cdot e^{-(105.97289)(0.0004534)t}} = \frac{0.0004534}{1 + 54.975 \cdot e^{-0.04805t}} \tag{4.15}$$

with t in days. Plotting this model over the measured plant data produces figure 4.4.

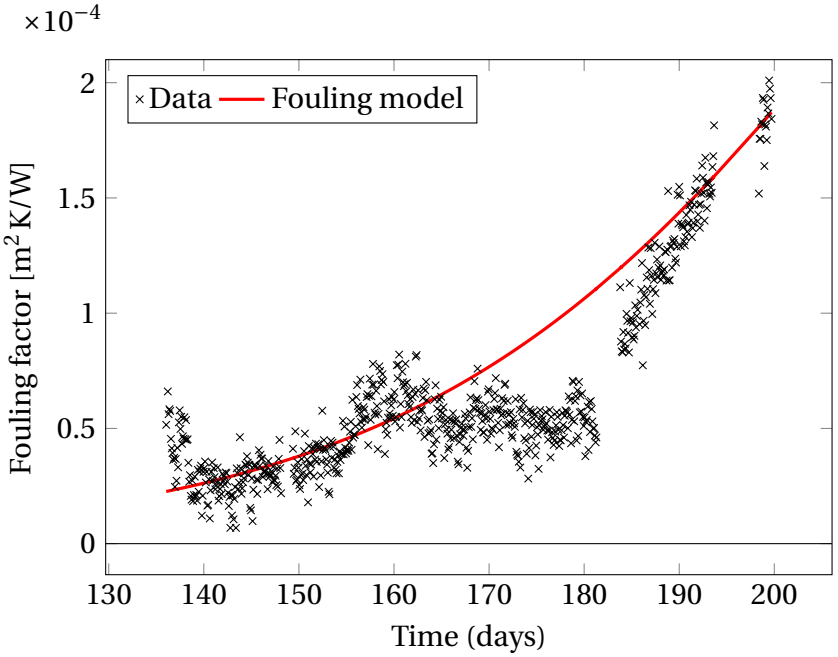

Figure 4.4: Model comparison to actual plant data

Good agreement between the actual condenser data and model is evident, notwithstanding all the fluctuations in operating parameters such as cooling water temperature, load variations, and air-ingress to name a few. The aforementioned method of determining the condenser fouling factor allows direct comparison with the single-tube tests. The fouling model is based on tests performed on a test tube of the same alloy and subjected to exactly the same fouling fluid, so this similarity is expected. In other words, using actual plant cooling water in the apparatus described in chapter 3 allows the dominant fouling mechanism to be replicated in real time and ultimately measured. It would be near impossible to realize such conditions during experiments using apparatuses that are not operated onsite with the fouling fluid. For example, even where fractions of cooling water are transported to offline apparatuses, the biological organisms in the transported water would obviously differ from those in the real fouling fluid. Thence the dominant fouling mechanism may not be directly measurable

in these apparatuses. Moreover point 2 in figure 4.3 shows comparatively a large level of scatter in the fouling factor. This indicates something other than water-side fouling impacting the thermal performance of the condenser, which is most likely the result of air-ingress into the steam space, i.e. the accumulation or ineffective extraction of non-condensible gases from the condenser. Effectively by measuring the waterside fouling in this way, the data can be used to separate the steam-side effects of the condenser from the water-side fouling as shown here.

Next to show the impact of the fouling between days 136 and 201 consider the cleanliness factor plotted in figure 4.5.

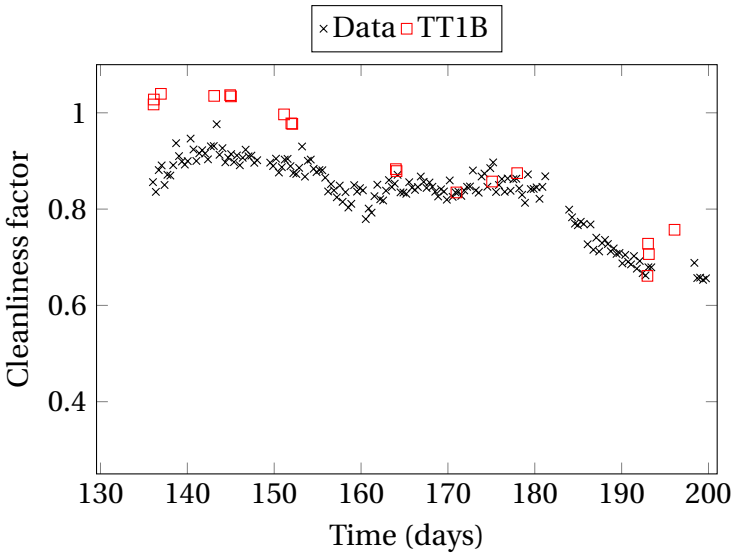

Figure 4.5: Cleanliness factor of the plant condenser compared to test tube TT1B

Initially the cleanliness factor after cleaning is around 0.9; some foulant may have not been removed during the cleaning process. Thereafter the increasing fouling corresponds to a decreasing cleanliness factor until the factor is less than 0.69 within 60 days of operation since cleaning. The condenser cleanliness factor agrees with data from TT1B as indicated in the figure.

4.6 Impact on the condenser performance and PPFs in the condenser life cycle

4.6.1 Parametric analysis comparing fouling of different PPFs on various tube alloys

Now that the actual condenser data has been successfully compared to the single-tube test data, it is necessary to compare all the results on a similar basis. To this effect, a parametric analysis is performed that uses a simple condenser model

(derived in section 4.4). The effect of tube alloy, fouling, and PPF application is parametrically considered by solving the resulting steam temperature (related to the back pressure since the condensation occurs within the vapor dome). The scope of this parametric model is to gain insight into the relative effect on thermal performance and therefore it does not consider the condenser-turbine interaction, although it may readily be extended to include this. Stated differently, the model supposes a constant heat duty, and solves the corresponding steam temperature based on the change in the thermal resistance. This approach will be somewhat conservative since in the real system as the steam temperature rises the condenser duty will also increase.

Using the design data in section 4.1, six cases are considered for three tube alloys: admiralty brass, stainless steel, and titanium.

Case 1. Clean – The fouling factor is set to zero and the model is solved in terms of the three different tube alloys, taking into consideration their differences in thermal conductivity and wall thicknesses. Thinner walls are achievable with stainless steel and titanium since these alloys have higher yield strengths (0.55 mm is assumed for them).

Case 2. Clean + PPF1 – The effective thermal conductivity of the tube-PPF composite is determined using the following

$$\frac{\ln\frac{d_3}{d_1}}{2\pi k_{\text{eff}} L} = \frac{\ln\frac{d_3}{d_2}}{2\pi k_t L} + \frac{\ln\frac{d_2}{d_1}}{2\pi k_{\text{PPF}} L} \tag{4.16}$$

where k_{eff} is the effective conductivity of the tube-PPF composite, k_t is the thermal conductivity of the tube, and k_{PPF} is the thermal conductivity of the PPF. In this case the conductivity of the thermally-enhanced PPF (non-biocidal) is used from test B of the experimentation (see table 3.7). A coating thickness of 50 µm is used.

Case 3. Clean + PPF2 – The effective thermal conductivity is equal to that of the type 2 prototype biocial PPF in test C of the experimentation (see table 3.7), and a coating thickness of 50 µm is used.

Case 4. Fouled – The same as case 1. except the fouling factor is included using the asymptotic values obtained in chapter 3.

Case 5. Fouled + PPF1 – The same as case 2 except the fouling factor is included.

Case 6. Fouled + PPF2 – The same as case 3 except the fouling factor is included

The input values used in the parametric analysis are given in table 4.3. The fouling factors in the table refer to the asymptotic values obtained in chapter 3.

Figure 4.6 summarizes the results. Case 1 shows that all the clean results are within 1 °C of the design condition (clean admiralty brass). The lower conductivities of the stainless steel and titanium alloys are slightly offset by the reduced

wall thickness. Consequently there is only a slight increase in steam temperature.

Table 4.3: Input values used in the parametric model

Input		Value		Unit
Tube outer diameter		24		mm
Tube length		12		m
PPF thickness		50		µm
Non-biocidal PPF conductivity		1.2		W/(m K)
Biocidal PPF conductivity		1.0		W/(m K)
Non-biocidal PPF fouling factor		6.48×10^{-4}		m^2 K/W
Biocidal PPF fouling factor		9.50×10^{-5}		m^2 K/W
Approach steam quality		0.96		
Cooling water inlet temperature		24		°C
Cooling water mass flow		9800		kg/s
Condenser duty		629.8		MW
Tube	Admiralty brass	Stainless steel	Titanium	
Tube wall thickness	1.2	0.55	0.55	mm
Tube conductivity	111	16	22	W/(m K)
Unmodified fouling factor	9.16×10^{-5}	4.53×10^{-4}	5.42×10^{-4}	m^2 K/W

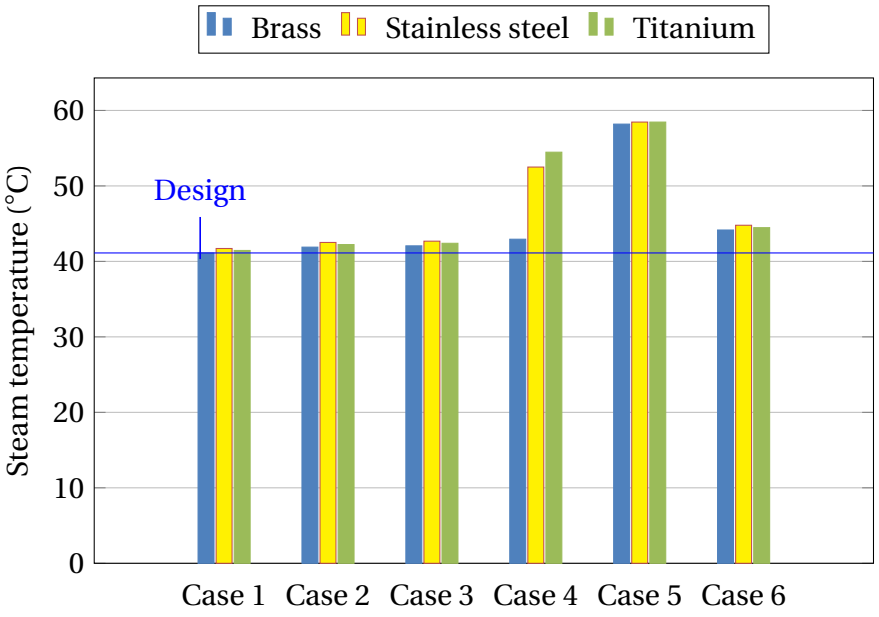

Figure 4.6: Comparison of the expected steam temperature for various tube options

Cases 2 and 3 show a further slight increase in the steam temperature, that is about 1 °C above the unmodified tube. This is because both PPFs are designed to be applied very thinly and their thermal performance is enhanced by careful selection and addition of fillers.

Case 4 shows an increase in steam surface temperature of about 1.8 °C for the admiralty brass but a significant increase of nearly 13 °C for the stainless steel and titanium. The toxicity of the copper ions in the brass means that this alloy resists the biofouling better than the other two alloys, which are dominated by the biofouling. In reality such high steam temperatures may be intolerable and necessitate derating the turbine. Furthermore this value is very close to the hotwell temperature recorded by the plant over the previously discussed period, shown in figure 4.7.

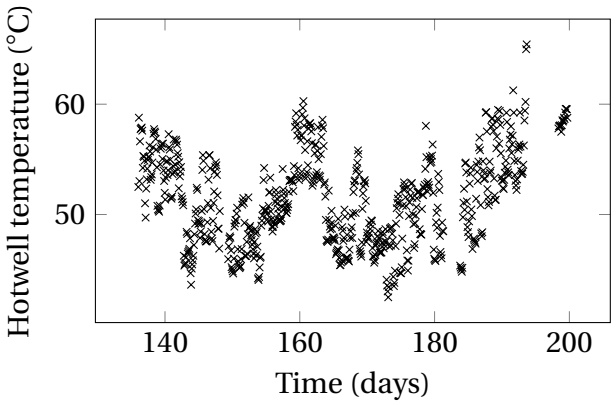

Figure 4.7: Measured hotwell temperature

Similar results are encountered for the non-biocidal PPF in case 5. The effect of the biocide in the PPF in case 6 is substantial. Here it is seen that all the tubes with the type 2 biocidal PPF behave similarly to the admiralty brass as a result of the inhibition of the biofilm formation. These illustratory results point to the significance that composite fouling can have on condenser performance, and moreover they show how critical it is to first understand the fouling mechanisms taking place before the PPF can be chosen.

4.6.2 Considerations of when to apply PPFs in the condenser life cyle

To establish when to use PPFs in the condenser life cycle, the preceding results have demonstrated that an investigation into the major fouling mechanisms is required. Such an investigation must be based on the exact fouling fluid for a particular condenser, for example using an onsite apparatus to measure the fouling (as is performed in this study). In particular this research is focused on new

tubes, and therefore is applicable to designers of new condensers or operators considering retubing an existing condenser.

If biofouling prevails as the predominant fouling mechanism there are several considerations that must be taken into account as shown in figure 4.8.

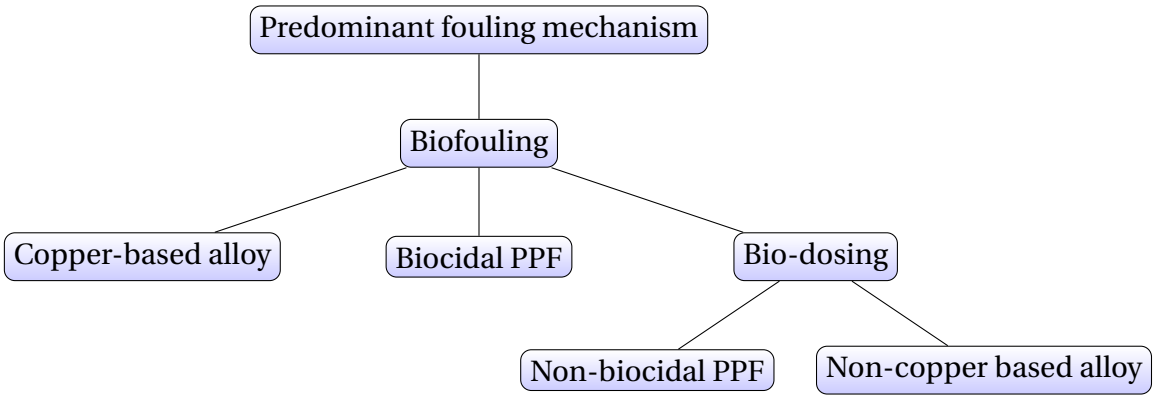

Figure 4.8: Decision tree for when to apply PPFs in the condenser life cycle

Firstly copper-based alloys without any PPFs should be considered. For example the inherent biocidal property of admiralty brass shows significant improvements in terms of biofouling mitigation as depicted in figure 4.6 (case 4). It must be noted that condensate corrosion must also be taken into account. Excessive levels of ammonia in the condensate (usually introduced into the boiler feed water as oxygen scavengers) can lead to premature failure of brasses by one such condensate corrosion mechanism known as ammonia grooving. The ammonia concentrations will depend on the condenser bundle design, non-condensible gas-removal efficiency, and condensate quality management. Brasses such as admiralty brass are susceptible to this type of corrosion of their outer surface, particularly in regions where ammonia concentrations in the condensate are highest, i.e. in and around the air extraction zone. In such cases brasses containing nickel, such as 90-10 copper-nickel brass, are better options since they have far greater resistance to this form of corrosion.

Secondly if a PPF is opted for instead, the results of this study highlight the importance of ensuring the selected PPF has sufficient biocidal action to combat intolerable levels of biofilm formation. In chapter 3 it is observed that application of a non-biocidal PPF to admiralty brass negated the toxicity of the brass thereby causing a larger fouling factor to ensue when biofouling dominates the fouling. The selected biocidal PPF must also meet the coating requirements (such as those given in section 1.4) to maintain structural integrity of the coating in service. Moreover, the thickness of the PPF and its thermal conductivity must be carefully controlled (Goodenough, 2013). If these conditions are met, then such a biocidal PPF can be considered as a viable option for application on new

tubes. The reason for this is that the initial thermal conductance penalty of applying the PPF is overshadowed by its long term performance provided the PPF limits the biofouling significantly. The type 2 biocidal PPF in chapter 3 shows this, although this PPF is still under development.

Thirdly the water treatment must be updated to work synergistically with the selected PPF or non-copper based alloy (figure 4.8). For example, bio-dosing with chlorine (one of the many ways of dealing with biofouling) can be implemented and / or increased since PPFs and certainly titanium are immune to high concentration levels of chlorides (this is not true for certain stainless steels that suffer from pitting corrosion when subjected to high chloride ion concentrations).

Otherwise PPFs can also be considered later in the condenser life cycle particularly to extend the lifespan of weathered tubes suffering from damage mechanisms such as corrosion and erosion. In such circumstances it may make economic sense to apply PPFs to extend the lifespan of ailing tubes until a retube becomes possible or other measures can be put in place such as water treatment upgrades, but the above mentioned considerations are still applicable.

Ultimately all these considerations are organized into the overall combined cost (capital plus operating costs). By way of example, this study demonstrates the significance of the performance losses due to biofouling and thence any PPF used in the condenser tube life cycle must account for this.

4.7 Summary

The actual fouling factor of a condenser is calculated using plant measured data including: inlet and outlet water temperatures, the steam flow, and hotwell condensate temperature. The overall heat transfer coefficient is determined by dividing the condenser duty but the product of the outer surface area and log mean temperature difference. Then the fouling factor can be found by subtracting the inverse of the overall heat transfer coefficient of the fouled condenser from the inverse of the calculated overall heat transfer coefficient of the same condenser in its unfouled state.

The unfouled overall heat transfer coefficient is calculated using the thermal resistance method, and a performance factor derived from the condenser design data. The performance factor accounts for steam-side phenomena, which influence the condensation convection, such as condensate inundation, vapor shearing, and the presence of non-condensible gases. The steam-side condensation convection coefficient is then the product of the performance factor and the single-tube condensation convection coefficient (calculated from literature correlations). The performance factor is regressed as a function of steam flow.

Data over a 60 day period is used to calculate the fouling factor and compared to the fouling model derived from experimental data on a single tube. The comparison of the fouling factor is within 10 % and the model is effective in separating the water-side fouling from the overall heat transfer coefficient of the

condenser. The impact of composite fouling is significant. Within 60 days the condenser cleanliness factor is less than 0.69, well below its design value.

A parametric study of three tube alloys with and without PPFs is performed to reveal the relative condenser performance impact of the different tube options in terms of fouling. The fouling factors measured in the previous chapter indicate that fouling has a significant effect on heat transfer resistance and particularly the biofouling characteristics of any tube-alloy-PPF combination are paramount in condenser performance. Considerations for PPF selection are discussed particularly for new tube applications.

Chapter 5

Conclusions and recommendations

5.1 Conclusions

A self-contained test apparatus is designed, built and installed at a power plant to simulate the water-side conditions experienced within actual steam surface condensers as closely as possible. The purpose of this apparatus is to replicate these conditions so that the dynamic effects of fouling, erosion and corrosion on tubes modified with paint-based protective films (PPFs) can be studied over time. The objectives of this project, stated in chapter 1, are reproduced here so that the conclusions can be suitably compared:

1. design, build, and operate an experimental testing facility at a power station, which is used to investigate fouling deposition and conditions inside condenser tubes with and without PPFs and evaluate their performance;
2. use this apparatus to gain a better understanding of the actual conditions condenser tubes experience in terms of combined fouling, erosion, and corrosion;
3. determine the time when PPFs should be applied within the condenser life cycle, by:
    a) investigating whether they can effectively reduce fouling, whilst mitigating corrosion, on several representative condenser tube materials, such as: admiralty brass, stainless steel, and titanium;
    b) comparing the relative performance over time of these tubes with and without PPFs ;
    c) validate these tests on single tubes with actual condenser data.

5.1.1 Objective 1

The apparatus is installed on an actual thermal power plant, with an open recirculating fresh-water cooling system. Fouling water from this cooling system is

tapped directly from the duct leading from the steam surface condenser outlet to the cooling tower. The apparatus is designed to simulate condensing steam on the outside of each of the six test tubes using heated potable water.

24 kW of direct electrical heating is used to heat the potable water to between 45 °C to 55 °C (depending on the temperature of the fouling fluid), which is then pumped through the annuli of six double-pipe heat exchangers. Repeatable convective heat transfer conditions are thus achievable and compare within ± 20 % of theoretical predictions; the differences are attributed to developing flow caused by edge effects of the heat exchangers.

The fouling water is distributed evenly through the inside of each test tube using purpose-built manifolds and diaphragm control valves. A total of 24 bulk fluid temperatures, 12 volumetric flow rates, and 6 static pressure drop measurements are recorded and used to measure the composite fouling on each test tube. Tubes are tested in pairs, that is to say one PPF-modified tube adjacent to a bare tube of the same alloy, so that plant operational fluctuations such as fluid temperature, bulk foulant concentrations, etc. are accounted for by the relative comparison to the control tube. The real-time relative performance of these tube pairs offers direct feedback on the condenser fouling phenomena.

5.1.2 Objective 2

Biological microfouling is found to be the most significant contributing mechanism to the thermal performance degradation of all the non-copper bearing alloy tubes. The stainless steel, titanium, and non-biocidal PPF modified tubes lack copper ions which would otherwise inhibit bacterial cellular respiration. The effect on thermal performance resulting from this biofouling, compounded by particulate and precipitation fouling, is considerable: the design allowance for fouling of the condenser is quickly exceeded after about 100 days of exposure. The asymptotic fouling factors measured on the non-copper tubes are about 5 times greater than that of admiralty brass. Analysis of bacterial swabs collected at the outlet of each test tube confirm this. The sessile bacterial counts, after 126 days of exposure, are 20 times higher on the stainless steel, titanium, and non-biocidal PPF modified tubes than the admiralty brass tube.

Mineralogical analysis of the foulant layer after testing reveals the majority of inorganic content to be calcium and magnesium scale, and to a lesser extent silicate scale. Particulate deposition of silt is also noted. Over the test duration no signs of corrosion or erosion are observed.

5.1.3 Objective 3

The thermally-enhanced PPF tested in this study that does not contain any biocidal agent, suffers from composite fouling, especially dominated by biological fouling, in an almost identical fashion to the stainless steel and titanium tubes tested. The result on performance is pronounced as a result of this fouling. And

for all the non-copper bearing tubes as well as the non-biocidal PPF-modified tubes the cleanliness factors are seen to decrease to around 0.4 after 185 days exposure. In comparison the admiralty brass tube has a cleanliness factor close to 0.8 in the same test. There are no signs of corrosion or erosion on neither the admiralty brass tubes, stainless steel tubes, titanium tubes, nor the non-biocidal PPF-modified tubes, as checked by visual inspection (for the admiralty brass) and electron scanning micrography.

The biocidal PPF-modified tube tested in a subsequent test shows the potential to resist the biofouling when compared to an unmodified stainless steel tube. Specifically after 85 days of exposure, the biocidal PPF has a cleanliness factor of 0.78 whereas the unmodified stainless steel has a cleanliness factor of 0.63. However, this is a prototype PPF and is currently undergoing further testing to determine its longevity.

A one-dimensional model is constructed based on the design data of the condenser at the power plant where the testing is performed. A design performance factor is calculated and then used to discount the single tube condensation correlations to better represent the actual condensation convection coefficient within the condenser that accounts for steam-side phenomena. Using the thermal resistance method of analysis this performance factor is used to calculate the actual fouling factor of the plant condenser following a cleaning operation performed on the condenser. The actual fouling factor of the condenser compares favorably to within about 10 % of the measured fouling factor obtained for the same tube alloy during single-tube tests. This model is further used to consider a parametric study of three tube alloys with and without PPFs to reveal the relative performance impact of the different tube options in terms of fouling. The fouling effects of composite fouling has a significant impact on the heat transfer resistance. In particular the biofouling characteristics of any tube-alloy-PPF combination are paramount in condenser performance.

As for the time when PPFs should be applied, these results indicate that the non-biocial PPF should not be applied to new tubes, or structurally intact tubes at this particular plant, because of the overwhelming influence of biofouling. It may be reserved for use as a short-term life extension when structural degradation of the tubes is imminent, and thereby prevent tube leaks from occurring. Alternatively, if the plant is able to implement effective biofouling control measures in the water treatment process, these PPFs can be reconsidered because of their good clean-ability properties. The same considerations are true for the installation of the other non-copper bearing alloy tubes. If the biocidal PPF successfully passes the required coating property tests, and continues to resist biofouling for a sustained period, this PPF may very well be considered for application onto new tubes such as stainless steel or titanium to be used in similar situations where biofouling prevails.

5.2 Recommendations

When choosing PPFs and new tube materials it is vital to research the fouling mechanisms present at the site (which have likely changed from the design values). It is also necessary to update the water chemistry management and cleaning regimes according to the PPF / tube material combination. The experimental procedures in this study have been shown to be an effective means of doing this. Particularly the complexity of biofouling together with its significant impact on thermal performance degradation, necessitates using the actual plant fouling fluid in such tests. Parallel testing of tubes also reduces uncertainties arising from changes in fouling fluid parameters such as temperature and foulant concentrations.

Research must now focus on developing PPFs which resist biological fouling. PPFs that provide antifouling properties rather than purely anti-corrosive properties are going to be highly sought after. Lastly when replacing copper-bearing alloys with PPF-modified tubes as well as corrosion-resistant alloys such as stainless steel or titanium, it is paramount that water management and fouling mitigation measures are accordingly re-designed to suit these PPFs and tube alloys. Economic comparisons between tubes of different alloys, with and without PPFs, should not only include the capital costs but importantly the operational costs must be included. The results herein have demonstrated by way of example the major impact on performance caused by biofouling that far outweighs the initial estimates of clean performance. These performance measurements should be calculated using experimental assays using the exact fouling fluid similar to the onsite technique conducted in this study.

List of references

Al-Otaibi, D. 2008. *Scale deposition on coated carbon steel and Titanium surfaces*. Lambert Academic Publishing.

ASME. 2010. PTC 12.2-2010, Steam surface condensers, performance test codes. Technical Report, American Society of Mechanical Engineers.

ASTM D4778-15. 2015. *Standard Test Method for Determination of Corrosion and Fouling Tendency of Cooling Water Under Heat Transfer Conditions*. ASTM International, West Conshohocken, PA, 2015.

ASTM D870-02. 2002. *Standard Practice for Testing Water Resistance of Coatings Using Water Immersion*. ASTM International, West Conshohocken, PA.

Awad, M.M., El-Wahab, I.F.A. & Gad, H.E. 2007. Effect of surface temperature on the fouling of heat transfer surfaces. In *Eleventh Internataional Water Technology Conference*. Sharm El-Sheikh, Egypt.

Balaraju, J., Narayanan, T.S. & Seshadri, S. 2003. Electroless ni-p composite coatings. *Journal of applied electrochemistry*, 33(9):807–816.

Bhatt, S.M. 2006. Effect of water side deposits on the energy performance of coal fired thermal power plants. *Energy Conversion and Management*, 47(9-10):1247–1263. Available at: `http://dx.doi.org/10.1016/j.enconman.2005.07.002`

Bhatti, M.S. & Shah, R.K. 1987. Turbulent and transition flow convective heat transfer. In S. Kakac, R.K. Shah & W. Aung (eds.), *Handbook of Single-Phase Convective Heat Transfer*. New York, USA: Wiley.

Bott, T.R. 1995. Fouling of heat exchangers. In *Chemical engineering monographs 26*, pages 247, 248. Elsevier.

Casanueva, J., Snchez, J., Garca-Morales, J., Casanueva-Robles, T., Lpez, J., Portela, J., Nebot, E. & Sales, D. 2003. Portable pilot plant for evaluating marine biofouling growth and control in heat exchangers-condensers. *Water Science & Technology*, 47(5):99–104.

Cengel, A.Y. & Ghajar, A. 2011. *Heat and Mass Transfer Fundamentals and Applications*. New York: McGraw Hill.

Characklis, W. & Marshall, K. 1990. *Biofilms*. Number v. 1 in Wiley Series in Ecological and Applied Microbiology. Wiley. ISBN 9780471826637. Available at: `https://books.google.co.za/books?id=soAXAQAAIAAJ`

Characklis, W.G. 1981. *Microbial fouling: a process analysis*, chapter Microbial fouling, pages 251–291. Hemisphere Publishing Corporation.

Characklis, W.G., Nevimons, M.J. & Picologlou, B.F. 1981. Influence of fouling biofilms on heat transfer. *Heat transfer engineering*, 3(1):23–37. DOI: 10.1080/01457638108939572.

Cho, Y.I., Kim, W. & Kim, D. 2006. Fouling mitigation in a heat exchanger: High cycles of concentration for a Cooling-Tower application. *Experimental Heat Transfer*, 19(2):113–128.
Available at: http://dx.doi.org/10.1080/08916150500479372

Coleman, H.W. & Steele, W.G. 2009. *Experimentation, Validation, and Uncertainty Analysis for Engineers*. 3rd edition. Hoboken, New Jersey: John Wiley and Sons, Inc.

Curran, E.L. 2009. Solving heat exchanger tube problems with thin film thermally conductive coating applications and novel tube and pipe cleaning as a precursor to coating application and NDT. In H. Müller-Steinhagen, M.R. Malayeri & A.P. Watkinson (eds.), *Proceedings of international conference on heat exchanger fouling and cleaning VIII*. Schaldming, Austria.

Davis, J.R. 2001. Copper and copper alloys. In *ASM Specialty Handbook*. ASM International.

Department of Water Affairs and Forestry (DWAF). 2006. Integrated water quality management plan for the vaal river system: Task 2: Water quality status assessment of the vaal river system. directorate national water resources planning. Department of Water Affairs and Forestry, Pretoria.

Department of Water Affairs (DWA). 2009. Adopt-a-river programme phase ii: Development of an implementation plan. water resource quality situation assessment. Prepared by H. Hendriks and J. N. Rossouw for Department of Water Affairs, Pretoria, South Africa.

Dirker, J. & Meyer, J.P. 2005. Convective heat transfer coefficients in concentric annuli. *Heat Transfer Engineering*, 26(2):38–44.

Epstein, N. 1981. *Fouling: technical aspects (afterward to fouling in heat exchangers)*, chapter Opening session, pages 31–53. Hemisphere publishing corporation.

Epstein, N. 1983. Thinking about heat transfer fouling: A 5 x 5 matrix. *Heat Transfer Engineering*, 4(1):43–56.
Available at: http://dx.doi.org/10.1080/01457638108939594

ESEERCO. 1987. Condenser tube coatings and inserts evaluation. Technical Report R. P. EP85-26, Stone & Webster Engineering Corporation.

Fan, S. & Zhong, Q. 2013. Prediction of fouling in condenser based on fuzzy stage identification and chebyshev neural network. *Measurement Science Review*, 13(2):94–99.
Available at: http://dx.doi.org/10.2478/msr-2013-0017

Fraze, R.O. & Woodruff, B.N. 1997. In-situ coating of condenser tubes as an alternative to retubing. Technical Report TR-107068, Electrical Power Research Institute, Palo Alto, California.

Fulford, J., Schutz, R. & Lisenbey, R. 1987. Characterization of titanium condenser tube hydriding at two florida power and light company plants. In *Joint ASME/IEEE Power Generation Conference. Miami Beach, Florida*.

Garey, J.F. 1997. On-line condenser fouling monitor development. Final report 109232, Bridger Scientific, Inc., Sandwich, Massachusetts. Prepared for Electric Power Research Institute.

Gawlik, K., Sugama, T., R., W. & Reams, W. 1998. Field testing of heat exchanger tube coatings. In *Geothermal resources council*. National renewable energy laboratory.

Gnielinski, V. 2009. Heat transfer coefficients for turbulent flow in concentric annular ducts. *Heat Transfer Engineering*, 30(6):431–436.

Goodenough, J. & Reuter, H. 2014. Performance characteristics of artificial coatings applied to steam surface condensers. *International Journal of Thermal Sciences*, 85:123–137.
Available at: `http://dx.doi.org/10.1016/j.ijthermalsci.2014.06.020`

Goodenough, J.L. 2013. Thermal performance evaluation of artificial protective coatings applied to steam surface condenser tubes. Master's thesis, Stellenbosch University.

Goodfellow Cambridge Ltd. 2013. Available: `http://www.goodfellow.com/E/Brass'.html`, [2013, August 22].

Hager, M., Mussalli, Y. & Tsou, J. 1988. Tube coatings for condensers and heat exchangers. In R. Coit (ed.), *Condenser Technology Symposium*, CS-5942-SR.

Heat Exchange Institute. 2012. *Standards for steam surface condensers*. Heat Exchange Institute (HEI), Cleveland, Ohio, 11th edition.

Honing, W. & Kröger, D.G. 2006. Thermal-flow characteristics of condenser tubes. Confidential report to Eskom, ITM/DGK/23/01/06, Stellenbosch University: Institute for Thermodynamics and Mechanics.

Horn, M.J. & Mitchell, J.E. 2002. The use of 100% solids epoxy coatings for full length condenser tube linings. In *Condenser Technology: Seminar and conference*, 1004116. Palo Alto, CA: EPRI.

Horn, M.J. & Mitchell, J.E. 2005. New developments in condenser tube coatings. In *Condenser Technology Conference*, TR-1010322, pages 429–436. Electrical Power Research Institute (EPRI).

Horn, M.J. & Woodruff, B.N. 1996. Condenser tube coatings as a means of extension and performance enhancement. In J.L. Tsou & Y.G. Mussalli (eds.), *Proceedings: condenser technology conference*, TR-1-6781. Electrical Power Research Institute.

IHS ESDU. 2008. Fouling in cooling systems using fresh water. Technical Report ESDU 08002, UK.

Incropera, F.P., Dewitt, D.P., Bergman, T.L. & Lavine, A.S. 2007. *Introduction to Heat Transfer*. 5th edition. United States of America: Wiley.

Izadi, M., Aidun, D., Marzocca, P. & Lee, H. 2011. Integrated experimental investigation of seawater composite fouling effect on the 90/10 Cu/Ni tube. *Applied Thermal Engineering*, 31(14-15):2464–2473.
Available at: `http://dx.doi.org/10.1016/j.applthermaleng.2011.04.012`

Kern, D.Q. & Seaton, R.E. 1959. A theoretical analysis of thermal surface fouling. *British Chemical Engineering*, 4:258–262.

Knudsen, J.G. 1981. Apparatus and techniques for measurement of fouling of heat transfer surfaces. In E.F.C. Somerscales & J.G. Knudsen (eds.), *Fouling of heat transfer equipment*, chapter Experimental Methods, pages 57–81. Hemisphere publishing corporation.

Konak, A.R. 1973. Prediction of fouling curves in heat transfer equipement. *Transactions of Institute Chemical Engineers*, 51:377.

Kröger, D.G. 1998. *Air-cooled Heat Exchangers and Cooling Towers: Thermal-flow performance evaluation and design*. Stellenbosch University: Department of Mechanical Engineering.

Kukulka, D.J. & Leising, P. 2010. Evaluation of heat exchanger surface coatings. *Applied Thermal Engineering*, 30(16):2333–2338.
Available at: `http://dx.doi.org/10.1016/j.applthermaleng.2009.12.013`

Lakshmi, B.V., Subrahmanyam, T., Rao, V.D. & Sharma, K.V. 2011. Turbulent film condensation of pure vapors flowing normal to a horizontal condenser tube - constant heat flux at the wall. *International Journal of Automotive and Mechanical Engineering*, 4:455–470.

Langelier, W.F. 1936. The analytical control of anti-corrosion water treatment. *Journal of American Water Works Association*, 28(10):1500–1521.

Lienhard, IV, J.H. & Lienhard, V, J.H. 2008. A heat transfer textbook. Phlogiston Press, Cambridge, Massachusetts, U.S.A.

Maurer, J.R. & Franson, I.A. 1988. Stainless steels: three decades of corrosion performance in steam surface condenser applications. In R. Coit (ed.), *Proceedings: condenser technology symposium*, CS-5942-SR.

McAllister, R.A., Eastham, D.H., Dougharty, N.A. & Hollier, M. 1961. A study of scaling and corrosion in condenser tubes exposed to river water. *Corrosion*, 17:579t–588t.

Michels, H.T., Kirk, W.W. & Tuthill, A.H. 1979. The influence of corrosion and fouling on steam condenser performance. *Journal of materials for energy systems*, 1:14–33.

Müller-Steinhagen, H. 2011. Heat transfer fouling: 50 years after the kern and seaton model. *Heat Transfer Engineering*, 32(1):1–13.

Müller-Steinhagen, H., Malayeri, M. & Watkinson, A. 2011. Heat exchanger fouling: Mitigation and cleaning strategies. *Heat Transfer Engineering*, 32(3-4):189–196. Available at: `http://dx.doi.org/10.1080/01457632.2010.503108`

Mussalli, Y.G. 1989. Heat exchanger tube coatings and liners. Final report 1689-18 GS-6203, Electrical Power Research Institute (EPRI).

Nebot, E., Casanueva, J., Casanueva, T. & Sales, D. 2007. Model for fouling deposition on power plant steam condensers cooled with seawater: Effect of water velocity and tube material. *International Journal of Heat and Mass Transfer*, 50(17-18):3351–3358. Available at: `http://dx.doi.org/10.1016/j.ijheatmasstransfer.2007.01.022`

Nimmons, M.J. 1979. Heat transfer effects in turbulent flow due to biofilm development. Master's thesis, Rice University, Houston, Texas. Pg 100.

Petukhov, B.S. & Krillov, V.V. 1958. On heat exchange at turbulent flow of liquids in pipes. *Teploenergetika*, 4:63–68.

Phull, B.S. 1991. Heat transfer evaluations of condenser tubes. Technical Report, Laque Center for Corrosion Technology. Prepared for Florida Power Corporation.

Plymouth Tube Co. 2013. Sea-cure® technical specifications, alloy application and data. [Accessed: 2016, November 12]. Available at: `http://www.plymouth.com/media/41927/SEA-CURE\%20Technical\%20Brochure.pdf`.

Prieto, M., Suarez, I. & Montanes, E. 2003. Analysis of the thermal performance of a church window steam condenser for different operational conditions using three models. *Applied thermal engineering*, 23(2):163–178.

Prieto, M., Vallina, J.M., Suárez, I. & Martin, I. 2001. Application of a design code for estimating fouling on-line in a power plant condenser cooled by seawater. *Experimental thermal and fluid science*, 25(5):329–336.

Pugh, S.J., Hewitt, G.F. & Müller-Steinhagen, H. 2009. Fouling during the use of fresh water as coolantant - development of a user guide. *Heat Transfer Engineering*, 30(10-11):851–858. Available at: `http://dx.doi.org/10.1080/01457630902753706`

Pullen, R.P. & Lherminier, F.P. 2005. The cost of dirty condenser tubes a contribution to condenser plant availability and efficiency improvements. In *EPRI (Electrical Power Research Institute) conference on heat rate and cost optimization.*

Putman, R.E. 2001. *Steam surface condensers: basic principles, performance monitoring, and maintenance*. ISBN 0-7918-0151-9. ASME Press. The American Soceity of Mechanical Engineers.

Putman, R.E. & Harpster, J.W. 2002. The measurement of condenser losses due to fouling and those due to air ingress. In J. Tsou (ed.), *Condenser technology: seminar and conference*, 1004116. Palo Alto, CA: EPRI.

Rabas, T.J. & Cane, D. 1983. An update of intube forced convection heat transfer coefficients of water. *Desalination*, 44:109–119.

Ramón, I. & González, M. 2001. Numerical study of the performance of a church window tube bundle condenser. *International Journal of Thermal Sciences*, 40(2):195–204. Available at: `http://dx.doi.org/10.1016/S1290-0729(00)01208-4`

Ranjbar, K. 2010. Effect of flow induced corrosion and erosion on failure of a tubular heat exchanger. *Materials and Design*, 31:613–619.

Reuter, H.C.R. 2010. *Performance evaluation of natural draught cooling towers with anisotropic fills*. Ph.D. thesis, Department of Mechanical and Mechatronic Engineering, Stellenbosch University.

Rhodes, N. & Hardy, C.D. 2005. A study of the effect of pant variables on the performance the Pilgrim condenser. In *Condenser technology conference*. Palo Alto: Electrical Power Research Institute.

Rice, J.K., Garey, J. & Puckorius, Y.G.Y.G.M. 1993. Condenser microbiofouling control handbook. Technical Report TR-102507, Electric Power Research Institute (EPRI).

Rose, J. 1980. Approximate equations for forced-convection condensation in the presence of a non-condensing gas on a flat plate and horizontal tube. *International Journal of Heat and Mass Transfer*, 23(4):539–546. Available at: `http://dx.doi.org/10.1016/0017-9310(80)90095-2`

Sato, S. & Nagata, K. 1985. Experiences of APF condenser tubes. In W. Chow & Y. Mussalli (eds.), *EPRI Condenser biofouling control symposium: the state-of-the-art*. Florida.

Sato, S., Nosetani, T. & Hotta, Y. 1985. Improvement of surface condenser performance by in-situ artificial protective film coating. In Y. Mussalli (ed.), *Effects of fouling and corrosion on heat transfer*. Florida. Presented at the winter annual meeting of the American Society of Mechanical Engineers.

Sheikholeslami, R. 2000. Composite fouling of heat transfer equipment in aqueous media-a review. *Heat Transfer Engineering*, 21(3):34–42.

Shinzato, K., Koyama, T., Watanabe, Y., Kawabe, A. & Fujii, T. 1990. A simple method for measuring the fouling factor inside a removed condenser tube by radiant heating. *Transactions of the Japan Society of Mechanical Engineers Series B*, 56(521):101–106.

Shor, S.W.W. 1988. Condenser tube material heat transfer testing cedar bayou unit 3 - hl& p. In R. Coit (ed.), *Proceedings: condenser technology symposium*, CS-5942-SR.

Silver, R.S. 1963. An approach to a general theory of surface condensers. In *Proceedings of the Institution of Mechanical*, pages 339–337. Institution of Mechanical Engineers.

Somerscales, E.F.C. 1981. *Introduction and summary: the fouling of heat transfer equipment*, page 2. Hemisphere publishing corporation.

Sommer, S., Ekin, A., Webster, D.C., Stafslien, S.J., Daniels, J., Vanerwal, L.J., Thompson, S.E.M., Callow, M.E. & Callow, J.A. 2010. A preliminary study on the performance and fouling-release performance of siloxane-polyurethane coatings prepared from poly(dimethylsiloxane) (pdms) macromers. *Biofouling: The journal of bioadhesion and biofilm research*, 26(8):961–972.

Stiebler, T.J. 1988. Experimence with sea-cure tubing in steam surface condensers. In R. Coit (ed.), *Proceedings: Condenser Technology Symposium*, CS-5942-SR, pages 13.1–13.8. Electrical Power Research Institute (EPRI).

Stringer, J. 1998. Coatings in the electricity supply industry: past, present, and opportunities for the future. *Surface and Coatings Technology*, 108-109:1–9.
Available at: `http://dx.doi.org/10.1016/S0257-8972(98)00642-2`

Sugama, T. 2006. High-performance coating materials. Technical Report BNL-77900-2007-IR, Brookhaven National Laboratory.

Tarrad, A.H. & Majeed, L.M. 2010. The application of a step by step technique for the performance prediction on thermal power plant surface condensers. *Journal of Engineering*, 16(1):4748–4770.

TEMA. 1999. Standards of the tubular exchanger manufacturers association. 8th ed.

Trueba, A., García, S. & Otero, F.M. 2006. Antifouling Ni-Cu-P-PTFE composite coatings for heat exchangers. *Advanced Coatings and Surface Technology*, 19(3):3–4.

Tsou, J.L. & Woodruff, B.N. 1994. Condenser tube coatings as an alternative to retubing. In *Joint Power Generating Conference*. Phoenix, AZ.

Vishwakarma, V., Josephine, J., George, R., Krishnan, R., Dash, S., Kamruddin, M., Kalavathi, S., Manoharan, N., Tyagi, A. & Dayal, R. 2009. Antibacterial copper-nickel bilayers and multilayer coatings by pulsed laser deposition on titanium. *Biofouling*, 25(8):705–710.
Available at: `http://dx.doi.org/10.1080/08927010903132183`

Walker, M.E., Safari, I., Theregowda, R.B., Hsieh, M., Abbasian, J., Arastoopour, H., Dzombak, D.A. & Miller, D.C. 2012. Economic impact of condenser fouling in existing thermoelectric power plants. *Energy*, 44(1):429–437.
Available at: `http://dx.doi.org/10.1016/j.energy.2012.06.010`

Wells, S. & Sytsma, M. 2009. A review of the use of coatings to mitigate biofouling in freshwater.

Wu, X. & Cremaschi, L. 2013. Effect of fouling on the thermal performance of condensers and on the water consumption in cooling tower systems. In H.M. M. R. Malayeri & A.P. Watkinson (eds.), *Heat Exchanger Fouling and Cleaning*, 14.

Yokouchi, H., Nonaka, T. & Kawabe, A. 1996. Japanese developments in condenser fouling control part IV: comparative tests of non-toxic antifouling pipe treating techniques using canals. In J.L.T.Y.G. Mussalli (ed.), *Proceedings: Condenser Technology Conference*. Boston, Massechusetts: EPRI.

Yu, H. 2007. *Composite fouling on heat exchanger surfaces.* Nova science publishers.

Appendices

Appendix A

Thermophysical property data

Thermophysical property data are given in terms of T, the temperature of the fluid (in kelvin).

A.1 Thermophysical properties of saturated water from 273.15 K to 380 K (Kröger, 1998)

- Density (kg/m^3):

$$\rho = (1.49343 \times 10^{-3} - 3.7164 \times 10^{-6} T + 7.09782 \times 10^{-9} T^2 - 1.90321 \times 10^{-20} T^6)^{-1} \tag{A.1}$$

- Specific heat (J/kg·K):

$$c_p = 8.15599 \times 10^3 - 2.80627 \times 10^1 T + 5.11283 \times 10^{-2} T^2 - 2.17582 \times 10^{-13} T^6 \tag{A.2}$$

- Dynamic viscosity (kg/m·s)

$$\mu = 2.414 \times 10^{-5} \times 10^{\frac{247.8}{(T-140)}} \tag{A.3}$$

- Thermal conductivity (W/m·K)

$$k_f = -6.14255 \times 10^{-1} + 6.9962 \times 10^{-3} T - 1.01075 \times^{-5} T^2 + 4.74737 \times 10^{-12} T^4 \tag{A.4}$$

- Prandtl number

$$\mathrm{Pr} = \frac{\mu c_p}{k_f} \tag{A.5}$$

- Latent heat of vaporization (J/kg)

$$i_{fg} = 3.4831814 \times 10^6 - 5.8627703 \times 10^3 T + 12.139568 T^2 - 0.0140290431 T^3 \tag{A.6}$$

A.2 Thermophysical properties of saturated water vapor from 273.15 K to 380 K (Kröger, 1998)

- Vapor pressure (Pa):

$$p_v = 10^z \tag{A.7}$$

with

$$\begin{aligned} z = {} & 10.79586(1 - 273.16/T) + 5.2808 \log_{10}(273.16/T) \\ & + 1.50474 \times 10^{-4} \left\{1 - 10^{-8.29692[(T/273.16)-1]}\right\} \\ & + 4.2873 \times 10^{-4} \left\{10^{4.76955(1-273.16/T)} - 1\right\} + 2.78618312 \end{aligned}$$

Appendix B

Supplementary data and photographs

B.1 Test facility specifications

Table B.1 provides some of the pertinent specifications and capacities of the test facility.

Table B.1: Specifications of the test facility

Overall dimensions (l×w×h)	7 m × 2.400 m × 2.600 m
Test tube length	3.199 m (+ entrance length)
Number of test tubes	6
Diameter range	22 mm - 25.40 mm
Heater	3-Phase 380 V 24 kW
Temperature controller	Solid state thyristor (60 A)
Temperature probes	24 × ϕ6.140 mm × 150 mm stainless steel sheath, PT1000, AA
Flow meter	Ultrasonic 0 – 10 L/s (1 % AR)

B.2 Supplementary photographs

The following list of photographs is included:

- Figure B.1: Assembled heat exchangers before placement in the container.
- Figure B.2: Hot pump showing all wetted parts are plastic including its housing and impeller.
- Figure B.3: Photograph during initial construction of apparatus showing the size of the container.

- Figure B.4: Transport of apparatus.
- Figure B.5: Apparatus after installation on-site.
- Figure B.6: Blocked strainer during test B.
- Figure B.7: Y-strainers arranged in parallel to enable online cleaning.

Figure B.1: Assembled heat exchangers before placement in the container

Figure B.2: Hot pump showing all wetted parts are plastic

Figure B.3: Photograph during initial construction of apparatus showing the size of the container

Figure B.4: Transport of apparatus

Figure B.5: Apparatus after installation on-site

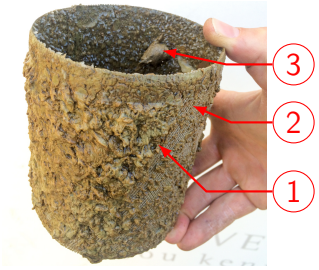

Figure B.6: Photograph of blocked strainer – (1) deposits, (2) 1 mm mesh, (3) dead fish

Figure B.7: Y-strainers arranged in parallel to enable online cleaning

Appendix C

Calibrations and commissioning tests

C.1 Temperature probe calibration and certification

Independent calibration tests, traceable to the South African National Accreditation System (SANAS), are performed on the entire measurement system, i.e. the datalogger, leads, and probes. The four probes that are calibrated at the three different temperature points are used as reference probes within the apparatus. Using the calibration data they are calibrated according to

$$T_{\text{actual}} = A_T T_{\text{measured}} + B_T \tag{C.1}$$

where the coefficients A_T and B_T are found by linear regression, and listed in table C.1.

Table C.1: Calibration coefficients for the reference heat exchanger probes

Probe	10 °C	30 °C	50 °C	A_T	B_T
T_{in}	9.982	30.026	50.056	0.9982	0.0341
T_{out}	10.014	30.048	50.065	0.9983	0.0209
$T_{\text{ann,in}}$	10.001	30.019	50.068	0.9981	0.0102
$T_{\text{ann,out}}$	10.014	30.048	50.065	0.9987	-0.0041

Next the respective temperature calibration certificates are presented in the following order:

- Four certificates showing the three point calibration at: 10 °C, 30 °C, and 50 °C.
- Twelve certificates showing the single point calibration at 30 °C.

unitemp®

Calibration and Services

calibration • validation • training

Calibration certificate

CAL-UG-S-T-150428L31

certificate number

sanas Calibration Laboratory 370

Lab measurement equipment with certified traceability to international standards

Description	Cert. No.	Equipment. Number
Testo 735 with PT100 probe	T59259	Unitemp34

Ambient conditions.

Temperature: 23 °C ± 5 °C

Measuring procedure (P0051)

The measurements read on this test item were obtained, in a thermostatic bath, while placed in very close proximity to the reference probe.

The result is calculated from an average of ***9*** *readings @* ***10*** *second intervals*

Measurement results for hi-accuracy digital thermometer with Pt1000 immersion probe

Indication from reference in °C	Indication from your measuring instrument in °C	Deviation in °C	G-Line allowed tolerance in °C	Expanded uncertainty of measurement in °C	Probe insertion depth in mm	Reference Equipment Used
10.153	10.167	**0.014**	0.1	± 0.06	90	Unitemp34
29.947	29.995	**0.048**	0.1	± 0.06	90	Unitemp34
50.027	50.092	**0.065**	0.1	± 0.06	90	Unitemp34

Validity of Certificate

The measurement results recorded in this certificate relate only to the instrument & attachments specified, and were correct at the time. A result with * next to it indicates this falls outside manufacture's specifications. Only the above points have been checked & performance at other points is not certain. Subsequent accuracy will depend on factors such as care, handling and frequency of use. It is recommended that recalibration be undertaken at an interval that will ensure that the instrument remains within the desired limits.

CALIBRATION AND SERVICES CALIBRATION LABORATORY unitemp 29 APR 2015 JOHANNESBURG MORE ASSURANCE, BETTER SERVICE

page 2 of 2

END

unitemp®

Calibration and Services

calibration • validation • training

Calibration certificate

CAL-UG-S-T-150428L32

certificate number

sanas Calibration Laboratory 370

Lab measurement equipment with certified traceability to international standards

Description	Cert. No.	Equipment. Number
Testo 735 with PT100 probe	T59259	Unitemp34

Ambient conditions.

Temperature: 23 °C ± 5 °C

Measuring procedure (P0051)

The measurements read on this test item were obtained, in a thermostatic bath, while placed in very close proximity to the reference probe.

The result is calculated from an average of ***8*** *readings @* ***10*** *second intervals*

Measurement results for hi-accuracy digital thermometer with Pt1000 immersion probe

Indication from reference in °C	Indication from your measuring instrument in °C	**Deviation in °C**	G-Line allowed tolerance in °C	Expanded uncertainty of measurement in °C	Probe insertion depth in mm	Reference Equipment Used
10.067	10.068	**0.001**	0.1	± 0.06	90	Unitemp34
29.973	29.992	**0.019**	0.1	± 0.05	90	Unitemp34
50.002	50.070	**0.068**	0.1	± 0.06	90	Unitemp34

Validity of Certificate

The measurement results recorded in this certificate relate only to the instrument & attachments specified, and were correct at the time. A result with * next to it indicates this falls outside manufacture's specifications. Only the above points have been checked & performance at other points is not certain. Subsequent accuracy will depend on factors such as care, handling and frequency of use. It is recommended that recalibration be undertaken at an interval that will ensure that the instrument remains within the desired limits.

CALIBRATION AND SERVICES / CALIBRATION LABORATORY / unitemp / 29 APR 2015 / JOHANNESBURG / MORE ASSURANCE, BETTER SERVICE

page 2 of 2

END

unitemp®

Calibration and Services

calibration • validation • training

Calibration certificate

CAL-UG-S-T-150428L33

certificate number

sanas Calibration Laboratory 370

Lab measurement equipment with certified traceability to international standards

Description	Cert. No.	Equipment. Number
Testo 735 with PT100 probe	T59259	Unitemp34

Ambient conditions.

Temperature: 23 °C ± 5 °C

Measuring procedure (P0051)

The measurements read on this test item were obtained, in a thermostatic bath, while placed in very close proximity to the reference probe.

The result is calculated from an average of ***6*** *readings @* ***10*** *second intervals*

Measurement results for hi-accuracy digital thermometer with Pt1000 immersion probe

Indication from reference in °C	Indication from your measuring instrument in °C	**Deviation in °C**	G-Line allowed tolerance in °C	Expanded uncertainty of measurement in °C	Probe insertion depth in mm	Reference Equipment Used
10.088	10.099	**0.011**	0.1	± 0.05	90	Unitemp34
29.950	29.991	**0.041**	0.1	± 0.05	90	Unitemp34
49.980	50.066	**0.086**	0.1	± 0.07	90	Unitemp34

Validity of Certificate

The measurement results recorded in this certificate relate only to the instrument & attachments specified, and were correct at the time. A result with * next to it indicates this falls outside manufacture's specifications. Only the above points have been checked & performance at other points is not certain. Subsequent accuracy will depend on factors such as care, handling and frequency of use. It is recommended that recalibration be undertaken at an interval that will ensure that the instrument remains within the desired limits.

CALIBRATION AND SERVICES CALIBRATION LABORATORY unitemp 29 APR 2015 JOHANNESBURG MORE ASSURANCE, BETTER SERVICE

page 2 of 2

END

unitemp®

Calibration and Services

calibration • validation • training

Calibration certificate

CAL-UG-S-T-150428L34
certificate number

sanas Calibration Laboratory 370

Lab measurement equipment with certified traceability to international standards

Description	Cert. No.	Equipment. Number
Testo 735 with PT100 probe	T59259	Unitemp34

Ambient conditions.

Temperature: 23 °C ± 5 °C

Measuring procedure (P0051)

The measurements read on this test item were obtained, in a thermostatic bath, while placed in very close proximity to the reference probe.

The result is calculated from an average of **7** *readings @* **10** *second intervals*

Measurement results for hi-accuracy digital thermometer with Pt1000 immersion probe

Indication from reference in °C	Indication from your measuring instrument in °C	**Deviation in °C**	G-Line allowed tolerance in °C	Expanded uncertainty of measurement in °C	Probe insertion depth in mm	Reference Equipment Used
10.076	10.058	**-0.018**	0.1	± 0.07	90	Unitemp34
29.968	29.994	**0.026**	0.1	± 0.05	90	Unitemp34
50.027	50.083	**0.056**	0.1	± 0.07	90	Unitemp34

Validity of Certificate

The measurement results recorded in this certificate relate only to the instrument & attachments specified, and were correct at the time. A result with * next to it indicates this falls outside manufacture's specifications. Only the above points have been checked & performance at other points is not certain. Subsequent accuracy will depend on factors such as care, handling and frequency of use. It is recommended that recalibration be undertaken at an interval that will ensure that the instrument remains within the desired limits.

CALIBRATION AND SERVICES CALIBRATION LABORATORY unitemp 29 APR 2015 JOHANNESBURG MORE ASSURANCE

page 2 of 2

END

unitemp®

Calibration and Services

calibration • validation • training

Calibration certificate

CAL-UG-S-T-150428L35

certificate number

sanas Calibration Laboratory 370

Lab measurement equipment with certified traceability to international standards

Description	Cert. No.	Equipment. Number
Testo 735 with PT100 probe	T59259	Unitemp34

Ambient conditions.

Temperature: 23 °C ± 5 °C

Measuring procedure (P0051)

The measurements read on this test item were obtained, in a thermostatic bath, while placed in very close proximity to the reference probe.

The result is calculated from an average of ***7*** *readings @* ***10*** *second intervals*

Measurement results for hi-accuracy digital thermometer with Pt1000 immersion probe

Indication from reference in °C	Indication from your measuring instrument in °C	**Deviation in °C**	G-Line allowed tolerance in °C	Expanded uncertainty of measurement in °C	Probe insertion depth in mm	Reference Equipment Used
29.996	30.063	**0.067**	0.1	± 0.06	90	Unitemp34

Validity of Certificate

The measurement results recorded in this certificate relate only to the instrument & attachments specified, and were correct at the time. A result with * next to it indicates this falls outside manufacture's specifications. Only the above points have been checked & performance at other points is not certain. Subsequent accuracy will depend on factors such as care, handling and frequency of use. It is recommended that recalibration be undertaken at an interval that will ensure that the instrument remains within the desired limits.

CALIBRATION AND SERVICES / MORE ASSURANCE / CALIBRATION LABORATORY unitemp 29 APR 2015 JOHANNESBURG

page 2 of 2

END

unitemp®

Calibration and Services

calibration • validation • training

Calibration certificate

CAL-UG-S-T-150428L36

certificate number

sanas Calibration Laboratory 370

Lab measurement equipment with certified traceability to international standards

Description	Cert. No.	Equipment. Number
Testo 735 with PT100 probe	T59259	Unitemp34

Ambient conditions.

Temperature: 23 °C ± 5 °C

Measuring procedure (P0051)

The measurements read on this test item were obtained, in a thermostatic bath, while placed in very close proximity to the reference probe.

The result is calculated from an average of ***8*** *readings @* ***10*** *second intervals*

Measurement results for hi-accuracy digital thermometer with Pt1000 immersion probe

Indication from reference in °C	Indication from your measuring instrument in °C	**Deviation in °C**	G-Line allowed tolerance in °C	Expanded uncertainty of measurement in °C	Probe insertion depth in mm	Reference Equipment Used
30.006	30.091	**0.085**	0.1	± 0.05	90	Unitemp34

Validity of Certificate

The measurement results recorded in this certificate relate only to the instrument & attachments specified, and were correct at the time. A result with * next to it indicates this falls outside manufacture's specifications. Only the above points have been checked & performance at other points is not certain. Subsequent accuracy will depend on factors such as care, handling and frequency of use. It is recommended that recalibration be undertaken at an interval that will ensure that the instrument remains within the desired limits.

CALIBRATION AND SERVICES CALIBRATION LABORATORY unitemp 29 APR 2015 JOHANNESBURG MORE ASSURANCE, BETTER SERVICE

page 2 of 2

END

unitemp®

Calibration and Services

calibration • validation • training

Calibration certificate

CAL-UG-S-T-150428L37

certificate number

sanas Calibration Laboratory 370

Lab measurement equipment with certified traceability to international standards

Description	Cert. No.	Equipment. Number
Testo 735 with PT100 probe	T59259	Unitemp34

Ambient conditions.

Temperature: 23 °C ± 5 °C

Measuring procedure (P0051)

The measurements read on this test item were obtained, in a thermostatic bath, while placed in very close proximity to the reference probe.

The result is calculated from an average of ***8*** *readings @* ***10*** *second intervals*

Measurement results for hi-accuracy digital thermometer with Pt1000 immersion probe

Indication from reference in °C	Indication from your measuring instrument in °C	**Deviation in °C**	G-Line allowed tolerance in °C	Expanded uncertainty of measurement in °C	Probe insertion depth in mm	Reference Equipment Used
29.906	29.908	**0.002**	0.1	± 0.05	90	Unitemp34

Validity of Certificate

The measurement results recorded in this certificate relate only to the instrument & attachments specified, and were correct at the time. A result with * next to it indicates this falls outside manufacture's specifications. Only the above points have been checked & performance at other points is not certain. Subsequent accuracy will depend on factors such as care, handling and frequency of use. It is recommended that recalibration be undertaken at an interval that will ensure that the instrument remains within the desired limits.

CALIBRATION AND SERVICES CALIBRATION LABORATORY unitemp 29 APR 2015 JOHANNESBURG MORE ASSURANCE

page 2 of 2

END

unitemp®

Calibration and Services

calibration • validation • training

Calibration certificate

CAL-UG-S-T-150428L38

certificate number

sanas Calibration Laboratory 370

Lab measurement equipment with certified traceability to international standards

Description	Cert. No.	Equipment. Number
Testo 735 with PT100 probe	T59259	Unitemp34

Ambient conditions.

Temperature: 23 °C ± 5 °C

Measuring procedure (P0051)

The measurements read on this test item were obtained, in a thermostatic bath, while placed in very close proximity to the reference probe.

The result is calculated from an average of ***8*** *readings @* ***10*** *second intervals*

Measurement results for hi-accuracy digital thermometer with Pt1000 immersion probe

Indication from reference in °C	Indication from your measuring instrument in °C	**Deviation in °C**	G-Line allowed tolerance in °C	Expanded uncertainty of measurement in °C	Probe insertion depth in mm	Reference Equipment Used
29.912	29.960	**0.048**	0.1	± 0.05	90	Unitemp34

Validity of Certificate

The measurement results recorded in this certificate relate only to the instrument & attachments specified, and were correct at the time. A result with * next to it indicates this falls outside manufacture's specifications. Only the above points have been checked & performance at other points is not certain. Subsequent accuracy will depend on factors such as care, handling and frequency of use. It is recommended that recalibration be undertaken at an interval that will ensure that the instrument remains within the desired limits.

CALIBRATION AND SERVICES / CALIBRATION LABORATORY / unitemp / 29 APR 2015 / JOHANNESBURG / MORE ASSURANCE, BETTER SERVICE

page 2 of 2

END

unitemp®

Calibration and Services

calibration • validation • training

Calibration certificate

CAL-UG-S-T-150428L39

certificate number

sanas Calibration Laboratory 370

Lab measurement equipment with certified traceability to international standards

Description	Cert. No.	Equipment. Number
Testo 735 with PT100 probe	T59259	Unitemp34

Ambient conditions.

Temperature: 23 °C ± 5 °C

Measuring procedure (P0051)

The measurements read on this test item were obtained, in a thermostatic bath, while placed in very close proximity to the reference probe.

The result is calculated from an average of ***7*** *readings @* ***10*** *second intervals*

Measurement results for hi-accuracy digital thermometer with Pt1000 immersion probe

Indication from reference in °C	Indication from your measuring instrument in °C	**Deviation in °C**	G-Line allowed tolerance in °C	Expanded uncertainty of measurement in °C	Probe insertion depth in mm	Reference Equipment Used
29.907	29.894	**-0.013**	0.1	± 0.05	90	Unitemp34

Validity of Certificate

The measurement results recorded in this certificate relate only to the instrument & attachments specified, and were correct at the time. A result with * next to it indicates this falls outside manufacture's specifications. Only the above points have been checked & performance at other points is not certain. Subsequent accuracy will depend on factors such as care, handling and frequency of use. It is recommended that recalibration be undertaken at an interval that will ensure that the instrument remains within the desired limits.

CALIBRATION LABORATORY unitemp 29 APR 2015 JOHANNESBURG

page 2 of 2

END

unitemp®

Calibration and Services

calibration • validation • training

Calibration certificate

CAL-UG-S-T-150428L40
certificate number

sanas Calibration Laboratory 370

Lab measurement equipment with certified traceability to international standards

Description	Cert. No.	Equipment. Number
Testo 735 with PT100 probe	T59259	Unitemp34

Ambient conditions.

Temperature: 23 °C ± 5 °C

Measuring procedure (P0051)

The measurements read on this test item were obtained, in a thermostatic bath, while placed in very close proximity to the reference probe.

The result is calculated from an average of ***6*** *readings @* ***10*** *second intervals*

Measurement results for hi-accuracy digital thermometer with Pt1000 immersion probe

Indication from reference in °C	Indication from your measuring instrument in °C	**Deviation in °C**	G-Line allowed tolerance in °C	Expanded uncertainty of measurement in °C	Probe insertion depth in mm	Reference Equipment Used
29.971	30.058	**0.087**	0.1	± 0.07	90	Unitemp34

Validity of Certificate

The measurement results recorded in this certificate relate only to the instrument & attachments specified, and were correct at the time. A result with * next to it indicates this falls outside manufacture's specifications. Only the above points have been checked & performance at other points is not certain. Subsequent accuracy will depend on factors such as care, handling and frequency of use. It is recommended that recalibration be undertaken at an interval that will ensure that the instrument remains within the desired limits.

CALIBRATION AND SERVICES CALIBRATION LABORATORY unitemp 29 APR 2015 JOHANNESBURG MORE ASSURANCE

page 2 of 2

END

unitemp®

Calibration and Services

calibration • validation • training

Calibration certificate

CAL-UG-S-T-150428L41
certificate number

sanas Calibration Laboratory 370

Lab measurement equipment with certified traceability to international standards

Description	Cert. No.	Equipment. Number
Testo 735 with PT100 probe	T59259	Unitemp34

Ambient conditions.

Temperature: 23 °C ± 5 °C

Measuring procedure (P0051)

The measurements read on this test item were obtained, in a thermostatic bath, while placed in very close proximity to the reference probe.

The result is calculated from an average of **7** *readings @* **10** *second intervals*

Measurement results for hi-accuracy digital thermometer with Pt1000 immersion probe

	Indication from reference in °C	Indication from your measuring instrument in °C	**Deviation in °C**	G-Line allowed tolerance in °C	Expanded uncertainty of measurement in °C	Probe insertion depth in mm	Reference Equipment Used
*	29.934	30.051	**0.117**	0.1	± 0.07	90	Unitemp34

Validity of Certificate

The measurement results recorded in this certificate relate only to the instrument & attachments specified, and were correct at the time. A result with * next to it indicates this falls outside manufacture's specifications. Only the above points have been checked & performance at other points is not certain. Subsequent accuracy will depend on factors such as care, handling and frequency of use. It is recommended that recalibration be undertaken at an interval that will ensure that the instrument remains within the desired limits.

CALIBRATION AND SERVICES / CALIBRATION LABORATORY / unitemp / 29 APR 2015 / JOHANNESBURG / MORE ASSURANCE, BETTER SERVICE

page 2 of 2

END

unitemp®

Calibration and Services

calibration • validation • training

Calibration certificate

CAL-UG-S-T-150428L42

certificate number

sanas Calibration Laboratory 370

Lab measurement equipment with certified traceability to international standards

Description	Cert. No.	Equipment. Number
Testo 735 with PT100 probe	T59259	Unitemp34

Ambient conditions.

Temperature: 23 °C ± 5 °C

Measuring procedure (P0051)

The measurements read on this test item were obtained, in a thermostatic bath, while placed in very close proximity to the reference probe.

The result is calculated from an average of ***7*** *readings @* ***10*** *second intervals*

Measurement results for hi-accuracy digital thermometer with Pt1000 immersion probe

Indication from reference in °C	Indication from your measuring instrument in °C	**Deviation in °C**	G-Line allowed tolerance in °C	Expanded uncertainty of measurement in °C	Probe insertion depth in mm	Reference Equipment Used
29.934	29.946	**0.012**	0.1	± 0.05	90	Unitemp34

Validity of Certificate

The measurement results recorded in this certificate relate only to the instrument & attachments specified, and were correct at the time. A result with * next to it indicates this falls outside manufacture's specifications. Only the above points have been checked & performance at other points is not certain. Subsequent accuracy will depend on factors such as care, handling and frequency of use. It is recommended that recalibration be undertaken at an interval that will ensure that the instrument remains within the desired limits.

CALIBRATION AND SERVICES CALIBRATION LABORATORY unitemp 29 APR 2015 JOHANNESBURG MORE ASSURANCE

page 2 of 2

END

Although the certificates are specified for a period of one year, most of the testing is performed within this period. Thereafter the probes are checked against one another during isothermal tests to ensure the probes have not gone out of calibration due to drift. In addition to the accuracy requirements the class AA RTD temperature probes are also chosen since they exhibit good longevity within the temperature ranges tested here, and no probes are seen to be out of calibration.

C.2 Regression coefficients resulting from the annular convection coefficient testing

Table C.2 shows the regressed coefficients for test A, test B, and test C.

Table C.2: Regression coefficients in the annular Nusselt number regression (equation (3.23))

	Test A		Test B		Test C	
Heat exchanger	A_{Nu}	B_{Nu}	A_{Nu}	B_{Nu}	A_{Nu}	B_{Nu}
1	0.55799	0.497	0.01360	0.859	0.01703	0.838
2	0.01705	0.827	0.06523	0.697	0.2309	0.588
3	0.11475	0.628	0.02541	0.772	0.1148	0.628
4	0.00062	1.179	0.03623	0.773	0.2309	0.588
5	0.07479	0.692	0.00047	1.174	0.03018	0.781
6	0.03857	0.738	0.01718	0.839	0.03857	0.738

C.3 Conductivities

The tube thermal conductivities and there references are tabulated in table C.3.

Table C.3: Constants used in the data processing

Thermal conductivities	Reference
Cartridge brass: 120,109-121 W/(m K)	Davis (2001); Goodfellow Cambridge Ltd. (2013)
Admiralty brass: 111 W/(m K)	Davis (2001); Heat Exchange Institute (2012)
Titanium (grade II): 22 W/(m K)	Heat Exchange Institute (2012)
Duplex stainless steel (TP 316): 14 W/(m K)	Heat Exchange Institute (2012)
Sea-cure®: 16 W/(m K)	Plymouth Tube Co (2013)
Epoxy type PPF: 0.5 W/(m K)	Goodenough (2013)
Thermally-enhanced PPF: 1.2 W/(m K)	Goodenough (2013)
Type 1 biocidal PPF: 1.0 W/(m K)	Measured

C.4 Flow metering calibration results

Table C.4 provides the flow rates recorded using the electromagnetic reference flow meter (denoted X) and the ultrasonic flow meter fitted to each branch of the manifold in succession (denoted Y). The resulting scaling factors are found by the method of least squares. Similarly for the annuli the results are given in table C.5.

Table C.4: Flow meter calibration results for the test tubes

Tube	JFC1	JFC2	JFC3	JFC4	JFC5	JFC6
Factor	0.9826	0.9833	0.9988	0.9786	0.9916	0.9973
X1	0.0000	0.0000	0.0000	0.0000	0.0000	0.0000
X2	0.3950	0.3197	0.2926		0.3113	0.5487
X3	0.6915	0.5991	0.3120	0.3371	0.4535	0.6892
X4	1.0350	0.8999	0.6327	0.8641	0.7855	0.3454
X5			0.8543	1.1176		1.1352
X6			1.0166			
Y1	0.0000	0.0000	0.0000	0.0000	0.0000	0.0000
Y2	0.4032	0.3288	0.2980		0.3207	0.5448
Y3	0.7139	0.6123	0.3147	0.3526	0.4612	0.6925
Y4	1.0503	0.9154	0.6414	0.8908	0.7927	0.3489
Y5			0.8663	1.1414		1.1387
Y6			1.0114			

Table C.5: Flow meter calibration results for the annuli

Tube	JFH1	JFH2	JFH3	JFH4	JFH5	JFH6
Factor	1.0004	0.9816	1.0200	0.9792	0.9874	1.0360
X1	0.0000	0.0000	0.0000	0.0000	0.0000	0.0000
X2	0.4085	0.3344	0.2820		0.3177	0.282
X3	0.7009	0.5919	0.6321	0.3147	0.4441	0.546
X4	1.0350	0.9126	0.8556		0.7913	0.674
X5			0.8170	0.6979		1.085
X6			1.0202	1.0924		1.134
Y1	0.0000	0.0000	0.0000	0.0000	0.0000	0.0000
Y2	0.4119	0.3462	0.2758		0.3314	0.2807
Y3	0.7075	0.6075	0.6212	0.3198	0.4569	0.537
Y4	1.0331	0.9299	0.8275		0.8020	0.65446
Y5			0.8025	0.7083		1.0568
Y6			1.0053	1.1163		1.09194

C.5 Comparison of annular Nusselt numbers

Figure C.1 compares the measured annular Nusselt numbers with the theoretical values as described in chapter 3.

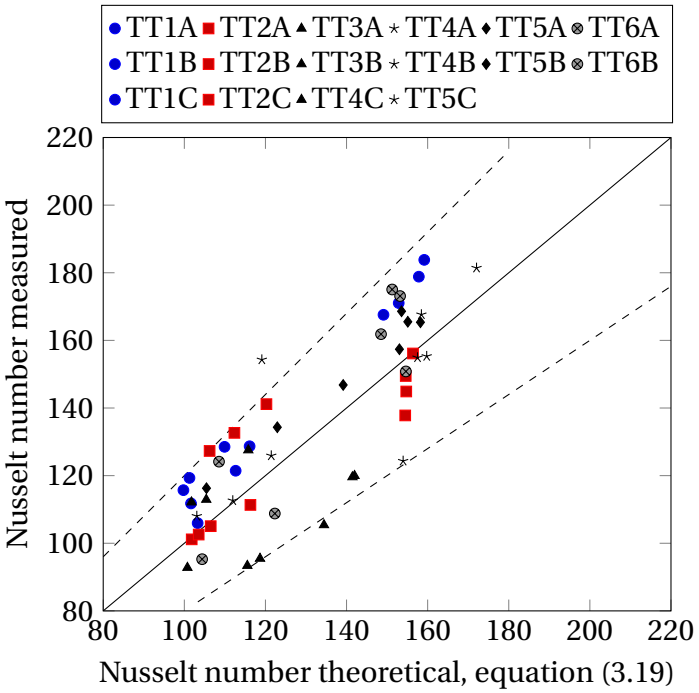

Figure C.1: Measured Nusselt numbers versus theoretical values (dashed lines ± 20%)

Appendix D

Experimental data

D.1 Presentation of data

The experimental data is presented in the following format:

- Section D.2 lists the raw data for test A, test B, and test C including the measured temperatures, flow rates, and height differentials of the manometers.
- Section D.3 gives the velocities, mass balances, heat transfers and log mean temperature differences.
- Section D.4 compares the theoretical annular Nusselt numbers to the measured values.
- Section D.5 lists the exposure times, measured friction factors, and fouling factors for test A, test B, and test C respectively.
- Section D.6 tabulates the total bacterial counts taken during test B.
- Section D.7 compares fouling factors measured in two ways from test B and test C.

The identifiers are labelled as follows:
→ C1 is the foulant inlet temperature to heat exchanger 1, and C1.1 is outlet temperature of the foulant from heat exchanger 1.
→ H1 is the annular fluid inlet temperature to heat exchanger 1, and C1.1 is outlet temperature of the annular fluid from heat exchanger 1.
→ JFC1 is the foulant flow rate through heat exchanger 1
→ JFH1 is the annular fluid flow rate through heat exchanger 1. This designation is continued similarly for the remaining five heat exchangers. Note that NaN is used as a place holder where no readings were taken.

D.2 Raw data

Raw data is tabulated in tables D.1, D.2, D.3,D.4, D.5 (test A), D.6, D.7, D.8, D.9, D.10, D.11, D.12 (test B), D.13, D.14, D.15, D.16 (test C).

Table D.1: Raw annular convection test data before the start of test A (1 of 2)

	Test number								
Measurement	OA1	OA2	OA3	OA4	OA5	OA6	OA7	OA8	Unit
C1	24.126	25.071	25.261	19.514	19.326	20.876		50.626	°C
C2	24.116	25.114	25.333	20.992	21.216	21.922		50.634	°C
C3	23.077	23.205	23.278	22.304	24.901	22.743		50.716	°C
C4	23.966	24.121	23.963	24.883	23.667	22.214	24.472	50.704	°C
C5	22.188	23.249	23.234	24.917	22.085	21.638	24.421	50.639	°C
C6	19.918	20.615	20.553	19.813	24.798	22.631		50.673	°C
H1	39.668	38.834	38.613	16.749	17.718	20.617		53.306	°C
H2	39.543	38.797	38.599	20.027	21.083	22.517		53.273	°C
H3	33.269	33.100	32.574	32.478	38.495	33.432		53.283	°C
H4	35.966	35.524	35.206	38.740	35.588	31.375	33.316	53.314	°C
H5	35.005	34.811	34.930	38.762	34.783	30.931	33.343	53.313	°C
H6	32.518	31.180	30.525	32.738	38.461	33.416		53.310	°C
C1.1	29.437	27.353	27.907	21.087	21.398	21.729		51.263	°C
C2.2	29.305	27.422	27.851	21.181	21.510	21.616		51.290	°C
C3.3	25.800	24.641	24.902	24.570	28.245	25.105		51.341	°C
C4.4	27.844	26.411	26.753	27.952	26.787	24.376	26.631	51.323	°C
C5.5	27.884	26.462	26.747	27.962	27.215	24.347	26.548	51.284	°C
C6.6	25.497	24.900	25.016	23.968	28.174	25.086		51.436	°C
H1.1	38.176	35.369	35.892	33.341	33.161	25.467		52.780	°C
H2.2	38.000	35.327	35.852	26.385	33.299	27.028		52.816	°C
H3.3	33.843	30.515	31.544	32.030	36.005	31.488		52.802	°C
H4.4	36.251	33.408	33.795	36.212	34.671	29.857	32.081	52.807	°C
H5.5	36.357	33.387	33.995	36.329	34.632	29.833	31.968	52.728	°C
H6.6	31.985	29.378	30.615	29.045	35.907	30.973		52.718	°C
Electromag	0.5920	1.3880	1.3740	1.6530	1.3710	1.3910	1.4940	4.2632	L/s
JFC1	0.3090	0.6882	0.6715	0.0000	0.0000	0.0000	0.0000	0.7643	L/s
JFC2	0.3264	0.6826	0.6955	0.0000	0.0000	0.0000	0.0000	0.7024	L/s
JFC3	0.0000	0.0000	0.0000	0.0000	0.6854	0.6654	0.0000	0.0000	L/s
JFC4	0.0000	0.0000	0.0000	0.8280	0.0000	0.0000	0.7567	0.7300	L/s
JFC5	0.0000	0.0000	0.0000	0.8040	0.0000	0.0000	0.7482	0.7573	L/s
JFC6	0.0000	0.0000	0.0000	0.0000	0.6459	0.7026	0.0000	0.7075	L/s
JFH1	1.0720	0.4484	0.6528	0.0000	0.0000	0.0000	0.0000	0.9762	L/s
JFH2	1.0751	0.4473	0.6534	0.0000	0.0000	0.0000	0.0000	0.9692	L/s
JFH3	0.0000	0.0000	0.0000	0.0000	0.8982	0.8044	0.0000	0.8758	L/s
JFH4	0.0000	0.0000	0.0000	0.9740	0.0000	0.0000	1.2829	1.0136	L/s
JFH5	0.0000	0.0000	0.0000	1.0100	0.0000	0.0000	1.1504	0.8498	L/s
JFH6	0.0000	0.0000	0.0000	0.0000	0.9076	0.7154	0.0000	0.9309	mm
Delta h1		464	451						mm
Delta h2		482	489						mm
Delta h3					556				mm
Delta h4				598					mm
Delta h5				669					mm
Delta h6					520				mm

Table D.2: Raw annular convection test data before the start of test A (2 of 2)

	Test number			
Measurement	OA9	OA10	OA11	Unit
C1	50.207	46.600	47.110	°C
C2	50.237	46.645	47.162	°C
C3	50.207	46.621	47.198	°C
C4	50.283	46.659	47.187	°C
C5	50.220	46.600	47.130	°C
C6	50.254	46.630	47.156	°C
H1	52.654	48.927	52.405	°C
H2	52.613	48.894	52.366	°C
H3	52.730	49.002	52.480	°C
H4	52.661	48.852	52.439	°C
H5	52.664	48.942	52.417	°C
H6	52.661	48.941	52.411	°C
C1.1	50.792	47.142	48.358	°C
C2.2	50.807	47.161	48.446	°C
C3.3	50.840	47.187	48.526	°C
C4.4	50.825	47.176	48.476	°C
C5.5	50.837	47.186	48.460	°C
C6.6	50.951	47.291	48.643	°C
H1.1	52.174	48.478	51.360	°C
H2.2	52.197	48.513	51.463	°C
H3.3	52.177	48.493	51.339	°C
H4.4	52.183	48.497	51.416	°C
H5.5	52.164	48.468	51.375	°C
H6.6	52.115	48.448	51.341	°C
Electromag	4.2480	4.1810	4.1984	L/s
JFC1	0.7540	0.7360	0.7470	L/s
JFC2	0.6980	0.7050	0.7109	L/s
JFC3	0.7180	0.6720	0.7039	L/s
JFC4	0.7720	0.7350	0.7410	L/s
JFC5	0.7510	0.7470	0.7489	L/s
JFC6	0.7220	0.7030	0.6930	L/s
JFH1	0.9900	0.9650	0.9176	L/s
JFH2	0.9740	0.9950	0.9897	L/s
JFH3	0.8620	0.8260	0.8610	L/s
JFH4	1.0000	0.9960	1.0104	L/s
JFH5	0.9730	0.9840	0.9603	L/s
JFH6	0.9200	0.9210	0.9480	mm
Delta h1				mm
Delta h2				mm
Delta h3				mm
Delta h4				mm
Delta h5				mm
Delta h6				mm

Table D.3: Test A raw data (1 of 3)

	Test number								
Measurement	DA1	DA2	DA3	DA4	DA5	DA6	DA7	DA8	Unit
C1	47.161	50.626	50.161	46.563	47.110	47.068	37.031	38.917	°C
C2	47.194	50.634	50.237	46.638	47.162	47.124	37.094	38.972	°C
C3	47.180	50.716	50.285	46.682	47.198	47.168	37.134	39.012	°C
C4	47.218	50.704	50.283	46.676	47.187	47.150	37.107	38.992	°C
C5	47.161	50.639	50.220	46.617	47.130	47.089	37.053	38.937	°C
C6	47.107	50.593	50.174	46.557	47.076	47.038	36.984	38.873	°C
H1	52.448	53.306	52.654	48.739	52.405	52.303	41.714	43.774	°C
H2	52.409	53.273	52.613	48.705	52.366	52.268	41.695	43.749	°C
H3	52.524	53.283	52.630	48.713	52.480	52.373	41.774	43.837	°C
H4	52.472	53.314	52.661	48.705	52.439	52.293	41.728	43.801	°C
H5	52.461	53.313	52.664	48.756	52.417	52.315	41.733	43.790	°C
H6	52.455	53.310	52.661	48.751	52.411	52.309	41.738	43.795	°C
C1.1	48.392	51.263	50.792	47.105	48.358	48.256	38.080	39.932	°C
C2.2	48.480	51.290	50.807	47.122	48.446	48.362	38.059	40.040	°C
C3.3	48.560	51.341	50.840	47.144	48.526	48.400	38.210	40.108	°C
C4.4	48.510	51.323	50.825	47.137	48.476	48.375	38.196	40.103	°C
C5.5	48.495	51.284	50.837	47.142	48.460	48.366	38.206	40.110	°C
C6.6	48.678	51.436	50.951	47.246	48.643	48.520	38.326	40.236	°C
H1.1	51.401	52.780	52.174	48.325	51.360	51.258	40.883	42.776	°C
H2.2	51.505	52.816	52.197	48.360	51.463	51.386	40.831	42.910	°C
H3.3	51.380	52.802	52.177	48.347	51.339	51.250	40.866	42.812	°C
H4.4	51.318	52.727	52.103	48.266	51.313	51.238	40.851	42.796	°C
H5.5	51.416	52.728	52.164	48.319	51.375	51.275	40.914	42.859	°C
H6.6	51.381	52.718	52.115	48.299	51.341	51.251	40.834	42.821	°C
Electromag	4.1984	4.2632	4.2500	4.1806	4.1984	4.2487	4.3975	4.3359	L/s
JFC1	0.747	0.764	0.754	0.736	0.747		0.763	0.779	L/s
JFC2	0.711	0.702	0.698	0.705	0.711	0.708	0.715	0.720	L/s
JFC3	0.704	0.683	0.718	0.672	0.704	0.686	0.708	0.718	L/s
JFC4	0.741	0.730	0.772	0.735	0.741	0.777	0.788	0.775	L/s
JFC5	0.749	0.757	0.751	0.747	0.749	0.767	0.785	0.768	L/s
JFC6	0.693	0.707	0.722	0.703	0.693	0.739	0.700	0.689	L/s
JFH1	0.918	0.976	0.990	0.965	0.918		0.994	0.793	L/s
JFH2	0.990	0.969	0.974	0.995	0.990	1.028	0.805	0.933	L/s
JFH3	0.861	0.876	0.862	0.826	0.861	0.846	0.904	0.797	L/s
JFH4	1.010	1.014	1.000	0.996	1.010	1.001	1.075	0.977	L/s
JFH5	0.960	0.850	0.973	0.984	0.960	0.937	1.086	0.974	L/s
JFH6	0.948	0.931	0.920	0.921	0.948	0.948	0.949	0.918	mm
Delta h1									mm
Delta h2									mm
Delta h3									mm
Delta h4									mm
Delta h5									mm
Delta h6									mm

Table D.4: Test A raw data (2 of 3)

	Test number								
Measurement	DA9	DA10	DA11	DA12	DA13	DA14	DA15	DA16	Unit
C1	50.277	50.040	50.563	41.320	42.069	29.888	48.557	43.086	°C
C2	50.328	50.118	50.636	41.393	42.145	29.953	48.643	43.159	°C
C3	50.362	50.163	50.672	41.437	42.175	29.996	48.673	43.191	°C
C4	50.351	50.060	50.582	41.324	42.074	29.871	48.573	43.092	°C
C5	50.286	50.078	50.600	41.348	42.096	29.898	48.588	43.111	°C
C6	50.244	50.036	50.620	41.350	42.092	29.872	48.602	43.113	°C
H1	54.941	54.717	55.300	46.726	47.022	35.676	54.261	49.055	°C
H2	54.899	54.729	55.313	46.742	47.029	35.693	54.270	49.064	°C
H3	55.012	54.731	55.312	46.718	47.016	35.640	54.278	49.056	°C
H4	54.922	54.768	55.349	46.761	47.059	35.693	54.314	49.095	°C
H5	54.942	54.772	55.353	46.776	47.073	35.722	54.319	49.109	°C
H6	54.940	54.776	55.358	46.786	47.081	35.737	54.322	49.116	°C
C1.1	51.379	51.192	51.728	42.614	43.200	31.129	49.730	44.250	°C
C2.2	51.443	51.254	51.794	42.674	43.219	31.134	49.858	44.363	°C
C3.3	51.485	51.335	51.872	42.667	43.165	31.106	49.665	44.188	°C
C4.4	51.474	51.269	51.808	42.691	43.285	31.236	49.830	44.345	°C
C5.5	51.499	51.291	51.831	42.711	43.309	31.241	49.761	44.379	°C
C6.6	51.595	51.306	51.851	42.644	43.176	31.089	49.682	44.193	°C
H1.1	54.024	53.876	54.442	45.793	46.164	34.744	53.366	48.161	°C
H2.2	54.082	53.899	54.466	45.824	46.166	34.717	53.384	48.186	°C
H3.3	53.975	53.859	54.423	45.875	46.396	34.978	53.638	48.415	°C
H4.4	53.944	53.760	54.327	45.676	46.103	34.689	53.325	48.114	°C
H5.5	54.021	53.832	54.397	45.746	46.144	34.719	53.354	48.137	°C
H6.6	53.929	53.744	54.309	45.762	46.243	34.832	53.469	48.253	°C
Electromag	4.1482	4.1414	4.1401	3.9898	3.9767	3.9332	3.8466	3.9298	L/s
JFC1	0.707	0.729	0.728	0.723	0.750	0.729	0.752	0.761	L/s
JFC2	0.707	0.686	0.689	0.676	0.685		0.593	0.598	L/s
JFC3	0.666	0.655	0.666	0.636	0.590		0.578	0.605	L/s
JFC4	0.747	0.713	0.741	0.715	0.733		0.715	0.739	L/s
JFC5	0.746	0.750	0.768	0.721	0.747	0.718	0.746	0.739	L/s
JFC6	0.639	0.680	0.666	0.613	0.561	0.543	0.569	0.583	L/s
JFH1	0.944	1.024	1.025	0.994	0.978	0.936	0.987	0.971	L/s
JFH2	0.972	0.957	0.954	0.919	0.862		0.806	0.800	L/s
JFH3	0.786	0.891	0.855	0.879	0.869		0.899	0.872	L/s
JFH4	0.948	0.935	0.941	0.949	0.955		0.976	0.970	L/s
JFH5	0.985	0.977	0.987	0.957	0.963		0.983	0.995	L/s
JFH6	0.853	0.860	0.843	0.812	0.791	0.775	0.791	0.779	mm
Delta h1				454	470	472	491	524	mm
Delta h2				430	451	410	348	377	mm
Delta h3				841	1173	1067	1188	1306	mm
Delta h4				406	409	407	406	458	mm
Delta h5				468	520	497	502	524	mm
Delta h6				832	1373	1349	1324	1362	mm

Table D.5: Test A raw data (3 of 3)

	Test number							
Measurement	DA16	DA17	DA18	DA19	DA20	DA21	DA22	Unit
C1	43.086	41.312	40.128	39.445	40.359	33.628	27.301	°C
C2	43.159	41.399	40.211	39.531	40.439	34.188	28.283	°C
C3	43.191	41.428	40.247	39.562	34.726	40.904	36.146	°C
C4	43.092	41.314	40.133	39.450	37.600	37.384	41.536	°C
C5	43.111	41.327	40.124	39.538	37.293	36.796	41.620	°C
C6	43.113	41.295	40.104	39.413	33.426	40.779	34.657	°C
H1	49.055	47.950	47.118	46.670	58.131	57.478	57.134	°C
H2	49.064	47.973	47.134	46.681	58.133	57.490	57.145	°C
H3	49.056	47.999	47.159	46.703	58.196	57.539	57.157	°C
H4	49.095	47.999	47.158	46.705	58.191	57.534	57.189	°C
H5	49.109	48.014	47.176	46.721	58.190	57.533	57.189	°C
H6	49.116	48.021	47.184	46.730	58.189	57.531	57.187	°C
C1.1	44.250	42.491	41.342	40.686	43.560	35.158	26.407	°C
C2.2	44.363	42.462	41.316	40.654	43.465	35.167	26.439	°C
C3.3	44.188	42.456	41.330	40.676	36.388	43.653	38.233	°C
C4.4	44.345	42.603	41.473	40.813	40.294	40.321	44.682	°C
C5.5	44.379	42.634	41.501	40.853	40.103	40.574	44.749	°C
C6.6	44.193	42.414	41.293	40.641	35.996	43.580	37.406	°C
H1.1	48.161	47.094	46.246	45.787	55.901	57.381	57.097	°C
H2.2	48.186	46.988	46.131	45.666	55.561	57.429	57.135	°C
H3.3	48.415	47.336	46.467	45.995	58.224	55.734	57.226	°C
H4.4	48.114	47.022	46.168	45.705	58.064	57.408	55.087	°C
H5.5	48.137	47.042	46.181	45.716	58.148	57.493	55.029	°C
H6.6	48.253	47.097	46.229	45.766	58.121	55.263	57.124	°C
Electromag	3.9298	3.8980	3.8555	3.8481	1.2935	1.2443	1.286	L/s
JFC1	0.761	0.726	0.731	0.716	0.701	0.000	0	L/s
JFC2	0.598	0.721	0.668	0.660	0.644	0.000	0	L/s
JFC3	0.605	0.603	0.581	0.580	0.000	0.613	0	L/s
JFC4	0.739	0.720	0.713	0.708	0.000	0.000	0.6661	L/s
JFC5	0.739	0.727	0.716	0.719	0.000	0.000	0.671825	L/s
JFC6	0.583	0.585	0.575	0.586	0.000	0.615	0	L/s
JFH1	0.971	1.002	0.989	0.998	0.998	0.000	0	L/s
JFH2	0.800	0.777	0.768	0.733	0.733	0.000	0	L/s
JFH3	0.872	0.897	0.862	0.877	0.000	0.877	0	L/s
JFH4	0.970	1.008	0.994	0.995	0.000	0.000	0.9953	L/s
JFH5	0.995	1.011	0.990	0.981	0.000	0.000	0.9809	L/s
JFH6	0.779	0.740	0.747	0.733	0.000	0.733	0	mm
Delta h1	524	543	530	514	484	0	0	mm
Delta h2	377	526	523	511	474	0	0	mm
Delta h3	1306	1201	1198	1193	0	1275	0	mm
Delta h4	458	461	456	442	0	0	416	mm
Delta h5	524	524	520	516	0	0	435	mm
Delta h6	1362	1387	1348	1326	0	1439	0	mm

Table D.6: Raw annular convection test data before the start of test B (1 of 1)

	Test number						
Identifier	OB1	OB2	OB3	OB4	OB5	OB6	Unit
C1	42.999			44.346	44.360	43.219	°C
C2	43.044			44.422	44.438	43.301	°C
C3		43.800			44.470	43.328	°C
C4			43.857	44.356		43.227	°C
C5			43.908	44.414		43.266	°C
C6		43.694			44.370	43.229	°C
H1	56.771			52.513	52.773	48.481	°C
H2	56.783			52.509	52.778	48.488	°C
H3		55.838			52.784	48.482	°C
H4			55.335	52.557		48.522	°C
H5			55.339	52.564		48.534	°C
H6		55.878			52.832	48.542	°C
C1.1	46.043			45.808	45.982	44.335	°C
C2.2	45.699			45.676	45.823	44.241	°C
C3.3		46.331			45.985	44.387	°C
C4.4			46.203	45.780		44.340	°C
C5.5			46.837	45.961		44.493	°C
C6.6		46.852			46.168	44.513	°C
H1.1	53.720			50.357	50.638	47.300	°C
H2.2	54.200			50.757	50.996	47.525	°C
H3.3		53.179			50.699	47.460	°C
H4.4			52.604	50.464		47.425	°C
H5.5			52.904	50.280		47.323	°C
H6.6		53.128			50.482	47.290	°C
Electromag	1.482	1.396	1.404	3.343	2.995	4.112	L/s
JFC1	0.695			0.856	0.779	0.710	L/s
JFC2	0.700			0.850	0.765	0.700	L/s
JFC3		0.708			0.784	0.708	L/s
JFC4			0.718	0.867		0.739	L/s
JFC5			0.722	0.886		0.726	L/s
JFC6		0.699			0.786	0.711	L/s
JFH1	0.683			0.564	0.574	0.650	L/s
JFH2	0.713			0.621	0.599	0.708	L/s
JFH3		0.663			0.568	0.688	L/s
JFH4			0.573	0.580		0.733	L/s
JFH5			0.834	0.611		0.753	L/s
JFH6		0.828			0.588	0.730	mm
Delta h1	441			609	497.5	421	mm
Delta h2	442			627	512	434	mm
Delta h3		480			582	487	mm
Delta h4			438	629		433	mm
Delta h5			449	641		445	mm
Delta h6		478			599	501	mm

Table D.7: Test B raw data (1 of 6)

	Test number								
Measurement	DB1	DB2	DB3	DB4	DB5	DB6	DB7	DB8	Unit
C1	42.999			44.346	44.360	43.219	42.224	40.407	
C2	43.044			44.422	44.438	43.301	42.309	40.485	°C
C3		43.800			44.470	43.328	42.345	40.516	°C
C4			43.857	44.356		43.227	42.237	40.414	°C
C5			43.908	44.414		43.266	42.314	40.484	°C
C6		43.664			44.340	43.199	42.205	40.381	°C
H1	56.771			52.513	52.773	48.481	47.421	45.939	°C
H2	56.783			52.509	52.778	48.488	47.427	45.953	°C
H3		55.838			52.784	48.482	47.425	45.933	°C
H4			55.335	52.557		48.522	47.463	45.976	°C
H5			55.339	52.564		48.534	47.475	45.991	°C
H6		55.878			52.832	48.542	47.482	46.003	°C
C1.1	46.043			45.808	45.982	44.335	43.310	41.550	°C
C2.2	45.699			45.676	45.823	44.241	43.210	41.439	°C
C3.3		46.331			45.985	44.387	43.374	41.616	°C
C4.4			46.203	45.780		44.340	43.350	41.592	°C
C5.5			46.837	45.961		44.493	43.429	41.671	°C
C6.6		46.852			46.168	44.513	43.460	41.700	°C
H1.1	53.720			50.357	50.638	47.300	46.253	44.712	°C
H2.2	54.200			50.757	50.996	47.525	46.448	44.910	°C
H3.3		53.179			50.699	47.460	46.409	44.862	°C
H4.4			52.574	50.434		47.395	46.408	44.739	°C
H5.5			52.904	50.280		47.323	46.237	44.687	°C
H6.6		53.128			50.482	47.290	46.213	44.665	°C
Electromag	1.4818	1.3960	1.4043	3.3433	2.9945	4.1119	4.1349	4.2082	°C
JFC1	0.6953			0.8555	0.7786	0.7100	0.7134	0.7241	L/s
JFC2	0.7001			0.8498	0.7649	0.7001	0.7115	0.7230	L/s
JFC3		0.7084			0.7841	0.7077	0.6920	0.7431	L/s
JFC4			0.7178	0.8673		0.7390	0.7364	0.7572	L/s
JFC5			0.7216	0.8855		0.7260	0.7270	0.7330	L/s
JFC6		0.6993			0.7860	0.7110	0.7100	0.7266	L/s
JFH1	0.6834			0.5642	0.5735	0.6499	0.6445	0.6598	L/s
JFH2	0.7133			0.6211	0.5991	0.7080	0.6673	0.6968	L/s
JFH3		0.6633			0.5682	0.6881	0.6947	0.6805	L/s
JFH4			0.5726	0.5803		0.7330	0.8212	0.6777	L/s
JFH5			0.8336	0.6108		0.7531	0.6800	0.7278	L/s
JFH6		0.8278			0.5877	0.7304	0.6839	0.7247	L/s
Delta h1	441			609	497.5	421	423	443	mm
Delta h2	442			627	512	434	445	471	mm
Delta h3		480			582	487	494	520	mm
Delta h4			438	629		433	442	453	mm
Delta h5			449	641		445	447	472	mm
Delta h6		478			599	501	501	528	mm

Table D.8: Test B raw data (2 of 6)

	Test number								
Measurement	DB9	DB10	DB11	DB12	DB13	DB14	DB15	DB16	Unit
C1	40.445	47.020	39.109	41.580	38.045	38.388	38.830	48.718	
C2	40.525	47.122	39.195	41.667	38.124	38.474	38.915	48.798	°C
C3	40.552	47.140	39.216	41.687	38.149	38.498	38.938	48.828	°C
C4	40.448	47.037	39.108	41.585	38.044	38.389	38.831	48.736	°C
C5	40.458	47.075	39.138	41.617	38.078	38.404	38.849	48.737	°C
C6	40.417	47.016	39.076	41.556	38.008	38.353	38.796	48.714	°C
H1	45.709	52.273	44.835	46.942	44.348	44.555	44.983	54.542	°C
H2	45.720	52.282	44.846	46.947	44.358	44.567	44.993	54.547	°C
H3	45.702	52.284	44.824	46.938	44.333	44.542	44.970	54.558	°C
H4	45.746	52.322	44.868	46.980	44.378	44.586	45.014	54.594	°C
H5	45.761	52.330	44.885	46.995	44.395	44.604	45.032	54.598	°C
H6	45.769	52.332	44.896	47.003	44.409	44.617	45.044	54.600	°C
C1.1	41.535	48.111	40.252	42.673	39.265	39.559	39.996	49.805	°C
C2.2	41.425	48.004	40.130	42.555	39.136	39.435	39.874	49.716	°C
C3.3	41.554	48.135	40.264	42.673	39.274	39.570	40.010	49.834	°C
C4.4	41.508	48.080	40.213	42.640	39.213	39.504	39.943	49.775	°C
C5.5	41.662	48.235	40.346	42.754	39.306	39.599	40.037	49.881	°C
C6.6	41.701	48.300	40.424	42.835	39.467	39.752	40.200	50.084	°C
H1.1	44.581	51.141	43.666	45.844	43.170	43.391	43.820	53.418	°C
H2.2	44.779	51.349	43.867	46.029	43.361	43.583	44.011	53.619	°C
H3.3	44.672	51.290	43.795	45.964	43.287	43.502	43.931	53.557	°C
H4.4	44.623	51.201	43.706	45.885	43.200	43.420	43.850	53.467	°C
H5.5	44.583	51.172	43.637	45.798	43.060	43.283	43.713	53.387	°C
H6.6	44.546	51.063	43.557	45.740	42.988	43.210	43.636	53.235	°C
Electromag	4.2369	4.1859	4.2017	4.1614	4.2507	4.1571	4.1553	4.1146	°C
JFC1	0.7377	0.7299	0.7366	0.7159		0.7097	0.7026	0.7011	L/s
JFC2	0.7204	0.7095	0.7182	0.7029	0.7225	0.7091	0.7155	0.7012	L/s
JFC3	0.7346	0.7162	0.7113	0.7204		0.7084	0.7174	0.6968	L/s
JFC4	0.7483	0.7251	0.7465	0.7352		0.7386	0.7494	0.7228	L/s
JFC5	0.7404	0.7399	0.7177	0.7187		0.7254	0.7277	0.7125	L/s
JFC6	0.7185	0.6994	0.7129	0.7113		0.6958	0.7041	0.6989	L/s
JFH1	0.6951	0.6901	0.6792	0.6968		0.6818	0.6870	0.6839	L/s
JFH2	0.7046	0.6846	0.7176	0.7071	0.7069	0.7134	0.7079	0.6989	L/s
JFH3	0.6652	0.6779	0.7057	0.7001		0.6987	0.7024	0.7219	L/s
JFH4	0.6769	0.6877	0.6987	0.7005		0.6991	0.6962	0.6659	L/s
JFH5	0.7452	0.7375	0.7105	0.7013		0.6447	0.6495	0.6584	L/s
JFH6	0.7503	0.7147	0.7019	0.7186		0.7025	0.7022	0.6980	L/s
Delta h1	449	433	451	444	496.5	487	486	456	mm
Delta h2	475.5	442	469	461	526	510	511	473	mm
Delta h3	525	508	538	525		559	557	527	mm
Delta h4	479	439	461	456		498	493	472	mm
Delta h5	475	466	472	460		498	496	475	mm
Delta h6	528	501	519	520		521	519	490	mm

Table D.9: Test B raw data (3 of 6)

	Test number								
Measurement	DB16	DB17	DB18	DB19	DB20	DB21	DB22	DB23	Unit
C1	48.718	38.970	38.403	27.247	30.367	33.162	40.927	40.178	
C2	48.798	39.044	38.476	27.292	30.413	33.219	40.972	40.236	°C
C3	48.828	39.078	38.506	27.338	30.456	33.260	41.024	40.277	°C
C4	48.736	38.970	38.402	27.224	30.348	33.149	40.926	40.176	°C
C5	48.737	38.996	38.431	27.223	30.374	33.180	40.947	40.195	°C
C6	48.714	38.935	38.364	27.256	30.300	33.104	40.893	40.142	°C
H1	54.542	45.237	44.575	36.977	37.729	40.316	48.000	47.393	°C
H2	54.547	45.248	44.585	36.984	37.738	40.325	48.012	47.405	°C
H3	54.558	45.228	44.563	36.945	37.697	40.291	47.998	47.390	°C
H4	54.594	45.271	44.607	36.995	37.747	40.339	48.039	47.432	°C
H5	54.598	45.287	44.625	37.023	37.774	40.362	48.052	47.445	°C
H6	54.600	45.297	44.637	37.038	37.790	40.378	48.060	47.453	°C
C1.1	49.805	40.109	39.541	29.088	31.593	34.389	42.172	41.376	°C
C2.2	49.716	39.998	39.421	28.899	31.442	34.245	42.041	41.252	°C
C3.3	49.834	40.124	39.541	29.077	31.530	34.354	42.154	41.349	°C
C4.4	49.775	40.061	39.494	29.006	31.512	34.313	42.109	41.306	°C
C5.5	49.881	40.159	39.602	29.138	31.625	34.305	42.119	41.406	°C
C6.6	50.084	40.373	39.782	29.613	31.818	34.605	42.353	41.625	°C
H1.1	53.418	44.103	43.425	35.846	36.584	39.165	46.802	46.259	°C
H2.2	53.619	44.296	43.622	36.004	36.772	39.355	46.995	46.427	°C
H3.3	53.557	44.207	43.504	35.931	36.697	39.258	46.902	46.366	°C
H4.4	53.467	44.141	43.463	35.855	36.625	39.207	46.897	46.270	°C
H5.5	53.387	44.031	43.365	35.763	36.513	39.095	46.746	46.243	°C
H6.6	53.235	43.885	43.225	35.535	36.358	38.956	46.576	46.033	°C
Electromag	4.1146	4.1295	4.1974	2.5425	3.9450	3.9603	3.9913	3.9352	°C
JFC1	0.7011	0.7423	0.7264	0.4423	0.6782	0.6310	0.6982	0.6819	L/s
JFC2	0.7012	0.7126	0.7125	0.4411	0.6873	0.6095	0.6990	0.6875	L/s
JFC3	0.6968	0.7046	0.7250	0.4354	0.6727	0.5940	0.6760	0.6660	L/s
JFC4	0.7228	0.7388	0.7488	0.4556	0.7160	0.6291	0.7110	0.7089	L/s
JFC5	0.7125	0.7266	0.7356	0.4504	0.6981	0.6351	0.7060	0.6940	L/s
JFC6	0.6989	0.6940	0.7167	0.4400	0.6929	0.6250	0.6880	0.6936	L/s
JFH1	0.6839	0.6963	0.6975	0.6848	0.6822	0.6196	0.6656	0.6890	L/s
JFH2	0.6989	0.7191	0.7081	0.7127	0.7059	0.6171	0.7088	0.7090	L/s
JFH3	0.7219	0.6985	0.6681	0.6739	0.6790	0.6057	0.6886	0.6830	L/s
JFH4	0.6659	0.6905	0.6958	0.6858	0.6890	0.5990	0.6710	0.6672	L/s
JFH5	0.6584	0.6674	0.6902	0.6827	0.6750	0.5917	0.6643	0.7250	L/s
JFH6	0.6980	0.6838	0.6926	0.6915	0.6819	0.6036	0.6907	0.6900	L/s
Delta h1	456	464	478	257	608	587.92	514	510	mm
Delta h2	473	487	512	252	646	630.92	562	556.5	mm
Delta h3	527	542	557	273	690	673.92	563	576	mm
Delta h4	472	473	492	249	594	582.92	528	529	mm
Delta h5	475	482	489	247	599	576.92	523	529	mm
Delta h6	490	505	517	237	532	519.92	499	504	mm

Table D.10: Test B raw data (4 of 6)

	Test number								
Measurement	DB24	DB25	DB26	DB27	DB28	DB29	DB30	DB31	Unit
C1	43.418	37.702	42.232	39.866	37.850	40.055	37.344	39.078	
C2	43.478	37.761	42.295	40.223	38.019	40.125	37.411	39.132	°C
C3	43.516	37.800	42.331	40.263	38.048	40.151	37.439	39.158	°C
C4	43.421	37.696	42.233	40.159	37.944	40.053	37.338	39.075	°C
C5	43.432	37.720	42.248	39.884	37.878	40.072	37.357	39.088	°C
C6	43.393	37.658	42.202	40.064	37.898	40.021	37.299	39.040	°C
H1	50.433	45.452	51.154	49.727	47.689	50.108	48.020	49.394	°C
H2	50.446	45.462	51.166	49.736	47.754	50.118	48.029	49.396	°C
H3	50.440	45.442	51.161	49.773	47.741	50.112	48.015	49.397	°C
H4	50.479	45.485	51.198	49.769	47.782	50.152	48.056	49.436	°C
H5	50.488	45.502	51.208	49.744	47.739	50.162	48.070	49.448	°C
H6	50.494	45.512	51.214	49.779	47.747	50.168	48.080	49.454	°C
C1.1	44.566	38.854	43.410	40.985	38.931	41.128	38.475	40.178	°C
C2.2	44.452	38.746	43.338	41.189	38.957	41.070	38.406	40.108	°C
C3.3	44.546	38.867	43.441	41.275	39.034	41.137	38.476	40.180	°C
C4.4	44.523	38.793	43.372	41.240	39.002	41.115	38.462	40.162	°C
C5.5	44.608	38.834	43.331	40.926	38.918	40.997	38.516	40.216	°C
C6.6	44.828	39.291	44.035	41.927	39.732	41.867	39.173	40.858	°C
H1.1	49.288	44.357	50.035	48.612	46.628	49.035	46.964	48.325	°C
H2.2	49.465	44.504	50.161	48.784	46.696	49.142	47.049	48.444	°C
H3.3	49.409	44.498	50.176	48.864	46.753	49.160	47.075	48.463	°C
H4.4	49.362	44.353	50.015	48.688	46.635	49.030	46.943	48.338	°C
H5.5	49.281	44.317	50.014	48.550	46.644	49.055	46.947	48.350	°C
H6.6	49.057	43.918	49.396	47.783	45.859	48.305	46.281	47.690	°C
Electromag	4.0706	3.9314	3.8932	3.9634	4.0091	4.0000	3.8025	3.8030	°C
JFC1	0.7186	0.6808	0.6867	0.6896	0.6959	0.6954		0.6595	L/s
JFC2	0.7025	0.6731	0.6863	0.7078	0.6928	0.7023		0.6856	L/s
JFC3	0.6837	0.6785	0.6680	0.6890	0.6886	0.6890			L/s
JFC4	0.7332	0.7133	0.7053	0.7230	0.7148	0.7194			L/s
JFC5	0.7229	0.6978	0.6968	0.7168	0.7235	0.7154	0.6831	0.6817	L/s
JFC6	0.7129	0.7036	0.6920	0.7108	0.7158	0.7205		0.6890	L/s
JFH1	0.6785	0.6748	0.6844	0.6767	0.6759	0.6650		0.6629	L/s
JFH2	0.6818	0.6850	0.6914	0.6933	0.6417	0.6702		0.6978	L/s
JFH3	0.6675	0.7307	0.7234	0.7089	0.6991	0.6932			L/s
JFH4	0.7095	0.6680	0.6513	0.7226	0.6560	0.6760			L/s
JFH5	0.6900	0.6895	0.6792	0.6471	0.7090	0.6931	0.6894	0.6851	L/s
JFH6	0.7021	0.6751	0.6732	0.6265	0.7123	0.6960		0.6688	L/s
Delta h1	548	510	552	605	610	616		599	mm
Delta h2	598	548	594	654	650	672		663	mm
Delta h3	650	575	637	670	661	675		654	mm
Delta h4	582	523	562	614	611.5	625			mm
Delta h5	570	528	567.5	610	615	631	618	603	mm
Delta h6	530	486	492	521	529	538		511	mm

Table D.11: Test B raw data (5 of 6)

	Test number								
Measurement	DB32	DB33	DB34	DB35	DB36	DB37	DB38	DB39	Unit
C1	39.376	39.078	38.815	34.678	37.586	36.848	38.460	36.425	
C2	39.446	39.132	38.888	34.741	37.652	36.925	38.536	36.496	°C
C3	39.472	39.472	38.799	34.803	32.805	37.007	38.555	36.518	°C
C4	39.372	39.372	38.811	34.667	34.607	36.841	38.456	36.417	°C
C5	39.387	39.088	38.838	34.695	34.366	36.866	38.484	36.585	°C
C6	39.338	39.040	38.777	34.628	31.604	36.804	38.422	36.524	°C
H1	49.851	49.394	49.561	45.362	48.863	47.264	49.317	47.463	°C
H2	49.860	49.396	49.570	45.364	48.873	47.275	49.326	47.471	°C
H3	49.854	49.854	49.384	45.382	48.860	47.254	49.318	47.458	°C
H4	49.893	49.893	49.602	45.396	48.902	47.300	49.359	47.499	°C
H5	49.905	49.448	49.615	45.414	48.914	47.315	49.371	47.713	°C
H6	49.912	49.454	49.622	45.423	48.921	47.324	49.378	47.722	°C
C1.1	40.493	40.178	39.932	35.786	38.532	38.187	39.673	37.583	°C
C2.2	40.426	40.108	39.879	35.684	38.442	38.051	39.571	37.491	°C
C3.3	40.499	40.499	39.826	35.806	32.378	37.973	39.529	37.467	°C
C4.4	40.480	40.480	39.934	35.756	35.791	37.906	39.507	37.451	°C
C5.5	40.496	40.216	39.986	35.804	35.555	37.954	39.555	37.611	°C
C6.6	41.199	40.858	40.752	36.485	31.630	38.650	40.611	38.726	°C
H1.1	48.771	48.325	48.429	44.369	47.464	46.057	48.224	46.387	°C
H2.2	48.894	48.444	48.602	44.349	47.607	46.173	48.339	46.512	°C
H3.3	48.905	48.905	48.438	44.447	48.951	46.331	48.422	46.577	°C
H4.4	48.792	48.792	48.490	44.301	48.806	46.208	48.304	46.479	°C
H5.5	48.799	48.350	48.493	44.313	48.878	46.228	48.325	46.688	°C
H6.6	48.119	47.690	47.661	43.570	48.867	45.476	47.252	45.625	°C
Electromag	3.8030	3.8030	3.8248	3.8501	2.0385	3.8523	3.7351	3.7339	°C
JFC1		0.6595	0.6673	0.6753	1.0936	0.6577	0.6517	0.6561	L/s
JFC2		0.6856	0.6869	0.6920	1.1045	0.6764	0.6712	0.6619	L/s
JFC3	0.6652	0.6652	0.6723	0.6654		0.6657	0.6544	0.6478	L/s
JFC4	0.6835	0.6835	0.6884	0.7018		0.6821	0.6918	0.6836	L/s
JFC5		0.6817	0.7003	0.6926		0.6932	0.6920	0.6905	L/s
JFC6		0.6890	0.7212	0.7038		0.7218	0.7247	0.7183	L/s
JFH1		0.6629	0.6311	0.7156	0.6926	0.6947	0.6821	0.6647	L/s
JFH2		0.6978	0.6966	0.6241	0.6821	0.6936	0.6944	0.6796	L/s
JFH3	0.6689	0.6689	0.6750	0.6577		0.6426	0.6594	0.6486	L/s
JFH4	0.7056	0.7056	0.7014	0.6907		0.6884	0.6757	0.6932	L/s
JFH5		0.6851	0.7038	0.6916		0.6763	0.6767	0.6926	L/s
JFH6		0.6688	0.6675	0.6711		0.6676	0.6776	0.6852	L/s
Delta h1		599	843	793		812	879	813.5	mm
Delta h2		663	915	861		884	949	895	mm
Delta h3	657	657	904	848		851	963.5	896	mm
Delta h4	596	596	847	788		802	901.5	839	mm
Delta h5		603	844	795		800	914	843	mm
Delta h6		511	622	599		611	635.5	628	mm

Table D.12: Test B raw data (6 of 6)

	Test number		
Measurement	DB40	DB41	Unit
C1	39.668	43.785	
C2	39.745	43.862	°C
C3	39.765	43.880	°C
C4	39.666	43.788	°C
C5	39.682	43.796	°C
C6	39.820	43.763	°C
H1	50.219	54.473	°C
H2	50.228	54.482	°C
H3	50.223	54.489	°C
H4	50.263	54.524	°C
H5	50.274	54.529	°C
H6	50.443	54.532	°C
C1.1	40.793	44.975	°C
C2.2	40.698	44.916	°C
C3.3	40.674	44.872	°C
C4.4	40.660	44.858	°C
C5.5	40.718	44.902	°C
C6.6	41.872	45.919	°C
H1.1	49.145	53.368	°C
H2.2	49.276	53.513	°C
H3.3	49.348	53.582	°C
H4.4	49.245	53.478	°C
H5.5	49.259	53.489	°C
H6.6	48.421	52.471	°C
Electromag	3.8250	3.6210	°C
JFC1	0.6645	0.6411	L/s
JFC2	0.6878	0.6428	L/s
JFC3	0.6733	0.6289	L/s
JFC4	0.6910	0.6580	L/s
JFC5	0.7061	0.6801	L/s
JFC6	0.7290	0.6746	L/s
JFH1	0.6565	0.6620	L/s
JFH2	0.6840	0.6955	L/s
JFH3	0.6408	0.6373	L/s
JFH4	0.6806	0.6758	L/s
JFH5	0.6932	0.6858	L/s
JFH6	0.6773	0.6653	L/s
Delta h1	816	722	mm
Delta h2	904	783	mm
Delta h3	909	780	mm
Delta h4	836	759	mm
Delta h5	866	764	mm
Delta h6	621	525	mm

Table D.13: Raw annular convection test data before the start of test C (1 of 1)

	Test number				
Measurement	OC1	OC2	OC3	OC4	Unit
C1	40.231	40.936	37.256	40.144	°C
C2	40.305	41.013	37.334	40.217	°C
C3	40.325	41.029	37.356	40.230	°C
C4	40.229	40.935	37.249	40.142	°C
C5	40.246	40.962	37.286	40.173	°C
C6	40.197	40.905	37.214	40.112	°C
H1	46.949	47.899	46.509	47.315	°C
H2	46.959	47.908	46.517	47.324	°C
H3	46.944	47.896	40.231	47.312	°C
H4	46.986	47.939	46.546	47.353	°C
H5	47.000	47.951	46.561	47.368	°C
H6	47.010	47.959	39.424	47.377	°C
C1.1	41.508	42.236	39.121	41.694	°C
C2.2	41.567	42.299	39.182	41.731	°C
C3.3	40.869	41.613	37.237	40.954	°C
C4.4	41.744	42.458	39.382	41.825	°C
C5.5	41.445	42.191	39.037	41.639	°C
C6.6	41.533	42.313	37.237	41.781	°C
H1.1	45.651	46.462	44.853	46.031	°C
H2.2	45.721	46.538	44.918	46.078	°C
H3.3	46.356	47.277	39.980	46.812	°C
H4.4	45.509	46.295	44.593	45.736	°C
H5.5	45.665	46.510	44.903	46.071	°C
H6.6	45.654	46.558	39.002	46.146	°C
Electromag	3.9245	3.8420	3.7490	3.2670	L/s
JFC1	0.6907	0.6788	0.6664	0.5756	L/s
JFC2	0.7062	0.7120	0.6817	0.6076	L/s
JFC3	0.6702	0.6469		0.5613	L/s
JFC4	0.7257	0.6916	0.6862	0.6035	L/s
JFC5	0.7448	0.7291	0.7061	0.6114	L/s
JFC6	0.6976	0.7010		0.5781	L/s
JFH1	0.6523	0.5937	0.7051	0.6751	L/s
JFH2	0.7154	0.6380	0.7494	0.6854	L/s
JFH3	0.5830	0.5736		0.6966	L/s
JFH4	0.7301	0.6366	0.7212	0.6124	L/s
JFH5	0.6481	0.6122	0.7549	0.6792	L/s
JFH6	0.6403	0.6384		0.7297	mm
Delta h1	428	413	399	311	mm
Delta h2	439	415	406	311	mm
Delta h3	962	941	433	774	mm
Delta h4	470	465	429	338	mm
Delta h5	483	469	448	350	mm
Delta h6	524	500		370	mm

Table D.14: Test C raw data (1 of 3)

	Test number								
Measurement	DC1	DC2	DC3	DC4	DC5	DC6	DC7	DC8	Unit
C1	40.231	40.936	37.256	40.144	46.397	47.370	47.598	46.697	
C2	40.305	41.013	37.334	40.217	46.464	47.435	47.672	47.773	°C
C3	40.325	41.029	37.356	40.230	46.488	47.458	47.693	47.806	°C
C4	40.229	40.935	37.249	40.142	46.405	47.382	47.610	47.746	°C
C5	40.246	40.962	37.286	40.173	46.408	47.412	47.613	47.820	°C
C6	40.197	40.905	37.214	40.112	46.380	47.358	47.588	47.717	°C
H1	46.949	47.899	46.509	47.315	52.706	54.855	54.692	55.208	°C
H2	46.959	47.908	46.517	47.324	52.710	54.867	54.700	55.207	°C
H3	46.944	47.896	40.231	47.312	52.716	54.872	54.709	55.217	°C
H4	46.986	47.939	46.546	47.353	52.754	54.907	54.746	55.257	°C
H5	47.000	47.951	46.561	47.368	52.761	54.912	54.750	55.258	°C
H6	47.010	47.959	39.424	47.377	52.765	54.914	54.751	55.258	°C
C1.1	41.508	42.236	39.121	41.694	47.591	49.078	49.239	48.108	°C
C2.2	41.567	42.299	39.182	41.731	47.561	49.049	49.182	49.166	°C
C3.3	40.869	41.613	37.237	40.954	47.006	48.255	48.431	48.408	°C
C4.4	41.744	42.458	39.382	41.825	47.767	49.201	49.318	49.380	°C
C5.5	41.445	42.191	39.037	41.639	47.580	49.081	49.210	49.258	°C
C6.6	41.533	42.313	37.237	41.781	47.702	49.115	49.226	49.259	°C
H1.1	45.651	46.462	44.853	46.031	51.428	53.482	53.397	54.337	°C
H2.2	45.721	46.538	44.918	46.078	51.357	53.432	53.335	53.672	°C
H3.3	46.356	47.277	39.980	46.812	52.249	54.283	54.137	54.720	°C
H4.4	45.509	46.295	44.593	45.736	51.195	53.201	53.102	53.609	°C
H5.5	45.665	46.510	44.903	46.071	51.514	53.576	53.474	54.000	°C
H6.6	45.654	46.558	39.002	46.146	51.583	53.499	53.393	53.904	°C
Electromag	3.9245	3.8420	3.7490	3.2670	4.0260	3.1140	3.1140	3.1536	°C
JFC1	0.6907	0.6788	0.6664	0.5756	0.7211	0.5460			L/s
JFC2	0.7062	0.7120	0.6817	0.6076	0.7703	0.6133		0.6129	L/s
JFC3	0.6702	0.6469		0.5613	0.6745		0.5280	0.5294	L/s
JFC4	0.7257	0.6916	0.6862	0.6035	0.7151		0.6044	0.6460	L/s
JFC5	0.7448	0.7291	0.7061	0.6114	0.7613	0.5771		0.6040	L/s
JFC6	0.6976	0.7010		0.5781	0.7281	0.5488		0.5572	L/s
JFH1	0.6523	0.5937	0.7051	0.6751	0.6540	0.6599			L/s
JFH2	0.7154	0.6380	0.7494	0.6854	0.5985	0.5931	0.6209	0.5146	L/s
JFH3	0.5830	0.5736		0.6966	0.6935		0.6217	0.5727	L/s
JFH4	0.7301	0.6366	0.7212	0.6124	0.6254		0.6304	0.6257	L/s
JFH5	0.6481	0.6122	0.7549	0.6792	0.6867	0.6922		0.7029	L/s
JFH6	0.6403	0.6384		0.7297	0.7552	0.6270		0.5937	L/s
Delta h1	428	413	399	311	425	275		347	mm
Delta h2	439	415	406	311	462	287		346	mm
Delta h3	962	941	433	774	990		548	597	mm
Delta h4	470	465	429	338	427		299	329	mm
Delta h5	483	469	448	350	504	299		335	mm
Delta h6	524	500		370	543	330		393	mm

Table D.15: Test C raw data (2 of 3)

	Test number								
Measurement	DC9	DC10	DC11	DC12	DC13	DC14	DC15	DC16	Unit
C1	45.143	48.274	49.158	38.803	42.206	41.478	50.572	45.896	
C2	45.209	48.326	49.215	38.862	42.256	41.536	50.618	45.944	°C
C3	45.253	48.371	49.249	38.893	42.286	41.567	50.648	45.977	°C
C4	45.155	48.289	49.170	38.800	42.208	41.479	50.587	45.909	°C
C5	45.306	48.323	49.168	38.843	42.240	41.515	50.597	46.035	°C
C6	45.121	48.260	49.146	38.763	42.176	41.447	50.562	45.880	°C
H1	52.374	53.141	53.317	47.293	50.238	51.407	53.830	53.162	°C
H2	52.397	53.159	53.321	47.304	50.246	51.417	53.841	53.163	°C
H3	52.382	53.148	53.327	47.290	50.246	51.419	53.847	53.172	°C
H4	52.419	53.188	53.364	47.333	50.286	51.458	53.884	53.208	°C
H5	52.426	53.193	53.372	47.346	50.295	51.466	53.887	53.216	°C
H6	52.434	53.194	53.377	47.355	50.300	51.467	53.889	53.222	°C
C1.1	46.673	49.291	49.956	40.469	43.699	42.981	51.014	46.924	°C
C2.2	46.656	49.266	50.022	40.480	43.678	42.969	51.047	46.944	°C
C3.3	45.833	48.709	49.514	39.526	42.874	42.284	50.807	46.449	°C
C4.4	46.762	49.389	50.132	40.681	43.979	43.370	51.172	47.222	°C
C5.5	46.658	49.295	49.996	40.423	43.744	43.355	51.189	47.190	°C
C6.6	46.673	49.309	50.011	40.472	43.757	43.295	51.136	47.145	°C
H1.1	51.142	52.302	52.505	45.806	48.845	50.016	53.339	52.124	°C
H2.2	51.120	52.283	52.606	45.928	49.042	50.284	53.465	52.333	°C
H3.3	51.949	52.862	53.087	46.761	49.762	50.840	53.711	52.775	°C
H4.4	50.873	52.100	52.442	45.626	48.708	49.899	53.277	52.019	°C
H5.5	51.256	52.332	52.593	45.864	48.884	49.834	53.309	52.001	°C
H6.6	51.156	52.299	52.572	45.841	48.881	49.936	53.333	52.068	°C
Electromag	3.1450	3.1870	3.1610	3.0900	3.1033	2.9143	3.1385	3.1017	°C
JFC1	0.5488		0.5754	0.5336	0.5255	0.4979	0.5121	0.5121	L/s
JFC2	0.6129	0.6308	0.5803	0.5649	0.5760	0.5060	0.5312	0.5312	L/s
JFC3	0.5294		0.5708	0.5565	0.5716	0.5040	0.5244	0.5244	L/s
JFC4	0.6460		0.5815	0.5942	0.5983	0.5048	0.5564	0.5564	L/s
JFC5	0.6040		0.6040	0.6052	0.6071	0.5554	0.6062	0.6062	L/s
JFC6	0.5572		0.5600	0.5511	0.5497	0.4923	0.5215	0.5215	L/s
JFH1	0.6755		0.5579	0.5768	0.5571	0.5277	0.5305	0.5305	L/s
JFH2	0.6053	0.6112	0.6141	0.6177	0.6063	0.6197	0.6119	0.6119	L/s
JFH3	0.6158		0.5774	0.5826	0.5940	0.5763	0.5710	0.5710	L/s
JFH4	0.6323		0.6221	0.6161	0.6325	0.6344	0.6289	0.6289	L/s
JFH5	0.7099		0.6222	0.6327	0.6284	0.6321	0.6403	0.6403	L/s
JFH6	0.6168		0.5670	0.5657	0.5637	0.5707	0.5618	0.5618	L/s
Delta h1	347		341	339	349	413	470	470	mm
Delta h2	346	367	318	354	366	423	481	481	mm
Delta h3	597		651	655	691	708	774	774	mm
Delta h4	329		280	300	313	391	408	408	mm
Delta h5	335		355	347	349	390	400	400	mm
Delta h6	393		394	424	439	441	546	546	mm

Table D.16: Test C raw data (3 of 3)

	Test number				
Measurement	DC16	DC17	DC18	DC19	Unit
C1	45.896	50.330	49.493	50.920	
C2	45.944	50.377	49.531	50.959	°C
C3	45.977	50.416	49.562	50.989	°C
C4	45.909	50.350	49.508	50.936	°C
C5	46.035	50.419	49.529	50.953	°C
C6	45.880	50.324	49.481	50.911	°C
H1	53.162	53.925	53.818	54.060	°C
H2	53.163	53.945	53.831	54.073	°C
H3	53.172	53.944	53.835	54.076	°C
H4	53.208	53.976	53.872	54.114	°C
H5	53.216	53.981	53.876	54.118	°C
H6	53.222	53.985	53.879	54.120	°C
C1.1	46.924	50.794	50.057	51.262	°C
C2.2	46.944	50.827	50.095	51.307	°C
C3.3	46.449	50.589	49.821	51.137	°C
C4.4	47.222	50.972	50.259	51.417	°C
C5.5	47.190	50.978	50.292	51.472	°C
C6.6	47.145	50.939	50.227	51.402	°C
H1.1	52.124	53.445	53.284	53.650	°C
H2.2	52.333	53.573	53.437	53.785	°C
H3.3	52.775	53.811	53.673	53.975	°C
H4.4	52.019	53.371	53.218	53.623	°C
H5.5	52.001	53.397	53.226	53.618	°C
H6.6	52.068	53.418	53.261	53.658	°C
Electromag	3.1017	3.0209	2.6864	2.8294	°C
JFC1	0.5121	0.5042	0.4539	0.4798	L/s
JFC2	0.5312	0.5173	0.4665	0.4905	L/s
JFC3	0.5244	0.5033	0.4467	0.4801	L/s
JFC4	0.5564	0.5276	0.5067	0.5229	L/s
JFC5	0.6062	0.6018	0.5555	0.5791	L/s
JFC6	0.5215	0.5108	0.4587	0.4841	L/s
JFH1	0.5305	0.5131	0.4729	0.4404	L/s
JFH2	0.6119	0.5959	0.6196	0.5712	L/s
JFH3	0.5710	0.5728	0.5805	0.5562	L/s
JFH4	0.6289	0.6210	0.6246	0.6146	L/s
JFH5	0.6403	0.6397	0.6332	0.5927	L/s
JFH6	0.5618	0.5493	0.5567	0.5320	L/s
Delta h1	470	606	683	836	mm
Delta h2	481	609	710	870	mm
Delta h3	774	1094	1114	1128	mm
Delta h4	408	516	631	792	mm
Delta h5	400	500	586	735	mm
Delta h6	546	634	706	855	mm

D.3 Processed convection data

Processed convection data is tabulated in tables D.17, D.18, D.19, D.20, D.21, D.22 (test A), D.23, D.24, D.25, D.26, D.27, D.28 (test B), D.29, D.30, D.31, D.32 (test C).

Table D.17: Heat exchanger 1: processed convection data (test A)

Identifier	Vc	Vh	EB	MB	Q	ΔT	UA
OA1	0.7576	2.021	1.21	5.51	6677.5	12.04	554.64
OA2	1.687	0.8456	−0.351	−2.93	6439.9	10.88	591.98
OA3	1.646	1.231	−1.35	−2.21	7322.5	10.67	686.37
OA8	1.874	1.841	−6.81	−15.3	2046.8	2.098	975.59
OA9	1.849	1.867	−8.77	2.74	1875.4	1.914	979.84
OA10	1.804	1.820	−9.52	1.62	1705.7	1.831	931.51
OA11	1.831	1.730	−4.42	2.30	3870.3	4.147	933.17

Table D.18: Heat exchanger 2: processed convection data (test A)

Identifier	Vc	Vh	EB	MB	Q	ΔT	UA
OA1	0.8023	1.988	2.72	5.51	6844.7	11.97	571.88
OA2	1.678	0.8270	2.03	−2.93	6388.5	10.78	592.42
OA3	1.709	1.208	−1.91	−2.21	7242.6	10.63	681.16
OA8	1.726	1.792	4.10	−15.3	1831.8	2.081	880.30
OA9	1.715	1.801	−1.58	2.74	1628.1	1.882	865.11
OA10	1.733	1.840	−3.82	1.62	1508.1	1.800	838.02
OA11	1.747	1.830	2.46	2.30	3663.7	4.108	891.89

Table D.19: Heat exchanger 3: processed convection data (test A)

Identifier	Vc	Vh	EB	MB	Q	ΔT	UA
OA5	1.793	1.996	0.777	−3.08	9502.6	10.67	890.47
OA6	1.740	1.788	−1.29	−1.85	6588.6	8.534	772.05
OA9	1.878	1.916	−6.59	2.74	1940.2	1.930	1005.45
OA10	1.758	1.836	−11.4	1.62	1671.3	1.843	906.64
OA11	1.841	1.914	−6.78	2.30	3998.3	4.047	987.93

Table D.20: Heat exchanger 4: processed convection data (test A)

Identifier	Vc	Vh	EB	MB	Q	ΔT	UA
OA4	1.995	1.775	3.46	−2.75	10182	11.06	920.91
OA6	1.823	2.337	3.23	−0.775	6556.1	7.137	918.60
OA8	1.759	1.847	−12.1	−15.3	1950.3	2.046	953.01
OA9	1.860	1.822	−12.5	2.74	1810.8	1.868	969.45
OA10	1.771	1.815	6.96	1.62	1483.8	1.756	845.13
OA11	1.786	1.841	−7.53	2.30	4017.9	4.095	981.26

Table D.21: Heat exchanger 5: processed convection data (test A)

Identifier	Vc	Vh	EB	MB	Q	ΔT	UA
OA4	1.896	1.881	0.460	−2.75	10091	11.10	908.86
OA6	1.764	2.143	1.31	−0.775	6533.9	7.165	911.96
OA8	1.786	1.583	−1.27	−15.3	2012.2	2.059	977.34
OA9	1.771	1.812	−4.30	2.74	1939.6	1.885	1029.02
OA10	1.761	1.833	−5.70	1.62	1848.7	1.811	1020.60
OA11	1.766	1.789	0.110	2.30	4080.7	4.099	995.51

Table D.22: Heat exchanger 6: processed convection data (test A)

Identifier	Vc	Vh	EB	MB	Q	ΔT	UA
OA5	1.666	1.994	−9.05	−3.08	9508.8	10.69	889.29
OA6	1.812	1.572	−4.70	−1.85	7349.6	8.336	881.66
OA8	1.824	2.045	−5.61	−15.3	2288.1	1.958	1168.46
OA9	1.862	2.021	−3.47	2.74	2109.2	1.784	1181.98
OA10	1.813	2.023	−1.39	1.62	1929.3	1.733	1113.51
OA11	1.787	2.083	−2.12	2.30	4291.5	3.973	1080.17

Table D.23: Heat exchanger 1: convection data (test B)

Identifier	Vc	Vh	EB	MB	Q	ΔT	UA
OB1	1.713	1.287	0.0975	−7.43	8601.6	10.72	802.08
OB4	2.108	1.062	1.21	1.80	5053.5	6.352	795.61
OB5	1.918	1.080	1.52	2.98	5094.4	6.531	780.01
OB6	1.749	1.224	1.59	3.24	3198.8	4.113	777.66

Table D.24: Heat exchanger 2: convection data (test B)

Identifier	Vc	Vh	EB	MB	Q	ΔT	UA
OB1	1.764	1.316	1.45	−7.43	7506.6	11.12	675.04
OB4	2.141	1.146	−1.67	1.80	4371.7	6.581	664.30
OB5	1.927	1.105	−0.357	2.98	4317.0	6.755	639.13
OB6	1.764	1.306	−3.20	3.24	2721.0	4.236	642.38

Table D.25: Heat exchanger 3: convection data (test B)

Identifier	Vc	Vh	EB	MB	Q	ΔT	UA
OB2	1.783	1.447	−0.124	0.642	7413.0	9.443	785.04
OB5	1.973	1.239	−1.59	2.98	4947.8	6.510	760.06
OB6	1.781	1.501	4.32	3.24	3030.3	4.114	736.68

Table D.26: Heat exchanger 4: convection data (test B)

Identifier	Vc	Vh	EB	MB	Q	ΔT	UA
OB4	2.086	1.057	1.83	1.80	4954.1	6.437	769.66
OB6	1.778	1.336	2.29	3.24	3291.9	4.190	785.66

Table D.27: Heat exchanger 5: convection data (test B)

Identifier	Vc	Vh	EB	MB	Q	ΔT	UA
OB3	1.722	1.536	4.66	0.996	8467.2	8.747	968.04
OB4	2.113	1.126	−1.18	1.80	5652.7	6.227	907.74
OB6	1.733	1.388	−1.78	3.24	3690.1	4.049	911.41

Table D.28: Heat exchanger 6: convection data (test B)

Identifier	Vc	Vh	EB	MB	Q	ΔT	UA
OB2	1.742	1.805	−6.27	0.642	9415.0	9.228	1020.21
OB5	1.958	1.281	−1.23	2.98	5866.6	6.384	918.94
OB6	1.771	1.593	−3.73	3.24	3840.2	4.045	949.39

Table D.29: Heat exchanger 1: convection data (test C)

Identifier	Vc	Vh	EB	MB	Q	ΔT	UA
OC1	1.708	1.227	2.50	6.69	3547.7	5.431	653.26
OC2	1.679	1.117	1.76	7.03	3560.0	5.594	636.38
OC3	1.648	1.326	4.61	Nan	4948.4	7.492	660.49
OC4	1.424	1.270	1.28	7.04	3609.0	5.753	627.32

Table D.30: Heat exchanger 2: convection data (test C)

Identifier	Vc	Vh	EB	MB	Q	ΔT	UA
OC1	1.745	1.323	1.01	6.69	3612.8	5.403	668.61
OC2	1.759	1.180	4.89	7.03	3638.1	5.567	653.53
OC3	1.684	1.386	5.30	Nan	5001.5	7.459	670.55
OC4	1.501	1.268	7.51	7.04	3607.0	5.726	629.93

Table D.31: Heat exchanger 4: convection data (test C)

Identifier	Vc	Vh	EB	MB	Q	ΔT	UA
OC1	1.746	1.339	2.06	6.69	4412.5	5.261	838.71
OC2	1.664	1.167	0.779	7.03	4252.9	5.420	784.63
OC3	1.651	1.323	3.97	Nan	5822.5	7.254	802.71
OC4	1.452	1.123	2.65	7.04	4063.7	5.561	730.75

Table D.32: Heat exchanger 5: convection data (test C)

Identifier	Vc	Vh	EB	MB	Q	ΔT	UA
OC1	1.862	1.204	3.72	6.69	3602.3	5.487	656.54
OC2	1.823	1.138	2.15	7.03	3641.0	5.653	644.04
OC3	1.765	1.403	−0.536	Nan	5098.7	7.570	673.50
OC4	1.528	1.262	2.33	7.04	3639.7	5.813	626.12

D.4 Annular Nusselt numbers

Table D.33: Heat exchanger 1: annular Nusselt numbers at the start of test A

Identifier	Nu theor	Nu meas	%
OA1	157.5	153.7	2.39
OA2	75.66	79.66	−5.02
OA3	103.3	105.9	−2.50
OA8	157.8	178.8	−11.75
OA9	159.2	183.8	−13.41
OA10	152.9	171.0	−10.62
OA11	149.1	167.6	−11.01

Table D.34: Heat exchanger 2: annular Nusselt numbers at the start of test A

Identifier	Nu theor	Nu meas	%
OA1	155.4	154.6	0.51
OA2	74.37	78.57	−5.34
OA3	101.8	101.2	0.65
OA8	154.6	149.5	3.31
OA9	154.7	144.9	6.36
OA10	154.5	137.8	10.79
OA11	156.4	156.1	0.17

Table D.35: Heat exchanger 3: annular Nusselt numbers at the start of test A

Identifier	Nu theor	Nu meas	%
OA5	134.5	112.4	16.41
OA6	118.7	95.46	19.55
OA9	142.0	119.9	15.52
OA10	134.4	105.4	21.60
OA11	141.5	119.6	15.47

Table D.36: Heat exchanger 4: annular Nusselt numbers at the start of test A

Identifier	Nu theor	Nu meas	%
OA4	141.4	160.6	−11.99
OA6	172.0	181.4	−5.15
OA8	159.8	155.3	2.80
OA9	157.5	154.9	1.66
OA10	153.9	124.3	19.26
OA11	158.4	167.6	−5.46

Table D.37: Heat exchanger 5: annular Nusselt numbers at the start of test A

Identifier	Nu theor	Nu meas	%
OA4	146.8	128.9	12.20
OA6	158.2	165.4	−4.32
OA8	139.2	146.8	−5.21
OA9	155.1	165.5	−6.29
OA10	153.6	168.6	−8.93
OA11	153.0	157.4	−2.76

Table D.38: Heat exchanger 6: annular Nusselt numbers at the start of test A

Identifier	Nu theor	Nu meas	%
OA5	136.9	115.1	15.91
OA6	108.6	124.1	−12.55
OA8	153.2	173.1	−11.50
OA9	151.3	175.0	−13.59
OA10	148.5	161.8	−8.24
OA11	154.6	150.8	2.47

Table D.39: Heat exchanger 1: annular Nusselt numbers at the start of test B

Identifier	Nu theor	Nu meas	%
OB1	119.1	129.9	−8.35
OB4	99.78	115.7	−13.77
OB5	101.3	119.3	−15.13
OB6	109.9	128.5	−14.47

Table D.40: Heat exchanger 2: annular Nusselt numbers at the start of test B

Identifier	Nu theor	Nu meas	%
OB1	121.7	121.9	−0.16
OB4	106.5	105.1	1.36
OB5	103.5	102.6	0.94
OB6	116.3	111.3	4.27

Table D.41: Heat exchanger 3: annular Nusselt numbers at the start of test B

Identifier	Nu theor	Nu meas	%
OB2	116.0	105.7	8.87
OB5	100.8	92.78	7.92
OB6	115.5	93.37	19.19

Table D.42: Heat exchanger 4: annular Nusselt numbers at the start of test B

Identifier	Nu theor	Nu meas	%
OB4	100.2	123.1	−18.57
OB6	119.1	154.3	−22.80

Table D.43: Heat exchanger 5: annular Nusselt numbers at the start of test B

Identifier	Nu theor	Nu meas	%
OB3	138.0	146.7	−5.90
OB4	105.5	116.3	−9.30
OB6	122.9	134.3	−8.48

Table D.44: Heat exchanger 6: annular Nusselt numbers at the start of test B

Identifier	Nu theor	Nu meas	%
OB2	140.3	124.9	10.98
OB5	104.4	95.29	8.72
OB6	122.3	108.8	11.05

Table D.45: Heat exchanger 1: annular Nusselt numbers at the start of test C

Identifier	Nu theor	Nu meas	%
OC1	109.3	118.2	−7.59
OC2	101.6	111.8	−9.07
OC3	116.1	128.7	−9.78
OC4	112.7	121.4	−7.24

Table D.46: Heat exchanger 2: annular Nusselt numbers at the start of test C

Identifier	Nu theor	Nu meas	%
OC1	116.1	130.9	−11.24
OC2	106.2	127.3	−16.55
OC3	120.2	141.1	−14.81
OC4	112.4	132.7	−15.30

Table D.47: Heat exchanger 4: annular Nusselt numbers at the start of test C

Identifier	Nu theor	Nu meas	%
OC1	117.4	131.7	−10.86
OC2	105.4	112.9	−6.65
OC3	115.8	127.5	−9.22
OC4	101.8	112.1	−9.25

Table D.48: Heat exchanger 5: annular Nusselt numbers at the start of test C

Identifier	Nu theor	Nu meas	%
OC1	107.5	112.8	−4.71
OC2	103.1	108.0	−4.58
OC3	121.4	125.9	−3.54
OC4	111.9	112.6	−0.60

D.5 Heat transfer data

The calculated heat transfer data from test A is presented in tables D.49, D.50, D.51, D.53, D.54, and D.52. For test B the data is presented in tables D.55, D.56, D.57, D.59, D.60, D.58, and likewise for test C tables: D.61, D.62, D.63, D.65, D.66, D.64.

Table D.49: Heat transfer data: TT1A

Exposure (d)	UA (K/W)	f_d	R_f (m^2 K/W)
0.00	952.66	$1.90\cdot10^{-2}$	$-6.27\cdot10^{-6}$
16.33	1 001.54	$1.87\cdot10^{-2}$	$-7.51\cdot10^{-6}$
17.11	1 033.55	$1.88\cdot10^{-2}$	$-1.55\cdot10^{-5}$
18.04	990.08	$1.92\cdot10^{-2}$	$-1.64\cdot10^{-5}$
18.35	957.87	$1.90\cdot10^{-2}$	$-7.64\cdot10^{-6}$
19.08	NaN	NaN	NaN
28.25	912.61	$1.97\cdot10^{-2}$	$-6.99\cdot10^{-6}$
29.33	863.97	$1.95\cdot10^{-2}$	$-9.23\cdot10^{-6}$
33.34	944.93	$1.91\cdot10^{-2}$	$-2.06\cdot10^{-6}$
35.04	969.43	$1.89\cdot10^{-2}$	$7.33\cdot10^{-7}$
35.21	972.38	$1.89\cdot10^{-2}$	$7.99\cdot10^{-7}$
45.25	911.69	$1.83\cdot10^{-2}$	$-7.90\cdot10^{-6}$
75.16	892.82	$1.76\cdot10^{-2}$	$-2.02\cdot10^{-6}$
76.22	793.21	$1.87\cdot10^{-2}$	$-3.77\cdot10^{-6}$
93.14	786.52	$1.83\cdot10^{-2}$	$5.09\cdot10^{-5}$
101.03	738.49	$1.91\cdot10^{-2}$	$6.20\cdot10^{-5}$
114.05	632.56	$2.18\cdot10^{-2}$	$1.18\cdot10^{-4}$
120.04	609.67	$2.09\cdot10^{-2}$	$1.26\cdot10^{-4}$
121.03	595.27	$2.11\cdot10^{-2}$	$1.33\cdot10^{-4}$
121.13	614.58	$2.08\cdot10^{-2}$	$1.30\cdot10^{-4}$
121.17	NaN	NaN	NaN
121.21	NaN	NaN	NaN

Table D.50: Heat transfer data: TT2A

Exposure (d)	UA (K/W)	f_d	R_f (m^2 K/W)
0.00	912.95	$1.92\cdot10^{-2}$	$-1.03\cdot10^{-5}$
16.33	901.51	$1.91\cdot10^{-2}$	$-6.68\cdot10^{-6}$
17.11	884.33	$1.91\cdot10^{-2}$	$-2.82\cdot10^{-6}$
18.04	859.92	$1.93\cdot10^{-2}$	$1.05\cdot10^{-6}$
18.35	913.21	$1.92\cdot10^{-2}$	$-1.04\cdot10^{-5}$
19.08	906.88	$1.93\cdot10^{-2}$	$-6.22\cdot10^{-6}$
28.25	781.57	$2.00\cdot10^{-2}$	$-5.55\cdot10^{-6}$
29.33	843.65	$1.98\cdot10^{-2}$	$-8.49\cdot10^{-6}$
33.34	912.18	$1.90\cdot10^{-2}$	$-7.63\cdot10^{-6}$
35.04	901.40	$1.92\cdot10^{-2}$	$-8.89\cdot10^{-6}$
35.21	908.83	$1.91\cdot10^{-2}$	$-9.95\cdot10^{-6}$
45.25	837.10	$1.97\cdot10^{-2}$	$-9.19\cdot10^{-6}$
75.16	784.73	$2.01\cdot10^{-2}$	$7.84\cdot10^{-6}$
76.22	NaN	NaN	NaN
93.14	646.55	$2.08\cdot10^{-2}$	$6.43\cdot10^{-5}$
101.03	603.57	$2.21\cdot10^{-2}$	$8.35\cdot10^{-5}$
114.05	567.29	$2.12\cdot10^{-2}$	$1.19\cdot10^{-4}$
120.04	528.35	$2.46\cdot10^{-2}$	$1.48\cdot10^{-4}$
121.03	502.18	$2.46\cdot10^{-2}$	$1.63\cdot10^{-4}$
121.13	528.39	$2.40\cdot10^{-2}$	$1.50\cdot10^{-4}$
121.17	NaN	NaN	NaN
121.21	NaN	NaN	NaN

Table D.51: Heat transfer data: TT3A

Exposure (d)	UA (K/W)	f_d	R_f (m^2 K/W)
0.00	1033.29	$1.91 \cdot 10^{-2}$	$-1.14 \cdot 10^{-5}$
16.33	900.33	$1.90 \cdot 10^{-2}$	$2.24 \cdot 10^{-5}$
17.11	916.17	$1.88 \cdot 10^{-2}$	$2.01 \cdot 10^{-5}$
18.04	808.59	$1.94 \cdot 10^{-2}$	$3.63 \cdot 10^{-5}$
18.35	1020.21	$1.91 \cdot 10^{-2}$	$-8.72 \cdot 10^{-6}$
19.08	957.12	$1.92 \cdot 10^{-2}$	$1.65 \cdot 10^{-6}$
28.25	931.91	$1.99 \cdot 10^{-2}$	$-2.82 \cdot 10^{-6}$
29.33	915.18	$1.97 \cdot 10^{-2}$	$-5.08 \cdot 10^{-6}$
33.34	940.81	$1.91 \cdot 10^{-2}$	$1.44 \cdot 10^{-6}$
35.04	934.20	$1.92 \cdot 10^{-2}$	$1.22 \cdot 10^{-5}$
35.21	929.73	$1.91 \cdot 10^{-2}$	$1.22 \cdot 10^{-5}$
45.25	765.25	$3.75 \cdot 10^{-2}$	$8.87 \cdot 10^{-5}$
75.16	588.69	$6.09 \cdot 10^{-2}$	$1.98 \cdot 10^{-4}$
76.22	NaN	NaN	NaN
93.14	504.12	$6.43 \cdot 10^{-2}$	$2.72 \cdot 10^{-4}$
101.03	484.70	$6.44 \cdot 10^{-2}$	$2.83 \cdot 10^{-4}$
114.05	446.21	$5.97 \cdot 10^{-2}$	$3.22 \cdot 10^{-4}$
120.04	428.05	$6.42 \cdot 10^{-2}$	$3.38 \cdot 10^{-4}$
121.03	427.69	$6.41 \cdot 10^{-2}$	$3.39 \cdot 10^{-4}$
121.13	NaN	NaN	NaN
121.17	478.63	$6.12 \cdot 10^{-2}$	$2.96 \cdot 10^{-4}$
121.21	NaN	NaN	NaN

Table D.52: Heat transfer data: TT6A

Exposure (d)	UA (K/W)	f_d	R_f (m^2 K/W)
0.00	1139.53	$1.92 \cdot 10^{-2}$	$1.51 \cdot 10^{-6}$
16.33	1258.64	$1.89 \cdot 10^{-2}$	$-1.34 \cdot 10^{-5}$
17.11	1278.04	$1.89 \cdot 10^{-2}$	$-1.60 \cdot 10^{-5}$
18.04	1215.86	$1.92 \cdot 10^{-2}$	$-1.48 \cdot 10^{-5}$
18.35	1139.05	$1.92 \cdot 10^{-2}$	$1.54 \cdot 10^{-6}$
19.08	1138.71	$1.90 \cdot 10^{-2}$	$6.91 \cdot 10^{-6}$
28.25	1077.15	$2.00 \cdot 10^{-2}$	$-3.72 \cdot 10^{-6}$
29.33	1063.74	$1.99 \cdot 10^{-2}$	$-1.27 \cdot 10^{-6}$
33.34	1071.25	$1.93 \cdot 10^{-2}$	$3.83 \cdot 10^{-6}$
35.04	1059.82	$1.91 \cdot 10^{-2}$	$1.18 \cdot 10^{-5}$
35.21	1028.28	$1.91 \cdot 10^{-2}$	$1.59 \cdot 10^{-5}$
45.25	819.97	$4.14 \cdot 10^{-2}$	$9.50 \cdot 10^{-5}$
75.16	676.88	$8.16 \cdot 10^{-2}$	$1.72 \cdot 10^{-4}$
76.22	609.97	$7.47 \cdot 10^{-2}$	$1.88 \cdot 10^{-4}$
93.14	577.34	$7.65 \cdot 10^{-2}$	$2.38 \cdot 10^{-4}$
101.03	551.23	$7.49 \cdot 10^{-2}$	$2.49 \cdot 10^{-4}$
114.05	498.58	$7.59 \cdot 10^{-2}$	$2.86 \cdot 10^{-4}$
120.04	494.21	$7.64 \cdot 10^{-2}$	$2.89 \cdot 10^{-4}$
121.03	487.09	$7.23 \cdot 10^{-2}$	$2.94 \cdot 10^{-4}$
121.13	NaN	NaN	NaN
121.17	504.95	$7.12 \cdot 10^{-2}$	$2.90 \cdot 10^{-4}$
121.21	NaN	NaN	NaN

Table D.53: Heat transfer data: TT4A

Exposure (d)	UA (K/W)	f_d	R_f (m^2 K/W)
0.00	1 099.75	$1.91 \cdot 10^{-2}$	$-1.36 \cdot 10^{-5}$
16.33	1 086.91	$1.90 \cdot 10^{-2}$	$-9.11 \cdot 10^{-6}$
17.11	1 114.09	$1.88 \cdot 10^{-2}$	$-1.12 \cdot 10^{-5}$
18.04	1 022.60	$1.92 \cdot 10^{-2}$	$-3.16 \cdot 10^{-6}$
18.35	1 078.21	$1.91 \cdot 10^{-2}$	$-9.46 \cdot 10^{-6}$
19.08	1 042.24	$1.89 \cdot 10^{-2}$	$1.10 \cdot 10^{-6}$
28.25	1 030.50	$1.96 \cdot 10^{-2}$	$-7.14 \cdot 10^{-6}$
29.33	1 023.42	$1.95 \cdot 10^{-2}$	$-1.08 \cdot 10^{-5}$
33.34	1 044.56	$1.89 \cdot 10^{-2}$	$-2.31 \cdot 10^{-6}$
35.04	1 045.69	$1.91 \cdot 10^{-2}$	$-7.90 \cdot 10^{-6}$
35.21	1 071.44	$1.89 \cdot 10^{-2}$	$-8.51 \cdot 10^{-6}$
45.25	994.30	$1.74 \cdot 10^{-2}$	$-1.98 \cdot 10^{-5}$
75.16	960.54	$1.67 \cdot 10^{-2}$	$-1.09 \cdot 10^{-5}$
76.22	NaN	NaN	NaN
93.14	831.41	$1.75 \cdot 10^{-2}$	$4.23 \cdot 10^{-5}$
101.03	792.13	$1.84 \cdot 10^{-2}$	$5.36 \cdot 10^{-5}$
114.05	707.48	$1.96 \cdot 10^{-2}$	$9.00 \cdot 10^{-5}$
120.04	679.44	$1.97 \cdot 10^{-2}$	$9.97 \cdot 10^{-5}$
121.03	662.42	$1.94 \cdot 10^{-2}$	$1.05 \cdot 10^{-4}$
121.13	NaN	NaN	NaN
121.17	NaN	NaN	NaN
121.21	658.81	$2.06 \cdot 10^{-2}$	$1.17 \cdot 10^{-4}$

Table D.54: Heat transfer data: TT5A

Exposure (d)	UA (K/W)	f_d	R_f (m^2 K/W)
0.00	1 024.66	$1.91 \cdot 10^{-2}$	$-2.06 \cdot 10^{-6}$
16.33	1 007.99	$1.88 \cdot 10^{-2}$	$-9.18 \cdot 10^{-6}$
17.11	1 059.37	$1.89 \cdot 10^{-2}$	$-4.96 \cdot 10^{-6}$
18.04	1 044.11	$1.92 \cdot 10^{-2}$	$-9.76 \cdot 10^{-6}$
18.35	1 024.34	$1.91 \cdot 10^{-2}$	$-2.08 \cdot 10^{-6}$
19.08	1 009.41	$1.90 \cdot 10^{-2}$	$8.28 \cdot 10^{-8}$
28.25	1 021.92	$1.97 \cdot 10^{-2}$	$-8.52 \cdot 10^{-6}$
29.33	1 000.34	$1.96 \cdot 10^{-2}$	$-1.45 \cdot 10^{-5}$
33.34	1 062.21	$1.89 \cdot 10^{-2}$	$-1.48 \cdot 10^{-6}$
35.04	1 063.58	$1.89 \cdot 10^{-2}$	$-2.66 \cdot 10^{-6}$
35.21	1 086.55	$1.88 \cdot 10^{-2}$	$-2.89 \cdot 10^{-6}$
45.25	978.81	$2.11 \cdot 10^{-2}$	$-4.14 \cdot 10^{-6}$
75.16	968.78	$2.17 \cdot 10^{-2}$	$6.91 \cdot 10^{-6}$
76.22	NaN	$2.25 \cdot 10^{-2}$	NaN
93.14	813.51	$2.11 \cdot 10^{-2}$	$7.12 \cdot 10^{-5}$
101.03	813.51	$2.24 \cdot 10^{-2}$	$6.27 \cdot 10^{-5}$
114.05	723.90	$2.31 \cdot 10^{-2}$	$9.70 \cdot 10^{-5}$
120.04	698.12	$2.37 \cdot 10^{-2}$	$1.04 \cdot 10^{-4}$
121.03	665.08	$2.33 \cdot 10^{-2}$	$1.17 \cdot 10^{-4}$
121.13	NaN	NaN	NaN
121.17	NaN	NaN	NaN
121.21	676.87	$2.25 \cdot 10^{-2}$	$1.20 \cdot 10^{-4}$

Table D.55: Heat transfer data: TT1B

Exposure (d)	UA (K/W)	f_d	R_f (m^2 K/W)
0.00	824.75	$1.90 \cdot 10^{-2}$	$-1.42 \cdot 10^{-5}$
$2.57 \cdot 10^{-2}$	NaN	NaN	NaN
$5.07 \cdot 10^{-2}$	NaN	NaN	NaN
0.11	817.46	$1.73 \cdot 10^{-2}$	$-1.14 \cdot 10^{-5}$
0.14	802.28	$1.71 \cdot 10^{-2}$	$-1.58 \cdot 10^{-5}$
0.95	798.86	$1.74 \cdot 10^{-2}$	$-1.90 \cdot 10^{-5}$
7.09	790.08	$1.73 \cdot 10^{-2}$	$-1.82 \cdot 10^{-5}$
8.93	793.43	$1.76 \cdot 10^{-2}$	$-1.77 \cdot 10^{-5}$
9.02	803.92	$1.71 \cdot 10^{-2}$	$-1.80 \cdot 10^{-5}$
15.13	799.50	$1.69 \cdot 10^{-2}$	$-7.96 \cdot 10^{-6}$
15.97	751.14	$1.73 \cdot 10^{-2}$	$-1.46 \cdot 10^{-6}$
16.08	761.42	$1.80 \cdot 10^{-2}$	$9.06 \cdot 10^{-7}$
27.98	NaN	NaN	NaN
28.01	679.71	$2.01 \cdot 10^{-2}$	$3.83 \cdot 10^{-5}$
28.09	678.60	$2.05 \cdot 10^{-2}$	$4.06 \cdot 10^{-5}$
34.98	676.18	$1.93 \cdot 10^{-2}$	$5.30 \cdot 10^{-5}$
39.08	665.22	$1.75 \cdot 10^{-2}$	$4.13 \cdot 10^{-5}$
41.97	677.24	$1.88 \cdot 10^{-2}$	$3.81 \cdot 10^{-5}$
56.97	401.58	$2.73 \cdot 10^{-2}$	$2.10 \cdot 10^{-4}$
57.04	544.42	$2.75 \cdot 10^{-2}$	$1.25 \cdot 10^{-4}$
57.13	519.84	$3.07 \cdot 10^{-2}$	$1.45 \cdot 10^{-4}$
60.09	592.82	$2.19 \cdot 10^{-2}$	$9.61 \cdot 10^{-5}$
70.10	548.96	$2.28 \cdot 10^{-2}$	$1.28 \cdot 10^{-4}$
70.97	566.79	$2.20 \cdot 10^{-2}$	$1.22 \cdot 10^{-4}$
84.08	476.58	$2.29 \cdot 10^{-2}$	$1.85 \cdot 10^{-4}$
93.12	418.22	$2.43 \cdot 10^{-2}$	$2.67 \cdot 10^{-4}$
106.00	360.20	$2.64 \cdot 10^{-2}$	$3.56 \cdot 10^{-4}$
113.09	345.62	$2.62 \cdot 10^{-2}$	$3.79 \cdot 10^{-4}$
120.10	334.93	$2.65 \cdot 10^{-2}$	$4.04 \cdot 10^{-4}$
125.93	NaN	NaN	NaN
126.08	320.16	$2.86 \cdot 10^{-2}$	$4.34 \cdot 10^{-4}$
126.13	NaN	NaN	NaN
126.13	320.16	$2.86 \cdot 10^{-2}$	$4.34 \cdot 10^{-4}$
132.16	312.67	$3.93 \cdot 10^{-2}$	$4.67 \cdot 10^{-4}$
137.95	312.44	$3.61 \cdot 10^{-2}$	$4.65 \cdot 10^{-4}$
138.05	408.61	$1.82 \cdot 10^{-2}$	$2.97 \cdot 10^{-4}$
138.11	388.46	$3.90 \cdot 10^{-2}$	$3.27 \cdot 10^{-4}$
152.08	326.44	$4.30 \cdot 10^{-2}$	$4.44 \cdot 10^{-4}$
169.05	306.50	$3.93 \cdot 10^{-2}$	$4.80 \cdot 10^{-4}$
180.04	316.60	$3.84 \cdot 10^{-2}$	$4.60 \cdot 10^{-4}$
188.09	322.28	$3.65 \cdot 10^{-2}$	$4.49 \cdot 10^{-4}$

Table D.56: Heat transfer data: TT2B

Exposure (d)	UA (K/W)	f_d	R_f (m^2 K/W)
0.00	687.96	$1.77 \cdot 10^{-2}$	$-1.49 \cdot 10^{-5}$
$2.57 \cdot 10^{-2}$	NaN	NaN	NaN
$5.07 \cdot 10^{-2}$	NaN	NaN	NaN
0.11	675.87	$1.71 \cdot 10^{-2}$	$-1.28 \cdot 10^{-5}$
0.14	651.14	$1.72 \cdot 10^{-2}$	$-1.48 \cdot 10^{-5}$
0.95	653.52	$1.74 \cdot 10^{-2}$	$-1.12 \cdot 10^{-5}$
7.09	640.57	$1.73 \cdot 10^{-2}$	$-1.33 \cdot 10^{-5}$
8.93	655.53	$1.77 \cdot 10^{-2}$	$-1.62 \cdot 10^{-5}$
9.02	634.05	$1.80 \cdot 10^{-2}$	$-2.46 \cdot 10^{-6}$
15.13	612.72	$1.73 \cdot 10^{-2}$	$1.82 \cdot 10^{-5}$
15.97	603.81	$1.79 \cdot 10^{-2}$	$1.34 \cdot 10^{-5}$
16.08	599.58	$1.83 \cdot 10^{-2}$	$2.04 \cdot 10^{-5}$
27.98	565.84	$1.98 \cdot 10^{-2}$	$4.38 \cdot 10^{-5}$
28.01	556.69	$1.99 \cdot 10^{-2}$	$5.07 \cdot 10^{-5}$
28.09	557.15	$1.96 \cdot 10^{-2}$	$5.03 \cdot 10^{-5}$
34.98	549.79	$1.89 \cdot 10^{-2}$	$7.39 \cdot 10^{-5}$
39.08	534.83	$1.89 \cdot 10^{-2}$	$6.58 \cdot 10^{-5}$
41.97	541.14	$1.98 \cdot 10^{-2}$	$6.14 \cdot 10^{-5}$
56.97	344.98	$2.55 \cdot 10^{-2}$	$2.23 \cdot 10^{-4}$
57.04	451.80	$2.69 \cdot 10^{-2}$	$1.40 \cdot 10^{-4}$
57.13	412.38	$3.34 \cdot 10^{-2}$	$1.80 \cdot 10^{-4}$
60.09	502.47	$2.26 \cdot 10^{-2}$	$1.10 \cdot 10^{-4}$
70.10	462.61	$2.31 \cdot 10^{-2}$	$1.47 \cdot 10^{-4}$
70.97	462.81	$2.38 \cdot 10^{-2}$	$1.54 \cdot 10^{-4}$
84.08	401.76	$2.38 \cdot 10^{-2}$	$2.10 \cdot 10^{-4}$
93.12	367.09	$2.48 \cdot 10^{-2}$	$2.82 \cdot 10^{-4}$
106.00	320.60	$2.57 \cdot 10^{-2}$	$3.72 \cdot 10^{-4}$
113.09	310.67	$2.66 \cdot 10^{-2}$	$3.80 \cdot 10^{-4}$
120.10	297.62	$2.68 \cdot 10^{-2}$	$4.24 \cdot 10^{-4}$
125.93	NaN	NaN	NaN
126.08	292.53	$2.77 \cdot 10^{-2}$	$4.41 \cdot 10^{-4}$
126.13	NaN	NaN	NaN
126.13	292.53	$2.77 \cdot 10^{-2}$	$4.41 \cdot 10^{-4}$
132.16	285.07	$3.81 \cdot 10^{-2}$	$4.79 \cdot 10^{-4}$
137.95	272.43	$3.53 \cdot 10^{-2}$	$4.87 \cdot 10^{-4}$
138.05	347.60	$1.81 \cdot 10^{-2}$	$3.28 \cdot 10^{-4}$
138.11	337.67	$3.80 \cdot 10^{-2}$	$3.49 \cdot 10^{-4}$
152.08	288.10	$4.14 \cdot 10^{-2}$	$4.72 \cdot 10^{-4}$
169.05	267.57	$4.02 \cdot 10^{-2}$	$5.22 \cdot 10^{-4}$
180.04	279.57	$3.76 \cdot 10^{-2}$	$4.93 \cdot 10^{-4}$
188.09	286.47	$3.73 \cdot 10^{-2}$	$4.80 \cdot 10^{-4}$

Table D.57: Heat transfer data: TT3B

Exposure (d)	UA (K/W)	f_d	R_f (m^2 K/W)
0.00	NaN	NaN	NaN
$2.57 \cdot 10^{-2}$	805.80	$1.90 \cdot 10^{-2}$	$-2.06 \cdot 10^{-5}$
$5.07 \cdot 10^{-2}$	NaN	NaN	NaN
0.11	NaN	NaN	NaN
0.14	779.69	$1.88 \cdot 10^{-2}$	$-1.77 \cdot 10^{-5}$
0.95	753.00	$1.93 \cdot 10^{-2}$	$-3.64 \cdot 10^{-6}$
7.09	745.84	$2.05 \cdot 10^{-2}$	$3.53 \cdot 10^{-7}$
8.93	761.86	$1.87 \cdot 10^{-2}$	$-1.11 \cdot 10^{-5}$
9.02	733.03	$1.93 \cdot 10^{-2}$	$-2.62 \cdot 10^{-7}$
15.13	709.59	$1.97 \cdot 10^{-2}$	$2.36 \cdot 10^{-5}$
15.97	685.07	$2.11 \cdot 10^{-2}$	$2.78 \cdot 10^{-5}$
16.08	693.08	$2.01 \cdot 10^{-2}$	$2.56 \cdot 10^{-5}$
27.98	NaN	NaN	NaN
28.01	632.41	$2.21 \cdot 10^{-2}$	$5.64 \cdot 10^{-5}$
28.09	639.33	$2.15 \cdot 10^{-2}$	$5.31 \cdot 10^{-5}$
34.98	636.89	$2.16 \cdot 10^{-2}$	$7.30 \cdot 10^{-5}$
39.08	600.70	$2.17 \cdot 10^{-2}$	$7.45 \cdot 10^{-5}$
41.97	617.44	$2.10 \cdot 10^{-2}$	$5.96 \cdot 10^{-5}$
56.97	370.56	$2.86 \cdot 10^{-2}$	$2.39 \cdot 10^{-4}$
57.04	478.04	$3.03 \cdot 10^{-2}$	$1.69 \cdot 10^{-4}$
57.13	452.37	$3.79 \cdot 10^{-2}$	$1.94 \cdot 10^{-4}$
60.09	547.48	$2.45 \cdot 10^{-2}$	$1.20 \cdot 10^{-4}$
70.10	491.71	$2.58 \cdot 10^{-2}$	$1.67 \cdot 10^{-4}$
70.97	498.14	$2.76 \cdot 10^{-2}$	$1.72 \cdot 10^{-4}$
84.08	448.78	$2.48 \cdot 10^{-2}$	$2.11 \cdot 10^{-4}$
93.12	392.18	$2.84 \cdot 10^{-2}$	$3.00 \cdot 10^{-4}$
106.00	328.90	$2.80 \cdot 10^{-2}$	$4.08 \cdot 10^{-4}$
113.09	330.27	$2.77 \cdot 10^{-2}$	$3.99 \cdot 10^{-4}$
120.10	312.16	$2.82 \cdot 10^{-2}$	$4.44 \cdot 10^{-4}$
125.93	NaN	NaN	NaN
126.08	NaN	NaN	NaN
126.13	293.98	$2.95 \cdot 10^{-2}$	$4.84 \cdot 10^{-4}$
126.13	293.98	$2.95 \cdot 10^{-2}$	$4.84 \cdot 10^{-4}$
132.16	290.08	$3.97 \cdot 10^{-2}$	$5.12 \cdot 10^{-4}$
137.95	280.15	$3.80 \cdot 10^{-2}$	$5.26 \cdot 10^{-4}$
138.05	NaN	NaN	NaN
138.11	278.65	$3.81 \cdot 10^{-2}$	$5.33 \cdot 10^{-4}$
152.08	261.80	$4.47 \cdot 10^{-2}$	$5.97 \cdot 10^{-4}$
169.05	248.00	$4.24 \cdot 10^{-2}$	$6.37 \cdot 10^{-4}$
180.04	256.64	$3.98 \cdot 10^{-2}$	$6.11 \cdot 10^{-4}$
188.09	260.16	$3.92 \cdot 10^{-2}$	$6.00 \cdot 10^{-4}$

Table D.58: Heat transfer data: TT6B

Exposure (d)	UA (K/W)	f_d	R_f (m^2 K/W)
0.00	NaN	NaN	NaN
$2.57 \cdot 10^{-2}$	1 060.60	$1.99 \cdot 10^{-2}$	$-1.56 \cdot 10^{-5}$
$5.07 \cdot 10^{-2}$	NaN	NaN	NaN
0.11	NaN	NaN	NaN
0.14	958.87	$1.98 \cdot 10^{-2}$	$-1.68 \cdot 10^{-5}$
0.95	990.61	$2.02 \cdot 10^{-2}$	$-1.66 \cdot 10^{-5}$
7.09	953.03	$2.02 \cdot 10^{-2}$	$-1.63 \cdot 10^{-5}$
8.93	977.05	$2.04 \cdot 10^{-2}$	$-1.73 \cdot 10^{-5}$
9.02	976.09	$2.08 \cdot 10^{-2}$	$-1.34 \cdot 10^{-5}$
15.13	971.27	$2.09 \cdot 10^{-2}$	$-5.16 \cdot 10^{-6}$
15.97	921.95	$2.08 \cdot 10^{-2}$	$-9.84 \cdot 10^{-6}$
16.08	945.09	$2.09 \cdot 10^{-2}$	$-7.85 \cdot 10^{-6}$
27.98	NaN	NaN	NaN
28.01	874.38	$2.19 \cdot 10^{-2}$	$3.94 \cdot 10^{-6}$
28.09	884.98	$2.13 \cdot 10^{-2}$	$9.59 \cdot 10^{-7}$
34.98	915.20	$2.04 \cdot 10^{-2}$	$9.27 \cdot 10^{-6}$
39.08	861.50	$2.14 \cdot 10^{-2}$	$4.31 \cdot 10^{-6}$
41.97	889.82	$2.05 \cdot 10^{-2}$	$-4.10 \cdot 10^{-6}$
56.97	570.27	$2.49 \cdot 10^{-2}$	$6.05 \cdot 10^{-5}$
57.04	726.18	$2.26 \cdot 10^{-2}$	$3.55 \cdot 10^{-5}$
57.13	665.37	$2.71 \cdot 10^{-2}$	$6.12 \cdot 10^{-5}$
60.09	766.95	$2.15 \cdot 10^{-2}$	$4.29 \cdot 10^{-5}$
70.10	736.23	$2.13 \cdot 10^{-2}$	$5.40 \cdot 10^{-5}$
70.97	770.15	$2.12 \cdot 10^{-2}$	$5.17 \cdot 10^{-5}$
84.08	767.71	$2.00 \cdot 10^{-2}$	$2.99 \cdot 10^{-5}$
93.12	744.56	$2.09 \cdot 10^{-2}$	$5.30 \cdot 10^{-5}$
106.00	709.83	$2.10 \cdot 10^{-2}$	$5.95 \cdot 10^{-5}$
113.09	713.31	$2.10 \cdot 10^{-2}$	$6.68 \cdot 10^{-5}$
120.10	677.28	$2.11 \cdot 10^{-2}$	$8.78 \cdot 10^{-5}$
125.93	NaN	NaN	NaN
126.08	601.70	$2.19 \cdot 10^{-2}$	$1.22 \cdot 10^{-4}$
126.13	NaN	NaN	NaN
126.13	601.70	$2.19 \cdot 10^{-2}$	$1.22 \cdot 10^{-4}$
132.16	657.82	$2.44 \cdot 10^{-2}$	$1.02 \cdot 10^{-4}$
137.95	609.49	$2.46 \cdot 10^{-2}$	$1.18 \cdot 10^{-4}$
138.05	NaN	NaN	NaN
138.11	631.99	$2.39 \cdot 10^{-2}$	$1.10 \cdot 10^{-4}$
152.08	738.01	$2.46 \cdot 10^{-2}$	$6.68 \cdot 10^{-5}$
169.05	715.10	$2.48 \cdot 10^{-2}$	$7.33 \cdot 10^{-5}$
180.04	714.74	$2.38 \cdot 10^{-2}$	$7.77 \cdot 10^{-5}$
188.09	698.61	$2.35 \cdot 10^{-2}$	$8.35 \cdot 10^{-5}$

Table D.59: Heat transfer data: TT4B

Exposure (d)	UA (K/W)	f_d	R_f (m^2 K/W)
0.00	NaN	NaN	NaN
$2.57 \cdot 10^{-2}$	NaN	NaN	NaN
$5.07 \cdot 10^{-2}$	760.80	$1.87 \cdot 10^{-2}$	$-1.85 \cdot 10^{-5}$
0.11	796.75	$1.84 \cdot 10^{-2}$	$-1.64 \cdot 10^{-5}$
0.14	NaN	NaN	NaN
0.95	819.17	$1.74 \cdot 10^{-2}$	$-1.97 \cdot 10^{-5}$
7.09	844.02	$1.79 \cdot 10^{-2}$	$-1.48 \cdot 10^{-5}$
8.93	826.82	$1.74 \cdot 10^{-2}$	$-3.92 \cdot 10^{-5}$
9.02	765.46	$1.88 \cdot 10^{-2}$	$-1.20 \cdot 10^{-5}$
15.13	751.43	$1.84 \cdot 10^{-2}$	$1.04 \cdot 10^{-5}$
15.97	731.74	$1.82 \cdot 10^{-2}$	$-2.77 \cdot 10^{-7}$
16.08	738.74	$1.86 \cdot 10^{-2}$	$4.52 \cdot 10^{-6}$
27.98	NaN	NaN	NaN
28.01	668.56	$2.01 \cdot 10^{-2}$	$3.51 \cdot 10^{-5}$
28.09	672.04	$1.93 \cdot 10^{-2}$	$3.25 \cdot 10^{-5}$
34.98	646.21	$1.99 \cdot 10^{-2}$	$6.75 \cdot 10^{-5}$
39.08	629.43	$1.91 \cdot 10^{-2}$	$5.23 \cdot 10^{-5}$
41.97	653.84	$1.93 \cdot 10^{-2}$	$4.04 \cdot 10^{-5}$
56.97	394.27	$2.64 \cdot 10^{-2}$	$1.93 \cdot 10^{-4}$
57.04	528.10	$2.55 \cdot 10^{-2}$	$1.12 \cdot 10^{-4}$
57.13	479.75	$3.24 \cdot 10^{-2}$	$1.46 \cdot 10^{-4}$
60.09	554.21	$2.30 \cdot 10^{-2}$	$1.16 \cdot 10^{-4}$
70.10	528.93	$2.32 \cdot 10^{-2}$	$1.33 \cdot 10^{-4}$
70.97	550.62	$2.38 \cdot 10^{-2}$	$1.40 \cdot 10^{-4}$
84.08	471.77	$2.26 \cdot 10^{-2}$	$1.78 \cdot 10^{-4}$
93.12	411.11	$2.49 \cdot 10^{-2}$	$2.68 \cdot 10^{-4}$
106.00	372.87	$2.58 \cdot 10^{-2}$	$3.40 \cdot 10^{-4}$
113.09	351.91	$2.63 \cdot 10^{-2}$	$3.57 \cdot 10^{-4}$
120.10	343.95	$2.66 \cdot 10^{-2}$	$3.84 \cdot 10^{-4}$
125.93	NaN	NaN	NaN
126.08	NaN	NaN	NaN
126.13	331.47	$2.81 \cdot 10^{-2}$	$4.13 \cdot 10^{-4}$
126.13	331.47	$2.81 \cdot 10^{-2}$	$4.13 \cdot 10^{-4}$
132.16	326.52	$3.93 \cdot 10^{-2}$	$4.42 \cdot 10^{-4}$
137.95	321.44	$3.52 \cdot 10^{-2}$	$4.34 \cdot 10^{-4}$
138.05	NaN	NaN	NaN
138.11	320.78	$3.79 \cdot 10^{-2}$	$4.43 \cdot 10^{-4}$
152.08	297.22	$4.15 \cdot 10^{-2}$	$5.08 \cdot 10^{-4}$
169.05	286.07	$3.95 \cdot 10^{-2}$	$5.33 \cdot 10^{-4}$
180.04	292.36	$3.85 \cdot 10^{-2}$	$5.21 \cdot 10^{-4}$
188.09	295.93	$3.86 \cdot 10^{-2}$	$5.19 \cdot 10^{-4}$

Table D.60: Heat transfer data: TT5B

Exposure (d)	UA (K/W)	f_d	R_f (m^2 K/W)
0.00	NaN	NaN	NaN
$2.57 \cdot 10^{-2}$	NaN	NaN	NaN
$5.07 \cdot 10^{-2}$	999.93	$1.95 \cdot 10^{-2}$	$-1.42 \cdot 10^{-5}$
0.11	936.90	$1.85 \cdot 10^{-2}$	$-1.31 \cdot 10^{-5}$
0.14	NaN	NaN	NaN
0.95	940.57	$1.91 \cdot 10^{-2}$	$-1.69 \cdot 10^{-5}$
7.09	875.37	$1.91 \cdot 10^{-2}$	$-1.03 \cdot 10^{-5}$
8.93	900.62	$1.98 \cdot 10^{-2}$	$-1.08 \cdot 10^{-5}$
9.02	907.04	$1.96 \cdot 10^{-2}$	$-1.07 \cdot 10^{-5}$
15.13	878.18	$1.92 \cdot 10^{-2}$	$9.39 \cdot 10^{-6}$
15.97	815.39	$2.07 \cdot 10^{-2}$	$1.20 \cdot 10^{-5}$
16.08	826.91	$2.01 \cdot 10^{-2}$	$9.95 \cdot 10^{-6}$
27.98	NaN	NaN	NaN
28.01	728.44	$2.14 \cdot 10^{-2}$	$3.85 \cdot 10^{-5}$
28.09	731.98	$2.12 \cdot 10^{-2}$	$3.84 \cdot 10^{-5}$
34.98	718.57	$2.11 \cdot 10^{-2}$	$6.49 \cdot 10^{-5}$
39.08	692.22	$2.06 \cdot 10^{-2}$	$5.75 \cdot 10^{-5}$
41.97	727.41	$2.04 \cdot 10^{-2}$	$4.38 \cdot 10^{-5}$
56.97	437.01	$2.75 \cdot 10^{-2}$	$1.86 \cdot 10^{-4}$
57.04	585.29	$2.78 \cdot 10^{-2}$	$1.17 \cdot 10^{-4}$
57.13	509.10	$3.23 \cdot 10^{-2}$	$1.70 \cdot 10^{-4}$
60.09	600.48	$2.37 \cdot 10^{-2}$	$1.22 \cdot 10^{-4}$
70.10	587.89	$2.48 \cdot 10^{-2}$	$1.38 \cdot 10^{-4}$
70.97	595.09	$2.46 \cdot 10^{-2}$	$1.39 \cdot 10^{-4}$
84.08	497.59	$2.45 \cdot 10^{-2}$	$1.99 \cdot 10^{-4}$
93.12	412.47	$2.64 \cdot 10^{-2}$	$3.10 \cdot 10^{-4}$
106.00	357.84	$2.68 \cdot 10^{-2}$	$3.91 \cdot 10^{-4}$
113.09	357.97	$2.65 \cdot 10^{-2}$	$3.95 \cdot 10^{-4}$
120.10	323.68	$2.79 \cdot 10^{-2}$	$4.69 \cdot 10^{-4}$
125.93	336.86	$2.99 \cdot 10^{-2}$	$4.36 \cdot 10^{-4}$
126.08	338.49	$2.93 \cdot 10^{-2}$	$4.34 \cdot 10^{-4}$
126.13	NaN	NaN	NaN
126.13	338.49	$2.93 \cdot 10^{-2}$	$4.34 \cdot 10^{-4}$
132.16	339.90	$3.89 \cdot 10^{-2}$	$4.52 \cdot 10^{-4}$
137.95	327.66	$3.74 \cdot 10^{-2}$	$4.64 \cdot 10^{-4}$
138.05	NaN	NaN	NaN
138.11	327.49	$3.76 \cdot 10^{-2}$	$4.67 \cdot 10^{-4}$
152.08	303.11	$4.31 \cdot 10^{-2}$	$5.34 \cdot 10^{-4}$
169.05	288.77	$3.99 \cdot 10^{-2}$	$5.67 \cdot 10^{-4}$
180.04	308.29	$3.92 \cdot 10^{-2}$	$5.23 \cdot 10^{-4}$
188.09	311.36	$3.73 \cdot 10^{-2}$	$5.17 \cdot 10^{-4}$

Table D.61: Heat transfer data: TT1C

Exposure (d)	UA (K/W)	f_d	R_f (m^2 K/W)
0.00	665.93	$1.85 \cdot 10^{-2}$	$-1.33 \cdot 10^{-5}$
$6.18 \cdot 10^{-2}$	649.52	$1.84 \cdot 10^{-2}$	$-1.62 \cdot 10^{-5}$
0.11	673.02	$1.85 \cdot 10^{-2}$	$-1.68 \cdot 10^{-5}$
0.89	640.37	$1.93 \cdot 10^{-2}$	$-1.46 \cdot 10^{-5}$
6.91	698.74	$1.68 \cdot 10^{-2}$	$-1.69 \cdot 10^{-5}$
7.00	647.60	$1.90 \cdot 10^{-2}$	$-9.84 \cdot 10^{-6}$
7.02	NaN	NaN	NaN
29.05	NaN	NaN	NaN
29.14	596.48	$2.37 \cdot 10^{-2}$	$3.91 \cdot 10^{-5}$
35.10	NaN	NaN	NaN
35.95	567.56	$2.12 \cdot 10^{-2}$	$3.75 \cdot 10^{-5}$
40.90	527.73	$2.45 \cdot 10^{-2}$	$5.29 \cdot 10^{-5}$
48.90	493.53	$2.60 \cdot 10^{-2}$	$9.11 \cdot 10^{-5}$
67.02	361.67	$3.43 \cdot 10^{-2}$	$2.68 \cdot 10^{-4}$
77.02	360.15	$3.69 \cdot 10^{-2}$	$2.94 \cdot 10^{-4}$
85.78	357.11	$3.69 \cdot 10^{-2}$	$2.93 \cdot 10^{-4}$

Table D.62: Heat transfer data: TT2C

Exposure (d)	UA (K/W)	f_d	R_f (m^2 K/W)
0.00	680.93	$1.82 \cdot 10^{-2}$	$-1.00 \cdot 10^{-5}$
$6.18 \cdot 10^{-2}$	666.35	$1.69 \cdot 10^{-2}$	$-1.55 \cdot 10^{-5}$
0.11	682.81	$1.80 \cdot 10^{-2}$	$-1.68 \cdot 10^{-5}$
0.89	642.45	$1.74 \cdot 10^{-2}$	$-1.72 \cdot 10^{-5}$
6.91	682.42	$1.61 \cdot 10^{-2}$	$-1.36 \cdot 10^{-5}$
7.00	646.58	$1.57 \cdot 10^{-2}$	$-2.42 \cdot 10^{-5}$
7.02	NaN	NaN	NaN
29.05	569.87	$1.90 \cdot 10^{-2}$	$3.13 \cdot 10^{-5}$
29.14	589.11	$1.90 \cdot 10^{-2}$	$2.64 \cdot 10^{-5}$
35.10	593.75	$1.90 \cdot 10^{-2}$	$3.20 \cdot 10^{-5}$
35.95	559.83	$1.95 \cdot 10^{-2}$	$4.86 \cdot 10^{-5}$
40.90	524.80	$2.29 \cdot 10^{-2}$	$6.97 \cdot 10^{-5}$
48.90	477.76	$2.28 \cdot 10^{-2}$	$1.20 \cdot 10^{-4}$
67.02	339.79	$3.41 \cdot 10^{-2}$	$3.32 \cdot 10^{-4}$
77.02	331.39	$3.52 \cdot 10^{-2}$	$3.67 \cdot 10^{-4}$
85.78	337.00	$3.52 \cdot 10^{-2}$	$3.50 \cdot 10^{-4}$

Table D.63: Heat transfer data: TT3C

Exposure (d)	UA (K/W)	f_d	R_f (m^2 K/W)
0.00	244.98	$4.25 \cdot 10^{-2}$	$6.44 \cdot 10^{-4}$
$6.18 \cdot 10^{-2}$	244.97	$4.47 \cdot 10^{-2}$	$6.44 \cdot 10^{-4}$
0.11	NaN	NaN	NaN
0.89	244.23	$4.88 \cdot 10^{-2}$	$6.73 \cdot 10^{-4}$
6.91	245.08	$4.32 \cdot 10^{-2}$	$6.71 \cdot 10^{-4}$
7.00	NaN	NaN	NaN
7.02	244.85	$3.90 \cdot 10^{-2}$	$6.42 \cdot 10^{-4}$
29.05	183.35	$4.23 \cdot 10^{-2}$	$9.50 \cdot 10^{-4}$
29.14	180.92	$4.23 \cdot 10^{-2}$	$9.68 \cdot 10^{-4}$
35.10	NaN	NaN	NaN
35.95	158.00	$3.97 \cdot 10^{-2}$	$1.15 \cdot 10^{-3}$
40.90	176.72	$4.20 \cdot 10^{-2}$	$9.84 \cdot 10^{-4}$
48.90	175.45	$4.20 \cdot 10^{-2}$	$1.00 \cdot 10^{-3}$
67.02	157.80	$5.54 \cdot 10^{-2}$	$1.16 \cdot 10^{-3}$
77.02	110.00	$5.59 \cdot 10^{-2}$	$1.79 \cdot 10^{-3}$
85.78	146.41	$5.59 \cdot 10^{-2}$	$1.28 \cdot 10^{-3}$

Table D.64: Heat transfer data: TT6C

Exposure (d)	UA (K/W)	f_d	R_f (m^2 K/W)
0.00	706.55	$2.19 \cdot 10^{-2}$	$6.15 \cdot 10^{-5}$
$6.18 \cdot 10^{-2}$	714.72	$2.07 \cdot 10^{-2}$	$5.56 \cdot 10^{-5}$
0.11	NaN	NaN	NaN
0.89	688.03	$2.26 \cdot 10^{-2}$	$6.48 \cdot 10^{-5}$
6.91	773.77	$2.09 \cdot 10^{-2}$	$6.34 \cdot 10^{-5}$
7.00	666.05	$2.23 \cdot 10^{-2}$	$7.13 \cdot 10^{-5}$
7.02	NaN	NaN	NaN
29.05	583.32	$2.58 \cdot 10^{-2}$	$1.29 \cdot 10^{-4}$
29.14	599.78	$2.58 \cdot 10^{-2}$	$1.16 \cdot 10^{-4}$
35.10	NaN	NaN	NaN
35.95	592.99	$2.56 \cdot 10^{-2}$	$1.17 \cdot 10^{-4}$
40.90	551.70	$2.84 \cdot 10^{-2}$	$1.32 \cdot 10^{-4}$
48.90	538.29	$2.96 \cdot 10^{-2}$	$1.53 \cdot 10^{-4}$
67.02	456.17	$3.71 \cdot 10^{-2}$	$2.36 \cdot 10^{-4}$
77.02	471.06	$4.09 \cdot 10^{-2}$	$2.43 \cdot 10^{-4}$
85.78	453.47	$4.09 \cdot 10^{-2}$	$2.56 \cdot 10^{-4}$

Table D.65: Heat transfer data: TT4C

Exposure (d)	UA (K/W)	f_d	R_f (m^2 K/W)
0.00	862.48	$1.96 \cdot 10^{-2}$	$-1.08 \cdot 10^{-5}$
$6.18 \cdot 10^{-2}$	808.14	$2.14 \cdot 10^{-2}$	$-5.83 \cdot 10^{-8}$
0.11	824.96	$2.00 \cdot 10^{-2}$	$-8.42 \cdot 10^{-6}$
0.89	753.40	$2.04 \cdot 10^{-2}$	$-4.77 \cdot 10^{-6}$
6.91	830.87	$1.84 \cdot 10^{-2}$	$-8.26 \cdot 10^{-6}$
7.00	NaN	NaN	NaN
7.02	790.91	$1.80 \cdot 10^{-2}$	$-1.34 \cdot 10^{-5}$
29.05	737.74	$1.73 \cdot 10^{-2}$	$1.23 \cdot 10^{-5}$
29.14	735.59	$1.73 \cdot 10^{-2}$	$8.69 \cdot 10^{-6}$
35.10	NaN	NaN	NaN
35.95	724.54	$1.82 \cdot 10^{-2}$	$8.80 \cdot 10^{-6}$
40.90	668.49	$1.87 \cdot 10^{-2}$	$2.10 \cdot 10^{-5}$
48.90	665.95	$1.92 \cdot 10^{-2}$	$3.60 \cdot 10^{-5}$
67.02	483.58	$3.38 \cdot 10^{-2}$	$1.95 \cdot 10^{-4}$
77.02	537.34	$2.90 \cdot 10^{-2}$	$1.58 \cdot 10^{-4}$
85.78	501.28	$2.90 \cdot 10^{-2}$	$1.83 \cdot 10^{-4}$

Table D.66: Heat transfer data: TT5C

Exposure (d)	UA (K/W)	f_d	R_f (m^2 K/W)
0.00	668.57	$1.75 \cdot 10^{-2}$	$-9.50 \cdot 10^{-6}$
$6.18 \cdot 10^{-2}$	656.35	$1.78 \cdot 10^{-2}$	$-8.93 \cdot 10^{-6}$
0.11	685.23	$1.81 \cdot 10^{-2}$	$-9.28 \cdot 10^{-6}$
0.89	638.28	$1.88 \cdot 10^{-2}$	$-5.49 \cdot 10^{-6}$
6.91	707.98	$1.75 \cdot 10^{-2}$	$-5.53 \cdot 10^{-6}$
7.00	656.90	$1.81 \cdot 10^{-2}$	$-6.57 \cdot 10^{-6}$
7.02	NaN	NaN	NaN
29.05	597.63	$1.85 \cdot 10^{-2}$	$3.81 \cdot 10^{-5}$
29.14	584.03	$1.85 \cdot 10^{-2}$	$4.16 \cdot 10^{-5}$
35.10	NaN	NaN	NaN
35.95	602.86	$1.96 \cdot 10^{-2}$	$2.71 \cdot 10^{-5}$
40.90	565.76	$1.91 \cdot 10^{-2}$	$2.97 \cdot 10^{-5}$
48.90	567.79	$1.91 \cdot 10^{-2}$	$3.67 \cdot 10^{-5}$
67.02	519.29	$2.54 \cdot 10^{-2}$	$9.08 \cdot 10^{-5}$
77.02	558.99	$2.19 \cdot 10^{-2}$	$7.21 \cdot 10^{-5}$
85.78	510.26	$2.19 \cdot 10^{-2}$	$1.05 \cdot 10^{-4}$

D.6 Bacterial counts

The total aerobic and anaerobic bacterial counts are summarized in table D.67 together with the total number of hydrogen sulphide producing bacteria.

Table D.67: Total bacteria counts

Tube	Total bacteria CFU/mL	H_2S producers CFU/mL
PPF-modified admiralty brass	39 800	>50
Admiralty brass	1337	41
Ti coated	26 050	>50
Ti uncoated	37 750	>50
SS coated	> 49 250	>50
SS uncoated	40 250	>50

D.7 Comparison of R_f and $R_f{}^*$ from test B and test C

Figures D.68 and D.69 compare the fouling factors from test B and C respectively.

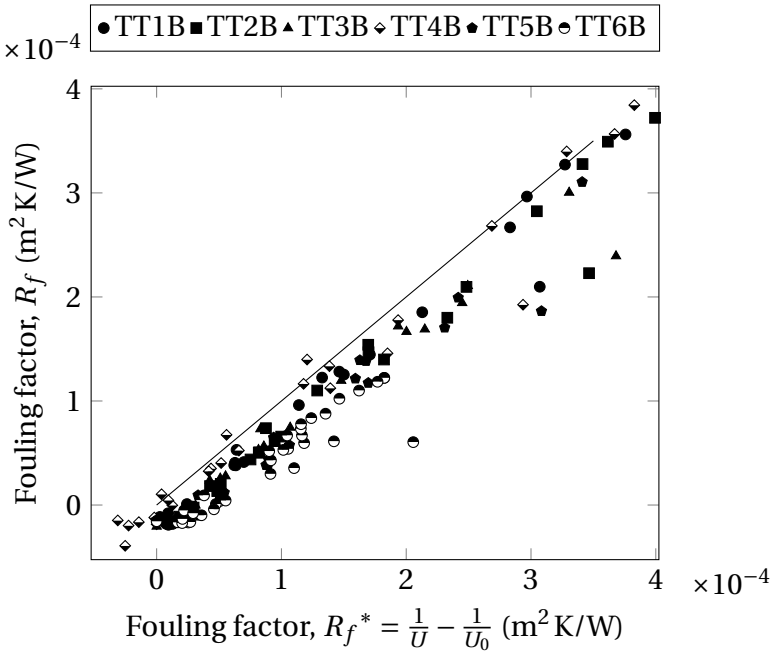

Table D.68: Measured fouling factors compared using equations (3.24) and (3.30)

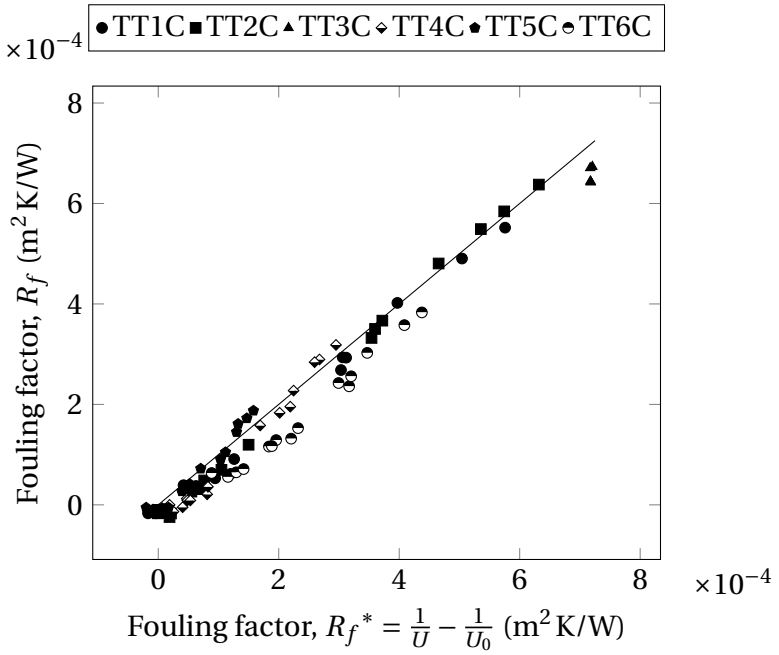

Table D.69: Measured fouling factors compared using equations (3.24) and (3.30

Appendix E

Sample calculations

E.1 Determining the friction factor at the start of testing

E.1.1 Test data

Consider test number DW4D20151121T1339, heat exchanger number 1. The measured geometry and recorded variables of this test are

Effective heat transfer length	L	=	3.199	m
Annulus diameter	d_4	=	0.0353	m
Tube outer diameter	d_3	=	0.0239	m
Tube inner diameter	d_2	=	0.0226	m
Cold inlet temperature	T_{in}	=	41.32	°C
Cold outlet temperature	T_{out}	=	42.614	°C
Annulus inlet temperature	$T_{\text{ann,in}}$	=	46.726	°C
Annulus outlet temperature	$T_{\text{ann,out}}$	=	45.793	°C
Cold volumetric flow rate	F	=	0.7107	l/s
Hot volumetric flow rate	F_{ann}	=	0.9948	l/s
Thermal conductivity of tube	k_t	=	16.1	W/m·K
Cold stream temperature difference	ΔT	=	5.406	K
Hot stream temperature difference	ΔT_{ann}	=	3.179	K
Length between pressure tappings	$L_{\Delta p}$	=	3.489	K
Manometer height difference	ΔH	=	454	mm

E.1.2 Thermophysical property data calculations

The bulk mean temperature of the foulant is

$$T_m = \frac{41.320\,^\circ\text{C} + 42.61\,^\circ\text{C}}{2} + 273.15\,\text{K} = 315.117\,\text{K} \tag{E.1}$$

- the density using equation A.1

$$\begin{aligned}\rho &= \Big[1.49343\times10^{-3} - 3.7164\times10^{-6}(315.117) + 7.09782\times10^{-9}(315.117)^2 \\ &\quad - 1.90321\times10^{-20}(315.117)^6\Big]^{-1} \\ &= 991.6\,\text{kg/m}^3 \end{aligned} \tag{E.2}$$

- the specific heat according to equation A.2

$$\begin{aligned}c_p &= 8.15599\times10^{3} - 2.80627\times10^{1}(315.117) + 5.11283\times10^{-2}(315.117)^2 \\ &\quad - 2.17582\times10^{-13}(315.117)^6 \\ &= 4\,177\,\text{J/kg}\cdot\text{K}\end{aligned} \tag{E.3}$$

- the viscosity using equation A.3

$$\begin{aligned}\mu &= 2.414\times10^{-5}\times10^{\frac{247.8}{(315.117-140)}} \\ &= 0.0006280\,\text{kg/(s m)}\end{aligned} \tag{E.4}$$

- the thermal conductivity according to equation A.4

$$\begin{aligned}k_f &= 6.14255\times10^{-1} + 6.9962\times10^{-3}\times(315.117) - 1.01075\times10^{-5}\times(315.117)^2 \\ &\quad + 4.74737\times10^{-12}\times(315.117)^4 \\ &= 0.6340\,\text{W/(m K)}\end{aligned}$$

- the Prandtl number according to equation A.5

$$\begin{aligned}\text{Pr} &= \frac{(6.278\times10^{-4})(4176.895)}{(0.634)} \\ &= 4.14\end{aligned} \tag{E.5}$$

E.1.3 Flow rate

The mass flow rate of the foulant is

$$m = \rho\cdot\text{F} \Rightarrow (991.6)(0.7107)\left|\frac{\text{l}}{\text{s}}\right|\left|\frac{1}{1000\,\text{l}}\right| = 0.7047\text{kg/s} \tag{E.6}$$

The cross-sectional flow area of the inside of the test tube is calculated using the internal diameter

$$A_c = \frac{\pi {d_1}^2}{4} \Rightarrow \frac{\pi(0.02260)^2}{4} = 0.0004012\,\text{m}^2 \tag{E.7}$$

which means the velocity of the foulant is

$$v = \frac{0.7107}{0.0004012}\left|\frac{\text{l}}{\text{s}}\right|\left|\frac{1}{1000\,\text{l}}\right| = 1.772\,\text{m/s} \tag{E.8}$$

E.1.4 Reynolds number

The Reynolds number characterizing the foulant is

$$Re = \frac{\rho \cdot v \cdot d_1}{\mu} \Rightarrow \frac{991.6 \cdot 1.772 \cdot 0.02260}{0.0006278} = 63244 \tag{E.9}$$

which is indeed fully turbulent.

E.1.5 Friction factor

The friction factor inside the test tube can be evaluated using

$$f_d = \frac{\rho g \Delta H}{\frac{L_{\Delta P} \rho v^2}{2 d_1}} \Rightarrow \frac{(991.6)(9.79)(454/1000)}{\frac{(3.4890)(991.6)(1.772)^2}{2(0.0226)}} = 0.0183 \tag{E.10}$$

Compare this to the theoretical smooth-tube friction factor

$$f_d = \left[1.8 \log_{10}(Re) - 1.5\right]^{-2} \Rightarrow \left[1.8 \log_{10}(63244) - 1.5\right]^{-2} = 0.0196 \tag{E.11}$$

an absolute difference of 6.4 % which is within the measurement uncertainty.

E.2 Determining the fouling factor

E.2.1 Test data

Consider test number DW4D20160627T1125-B, heat exchanger number 1. The measured geometry and recorded variables of this test are

Effective heat transfer length	L	=	3.199	m
Annulus diameter	d_4	=	0.0353	m
Tube outer diameter	d_3	=	0.0239	m
Tube inner diameter	d_2	=	0.0225	m
Cold inlet temperature	T_{in}	=	36.848	°C
Cold outlet temperature	T_{out}	=	38.187	°C
Annulus inlet temperature	$T_{\text{ann,in}}$	=	47.264	°C
Annulus outlet temperature	$T_{\text{ann,out}}$	=	46.057	°C
Cold volumetric flow rate	F	=	0.6463	l/s
Hot volumetric flow rate	F_{ann}	=	0.695	l/s
Thermal conductivity of tube	k_t	=	14	W/m·K
Cold stream temperature difference	ΔT	=	10.416	K
Hot stream temperature difference	ΔT_{ann}	=	7.87	K
Length between pressure tappings	$L_{\Delta p}$	=	3.499	K
Manometer height difference	ΔH	=	812	mm
Coefficient	A_{Nu}	=	0.558	
Exponent	B_{Nu}	=	0.4971	

E.2.2 Thermophysical property data calculations

The bulk mean temperature of the foulant is

$$T_m = \frac{36.848\,^\circ\text{C} + 38.19\,^\circ\text{C}}{2} + 273.15\,\text{K} = 310.667\,\text{K} \tag{E.12}$$

- the density using equation A.1

$$\begin{aligned}\rho = \Big[&1.49343 \times 10^{-3} - 3.7164 \times 10^{-6}(310.667) + 7.09782 \times 10^{-9}(310.667)^2 \\ &- 1.90321 \times 10^{-20}(310.667)^6\Big]^{-1} \\ &= 993.2\,\text{kg/m}^3\end{aligned} \tag{E.13}$$

- the specific heat according to equation A.2

$$\begin{aligned}c_p = &8.15599 \times 10^3 - 2.80627 \times 10^1(310.667) + 5.11283 \times 10^{-2}(310.667)^2 \\ &- 2.17582 \times 10^{-13}(310.667)^6 \\ &= 4\,177\,\text{J/(kgK)}\end{aligned} \tag{E.14}$$

- the viscosity using equation A.3

$$\begin{aligned}\mu &= 2.414 \times 10^{-5} \times 10^{\frac{247.8}{(310.667-140)}} \\ &= 0.0006830\,\text{kg/(sm)}\end{aligned} \tag{E.15}$$

- the thermal conductivity according to equation A.4

$$\begin{aligned}k_f = &6.14255 \times 10^{-1} + 6.9962 \times 10^{-3} \times (310.667) - 1.01075 \times 10^{-5} \times (310.667)^2 \\ &+ 4.74737 \times 10^{-12} \times (310.667)^4 \\ &= 0.6280\,\text{W/(mK)}\end{aligned} \tag{E.16}$$

- the Prandtl number according to equation A.5

$$\begin{aligned}\text{Pr} &= \frac{(6.834 \times 10^{-4})(4176.820)}{(0.628)} \\ &= 4.55\end{aligned} \tag{E.17}$$

The bulk mean temperature of the annular fluid is

$$T_{m,\text{ann}} = \frac{47.3\,^\circ\text{C} + 46.3\,^\circ\text{C}}{2} + 273.15\,\text{K} = 319.3\,\text{K} \tag{E.18}$$

Similarly for the annular stream find

$$\begin{aligned} \rho_{\text{ann}} &= 989.6\,\text{kg/m}^3 \\ c_{p,\text{ann}} &= 4177.8\,\text{J K/kg} \\ \mu_{\text{ann}} &= 0.0005800\,\text{kg/(s s)} \\ k_{f,\text{ann}} &= 0.6391\,\text{W/(m K)} \\ \text{Pr}_{\text{ann}} &= 3.77 \end{aligned}$$

E.2.3 Flow rates

The mass flow rate of the foulant is

$$m = \rho \cdot \text{F} \Rightarrow (993.2)(0.6463) \left|\frac{\text{l}}{\text{s}}\right| \left|\frac{1}{1000\,\text{l}}\right| = 0.6419\text{kg/s} \tag{E.19}$$

The cross-sectional flow area of the inside of the test tube is calculated using the internal diameter

$$A_c = \frac{\pi {d_1}^2}{4} \Rightarrow \frac{\pi(0.02250)^2}{4} = 0.0003976\,\text{m}^2 \tag{E.20}$$

which means the velocity of the foulant is

$$v = \frac{0.6463}{0.0003976} \left|\frac{\text{l}}{\text{s}}\right| \left|\frac{1}{1000\,\text{l}}\right| = 1.625\,\text{m/s} \tag{E.21}$$

And for the annulus the mass flow rate is

$$m_{\text{ann}} = \rho_{\text{ann}} \cdot \text{F}_{\text{ann}} \Rightarrow (989.6)(0.6950) \left|\frac{\text{l}}{\text{s}}\right| \left|\frac{1}{1000\,\text{l}}\right| = 0.6878\text{kg/s} \tag{E.22}$$

The cross-sectional flow area of the annulus is

$$A_{\text{ann}} = \frac{\pi {d_4}^2 - \pi {d_3}^2}{4} \Rightarrow \frac{\pi(0.03530)^2 - \pi(0.02390)^2}{4} = 0.0005301\,\text{m}^2 \tag{E.23}$$

which means the velocity through the annulus is

$$v_{\text{ann}} = \frac{0.6950}{0.0005301} \left|\frac{\text{l}}{\text{s}}\right| \left|\frac{1}{1000\,\text{l}}\right| = 1.311\,\text{m/s} \tag{E.24}$$

E.2.4 Reynolds number

The Reynolds number characterizing the foulant is

$$Re = \frac{\rho \cdot v \cdot d_1}{\mu} \Rightarrow \frac{993.2 \cdot 1.625 \cdot 0.02250}{0.0006834} = 53154 \tag{E.25}$$

which is indeed fully turbulent.

E.2.5 Friction factor

The friction factor inside the test tube can be evaluated using

$$f_D = \frac{\rho g \Delta h}{\frac{L_{\Delta P} \rho v^2}{2 d_1}} \Rightarrow \frac{(993.2)(9.79)(812/1000)}{\frac{(3.4990)(993.2)(1.625)^2}{2(0.0225)}} = 0.0387 \tag{E.26}$$

Compare this to the theoretical smooth-tube friction factor

$$f_D = \left[1.8 \log_{10}(Re) - 1.5\right]^{-2} \Rightarrow \left[1.8 \log_{10}(53154) - 1.5\right]^{-2} = 0.0204 \tag{E.27}$$

an absolute difference of 47.3 % which is attributable to the increased roughness caused from the presence of the foulant.

E.2.6 Nusselt number

The relative roughness is determined from equation (3.16):

$$\frac{\epsilon}{d_1} = e^{((1.14 - 0.038694^{-0.5})/0.86)} = 0.010197 \tag{E.28}$$

Next calculate the roughness Reynolds number which characterizes whether the internal heat transfer coefficient is smooth, transitionally rough, or fully rough:

$$\mathrm{Re}_\epsilon = \mathrm{Re} \cdot \frac{\epsilon}{d_1} \cdot (f_d/8)^{0.5} \Rightarrow (53154)(0.010197)(0.0387/8)^{0.5} = 37.7 \tag{E.29}$$

which is greater than 5 but less than 70 and therefore transitionally rough, so the internal Nusselt number is

$$\begin{aligned} \mathrm{Nu} &= \frac{(f_d/8)\mathrm{Re}\,\mathrm{Pr}}{(1 + 12.7(f_d/8)^{0.5}(\mathrm{Pr}^{2/3} - 1)}) \\ &\Rightarrow \frac{(0.0387/8)(53154)(4.55)}{(1 + 12.7(0.0387/8)^{0.5}(4.55^{2/3} - 1)}) = 460.0 \end{aligned} \tag{E.30}$$

The convection coefficient for the foulant is

$$h = \frac{\mathrm{Nu}^* k_f}{D_h} \Rightarrow \frac{(460.0)(0.62794)}{(0.0225)} = 12\,840\,\mathrm{W/(m^2\,K)} \tag{E.31}$$

Similarly the annular Reynolds number is determined using the equation (3.18)

$$\mathrm{Re}_{\mathrm{ann}} = \frac{989.6\times, 1.311\,(0.0353 - 0.0239)}{0.000577} = 25656 \tag{E.32}$$

Then the annular convection coefficient is determined using the regression (equation: 3.23)

$$\begin{aligned} h_{\mathrm{ann}} &= \mathrm{A_{Nu}} \mathrm{Re_{ann}}^{\mathrm{B_{Nu}}} \mathrm{Pr}^{0.3} \times \left(\frac{k_f, \mathrm{ann}}{D_{h,\mathrm{ann}}}\right) \\ &\Rightarrow (0.558000)(25656)^{(0.497100)}(3.769)^{0.3} \times \frac{(0.63908)}{(0.0114)} = 7\,244\,\mathrm{W/(m^2\,K)} \end{aligned} \tag{E.33}$$

E.2.7 The total thermal resistance

The total thermal resistance is equal to the sum of each of the thermal resistances and thus can be written in terms of the fouling factor as

$$\begin{aligned}\Sigma R - R_f &= \frac{1}{hA_s} + \frac{\ln\frac{d_3}{d_1}}{2\pi k_{\text{eff}} L_{eff}} + \frac{1}{h_{ann}A_{ann}} \\ &\Rightarrow \frac{1}{(12838.7)(0.2261)} + \frac{\ln\frac{(0.0239)}{(0.0225)}}{2\pi(14.0)(3.199)} + \frac{1}{(7243.8)(0.2402)} \\ &= 0.001134\,\text{K/W}\end{aligned} \tag{E.34}$$

E.2.8 Heat transfer

The rate of heat transfer to the foulant is calculated assuming constant specific heat, thus

$$Q = mc_p\Delta T \Rightarrow (0.6419)(4176.8)(38.187 - 36.848) = 3\,590\,\text{W} \tag{E.35}$$

Similarly the rate of heat transfer from the annulus is

$$Q_{\text{ann}} = m_{\text{ann}}c_{p,\text{ann}}\Delta T_{\text{ann}} \Rightarrow (0.6878)(4177.8)(47.264 - 46.057) = 3\,468\,\text{W} \tag{E.36}$$

and the mean heat transfer rate

$$\bar{Q} = 0.5(Q + Q_{\text{ann}}) \Rightarrow 0.5(3590.2 + 3468.3) = 3\,529\,\text{W} \tag{E.37}$$

The energy balance term calculated using equation (3.37) is

$$\text{EB} = \frac{Q - Q_{\text{ann}}}{\max(Q, Q_{\text{ann}})} \Rightarrow \frac{(3590.2) - (3468.3)}{(3590.2)} = 3.397\,\% \tag{E.38}$$

The log mean temperature difference

$$\Delta T_{\text{LM}} = \frac{\Delta T_1 - \Delta T_2}{\ln\frac{\Delta T_1}{\Delta T_2}} \Rightarrow \frac{(10.416) - (7.870)}{(0.2803)} = 9.084\,\text{K} \tag{E.39}$$

E.2.9 The overall heat transfer coefficient

The overall heat transfer coefficient is defined to be

$$UA = \frac{\bar{Q}}{\Delta T_{\text{LM}}} = (\Sigma R - R_f)^{-1} \tag{E.40}$$

Then

$$UA = 388.5\,\text{W/K} \tag{E.41}$$

And the overall heat transfer coefficient

$$U = \frac{388.5\,\text{W/K}}{0.2402\,\text{m}^2} = 1\,617.6\,\text{W/(m}^2\,\text{K)} \tag{E.42}$$

E.2.10 The fouling factor

Substituting equations (E.37), (E.39), and (E.34) find

$$R_f = 0.0003257\,\mathrm{m^2\,K/W} \tag{E.43}$$

Finally compare this to $R_f{}^*$ by recalling at the start of the test the overall heat transfer coefficient is

$$U_0 = \frac{8601.1}{0.240 \times 10.4} = 3\,432\,\mathrm{W/(m^2\,K)} \tag{E.44}$$

Which means $R_f{}^*$ is

$$R_f{}^* = \frac{1}{1\,618\,\mathrm{W/(m^2\,K)}} - \frac{1}{3\,432\,\mathrm{W/(m^2\,K)}} = 0.0003269\,\mathrm{m^2/(W\,K)} \tag{E.45}$$

Appendix F

Water analysis

F.1 Cooling water analysis

Table F.1 includes the complete water sample quality analysis.

Table F.1: Water analysis comparison

		Sample point			
Descriptor	Limits	Station clarifier		Apparatus	
Sample date		2015/12/24	2016/1/27	2016/4/2	2016/8/5
pH 25 degC pH	8.1-8.6	8.85	8.64	8.59	8.88
Electrical conductivity (EC) @ 25 C mS/m			293	221	207
Total dissolved solids (TDS) mg/l			2040	1511	1638
Total alkalinity mg CaCO3/l			185	160	337
Chloride (Cl) mg/l	400	174	268	172	173
Sulphate (SO4)	1000	688	946	727	695
Nitrate (NO3) as N mg/l		2.71	3.55	2.06	5.53
Ammonium (NH4) as N mg/l	40	1.5	0.029	<0.005	0.254
Orthophosphate (PO4) as P mg/l			0.053	0.013	0.070
Fluoride (F) mg/l			1.65	1.72	2.13
Calcium (Ca) mg/l			108	72.5	59.5
Magnesium (Mg) mg/l			117	86.7	118
Sodium (Na) mg/l	500	287	369	272	301
Potassium (K) mg/l		72	101	71.4	58.2
Aluminium (Al) mg/l			<0.002	<0.002	<0.002
Iron (Fe) mg/l			<0.004	<0.004	<0.004
Manganese (Mn) mg/l			<0.001	<0.001	<0.001
Turbidity NTU	100	81.3	32.2	32.9	274
Total hardness mg $CaCO_3$/l			752	538	636
Suspended solids (SS) mg/l			60	43	374
Langelier Saturation Index LSI	0		0.92	0.65	1.17
Ryznar Stability Index RSI	6		6.79	7.29	6.55
Legionella CFU/ml			<60		
Cycles of concentration		16.9			